Shining a Light on Silica Production in the Oceans: Using a Fluorescent Tracer to Measure Silica Deposition in Marine Diatoms

by

Jennifer Long
B.Sc., University of British Columbia, 2010

A Thesis Submitted in Partial Fulfillment
of the Requirements for the Degree of

MASTER OF SCIENCE

in the Department of Biology

Supervisory Committee

Shining a Light on Silica Production in the Oceans: Using a Fluorescent Tracer to Measure Silica Deposition in Marine Diatoms

by

Jennifer Long
B.Sc., University of British Columbia, 2010

Supervisory Committee

Dr. Diana E. Varela (Department of Biology, and School of Earth and Ocean Sciences)
Supervisor

Dr. Kerry R. Delaney (Department of Biology)
Departmental Member

Dr. Roberta C. Hamme (School of Earth and Ocean Sciences)
Outside Member

Abstract

Supervisory Committee
Dr. Diana E. Varela (Department of Biology, and School of Earth and Ocean Sciences)
Supervisor
Dr. Kerry R. Delaney (Department of Biology)
Departmental Member
Dr. Roberta C. Hamme (School of Earth and Ocean Sciences)
Outside Member

This thesis presents improvements to a method for measuring the production of biogenic silica ($bSiO_2$) by diatoms, a group of microscopic algae with siliceous cell walls (frustules) that dominate the marine cycling of silicon (Si) and account for a significant proportion of global marine primary productivity. Using the fluorescent dye PDMPO, diatom $bSiO_2$ can be labeled as it is produced and then quantified using fluorometry to determine community-wide $bSiO_2$ production. A distinct advantage of PDMPO over more traditional tracers of $bSiO_2$ production is that the combination of measurements of PDMPO by fluorometry and by fluorescence microscopy allows for the quantification of cell (and thus taxa) specific $bSiO_2$ production within a mixed community. However, the robustness of PDMPO as a quantitative tracer of diatom $bSiO_2$ production has not been sufficiently investigated. To address this, experiments were conducted both in the lab, and at two field locations where diatoms are known to be abundant, namely the continental shelf off the west coast of Vancouver Island, and Saanich Inlet, a highly productive fjord located on southern Vancouver Island.

Laboratory culture experiments demonstrated that concentrations of PDMPO >500 nmol L^{-1} reduced growth rate in the diatom *Thalassiosira pseudonana*, and affected the Si:PDMPO ratio of incorporation. The relationship between SiO_2 and PDMPO incorporation was significantly affected by diatom species, though this effect was small (8%) when cells were lysed. From these experiments, a Si:PDMPO incorporation ratio of 4200 ± 380:1 was determined, which predicted 30% more $bSiO_2$ production for PDMPO incorporation than previous studies, and better agreed with $bSiO_2$ production rates determined using established methods in Saanich Inlet. However, $bSiO_2$ production rates were over-estimated by the PDMPO method when rates were less than 1 µmol L^{-1} d^{-1}. In

a few cases, this occurred when dinoflagellates were numerically dominant, but for the majority of samples, dinoflagellates were low in abundance, and over-estimation by PDMPO may be related to low dissolved $Si(OH)_4$ concentration.

Protocols for quantifying PDMPO fluorescence by microscopy were optimized by using a low numerical aperture microscope objective. Additionally, measurements of fluorescence intensity were calibrated using a fluorescent microscope slide as a standard, which served to correct for unevenness of illumination across the field of view. With these protocol modifications, quantification of PDMPO by microscopy agreed with PDMPO measured by fluorometry. When PDMPO was measured by microscopy in the field, the contribution of diatom taxa to PDMPO fluorescence differed from their contribution to cell numbers. In many cases this was due to large diatom taxa producing more $bSiO_2$ per cell than smaller taxa. However, much of the difference between cell numbers and PDMPO fluorescence was not explained by differences in cell size. This suggests that the diatom taxa had different specific $bSiO_2$ production rates, which could be estimated using PDMPO. This thesis highlights the strength of the PDMPO tracer for understanding diatom community dynamics. The use of PDMPO should allow the relationship between diatom community composition, growth and productivity to be better illuminated in the oceans.

Table of Contents

List of Tables

List of Figures

Acknowledgments

First, I would like to thank my supervisor, Diana Varela for giving me a wealth of opportunities. Beyond her continual support of my research, Diana has always encouraged me to aim higher. In addition to supporting my graduate study, I have also learned much about the intricacies of the academic system from many candid conversations about science in general.

Next, I would like to thank Kerry Delaney for many enlightening discussions about fluorescence microscopy, as well as his contributions to the design of this project. Kerry has taught me almost everything I know about fluorescence microscopy, from broad principals of optics to the basic details of imaging. He has also constantly debated new and improved microscope configurations optimal for the unique challenges of my project, and in doing so pushed me to think beyond the present.

I would also like to thank Roberta Hamme for her contributions to the design of this project, as well as providing a calm and down to earth perspective in guiding my research. In addition, my studies have profited from her patient assistance with data interpretation.

This research would not have been possible without the support of many Varela lab group members over the years. First I would like to thank Karina Giesbrecht, who taught me much of what I know about working in the lab, and has been a wonderful mentor. Karina has helped me with almost all aspects of this project: teaching me analytical chemistry, showing me the ropes on my first oceanographic research cruise, and being there for me through all the highs and lows of graduate research. Next, I'd like to thank Marcos Lagunas, who was my partner for much of my field work in Saanich Inlet and my second cruise to the west coast of Vancouver Island. With Marcos' help I was able to accomplish so much, even when we were both seasick. I would also like to thank Jill Sutton, for patiently teaching me how to culture diatoms, and also Rhiannon Pretty, Robert Izett, Pam Dheri, Sarah Garner, and Lincoln Hood for assistance growing cultures through the years. Other members of the Varela lab that played a less direct role in my project but provided substantial moral support include Arielle Kobryn and Curtis Martin.

The collection of my field samples would not have been possible without the help of many people. Thank you to Doug Yelland and Marie Robert for co-ordinating cruises to the west coast of Vancouver Island, and the captain and crew of the CCGS John P. Tully for enabling the collection of these samples. Cruises to Saanich Inlet would not have been possible without collaboration with the Hallam lab at the University of British Columbia, in particular the ever cheery Monica Torres Beltrán. Also, I would like to thank Captain Ken Brown of the RV Strickland for making collection of these samples possible.

Sample analysis was also supported by many people. I would like to thank Lisa Miller at the Fisheries and Oceans Canada who allowed Karina and I to use her beta counter for the measurement of ^{32}Si samples, and assisted with sample analysis as did Marty Davelaar. Jody Spence taught me how to use HF safely and provided safe space to work with this toxic substance. Measurements of PDMPO samples were aided by the Mazumder lab, who allowed me to use their Turner Trilogy fluorometer. I would also like to acknowledge assistance from Linghong Lu who provided assistance modelling PDMPO incorporation in R.

During my time at the University of Victoria, I have also enjoyed support from many friends and colleagues. I would like to thank Christina Schallenberg and David Janssen for illuminating discussions about the chemical side of oceanography, among many other things. I would also like to thank Jessica Nephin, Jackson Chu, Jonathan Rose and Katie Gale for many productive discussions on a wide range of subjects from Saanich Inlet to statistics to technology. In addition to helping me to better understand my research topic, these individuals have also provided invaluable support managing the day to day challenges of being a graduate student.

I would also like to thank my family for their continued support and grounded perspectives throughout my degree. Kathy Wellburn and Anne Labelle have both helped me to make many important decisions during my studies, and encouraged me to think about my long term goals, both academic and otherwise. Malcolm Long has always provided important diversions, and a very different perspective to my own. I would also like to thank Jean Long for her unconditional love and support.

Lastly I would like to acknowledge the funding sources without which this research would not have been possible. My research has been supported by a National Sciences and Engineering Research Council of Canada (NSERC) Discovery Grant awarded to Diana Varela. In addition, I received NSERC funding from an NSERC Alexander Graham Bell Canada Graduate Scholarship. I was also fortunate to have support from the University of Victoria, in the form of a University of Victoria President's Research Scholarship and a University of Victoria Fellowship. I also appreciate the support I received from the Lewis J. Clark Memorial Fellowship, the W. Gordon Fields Memorial Fellowship, and the CUPE 4163 Conference Award.

Glossary of Terms

2P – Two photon. Two photon microscopy is an optical sectioning method that excites and detects fluorescence by scanning a focused spot of light across the field of view.
Absolute fluorescence – When fluorescence intensity is quantified as a numerical value, such that it can be compared with measurements from a separate sample.
Bq – Becquerel. Unit of radioactivity. Equivalent to one radioactive decay per second.
Brightfield microscopy – When white light is transmitted through a sample and detected through a microscope.
bSiO$_2$ – Particulate biogenic silica. In seawater, mostly from diatom frustules. A component of total particulate SiO_2 in field samples, as particulate SiO_2 in marine waters is composed of biogenic and lithogenic fractions.
Bulk – Used in this thesis to refer to a measurement of the whole community, when all cells present in a sample are collected on a filter and then analyzed together.
Calibration image – Image of a calibration slide. An average image of 10 different fields of view of a calibration slide.
Calibration slide – A fluorescent slide used as a standard to calibrate illumination intensity and flat-field correct images of fluorescence for quantitative microscopy.
CCMP – National Center for Marine Algae and Microbiota strain.
Chl *a* – Chlorophyll *a*. Pigment central to photosynthesis in autotrophic organisms, and often used as an indicator of autotrophic biomass.
Ci – Curie. Unit of radioactive activity. Equivalent to 3.7×10^{10} Bq.
CTD – Conductivity, temperature and depth sensor package. Used to profile conductivity and temperature with depth through the water column, and may be equipped with additional sensors such as for chlorophyll *a* fluorescence and irradiance.
DPM- Disintegration per minute. The number of decays of a radioactive substance (e.g. ^{32}Si) that occur during one minute.
Emission – Light released from a fluorophore during fluorescence.
ESAW – Enriched seawater, artificial water. Artificial seawater medium for the culture of diatoms. Recipe described in Berges et al. (2001).
Excitation – The absorbance of light by a fluorophore that causes the electrons in a fluorophore to reach a higher energy level. When the fluorophore returns to its ground state fluorescence is emitted.
FOV – Field of view. The area of a slide visible through the oculars, or captured as an image by a camera using a microscope.
Flat-field correction – When fluorescence intensities measured from a sample image are normalized to a calibration image. This corrects for unevenness in illumination (and therefore fluorescence detected) across the field of view. The fluorescence intensity of each pixel within the sample image is divided by the intensity of the pixel at the same location within the field of view from the calibration image.
Frustule – SiO_2 cell wall of diatoms.
FSW – Filtered sea water. Filtered to remove particle larger than 0.7 µm.
GF – Glass fiber filter.
Incorporation – The process by which a constituent becomes part of a diatom cell.

iPDMPO – PDMPO incorporated into cells, quantified by fluorescence microscopy.
K_{Si} – The half saturation constant for $Si(OH)_4$. The concentration of $Si(OH)_4$ at which uptake rate is half the maximum rate.
Linear mixed effects model - A linear model that accounts for non-independence of measurements by imposing a grouping structure between measurements. Follows the same form as a linear model, except with multiple values for b (intercept), each corresponding to a different group.
Linear model - Relationship between two parameters in the form $y = mx + b$.
Ln – Natural logarithm.
Mountant – Substance applied to a sample on a microscope slide which is subsequently covered with a coverslip.
n – The number of replicate samples.
NA – Numerical aperture. A measure of the range of angles of light that can be captured by a microscope objective lens.
NO_3^- - Nitrate. The dominant form of bioavailable nitrogen in high nutrient seawater. In some cases, NO_3^- values reported represent the total concentration of NO_3^- and nitrite (NO_2^-) as these species were not distinguished during analysis in this thesis.
NO_2^- - Nitrite. A form of bioavailable nitrogen in seawater.
Optical sectioning – Method for microscopic imaging in which images are captured from precisely focused planes at regular intervals throughout the cell depth.
PC – Polycarbonate, a type of plastic.
PDMPO – 2-(4-pyridyl)-5-((4-(2-dimethylaminoethylaminocarbamoyl)methoxy)-phenyl)oxazole. Also known as Lysosensor DND-160, a fluorescent dye manufactured by Life Technologies.
Plane of focus – The region where generation and collection of fluorescence by a microscope is maximal.
PP- Polyproylene, a type of plastic.
pPDMPO – PDMPO incorporated into particles. In this thesis, samples were filtered, diatom frustules were digested, and the PDMPO concentration determined by measurement on a fluorometer.
PO_4^{-3} – Orthophosphate. In this thesis, refers to dissolved inorganic phosphorus in the form of PO_4^{-3} and HPO_4^{-2} which are the forms readily taken up by phytoplankton.
Primary productivity - Rate of organic carbon production by autotrophic organisms.
R – Language and environment for statistical analysis and graphics.
Relative fluorescence –The proportion of PDMPO fluorescence for different cells (or species) determined within the same microscope slide.
S - Salinity.
SA – Surface area. In this thesis, it may refer to the surface area of a diatom cell, or the total surface area of a taxonomic group within an assemblage.
SA:V – Surface area to volume ratio.
SD – Standard deviation.
SDV – Silicon deposition vesicle. The acidic vesicle where polymerization of SiO_2 occurs within a diatom.
SE – Standard error. SD divided by the square root of n.
Si – The element silicon.
^{30}Si – A stable isotope of silicon, 3% of natural isotope abundance.

^{32}Si – A radioactive isotope of silicon. Used as a tracer for measuring gross $bSiO_2$ production rates.
SiO_2 – Silica. Abbreviation of $SiO_2 \cdot nH_2O$, the chemical form of silicon in diatom frustules.
$Si(OH)_4$ – Silicic acid. Dissolved form of Si which is most abundant in seawater and taken up by diatom cells.
Si:PDMPO – The ratio of Si to PDMPO incorporated into a diatom frustule.
Stoke's shift – The difference in wavelengths between excitation and emission spectra of a fluorophore.
T- Temperature.
Uptake – Transport of a constituent across the cell membrane.
V_{PDMPO} – PDMPO incorporation for a genus normalized to its cumulative surface area, and a proxy for specific SiO_2 production rate.
Widefield microscopy – Fluorescence microscopy that simultaneously illuminates and detects the entire FOV.
$\Delta[SiO_2]$ – The concentration of SiO_2 produced by diatoms since the addition of PDMPO.
μ - Growth rate. The number of cell divisions per day (units of d^{-1}).
ρ – $bSiO_2$ production rate. In units of µmol SiO_2 L^{-1} d^{-1}.
ρ_{NET} – Net biogenic silica production rate. Determined as the difference between $bSiO_2$ concentration between the start and end of a given period of time.
ρ_{GROSS} – Gross biogenic silica production rate. Determined using the tracer ^{32}Si.
ρ_{PDMPO} – Biogenic silica production rate determined using PDMPO.

Chapter 1: General Introduction

1.1. Introduction

Marine diatoms are microscopic phytoplankton which are responsible for ~40% of marine primary productivity (Nelson et al. 1995). For my thesis, I have improved and implemented a technique that uses a fluorescent tracer quantified by fluorometry and microscopy to investigate diatom silica production. The following introduction begins with a brief history of diatoms and microscopy, and continues with an overview of the role of diatoms in the marine carbon and silicon cycles. This is followed by a discussion of different approaches to quantify diatom productivity, and finally the focus and outline of this thesis.

1.2. A Brief History of Diatoms and Microscopy

"In all the range of microscopic research there is confessedly nothing which offers more seductive attraction than that department of botany which comprises the Diatomaceae"

-Johnston, in The Lens (1872)

Ever since their first observation in 1703 (Mr. C 1703), people have been fascinated by diatoms. The beauty of their ornate geometric shapes has been appreciated since we first had the power to see them. Although the anonymous country gentleman Mr. C was the first to unambiguously describe and sketch diatom cells when he discovered them in a ditch, the study of diatoms was limited by the resolution of microscopes at the time (Round et al. 1990). Not until the 1800s were microscopes good enough to resolve diatom structures beyond the outline of the cell (Bradbury and Turner 1967).

Once microscopy had advanced sufficiently to distinguish different species of diatoms, research into aspects of diatom biology flourished. Many topics investigated during this time are still actively studied today, though techniques have advanced. Light microscopy allowed the classification of different diatom species based on morphology (Walker-Arnott 1860; Bessey 1900), and the taxonomic relationships of diatom species are

currently still investigated, aided by modern phylogenetic techniques (Theriot 2010). Early diatomists observed seasonal changes in diatom abundance, and commented on the causes of such fluctuations (Donkin 1858). The factors controlling diatom abundance and biomass are still explored, and have been greatly aided by the development of computer models that account for environmental and biological factors (e.g. Collins et al. 2009). In an 1889 publication, Kain used diatom species composition from sediments to infer the paleo-environment in which they had grown. Diatoms are used in contemporary studies as indicators of past nutrient availability and productivity, although using more sophisticated techniques such as stable silicon (Si) isotope ratios (Hendry and Brzezinski 2014). Both the structure and synthesis of diatom frustules were investigated by early diatomists (Durkee 1884; Cox 1885; Palmer and Keeley 1900), a research area that has profited from further advancements in microscopy such as the capability to image fluorescently labelled cellular structures (Hazelaar et al. 2005; Heredia et al. 2008; Tesson and Hildebrand 2010a).

While advances in microscopy allowed for increased investigation of diatoms, diatoms in turn facilitated advances in microscopy. Starting in the 1820s, microscopists used test objects to determine the capabilities of their microscope configurations, a process that was crucial to the development of microscopy (Schickore 2003). Due to their fine scale geometric features, diatoms were preferred as test objects (Hogg 1869; Round et al. 1990), with Spitta (1920) even recommending several different diatom species, each optimal for testing a different microscopic capability. Competition among gentleman scholars ensued to describe more and more details of different diatom frustules (Round et al. 1990). But despite much interest in their appearance, understanding of diatom biology was limited in the 19th century. Debate about whether diatoms were plants or animals continued into the 1850s, at which point they were generally agreed to be "plants" (Round et al. 1990).

Today, we have a much better understanding of diatom biology, as well as the significant role that diatoms play in marine and freshwater ecosystems and global biogeochemical cycles. The magnitude of the importance of diatoms on a global scale

likely could not have been imagined by the diatomists of two centuries ago, and advances in microscopy continue to improve our understanding of the ecology and physiology of diatoms. Yet the aesthetic fascination with diatoms remains timeless, as is evident in the leading role that diatoms play in contemporary microscopic art (Nikon Instruments Inc. 2013).

1.3. Diatoms and the Carbon Cycle

Diatoms are autotrophic organisms which use energy from sunlight to convert carbon dioxide (CO_2) into organic carbon. They play a large role in global carbon (C) cycling, and are responsible for an estimated 20% of global primary productivity, a share larger than that of all tropical rainforests (Nelson et al. 1995; Field et al. 1998). In the marine environment, the biomass of primary producers at the bottom of a food web is the dominant determinant of the biomass of higher trophic levels (Ware and Thomson 2005; Chassot et al. 2010). Among the phytoplankton, diatoms tend to dominate in regions of high primary productivity (Nelson et al. 1995), such as high nutrient upwelling and coastal regions (Lalli and Parsons 1997). These are areas which also support productive fisheries, and therefore diatom biomass is an important determinant of fisheries productivity.

Diatoms also impact the global C cycle through their contribution to the biological C pump, the process by which C is moved from the atmosphere and surface ocean to the deep ocean by biologically produced particles. When diatoms grow, they fix CO_2 in the surface ocean, and when they die, some fraction of this C sinks to the deep ocean. The biological C pump is responsible for 75% of the 15% higher dissolved inorganic C concentrations in the deep ocean relative to the surface (Riebesell et al., 2007; Sarmiento and Gruber, 2006). As a result, the biological C pump is important for C sequestration away from the atmosphere, as the deep ocean is the largest non-rock C reservoir on the planet and C is stored there on time scales of ~1000 years (Emerson and Hedges 2008). Carbon sequestration in the ocean is important for mitigating the increase in atmospheric CO_2 concentrations due to human activities that has occurred over the past ~200 years

(Falkowski 2000), and the oceans have already absorbed 30% of anthropogenic CO_2 emissions (Le Quéré et al. 2015). Export of C via the biological pump has likely occurred at a constant rate over the time scale of anthropogenic emissions, but if it were to change in magnitude it could have substantial implications for carbon sequestration.

Atmospheric concentrations of CO_2 affect global climate, and it has been hypothesized that past changes in phytoplankton, primarily diatom, productivity could be partially responsible for glacial-interglacial climate transitions (Martin 1990; Tréguer 2002; de Baar et al. 2005). Diatoms are thought to be particularly efficient at removing CO_2 from the surface ocean, and are often responsible for the majority of new and export production (Dugdale and Wilkerson 1998; Marchetti et al. 2010). This has been observed even in regions where diatoms are low in abundance (Brzezinski et al. 1998; Dugdale and Wilkerson 1998; Krause et al. 2009; Dugdale et al. 2011), although in some instances they may contribute less to C export if they are efficiently grazed (Benitez-Nelson et al. 2007). Diatoms are effective at exporting carbon to the deep ocean because they often sink rapidly which minimizes respiration of their carbon in the surface ocean. Large diatoms sink especially fast (Kemp et al. 2000; Mosseri et al. 2008), as do those species that form aggregates (Alldredge and Gotschalk 1989; Passow et al. 2003). Additionally, when diatoms are grazed, their silica frustules serve as ballast for the fecal pellets generated, enhancing carbon export to depth (Honjo et al. 2008). Since diatoms are important for both the fixation of C into organic matter and the sequestration of C in deep waters, determining the controls on the productivity of diatoms is important to our understanding of the global carbon cycle and its response to anthropogenic perturbations.

1.4. Diatoms and the Silicon Cycle

Unlike other groups of phytoplankton, diatoms require silicon (Si). They take up Si in the form of silicic acid ($Si(OH)_4$, Del Amo and Brzezinski, 1999), which they use to build frustules of non-crystalline hydrated opal, with the chemical form $SiO_2 \bullet nH_2O$ (Kröger 2007; Armbrust 2009). Silicic acid uptake requires cellular energy (Azam et al. 1974) and increases cell density requiring diatom cells to expend even more energy to resist

sinking out of the sunlit euphotic zone (Raven and Waite 2004). Therefore, the silica (SiO_2) cell wall must confer some selective advantage to compensate for these physiological costs. However, there is still speculation about what this advantage might be. Raven and Waite (2004) suggest many possible functions for the silica frustule such as grazer protection, turgor resistance and buffering carbonic anhydrase activity. Diatom frustules also affect light entering the cell; for example, they may focus light (De Stefano et al. 2007) or reduce UV radiation reaching the cell (Ingalls et al. 2010). Although producing a SiO_2 frustule requires energy, it requires less than the production of potential alternatives such as polysaccharides or lignin (Martin-Jézéquel et al. 2000). Interestingly, ancestral diatoms did not have SiO_2 frustules, and evolved to produce them at a time when $Si(OH)_4$ concentrations in seawater were much higher than today (Raven and Waite 2004).

Presently, $Si(OH)_4$ concentrations are low in much of the surface ocean (Sarmiento and Gruber 2006), and may limit the growth of diatoms. Silicon cycling in the ocean is largely controlled by diatoms, and a single atom of Si will cycle through 25 different diatom cells before it is buried at the sea floor (Tréguer and De La Rocha 2012). Although diatom productivity may be limited directly by $Si(OH)_4$ availability (Martin-Jézéquel et al. 2000; Dugdale et al. 2011), the amount of Si per cell (the cellular Si quota), is flexible and may vary with respect to other cellular constituents such as C and nitrogen (N). It is possible for $Si(OH)_4$ concentrations to limit SiO_2 formation but not affect growth rate overall (Paasche 1973). Conversely, it is possible for low growth rates to result in an increase in SiO_2 per cell (Claquin et al. 2002). The SiO_2 in a diatom cell is located in the cell wall, and the amount of SiO_2 per cell is determined by the thickness of the frustule and the cell's surface area (SA). Therefore, SA is useful as a proxy for a diatom cell's SiO_2 content. The SiO_2 content of different diatom species can be estimated by calculating their surface area based on their morphology (Brzezinski 1985). In contrast, most other cellular constituents (e.g. C, nitrogen) are found within the cell, and their amount per cell is more closely related to the cell volume. Therefore factors that affect cell size and surface area to volume ratios (SA:V) will affect the quotas of Si and intracellular elements differently.

Changes in cellular Si quota have significant consequences for the biological C pump. Because SiO_2 is dense, an increase in the amount of SiO_2 per cell may increase particle sinking rate and enhance carbon transport to the deep ocean (Annett et al. 2009; Marchetti et al. 2010; Durkin et al. 2013). The Si requirement of diatoms also has ecological consequences: if $Si(OH)_4$ concentrations are low relative to other nutrients, non-diatom phytoplankton may outcompete diatoms. In certain instances, this can cause a shift towards the dominance of other phytoplankton such as those responsible for harmful algal blooms (Laruelle et al. 2009) or towards coccolithophorids, which are less efficient at sequestering C (Emerson and Hedges 2008).

1.5. Measuring Diatom Biomass and Productivity

Since diatoms are the dominant producers of particulate SiO_2 in the oceans, biogenic SiO_2 ($bSiO_2$, to distinguish from lithogenic SiO_2) is often used as a proxy for diatom biomass. In order to determine $bSiO_2$ concentrations, water samples are filtered to collect diatom cells, then cells are digested to convert $bSiO_2$ to $Si(OH)_4$, which can be measured using a colorimetric assay (Brzezinski and Nelson 1986). However, in order to quantify fluxes, the rates of processes must be known, and therefore it is more useful to determine a production rate than the standing stock. Normally production rates are measured using live diatom experiments, for which a water sample is collected and incubated for an amount of time in conditions that approximate the characteristics of the environment from where the sample was collected. The simplest way to measure $bSiO_2$ production rates is to determine $bSiO_2$ concentrations at the start and end of the incubation period, and calculate the rate of increase of $bSiO_2$. This method yields a net rate, as both $bSiO_2$ production and dissolution will affect the accumulation of $bSiO_2$ over time. This technique has been used previously in the field to determine net $bSiO_2$ production rates (Pondaven et al. 2007; Adjou et al. 2011; Demarest et al. 2011); however, it suffers from low sensitivity and requires long periods of incubation time and large volumes of water to detect accurate rates of change.

More sensitive methods for detecting of $bSiO_2$ production measure the incorporation of tracers into $bSiO_2$. Nelson and Goering (1977) first used this approach to measure $bSiO_2$ production with the stable isotope ^{30}Si. They enriched their samples with ^{30}Si-labelled $Si(OH)_4$ and measured the incorporation of this isotope which is heavier and far less abundant (3% of naturally occurring Si) than ^{28}Si (92% of naturally occurring Si, Nelson and Goering 1977). The $bSiO_2$ production rate determined using this technique is closer to a gross rate, as the dissolution rates of healthy diatom cells are low (Bidle and Azam 1999). Therefore, the probability of a diatom cell incorporating ^{30}Si and this $^{30}SiO_2$ subsequently dissolving on the time scale of an incubation experiment (usually 1-2 days) is small.

More recently, the radioisotope ^{32}Si has been used as a tracer of $bSiO_2$ production. ^{32}Si is a radioactive isotope, and emits beta radiation as it decays. Low levels of this radiation can be accurately detected, and as a result $bSiO_2$ production rates can be determined when fewer atoms of ^{32}Si are incorporated than unlabeled or ^{30}Si. This technique was first described by Brzezinski and Phillips (1997), and has been used in a number of field studies (Blain et al. 1997; Brzezinski et al. 1998; Allen et al. 2005; Mosseri et al. 2008; Krause et al. 2009, 2011, 2015; Marchetti et al. 2010; Dugdale et al. 2011; Fripiat et al. 2011). Although ^{32}Si was suggested as an ideal tracer in 1977 by Nelson and Goering, there are several challenges in using this isotope. Due to its radioactivity, additional restrictions apply to the use of ^{32}Si, which may prevent its use in the field and on board oceanographic research vessels. Additionally, ^{32}Si is expensive relative to other tracers used in productivity measurements. Furthermore, ^{32}Si is not commercially available, and must be produced within particle colliders and then refined. Consequently, the isotope is difficult to acquire, and not readily available for use in research.

1.6. Higher Resolution Approaches

All of the methods described in the above section require filtration of sample water to concentrate diatom cells. These methods yield a $bSiO_2$ production rate for the whole $bSiO_2$ producing community (a bulk rate). While this is useful, bulk measurements do

not provide information about the contribution of different taxa within the community to the total $bSiO_2$ production rate. In order to better understand the controls on $bSiO_2$ production, it would be useful to determine the roles of different diatom species within the community.

Although all diatoms require Si for growth, there is a large amount of genetic and physiological diversity within the group. The genomes of the first two diatom species to be sequenced are as distant from one another as fish and mammals (Bowler et al. 2008). Physiological parameters also vary; maximum growth rates between species differ by one order of magnitude and the half saturation constant for $Si(OH)_4$, an important parameter for determining susceptibility to $Si(OH)_4$ limitation, varies by two orders of magnitude (Sarthou et al. 2005). Differences in assemblage composition translate into differences in the community uptake or production rates measured in the field (Blain et al. 1997, 2007). Additionally, different diatom species have different nutrient uptake capabilities and requirements, and Poulton et al. (2007) even found different diatoms within the same assemblage to be limited by different nutrients. It is clear that diatom community composition is an important determinant of the total productivity of the assemblage.

The composition of the diatom community also has consequences for the rest of the ecosystem. As grazers are often size selective (Sunda and Hardison 2010), the size of diatom species will affect their consumption and transfer of energy up the food chain. Some diatom species form blooms that are harmful to other organisms, such as a few *Chaetoceros* sp. that have spines that are damaging to fish gills (Albright et al. 1993). Another genus, *Pseudo-nitzschia* sp., can produce the neurotoxin domoic acid, which is harmful to marine mammals, birds and humans (Scholin et al. 2000). Assemblage composition is also an important factor in C export, as different species are exported with different efficiencies (Waite and Nodder 2001; Annett et al. 2009; Smetacek et al. 2012; Twining et al. 2014). Together these factors determine the role of a diatom community within an ecosystem.

Characteristics of diatom species are usually determined and compared through unialgal culture experiments in a laboratory setting. While this is useful for investigating many aspects of diatom physiology, other factors such as grazing and competition that are not represented in culture experiments need to be considered.

In the field, the resolution of bulk methods can be increased by using different pore sizes during filtration in order to separate cells based on their size. As cell size is a major determinant of differences between species such as growth rate (Geider et al. 1986), grazing pressure (Frost 1972), and sinking rate (Waite and Nodder 2001), this is useful for making inferences about the community dynamics. However, the 2-3 size fractions separated this way may still represent a suite of distinct species, limiting understanding of community dynamics.

Within a sample, the abundance of different species can be determined using microscopy. The combination of cell counts with measurements of cell surface area (SA) and volume is useful for estimating the contribution of different species to community biomass. As SA is correlated with $bSiO_2$ per cell (Brzezinski 1985), determining SA together with cell counts can indicate the proportion of $bSiO_2$ present in each species; however, this relationship does not always hold as $bSiO_2$ thickness may be affected by other factors such as light, temperature, and nutrient concentrations (Martin-Jézéquel et al. 2000). Therefore it would be preferable to measure $bSiO_2$ directly for individual cells. Cell numbers from a seawater sample are also limited in that they indicate biomass and not a production rate, and the species that are abundant are not necessarily those that are contributing most to production.

1.7. Use of Microscopic Imaging to Quantify Biogenic Silica Production

In order to quantify $bSiO_2$ production per species, it is possible to combine the microscopy and tracer approaches. As with some bulk methods, a tracer is added and samples are incubated, but at the end of the incubation the incorporation of the tracer into cells is determined by microscopy. If the incorporation of the tracer is known to be

proportional to the incorporation of SiO_2 in the diatom cells, the tracer can be used as a quantitative proxy for SiO_2 incorporation. This allows relative comparisons between species or individuals within a mixed sample, and can be combined with bulk methods so that rates of $bSiO_2$ production can be determined for different cells in a mixed assemblage.

It is possible to use ^{32}Si as an indicator of cell specific $bSiO_2$ production, as beta emissions from the radioactive decay of the isotope can be detected with photographic emulsion. Shipe and Brzezinski (1999) described this method and used it to determine relative amounts of SiO_2 incorporation in individual cells within a *Rhizosolenia* spp. mat. However, this method is logistically challenging. As the decay product of ^{32}Si is ^{32}P, which is a much stronger beta emitter, samples must be stored until any ^{32}P taken up has decayed and ^{32}Si and ^{32}P are in secular equilibrium. This is necessary to ensure that all beta emissions detected are from isotopes that were ^{32}Si at the time of incorporation. Following this, samples must be exposed to photographic emulsion for several months in order to detect enough beta emissions for labelled structures to be clearly visible (Shipe and Brzezinski 1999). Due to these challenges, this technique has not been used in other studies.

More commonly, fluorescent dyes have been used to label $bSiO_2$ as it is produced. Unlike ^{32}Si, the incorporation of a given fluorescent dye may or may not behave similarly to SiO_2 incorporation, and may or may not be a quantitative tracer of $bSiO_2$ production. Most dyes that are used share similar properties that make them useful for imaging SiO_2 incorporation in diatoms: they enter cells quickly, they are non-toxic at the concentrations used, and they accumulate in the acidic silica deposition vesicle (SDV), resulting in their incorporation into SiO_2 as it is produced.

The first commonly used fluorescent dye for imaging SiO_2 deposition in diatoms was rhodamine 123 (R123), which was used by Li et al. (1989) to visualize the cellular location of SiO_2 production. The method was further developed by Brzezinski and Conley (1994) who found that R123 incorporation was linearly related to SiO_2

incorporation, and thus R123 could be used to quantify SiO_2 incorporation. Rhodamine 123 and other rhodamine dyes continue to be used to visualize SiO_2 deposition (Vrieling et al. 1999; Hildebrand et al. 2007; Wang et al. 2009; Kaluzhnaya and Likhoshway 2007; Kucki and Fuhrmann-Lieker 2012). However, R123 has a low incorporation efficiency of 17 million:1Si:R123 (Brzezinski and Conley 1994), making it difficult to image small structures such as girdle bands. Rhodmaine 123 also stains mitochondria, so it is necessary to remove cellular contents in order to visualize labelled SiO_2, so the method cannot be used with live cells (Brzezinski and Conley 1994).

Since 1989, many more fluorescent dyes that label SiO_2 in diatoms have been synthesized, including a suite of oligopropylamine dyes (Annenkov et al. 2010) and a fluorescent dye derived from silk worm cocoons (Kusurkar et al. 2013). However, the most popular dyes for use in diatoms are Lysotracker yellow HCK-123 (HCK-123, Desclés et al., 2008) and 2-(4-pyridyl)-5-((4-(2-dimethylaminoethylaminocarbamoyl)methoxy)-phenyl)oxazole (PDMPO, Lysosensor DND-160, Shimizu et al. 2001). Both dyes are available from Life Technologies (Life Technologies Corporation 2013) and are marketed for their ability to label acidic cellular compartments such as the diatom SDV. However, it is not known whether the dyes bind to SiO_2 within the SDV, or if they are simply trapped in the frustule as it forms.

A key difference between HCK-123 and PDMPO is that both the excitation and emission spectra of PDMPO are pH sensitive (Shimizu et al. 2001). Consequently, it is important that the pH of a sample be controlled when the concentration of PDMPO is determined by fluorometry, and appropriately matched to the standards used. Additionally, for PDMPO quantification by microscopy, microscope slides can be prepared with diatom cells within a buffered mountant that has a consistent pH. Therefore, pH can be controlled so that PDMPO can be accurately quantified, but this effect must be considered.

Both PDMPO and HCK-123 have been used in different SiO_2 producing organisms such as radiolarians (Ogane et al. 2009), sponges (Schroder et al. 2004), and rhizaria

(Nomura et al. 2014), but are more widely used in diatoms. Both dyes can be used to visualize the location of SiO_2 deposition through time and/or in relation to other cellular components (Hazelaar et al. 2005; Mock et al. 2008; Heredia et al. 2008; Vartanian et al. 2009; Tesson et al. 2009; Durkin et al. 2009; Tesson and Hildebrand 2010a; b, 2013). They have also been used to assess the effect of different experimental treatments (Znachor et al. 2011; Durkin et al. 2012, 2013; Hervé et al. 2012; Renzi et al. 2014), and to distinguish between cells that are not physiologically active and those that are actively depositing SiO_2 (Leblanc and Hutchins 2005; Gröger et al. 2008; Richthammer et al. 2011). Hervé et al. (2012) demonstrated that HCK-123 is a quantitative tracer of SiO_2 deposition, and Leblanc and Hutchins (2005) showed the same for PDMPO, but both conclusions are based on experiments with only one species (HCK-123), or two species and a field assemblage (PDMPO).

Although both HCK-123 and PDMPO have been used to visualize SiO_2 deposition in diatoms, HCK-123 has been used only in unialgal culture experiments, and never in mixed field assemblages. In contrast, PDMPO has been employed in several field studies in order to investigate $bSiO_2$ production using fluorescence microscopy (Leblanc and Hutchins 2005; Znachor et al. 2008, 2013; Znachor and Nedoma 2008; Iluz et al. 2009; Ichinomiya et al. 2010; Quéguiner et al. 2011; Durkin et al. 2012). PDMPO has also been used to quantify SiO_2 incorporation at the community scale: in a bulk water sample after filtering and digesting labelled diatom cells (Leblanc and Hutchins 2005; Saxton et al. 2012; Leng et al. 2015). Leblanc and Hutchins (2005) determined an average ratio of Si:PDMPO of 3230 ± 660:1 from their experiments, suggesting that measurements of PDMPO incorporation can be directly converted to SiO_2 incorporation using that ratio. Because PDMPO is more established as a tracer of $bSiO_2$ production in the field than HCK-123, and because the relationship between SiO_2 and PDMPO incorporation has been previously described for PDMPO, I chose to use PDMPO as a tracer of $bSiO_2$ production for my thesis.

1.8. Promise and Problems with the PDMPO Method

Application of the PDMPO method has the potential to increase our understanding of diatom ecology in the field by providing high taxonomic resolution quantification of $bSiO_2$ production. PDMPO can be used as tracer for determining whole community $bSiO_2$ production analogous to ^{32}Si, but more affordably and without radioactivity restrictions. Additionally, PDMPO can be applied to quantify $bSiO_2$ production per cell by microscopy in order to determine the relative contributions of different diatom species within a mixed field assemblage. Although the method of using PDMPO to quantify $bSiO_2$ production was published by Leblanc and Hutchins a decade ago, it has been applied in only one study to investigate whole community $bSiO_2$ production (Saxton et al. 2012), and only a few times to look at species contributions by microscopy (Leblanc and Hutchins 2005; Znachor et al. 2008, 2013; Znachor and Nedoma 2008; Iluz et al. 2009; Ichinomiya et al. 2010; Quéguiner et al. 2011; Durkin et al. 2012).

Despite the many potential advantages of the method, its lack of widespread implementation probably reflects remaining uncertainties about the technique. As the exact mechanism of PDMPO's incorporation into the frustule is unknown, it is possible that the incorporation of SiO_2 and PDMPO may be decoupled under certain environmental conditions. This could invalidate PDMPO as a quantitative tracer of SiO_2 deposition and confound measurements of $bSiO_2$ production based on PDMPO, at least under certain conditions. The mechanisms for uptake of $Si(OH)_4$ and PDMPO into the cell are different: $Si(OH)_4$ uptake occurs actively (Azam et al. 1974), whereas PDMPO diffuses freely into the cell (Life Technologies Corporation 2013) before selectively accumulating in the acidic SDV (Shimizu et al. 2001). Once in the SDV, PDMPO may bind SiO_2 directly or be trapped within the frustule as it forms. The process controlling PDMPO incorporation has important implications for the tracer's utility. If PDMPO were known to directly bind to SiO_2 with a fixed ratio of incorporation, processes that differentially affect PDMPO and SiO_2 incorporation into the SDV would not be expected to affect the final relationship of Si:PDMPO within the frustule. Conversely, if PDMPO is simply trapped as SiO_2 forms in the SDV, factors other than SiO_2 incorporation could affect PDMPO incorporation, confounding its utility as a tracer.

Even if the relationship between Si and PDMPO incorporation can be determined such that fluorometric measurements of PDMPO can be converted to SiO_2 production rates, another source of error may prevent reliable quantification of PDMPO by microscopy. The SiO_2 structures of diatom frustules vary in thickness from 1 µm (e.g. a *Chaetoceros* sp. spine) to 100 µm (e.g. a *Coscinodiscus* sp. frustule). This presents a challenge for fluorescence microscopy, as the plane of focus for the most common widefield microscope objectives used for visualizing diatom cells is less than 10 µm. Thus for thick cells, it is likely that some portion of the frustule bound PDMPO would be outside the plane of focus for most microscope objectives. The extent to which this out of focus fluorescence would be generated or collected by widefield fluorescence microscopy is not presently known. If out of focus fluorescence was captured less effectively than fluorescence from PDMPO within the plane of focus, this would cause under-estimation of PDMPO incorporation, and therefore SiO_2 production, from thicker diatom species. Consequently, comparisons of PDMPO fluorescence between different diatom taxa would be confounded by their cell thickness. In order to ensure that measurements of PDMPO fluorescence by microscopy reflect the amount of PDMPO incorporated, it is necessary to test different microscope configurations, and compare PDMPO microscopy to fluorometry to determine if PDMPO can be reliably quantified by microscopy.

Additionally, the performance of the PDMPO technique has not been well assessed in the field. Leblanc and Hutchins (2005) compared $bSiO_2$ production rates determined by ^{32}Si and PDMPO at one field site, but more comparisons are needed to build confidence in the method.

1.9. Thesis Focus

In this thesis I address several of the uncertainties of the PDMPO technique, as well as implement the method in the field to investigate diatom community dynamics.

Chapter 2 of this thesis presents optimizations for the measurement of PDMPO incorporation in bulk (using fluorometry) and for individual cells by microscopy. In addition, the results of several laboratory experiments are presented that determine how the relationship between SiO_2 and PDMPO incorporation is affected by a) initial PDMPO concentration, b) diatom species and c) cell lysis. From these laboratory experiments I also determined the relationship for conversion of PDMPO incorporation to SiO_2 incorporation which I have used in subsequent field work. Additionally, I present the results of tests that confirm that quantification of PDMPO by microscopy agrees with quantification by fluorometry, and a comparison of PDMPO and ^{32}Si based $bSiO_2$ production rates from monthly sampling in Saanich Inlet.

Chapter 3 presents results from two cruises to the west coast of Vancouver Island (Canada) where I compared $bSiO_2$ production rates determined from incubations of unlabelled, ^{32}Si labelled, and PDMPO labelled samples in order to assess the performance of the PDMPO method in the field. I also compared measurements of PDMPO by microscopy and fluorometry, and determined the contribution of non-diatoms to PDMPO fluorescence. In addition I examined the spatial and temporal distribution of diatom biomass and $bSiO_2$ production, and combined cell count and PDMPO measurements by microscopy to estimate the contribution of different diatom genera to cell numbers and $bSiO_2$ production.

Chapter 4 presents a comparison between the contribution of diatom taxa to cell numbers and to PDMPO fluorescence in Saanich Inlet. I also determined the contributions of different diatom genera to $bSiO_2$ production throughout the different seasons during two years. Additionally I examined the utility of PDMPO as an indicator of specific $bSiO_2$ production rate, and whether this could predict shifts in assemblage composition.

Chapter 5 presents the overall conclusions of this work and suggestions for further optimizations of the PDMPO method. In addition, I discuss potential applications of the technique to investigate diatom community dynamics.

Chapter 2: Improving the Use of PDMPO as a Tracer of Biosilicification in Marine Diatoms

2.1. Introduction

Diatoms are unicellular photoautotrophs that play important roles in marine ecology and biogeochemical cycling. They are the foundation of many marine food webs, and responsible for ~20% of global primary productivity (Nelson et al. 1995; Field et al. 1998). Diatoms often dominate export production and are significant contributors to the biological carbon pump (Alldredge and Gotschalk 1989; Dugdale and Wilkerson 1998; Kemp et al. 2006; Krause et al. 2009). Diatoms differ from other groups of phytoplankton in that they require silicon (Si), which they take up in the form of silicic acid ($Si(OH)_4$, Del Amo and Brzezinski, 1999). Once inside the cell, $Si(OH)_4$ is polymerized within the silicon deposition vesicle (SDV) to form silica ($SiO_2 \bullet nH_2O$, Armbrust 2009, referred to hereafter as SiO_2) that makes up the cell wall, or frustule, composed of two parts. Each time a diatom cell divides it produces two new frustule halves, with one half incorporated into each daughter cell. Therefore, because cell division requires Si for frustule formation, SiO_2 incorporation rates (i.e. SiO_2 production rates) can be used as index of diatom growth and biosilicification.

Silica production by diatoms in seawater can be measured using different methods. The SiO_2 incorporation rate can be determined by quantifying the amount of biogenic SiO_2 in seawater (referred to as $bSiO_2$ to distinguish from lithogenic SiO_2) before and after a period of incubation. This yields a net $bSiO_2$ production rate, as both production and dissolution processes occur during the incubation time (Krause et al. 2010). However, this method has low sensitivity, requiring large volumes of seawater and long incubation periods for the accurate detection of changes in $bSiO_2$. Diatom SiO_2 production rates can also be quantified by measuring the incorporation of the radioactive isotope ^{32}Si (Brzezinski and Phillips 1997). The ^{32}Si method is much more sensitive than measuring changes in $bSiO_2$ concentration; however, it is subject to time-consuming regulatory restrictions that apply to radioactive substances. Measuring the incorporation

rate of fluorescent dyes into $bSiO_2$ is another method for measuring SiO_2 production that has been used recently (Leblanc and Hutchins 2005; Desclés et al. 2008; Znachor and Nedoma 2008; Durkin et al. 2012). The fluorescent dye 2-(4-pyridyl)-5-((4-(2-dimethylaminoethylaminocarbamoyl)methoxy)-phenyl)oxazole (PDMPO, Lysosensor DND-160, Life Technologies) stains SiO_2 as it polymerizes in the SDV of a diatom cell (Shimizu et al. 2001). Like methods that use ^{32}Si, changes in PDMPO labelled SiO_2 can be detected with greater sensitivity than changes in unlabelled SiO_2, but PDMPO does not have the restrictions associated with using radioisotopes, and is also more affordable than ^{32}Si. Despite these advantages, few studies have used PDMPO as a method for determining SiO_2 production rates.

The PDMPO method may not have been widely adopted because there is still uncertainty regarding PDMPO's robustness as a tracer of SiO_2 incorporation. Previous work found a linear relationship between SiO_2 and PDMPO incorporation in diatoms (Leblanc and Hutchins 2005) suggesting that it can be used as a quantitative tracer like ^{32}Si. But unlike ^{32}Si, the mechanism of PDMPO incorporation into the frustule may differ from the incorporation of SiO_2. Uptake of $Si(OH)_4$ at the concentrations found in ocean surface waters is active via $Si(OH)_4$ transporters (Martin-Jézéquel et al. 2000), whereas PDMPO diffuses passively and rapidly into diatom cells (Life Technologies Corporation 2013) where it accumulates within acidic organelles such as the SDV (Shimizu et al. 2001). It is unknown whether PDMPO binds to molecules of SiO_2 within the SDV, or is simply trapped within SiO_2 as the frustule polymerizes.

If the processes that control SiO_2 and PDMPO incorporation into the frustule are different, the incorporation of SiO_2 and PDMPO could become decoupled, in which case PDMPO would not be useful as a tracer of SiO_2 incorporation in diatoms. Decoupling of SiO_2 and PDMPO incorporation could occur due to differential uptake of $Si(OH)_4$ and PDMPO into the cell, and consequently into the SDV. This could result from several conditions, such as the extracellular PDMPO concentration, and the taxonomic composition of the diatom assemblage present. Different extracellular concentrations of PDMPO would be expected to change the concentration of PDMPO within the diatom

cell without affecting $Si(OH)_4$ uptake. Consequently, higher extracellular concentrations of PDMPO would result in increased accumulation of PDMPO inside the cell, the SDV, and the frustule, without a concomitant accumulation of SiO_2.

Another factor that could affect the relationship between SiO_2 and PDMPO incorporation is which diatom taxa are responsible for SiO_2 production within the assemblage. Differences in Si metabolism between diatom species could affect $Si(OH)_4$ uptake without an effect on PDMPO uptake. Silicon metabolism varies widely between different diatoms; the half saturation constant for $Si(OH)_4$ (K_{Si}), an indicator of the affinity of $Si(OH)_4$ transporters for $Si(OH)_4$, varies by more than an order of magnitude between species (Sarthou et al. 2005). Diatom species could also have differential PDMPO uptake unrelated to differences in Si metabolism. Not all PDMPO that enters the diatom cell ends up in the SDV; some is stored within other parts of the cell and is likely unrelated to Si metabolism. For example, larger diatom cells could have lower cellular Si:PDMPO than small cells, as they would have a larger amount of PDMPO stored within the cytoplasm or vacuole due to their larger volume (Leblanc and Hutchins 2005). However, Leblanc and Hutchins (2005) found that when cells were lysed (i.e. internal contents removed) there were no differences in the ratio of Si:PDMPO incorporation between the *Chaetoceros* sp., *Thalassiosira* sp., and a mixed assemblage that they tested. They also suggested that a ratio of 3230 ± 660:1 Si:PDMPO can be used to convert measurements of PDMPO to SiO_2 incorporation. To further improve confidence in PDMPO as a tracer of SiO_2 production, it is critical to test the effect of extracellular PDMPO concentration, diatom species, and cell lysis on the Si:PDMPO relationship of incorporation. In addition, the relationship of Si:PDMPO incorporation must be investigated in more diatom species, to improve conversion of PDMPO measurements to SiO_2 .

To date, only two studies have used PDMPO in the field to determine SiO_2 production rates for the total diatom assemblage (Leblanc and Hutchins 2005; Saxton et al. 2012), and only one compared these rates to those determined with ^{32}Si (Leblanc and Hutchins 2005). Additional factors may affect measurements of PDMPO incorporation in field

samples that are not present in laboratory cultures, such as fluorescence by non-diatom cells. To ensure the reliability of the PDMPO method as a tracer of SiO_2 production in natural assemblages, more comparisons of PDMPO and $^{32}SiO_2$ incorporation rates are needed for natural diatom assemblages.

The incorporation of PDMPO into diatom frustules can be quantified by fluorometry. For these measurements, the total amount of PDMPO incorporated into all diatom cells filtered from a sample is determined using a fluorometer. This measurement reflects the PDMPO incorporated by the entire assemblage of diatoms in the sample, but does not distinguish between the contributions of different diatom taxa to the total. To determine the fluorescence from individual cells and species, PDMPO fluorescence can be detected by fluorescence microscopy. This would present a significant advantage over bulk measurements, but previous work has not tested whether measurements of PDMPO using microscopy agree with other methods for determining SiO_2 incorporation.

Diatom SiO_2 structures can be as thin as 1 µm (eg. a *Chaetoceros* sp. spine) or thicker than 100 µm (e.g. a *Coscinodiscus* sp. frustule), presenting a challenge for quantification using widefield fluorescence microscopy. Microscope objectives have fixed depths of focus (determined by the numerical aperture, NA, Figure 2.1), so PDMPO fluorescence outside the plane of focus may not be captured. This would cause the fluorescence of large or thick SiO_2 structures to be under-estimated, and confound the comparison of fluorescence signals from diatom species of different sizes measured by microscopy. Measurements made using microscope objectives with lower NAs have thicker planes of focus, and are expected to capture fluorescence from a greater range of diatom sizes (Figure 2.1A). But there is a trade-off between depth of focus and efficiency of light capture: higher NAs detect more angles of emitted fluorescence but have a shorter depth of focus (Figure 2.1B). As a result, different microscope objectives should be assessed to determine the optimal balance between light capture and depth of focus when quantifying PDMPO fluorescence in diatom cells.

The limited depth of focus inherent in widefield fluorescence microscopy can be overcome by using optical sectioning methods, such as two photon (2P) microscopy (Figure 2.1C). A 2P microscope images fluorescence in precisely focused planes at regular intervals throughout the depth of the cell. Therefore, the depth from which fluorescence is detected by the microscope can be adjusted to ensure that fluorescence from all labelled SiO_2 structures is captured. These measurements should be less affected by differences in cell thickness between diatom species than measurements by widefield microscopy, but they are more time consuming. Consequently, measuring PDMPO fluorescence in diatom cells by widefield microscopy would be preferred, but comparisons with 2P are needed to ensure that widefield measurements are not confounded by differences in diatom thickness and morphology.

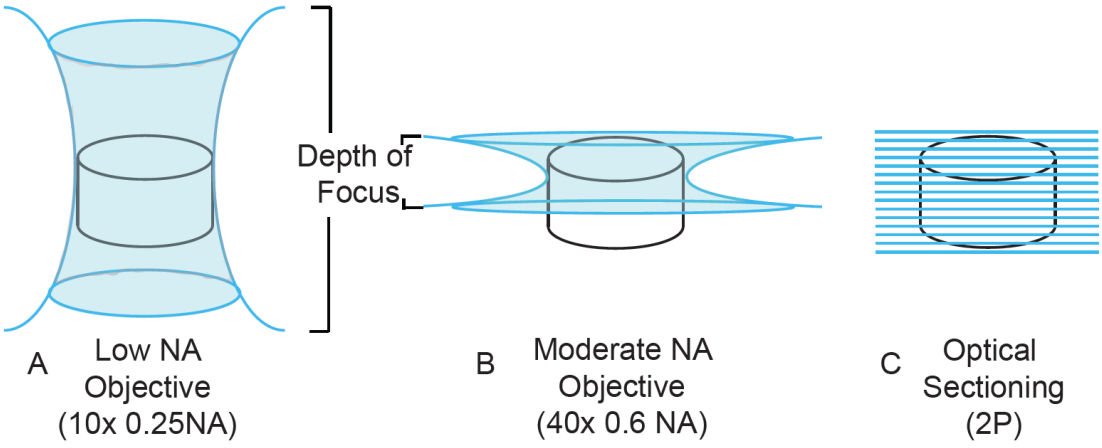

Figure 2.1: Diagram showing fluorescence captured by different microscope configurations. Black outline indicates a hypothetical diatom cell. Blue shading indicates the regions where fluorescence is excited and also detected. Diagrams shown for A) a widefield fluorescence microscope with low numerical objective, B) a widefield fluorescence microscope with moderate numerical aperture objective, and C) an optical sectioning method (2 photon microscopy). The specific configurations used in this study are indicated in brackets.

Once a suitable microscope configuration for quantifying PDMPO fluorescence has been determined, measurements of PDMPO fluorescence by microscopy and fluorometry should be compared to validate measurements of PDMPO by microscopy. Previous studies have quantified relative PDMPO fluorescence (i.e. the relative intensity of cells

within the same slide, such as the percentage from different species; Quéguiner et al. 2011, Durkin et al. 2012) as well as absolute PDMPO fluorescence (i.e., a numerical value for fluorescence intensity that can be compared between different samples, Znachor and Nedoma 2008, 2009; Durkin et al. 2012; Znachor et al. 2013) by microscopy in field assemblages. Even if different diatom species can be reliably quantified within the same sample, comparisons between different samples could be confounded by other factors such as minor differences in sample (slide) preparation, or storage time prior to analysis. If the methods do agree, this would suggest that measurements of PDMPO fluorescence by microscopy are reliable, and can be used to compare $bSiO_2$ production within and between samples in the field.

The overall goal of this study is to improve the quantification of diatom SiO_2 incorporation using the PDMPO tracer. The specific objectives addressed here are to:

1. Determine how the relationship between SiO_2 and PDMPO bulk incorporation is affected by
   1a. Extracellular PDMPO concentrations
   1b. Different diatom species
   1c. Lysis of diatom cells

2. Optimize the quantification of PDMPO using epifluorescence microscopy by investigating:
   2a. The effect of different microscope objectives
   2b. Relative PDMPO fluorescence within the same microscope slide
   2c. Absolute PDMPO fluorescence between different microscope slides

3. Test the improved method in a field scenario by comparing:
   3a. SiO_2 incorporation rates measured using bulk PDMPO and ^{32}Si methods
   3b. The contribution of different diatom taxa to cell numbers and PDMPO fluorescence microscopy

2.2. Materials and Procedures

2.2.1. Relationship Between PDMPO and SiO_2 Incorporation

2.2.1.a Effect of Extracellular PDMPO Concentration

Thalassiosira pseudonana was obtained from the National Center for Marine Algae and Microbiota (CCMP 1014), and maintained at 18°C in Enriched Seawater Artificial Water (ESAW) media (Berges et al. 2001), under continuous irradiance of optimal intensity (180 µmol photons m^2 s^{-1}, see Appendix A). Cultures were grown in triplicate and acclimated to growth conditions for ten generations prior to starting experiments. The effect of different concentrations of PDMPO on the relationship between SiO_2 and PDMPO incorporation in diatoms was determined by growing *Thalassiosira pseudonana* with 0 (control), 100, 125, 250, 500, 750 and 1000 nmol L^{-1} PDMPO for 24 hours.

Diatom cell numbers were determined using a Z series Coulter counter (Beckman Coulter) and growth rates were calculated as the difference between the natural logarithm of cell counts at the start and end of the 24 hour incubation with PDMPO. Therefore, a growth rate of 0.69 d^{-1} corresponds to one cell division per day. Samples (35 mL) for the measurement of SiO_2 and particulate PDMPO (pPDMPO) concentration were filtered onto 0.6 µm polycarbonate (PC) filters. These samples were digested using the hot NaOH method and the resulting $Si(OH)_4$ concentration was determined using the silicomolybdate assay with modified reagent blank (Brzezinski and Nelson 1986, 1989). Incorporated pPDMPO was determined from an aliquot of the same digest with a TD-700 fluorometer (ammonium filter set: 310-390 nm excitation, 410-600 nm emission). Sample PDMPO concentration was determined by comparing sample fluorescence with a standard curve over the 0 – 250 nmol L^{-1} range of PDMPO concentrations in the same NaOH-HCl matrix as samples (R^2 = 0.998). Samples for the determination of initial $bSiO_2$ concentration (at the time of PDMPO addition) were also collected and analyzed. The concentration of SiO_2 present initially was subtracted from the concentration of SiO_2 after 24 hours, to yield the amount of SiO_2 produced since the addition of PDMPO ($\Delta[SiO_2]$).

Differences between treatments (different PDMPO concentrations) were determined using ANOVA and Tukey HSD statistical tests in R with R studio (R Studio 2012; R Core Team 2013).

2.2.1.b Effect of Diatom Species

To assess the effect of diatom species on the relationship between SiO_2 and PDMPO incorporation, three temperate diatom species (*Asterionellopsis glacialis*, CCMP 139; *Skeletonema dohrnii*, CCMP 785; and *Chaetoceros contortus*, CCMP 1578) were used in addition to *T. pseudonana* (Table 2.1), and were grown using the same culture methods as section 2.2.1a. Species were chosen to match the dominant taxa present in Saanich Inlet, the location of marine tests of the method. Cultures were incubated for 48 hours with 125 nmol L^{-1} PDMPO, as this concentration was used previously to determine the relationship between SiO_2 and PDMPO incorporation by Leblanc and Hutchins (2005) and this concentration did not negatively affect diatom growth (see section 2.3.1a). Samples for determining SiO_2 and pPDMPO concentration were collected at 12, 18, 24, 36, and 48 hours, during exponential growth. Samples for determining SiO_2 concentrations were also collected immediately prior to PDMPO addition, and all SiO_2 samples were collected and analyzed as described above (section 2.2.1a). As in section 2.2.1a, SiO_2 concentrations presented here are for SiO_2 produced since the time of PDMPO addition, $\Delta[SiO_2]$. Therefore, the slope of the line between pPDMPO and $\Delta[SiO_2]$ reflects the ratio of Si:PDMPO incorporated into the frustule during the experiment.

Table 2.1: Growth information of the diatom species used to determine the relationship between PDMPO and $\Delta[SiO_2]$. Irradiances levels listed in the table are the optimal for growth (see Appendix A for growth vs. irradiance curves).

Species	Strain	Irradiance (µmol photons m^{-2} s^{-1})	Growth Rate (day^{-1})		
			Mean	SE	n
Asterionellopsis glacialis	CCMP 139	150	1.16	0.06	3
Chaetoceros contortus	CCMP 1578	100	1.08	0.02	3
Skeletonema dohrnii	CCMP 785	100	1.34	0.02	3
Thalassiosira pseudonana	CCMP 1014	180	1.79	0.01	4

For PDMPO measurements, duplicate samples were filtered and collected, with one filter rinsed with filtered seawater (FSW) in order to keep cells intact, and the other one immersed in 10% HCl for two minutes and then rinsed with deionized water to lyse cells and remove intracellular contents (Leblanc and Hutchins 2005). Filters were dried at 56°C for several days and stored dry until further analysis. This storage method preserves PDMPO fluorescence for at least one month while freezing samples has been found to decrease fluorescence by 40 ± 3% (Mean ± SE, Appendix B). Sample analysis procedures differed from section 2.2.1a as protocols had been further optimized. The hot NaOH digestion was found to decrease PDMPO fluorescence by 23 ± 3% (Appendix C) so pPDMPO samples were collected separately from SiO_2 samples and were instead digested with 0.5M HF for 3 hours (McNair and Brzezinski pers. comm.). This yielded pPDMPO concentrations 28 ± 3% higher than those digested with NaOH (Appendix D). Accordingly, sample fluorescence was compared to that of PDMPO standards from 0 – 100 nmol L^{-1} prepared in the HF-boric acid matrix ($R^2 = 0.997$). Concentrations of pPDMPO were determined using a Turner Trilogy Fluorometer (350/80 nm excitation 410 – 600 nm emission, crude oil module) which had better sensitivity than the Turner TD-700 model under acidic conditions.

2.2.1.c Effect of Diatom Cell Lysis

The effect of cell lysis on the relationship between SiO_2 and PDMPO incorporation was determined for the culture experiments described in section 2.2.1b. The percentage of pPDMPO lost due to rinsing with HCl was calculated as

$$\%pPDMPO\ loss = [(pPDMPO_{FSW} - pPDMPO_{HCl}) / pPDMPO_{FSW}] * 100$$

Equation 1

where $pPDMPO_{FSW}$ and $pPDMPO_{HCl}$ represent the pPDMPO concentration measured for paired samples rinsed with FSW and HCl respectively. Cell volumes were also calculated for the different species according to the geometric formulas of Sun and Liu (2003) to assess whether intracellular PDMPO loss correlated with diatom cell volume.

The relationship for conversion of pPDMPO to $\Delta[SiO_2]$ was determined for both lysed and unlysed cells. The relationship between pPDMPO and $\Delta[SiO_2]$ was modelled in R with R Studio (R Studio 2012; R Core Team 2013; Appendix E).

2.2.2. Quantification of PDMPO Fluorescence by Microscopy

2.2.2.a Effect of Microscope Objective

To test whether microscope objective depth of focus (proportional to NA) affected quantification of differently sized diatom species, an artificial mixed assemblage was created (Figure 2.2). Two diatom species were chosen that represented different diatom sizes: *Coscinodiscus wailesii* (CCMP 2513, ~100 µm thick) and *Pseudo-nitzschia* sp. (isolated from Strait of Georgia, <10 µm thick). These species were cultured separately under continuous illumination of 100 µmol photons m^{-2} s^{-1} with 125 nmol L^{-1} PDMPO. Due to the slow growth rate of *C. wailesii*, this species was cultured with PDMPO for 72 hours, to increase the proportion of PDMPO labelled cells. For *Pseudo-nitzschia* sp., a 24 hour incubation was sufficient to stain cells. At the end of both incubations, samples were collected for measurements of PDMPO using fluorometry and microscopy.

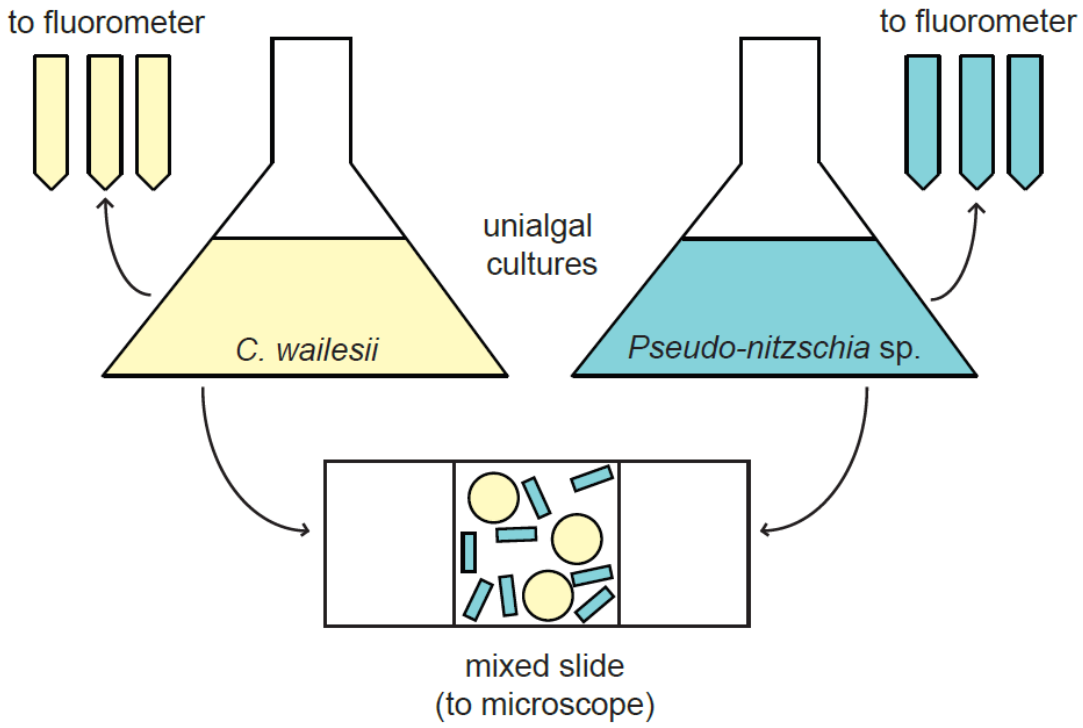

Figure 2.2: Experimental design for comparing PDMPO fluorescence measured using a microscope and a fluorometer described in section 2.2.2a and b. Cultures of a thick diatom (*Coscinodiscus wailesii*, ~100 µm thick, yellow) and a thin (*Pseudo-nitzschia* sp. <10 µm thick, teal) were labeled with PDMPO, and samples removed for determination of PDMPO by fluorometry. In addition, subsamples from each culture were mixed together in known proportions and an aliquot placed on a microscope slide, for quantification of PDMPO by microscopy.

Microscope slides were prepared with a mixture of both species. Homogenous subsamples of each culture were mixed together in known proportions and filtered onto a 0.6 µm PC filter. Cells were then freeze-transferred from the filter to a microscope slide as described in Hewes and Holm-Hansen (1983) and as modified by Franck and Brzezinski (pers. comm.). In short, a 15 µL droplet of deionized water was placed on a new microscope slide, and the filter was placed face down so that diatom cells were within the water droplet. The reverse of the slide was frozen, and the filter carefully peeled off. This procedure transferred cells effectively for a wide range of diatom sizes (Appendix F). Unlike the black filter protocol of Leblanc and Hutchins (2005), chlorophyll *a* fluorescence was not well preserved with the freeze-transfer technique; however, the freeze transfer method was preferred as freeze transferred cells could be

readily observed using brightfield illumination. Slides were dried at ambient temperature and then coverslipped using ProLong Gold mountant (Life Technologies Inc.). Slides were stored frozen until analysis.

To determine whether widefield measurements of PDMPO fluorescence from diatom cells of different thickness could be quantified reliably using widefield microscopy, measurements of diatom cells by widefield microscopy were compared with 2P measurements. A 2P microscope with 20x (0.95 NA) water immersion objective was coupled with a pulsed laser excitation light source (coherent MIRA 900) at 780nm. This excitation wavelength was chosen out of convenience, and because PDMPO has a high absorption cross section in this range, causing efficient 2P excitation of PDMPO. Although it is possible that a different wavelength would be superior for 2P PDMPO excitation, imaging was not light limited under these conditions.

Diatom cells were located on the 2P microscope, and then a stack of images throughout the cell depth was captured. Each image within a stack was 2 µm apart, and the vertical position of the first and last image was adjusted so that they were outside any part of the cell and had no detectable fluorescence. This ensured that the entire cell depth was captured. Images within the same stack were summed to generate a single image representing all fluorescence captured throughout the depth of the cell.

Next, cells were imaged using an Olympus IX-70 widefield microscope with 10x (0.25 NA) and 40x (0.6 NA) objectives. An X-cite 120 PC EXFO light source was used for excitation, and DAPI excitation (377/50 nm) and custom emission (510/140 nm) filters were used to capture PDMPO fluorescence. Images were captured using a 12-bit Retiga QImaging camera connected to a computer with µManager for ImageJ software (Edelstein et al. 2010; Rasband 2012).

Each time diatom cells were imaged, calibration images were also captured to correct for differences in excitation light intensity and unevenness of illumination across the FOV. A yellow fluorescent slide (1.5 mm thick, Chroma Technology Corp) was used for

calibration. In a comparison with fluorescein solutions used by previous authors (Model and Burkhardt 2001; Znachor and Nedoma 2008; the yellow Chroma slide corrected for unevenness in illumination similarly (Appendix G) but was preferred for its higher fluorescence intensity (~ 8 times) and the convenience of using a solid standard. Ten fields of view (FOVs) of the calibration slide were imaged to account for slight differences in fluorescence within the slide. These 10 FOV's were then averaged to generate the calibration image (Figure 2.3A).

Then the same diatom cells that were imaged with the 2P microscope were located on the widefield fluorescence microscope and imaged using both the 10x (0.25 NA) and 40x (0.6 NA) objectives. Once a cell was located, focus was adjusted manually. Exposure times were adjusted to be as long as possible without saturating pixels. Saturating pixels occur when the fluorescence intensity equals or exceeds the maximum intensity detectable by the camera (for a 12-bit camera, 4096). Over-saturated pixels have intensities greater than this maximum, but are instead measured as the maximum value, causing under-estimation of the actual fluorescence intensity. Exposure times were adjusted so that the brightest pixels were near this limit, to maximize detection of faintly labelled structures. Once the optimal exposure time had been determined, images were captured (Figure 2.3B).

Images were then analyzed to measure fluorescence from each diatom particle. ImageJ was used for all image analysis (Rasband 2010). First, the original image was normalized by the calibration image: for each pixel within the original image, the intensity was divided by the intensity of the pixel at the same location from the calibration image. This corrects for unevenness of illumination at different locations within the FOV and differences in excitation light intensity between different days of image collection (Figure 2.3C, Appendix G). Next, the background fluorescence was measured. Background occurs due to stray light and camera noise during imaging, and was low for the images collected (13 ± 6 and 9 ± 5 with 10x and 40x objectives respectively) relative to the detectable range (0-4096). Background was measured at five locations per FOV where no diatom cells were found, and approximately at each corner and the center of the FOV

(e.g. red boxes, Figure 2.3C). The average fluorescence per pixel for the five background regions was then subtracted from the image (Figure 2.3D). Following this, the image was duplicated to create a binary mask for particle analysis (Figure 2.3E). A binary mask was created by manually adjusting the threshold for detection of fluorescence. This created an image where fluorescent diatom cells were indicated in black and empty areas of the FOV in white. Thresholds were set as low as possible while excluding fluorescence not from diatom cells. If necessary, fluorescence was excluded if detected from mountant imperfections, or pixels where the two species overlapped (shown in red, Figure 2.3E). Next, automated particle analysis was conducted to measure the fluorescence of each particle. By using the binary mask to determine which pixels contained cells, the fluorescence of each cell in the calibrated, background subtracted image was measured. A drawing of particles analyzed was automatically produced (Figure 2.3F) so that fluorescence measurements could be assigned to each diatom cell. Finally, measured fluorescence intensities were normalized (divided) by exposure times (Znachor and Nedoma 2008) to account for differences in exposure time between images.

To determine whether the relative fluorescence for the two diatom species from 2P microscopy agreed with widefield measurements, fluorescence for each diatom cell using the 10x or 40x objective was divided by the fluorescence intensity of the same cell measured on the 2P microscope. Pairing measurements of the same cell for the different methods served to remove variability between individual cells to provide a more robust comparison between methods. Fluorescence measurements for the two species were compared in R (R Core Team 2013), and Wilcoxon rank sum test was used to determine significance as variance between groups was unequal. To distinguish measurements of PDMPO fluorescence by microscopy from those made by fluorometry, measurements by microscopy have been designated iPDMPO.

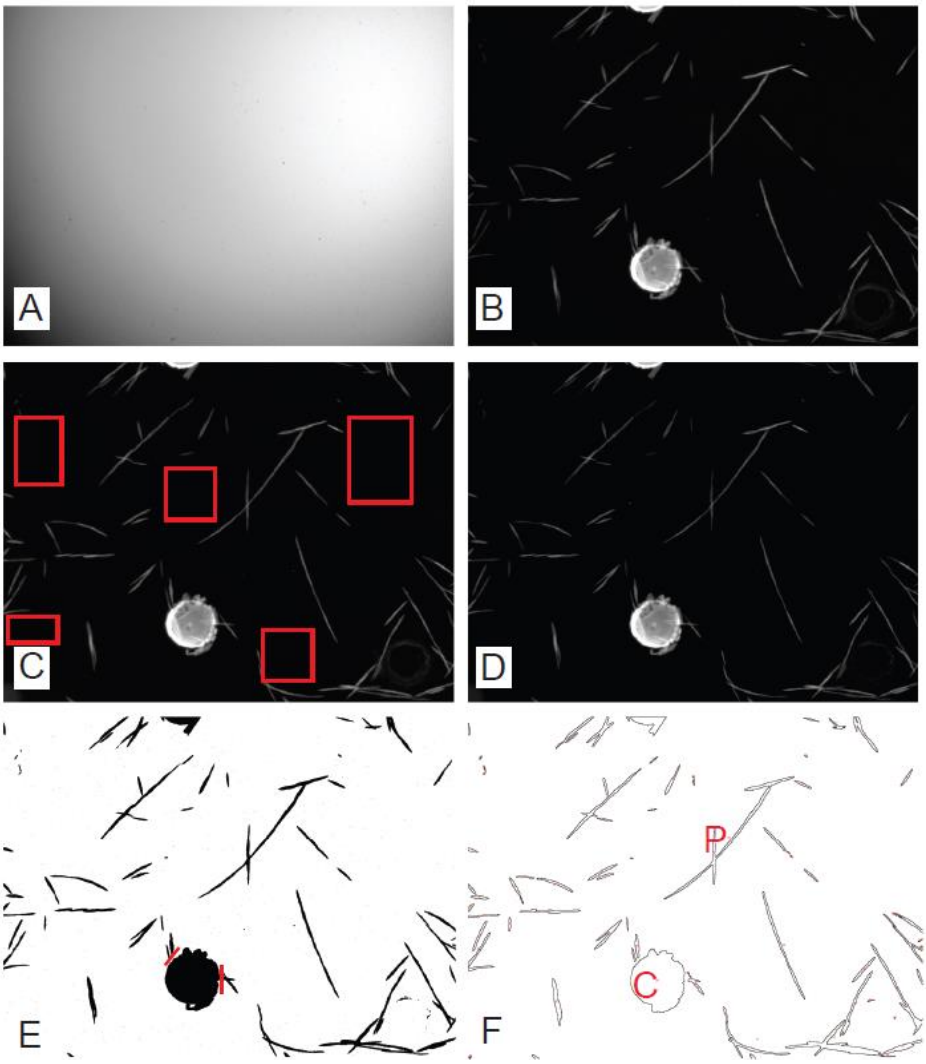

Figure 2.3: Example of images produced during fluorescence quantification from diatom cells by microscopy. A) A calibration slide was imaged to correct for differences in excitation light intensity between different times when slides were imaged and unevenness across the field of view. B) An image of a sample with diatom cells was captured. C) The sample image intensities were divided by the calibration image so that the intensity of each pixel in B was normalized by the intensity of each pixel in the same location from A. Also, background was measured in regions indicated by red boxes. D) Average background per pixel was subtracted from the entire FOV. E) A binary image was created to identify all particles. Pixels overlapping between the two species were manually excluded (red). F) A drawing of numbered particles was automatically generated during particle analysis so that measured fluorescence intensities could be matched to their respective particles. For example, one *C. wailesii* cell (C) and *Pseudo-nitzschia* sp. chain (P) are indicated.

2.2.2.b Testing Relative PDMPO Quantification

Measurements of PDMPO fluorescence obtained using microscopy and fluorometry were compared to determine the degree of agreement between the two methods. For the incubation experiment described previously (section 2.2.2a, Figure 2.2) samples for determination of PDMPO incorporation were collected from the separate incubations of *C. wailesii* and *Pseudo-nitzschia* sp. These samples were rinsed with HCl during filtration, and pPDMPO concentrations determined as described above (section 2.2.1b). Next, the same mixed microscope slide described above (section 2.2.2a) was imaged, but in this case the entire slide was imaged and the total fluorescence per diatom species was determined for each FOV. Then FOV's were randomly assigned to 3 pseudo-replicates, and the percentage fluorescence from each species averaged between pseudo-replicates. For this comparison, fluorescence per species was quantified within the same slide, and expressed as a proportion of the total (relative fluorescence). This approximates a field scenario in which PDMPO would be used to determine the contribution of different taxa to the SiO_2 production of the assemblage. Additionally, this test represents the most conservative test of quantification of PDMPO microscopy, as factors that may confound measurements between different slides (e.g. storage time, preparation conditions, mountant thickness, etc.) would not affect these relative measurements within the same slide.

2.2.2.c Testing Absolute PDMPO Quantification

In addition to relative PDMPO quantification within a microscope slide, measurements of absolute PDMPO fluorescence (fluorescence intensities quantified from different slides) measured by microscopy were compared to bulk measurements of $\Delta[SiO_2]$. Incubation experiments described in section 2.2.1b were subsampled to prepare microscope slides for analysis as described in section 2.2.2a, except that Immu-mount mountant was used instead of ProLong Gold. Slides from each one of the triplicate cultures at 12, 24 and 48 hours of incubation were analyzed for each of the four species. Particle analysis was conducted as described in section 2.2.2a and PDMPO fluorescence per mL was calculated as:

$$iPDMPO = \frac{Total}{\#\ FOVs} \times \frac{AFOV}{Afilt} \times \frac{1}{Vfilt}$$

Equation 2

where iPDMPO is the PDMPO fluorescence (mL^{-1}), Total is the sum of PDMPO fluorescence measured in all FOVs, # FOVs is the total number of FOVs analyzed, AFOV is the area of the FOV (mm^2), Afilt is the area of the filter used to prepare the slide (mm^2, in this case 491 mm^2 for the 25 mm diameter filter) and Vfilt is the volume of culture filtered to prepare the slide (mL). Finally, iPDMPO was modelled as a function of $\Delta[SiO_2]$ incorporation as in section 2.2.1b.

2.2.3. Assessing the Performance of the PDMPO Technique in the Field

To test the PDMPO method with natural assemblages, measurements of SiO_2 incorporation using PDMPO and ^{32}Si were compared at a marine location. Oceanographic cruises to Saanich Inlet (location 123.30 W, 48.36 N) on board the RV Strickland were conducted once a month from February to December during 2013. Seawater samples were collected with 12 L Go Flo bottles from the depth of the chlorophyll *a* maximum determined with an *in vivo* fluorescence sensor attached to a conductivity temperature depth CTD package, and kept cool and in the dark until return to shore. Diatom cell numbers and iPDMPO results are presented here only for March 2013, the month of the spring bloom with highest SiO_2 incorporation rates. The results from analysis of all Saanich Inlet microscope slides will be presented in Chapter 4 of this thesis.

Triplicate incubation experiments were conducted for 24 hours in a flow-through acrylic tank exposed to natural irradiance, supplied with water of surface seawater temperature, and screened with blue photographic film (Lee Filters 202 Half C. T. Blue) to simulate the intensity and wavelengths at the depth corresponding to 50% surface incident irradiance. The depth of the chl *a* maximum was less than 10 m in all months

with one exception (May 2013 depth of 20 m, Table 4.1). The irradiance at the chl *a* max varied considerably, and ranged from 2-100 % of surface PAR averaging 52%.

For pPDMPO concentration measurements, seawater samples (400 mL) were incubated with 125 nmol L^{-1} PDMPO in acid cleaned polycarbonate bottles for 24 hours. At the end of the incubation period, samples were filtered onto 0.6 µm PC filters, and filters were rinsed with HCl, and stored dry as described in section 2.2.1b. Samples were analyzed following digestion with HF and pPDMPO concentration determined as described in section 2.2.1b. Then pPDMPO concentrations were converted to $\Delta[SiO_2]$ using the Si:PDMPO ratio determined from culture experiments in section (2.3.1c) and also the ratio of 3230 ± 660:1 Si:PDMPO from Leblanc and Hutchins (2005). As incubations were conducted for 24 hours, the $\Delta[SiO_2]$ calculated is equivalent to the daily rate of $bSiO_2$ incorporation (denoted ρ_{PDMPO}, units of µmol SiO_2 L^{-1} d^{-1}).

Separate incubations were also conducted using ^{32}Si as a tracer of SiO_2 incorporation. Samples (300 mL) were spiked with to a final activity of 22.2 kBq (0.01 µCi) $^{32}Si(OH)_4$, and after 24 hours samples were filtered onto 0.6 µm PC filters. Next, filters were placed on nylon discs, allowed to dry at room temperature, and covered with Mylar film. Upon reaching secular equilibrium (~120 days), incorporation of ^{32}Si was determined by gas-flow proportional counting (Krause et al. 2011) with a multicounter system for low-level beta radiation (Risø GM-25-5A, DTU Nutech). Incorporation rates were calculated from ^{32}Si measurements as described in Brzezinski and Phillips (1997). Rates of $bSiO_2$ production determined using ^{32}Si are denoted ρ_{GROSS}.

Subsamples from PDMPO incubation bottles were collected to prepare slides for quantification of PDMPO by microscopy. Prior to filtration, cell density was assessed in order to determine the optimal filtration volume for slide preparation (Franck and Brzezinski pers. comm.). The optimal filtration volumes were such that cell density was maximized, while overlap between cells was minimized. Filtered cells were transferred to microscope slides by freeze transfer (section 2.2.2a). Samples were imaged using a 10x (0.25 NA) microscope objective and then the fluorescence intensity per cell was

determined by particle analysis (section 2.2.2a). If cells of different taxa overlapped, either the overlapping cells were excluded from the analysis, or the overlapping pixels were manually excluded. In addition to PDMPO fluorescence images, brightfield images were captured for each FOV to aid in species identification. Although 30 FOVs were imaged per slide, not all were analyzed as fluorescence was reliably quantified from fewer FOVs based on the following criteria. Fields of view were randomly selected for analysis, and the cumulative average and standard deviation of total fluorescence per diatom genus was calculated. Once the standard deviation was less than 15% of the cumulative average, a genus was considered adequately quantified. More FOVs were analyzed until the genera most important for PDMPO fluorescence (>10% of the total diatom fluorescence) were adequately quantified in this manner. Then the percentage contribution of the different genera to community PDMPO incorporation was calculated.

Samples were also collected for the enumeration and identification of phytoplankton. These samples (125 mL) were preserved in amber glass bottles with acidic Lugol's Iodine until analysis. In the laboratory, samples (50 mL) were settled for 24 hours in settling chambers, and then counted on an inverted Olympus IX-71 as per Utermöhl (1958).

2.3. Assessment

2.3.1. Relationship Between PDMPO and SiO_2 Incorporation

2.3.1.a Effect of Extracellular PDMPO Concentration

High concentrations of PDMPO (750 and 1000 nmol L^{-1}) significantly reduced *T. pseudonana* growth rates relative to the 0 nmol L^{-1} control (Figure 2.4A, $p < 0.005$ and $p < 0.0001$ respectively). The $\Delta[SiO_2]$ was significantly lower in the 1000 nmol L^{-1} and the 125 nmol L^{-1} treatment than in the control ($p < 0.01$, $p < 0.03$ respectively), though overall there did not seem to be a clear relationship of $\Delta[SiO_2]$ with PDMPO concentration (Figure 2.4B). In the 100, 125 and 250 nmol L^{-1} treatments, $\Delta[SiO_2]$ unexpectedly appeared reduced relative to the control, although the growth rates of these treatments

were not. It is unclear why these treatments could have reduced SiO_2 per cell during these experiments, as all cultures were acclimated to conditions for ten generations prior to the start of experiments. These treatments were started from the same initial culture flask, and separately from the 750, 500 and 1000 nmol L^{-1} treatments. Therefore, it is possible that the apparent reduction in $\Delta[SiO_2]$ for the 100 - 250 nmol L^{-1} treatments could be due to erroneous over-estimation of the initial concentration of SiO_2 in the parent culture.

The concentration of pPDMPO after 24 hours was higher in treatments with higher extracellular PDMPO concentrations (Figure 2.4C). The pPDMPO concentration increased with extracellular PDMPO concentration until 500 nmol L^{-1}. A plateau was reached at 750 nmol L^{-1}, perhaps due to the decreased growth rates at this concentration and at 1000 nmol L^{-1}. When all treatments are included, an average of 3.9 ± 0.5 % of the PDMPO added was incorporated into cells, and when treatments with reduced growth rate (750 and 1000 nmol L^{-1}) were excluded 7.0 ± 0.6% of PDMPO added was incorporated.

When $\Delta[SiO_2]$ was divided by pPDMPO to yield the ratio of Si:PDMPO of incorporation during the 24 hour incubation, the ratio decreased when more PDMPO was added (Figure 2.4D), driven by the increased incorporation of PDMPO at higher PDMPO concentrations.

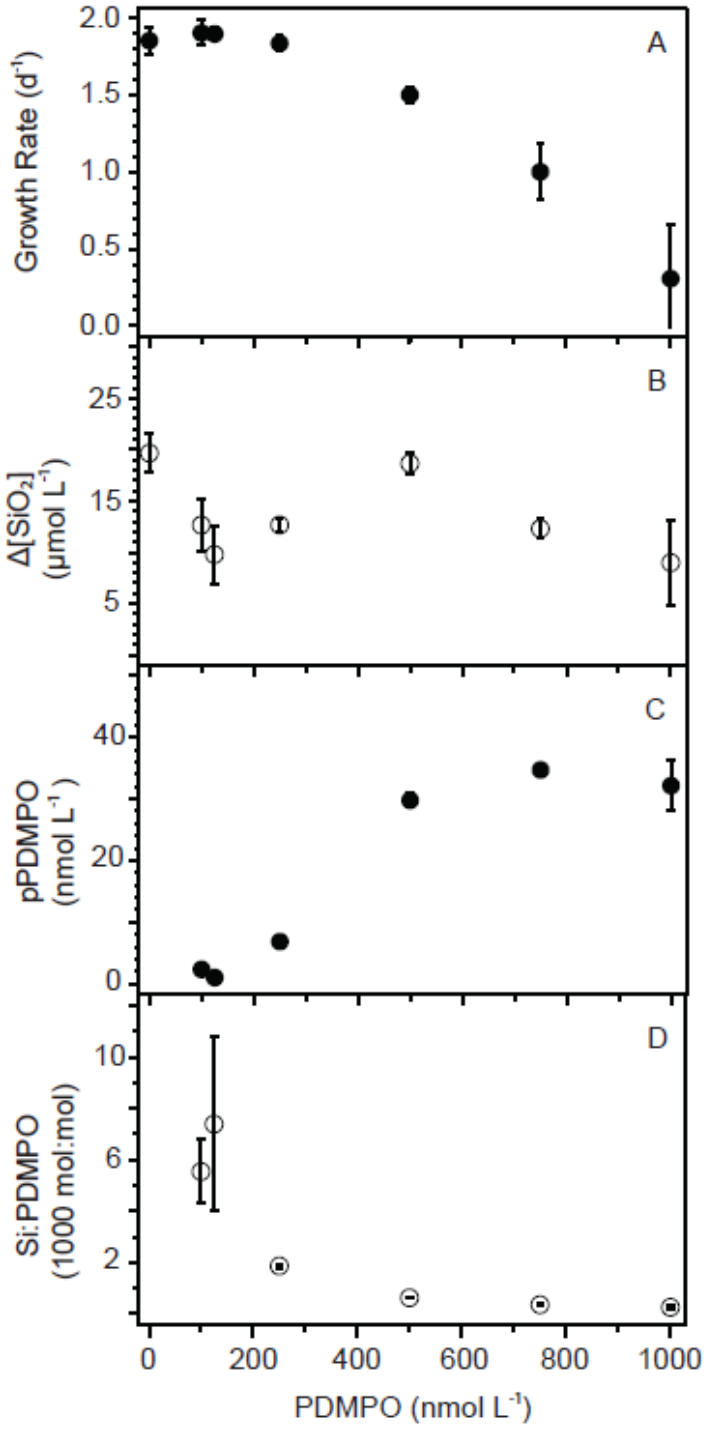

Figure 2.4: Effect of extracellular PDMPO concentration on A) growth rate B) $\Delta[SiO_2]$ C) pPDMPO concentration and D) the Si:PDMPO ratio of incorporation in *Thalassiosira pseudonana* cultures after a 24 hour experiment. Each symbol represents the mean of triplicate cultures ± 1 SE, except for n = 2 for the 125 nmol L^{-1} treatment in panel C. If error bars are not visible, they are smaller than the symbol.

2.3.1.b Effect of Diatom Species

For all further experiments, PDMPO was added to a final concentration of 125 nmol L^{-1} PDMPO. During experiments with four different diatom species, pPDMPO concentrations increased linearly with $\Delta[SiO_2]$ throughout the 48 hour incubation (Figure 2.5, Figure 2.6). As a result, the data points with the lowest $\Delta[SiO_2]$ and pPDMPO concentrations correspond to 12 hours after the addition of PDMPO, and $\Delta[SiO_2]$ and pPDMPO concentrations increased throughout the experiments to the greatest values at 48 hours. When cells were not lysed, species had a significant effect on the relationship between $\Delta[SiO_2]$ and PDMPO concentration ($p < 0.0001$). In all cases, the intercept of the line of best fit between pPDMPO and $\Delta[SiO_2]$ was not significant. Therefore, the relationship between SiO_2 and PDMPO incorporation is presented as a ratio between Si and PDMPO, calculated from the slope of best fit lines.

The ratio of Si:PDMPO incorporated into the frustule varied between the species tested by 3.1x when cells remained intact (Table 2.2). The highest ratio was measured in *A. glacialis* (4780 ± 380:1), while the other three species had much lower ratios that did not differ significantly among them and averaged 1750 ± 90:1. When all four species were analyzed together, the resulting best fit yielded a ratio of 2260 ± 190:1. When species was included as a predictor of the relationship between pPDMPO and $\Delta[SiO_2]$, the R^2 of the model was 0.90. However, when species was not included, as would be the case for a field assemblage of unknown composition, the R^2 decreased to 0.70.

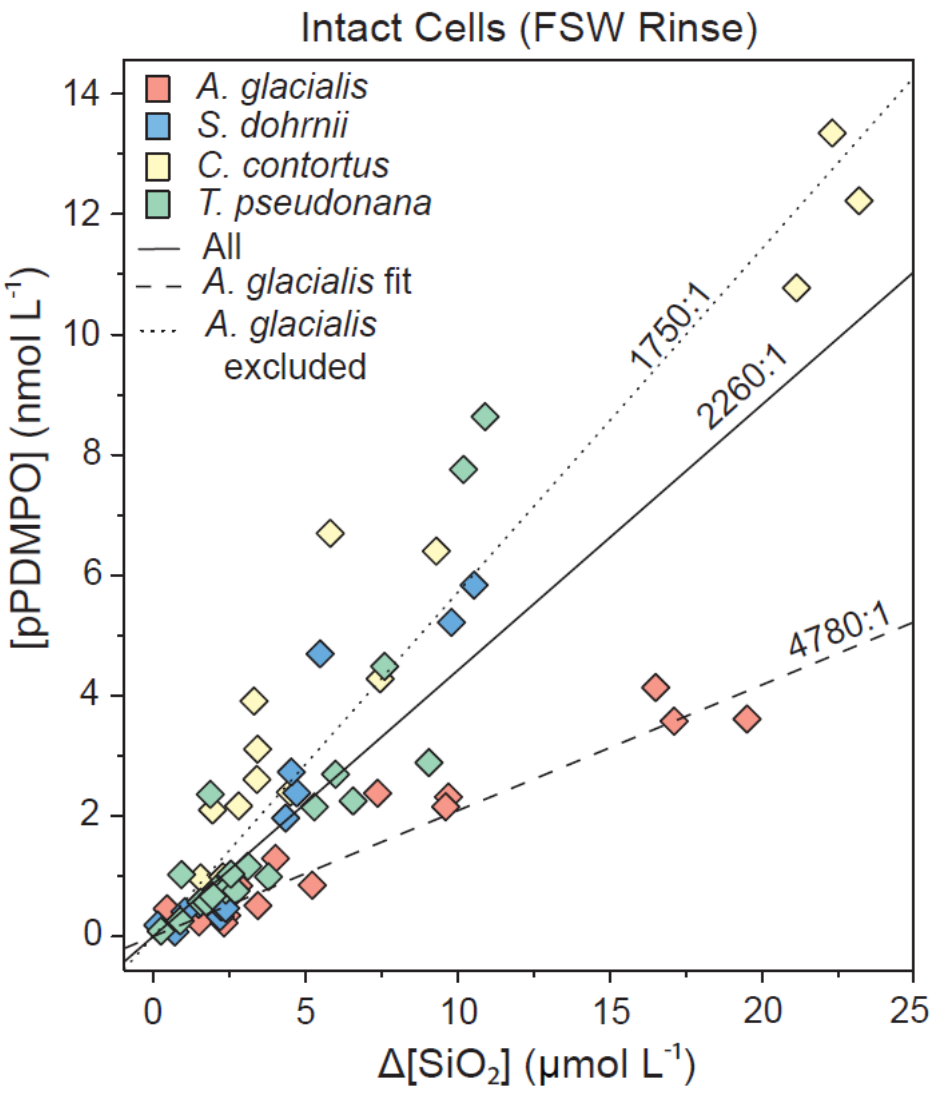

Figure 2.5: The concentration of pPDMPO vs. $\Delta[SiO_2]$. When incubations were terminated, cells on the filter were kept intact by rinsing cells with filtered sea water. Colours indicate the different species tested. For each species the consecutive data points correspond to different incubation times (12, 18, 24, 36 and 48 h), with the lowest and highest concentrations of pPDMPO and $\Delta[SiO_2]$ corresponding to 12 and 48 hours respectively. Lines of best fit are also shown with the corresponding Si:PDMPO ratio, with the solid line showing the best fit for all four species, the dashed line the fit for *A. glacialis* only, and the dotted line the fit for the remaining three species. Ratios of Si:PDMPO corresponding to the slope of each line of fit are indicated.

Table 2.2**:** Ratios of Si:PDMPO calculated from lines of best fit for pPDMPO concentration vs. $\Delta[SiO_2]$ for four diatom species presented in Figure 2.5 and Figure 2.6. Unlysed (FSW rinsed) and lysed (HCl rinsed) cells were analyzed separately for each species. R^2 values indicated are for the line of best fit for individual species.

Cells	**Species**	**Si:PDMPO (mol:mol)**		
		Mean	**SE**	**R^2**
Unlysed	*Asterionellopsis glacialis*	4780	380	0.92
	Skeletonema dohrnii	1640	140	0.91
	Chaetoceros contortus	1940	150	0.92
	Thalassiosira pseudonana	1550	190	0.78
	All	**2260**	**190**	**0.7**
	Excluding *A. glacialis*	**1750**	**90**	**0.89**
Lysed	*Asterionellopsis glacialis*	4300	430	0.89
	Skeletonema dohrnii	2850	480	0.71
	Chaetoceros contortus	4780	580	0.83
	Thalassiosira pseudonana	2150	360	0.66
	All	**4200**	**380**	**0.69**

2.3.1.c Effect of Diatom Cell Lysis

Loss of intracellular PDMPO from rinsing cells with HCl varied considerably between species (Table 2.3). In *A. glacialis*, intracellular PDMPO loss was not significantly different from zero, whereas in *Chaetoceros contortus* 53 ± 9 % of the pPDMPO measured was lost during rinsing with HCl.

Table 2.3: Percentage of intracellular PDMPO loss for the four diatom species for which the pPDMPO vs. $\Delta[SiO_2]$ relationship was determined (Figure 2.5). Loss was calculated as the difference in pPDMPO concentration between samples rinsed with FSW and samples rinsed with HCl (PDMPO stored intracellularly) as a percentage of the FSW pPDMPO (intracellular pPDMPO + pPDMPO in the frustule) for each pair of samples. Cell volumes are also listed for comparison.

Species	**Intracellular PDMPO Loss (%)**			**Cell Volume (μm^3)**
	Mean	SE	n	
Asterionellopsis glacialis	11	11	3	3000
Chaetoceros contortus	53	9	3	1000
Skeletonema dohrnii	23	11	3	450
Thalassiosira pseudonana	32	5	4	30

When data from HCl lysed cells was modelled as for unlysed cells (section 2.3.1b) diatom species had a significant effect on PDMPO incorporation ($p < 0.01$, Figure 2.6). When species was included as a predictor variable the model R^2 was 0.75, but decreased to 0.67 when species was not included. The range in Si:PDMPO between species when cells were lysed was less than when cells were unlysed (2.2x). Interestingly, the ratio of Si:PDMPO did not differ between lysed and unlysed cells of *A. glacialis* (4300 ± 430:1), while the large proportion of intracellular PDMPO loss from *C. contortus* caused it to have a higher Si:PDMPO ratio than *A. glacialis* (4780 ± 580:1). The Si:PDMPO ratio of *T. pseudonana* was significantly lower than both *A. glacialis* and *C. contortus*, while the Si:PDMPO ratio of *S. dohrnii* did not differ significantly from any of the other species. However, the low Si:PDMPO ratio of *T. pseudonana* seems to be largely due to two t = 48 measurements with high pPDMPO. The remaining two *T. pseudonana* t = 48 replicates were in line with the majority of data points from other species tested. When the two data points with high pPDMPO were removed from the analysis, the Si:PDMPO ratio of *T. pseudonana* increased, and no longer differed significantly from *A. glacialis* or *C. contortus*. It is possible that cells in these samples were not lysed effectively, although the pPDMPO concentrations measured are less than those from paired samples that were

rinsed with FSW. Regardless, excluding these two outliers increased the Si:PDMPO ratio calculated for the four species pooled together by less than 10%.

Although the effect of species was significant even when cells were lysed, species explained only 8% of the variability in pPDMPO concentrations (R^2 = 0.75 when species included as a predictor variable, R^2 = 0.67 when excluded), and was not a significant predictor of the ratio when the two *T. pseudonana* outliers were excluded. This suggests that were the taxonomic identity of diatom species unknown, a Si:PDMPO ratio of 4200 ± 320:1 could be used to convert pPDMPO measurements to $\Delta[SiO_2]$.

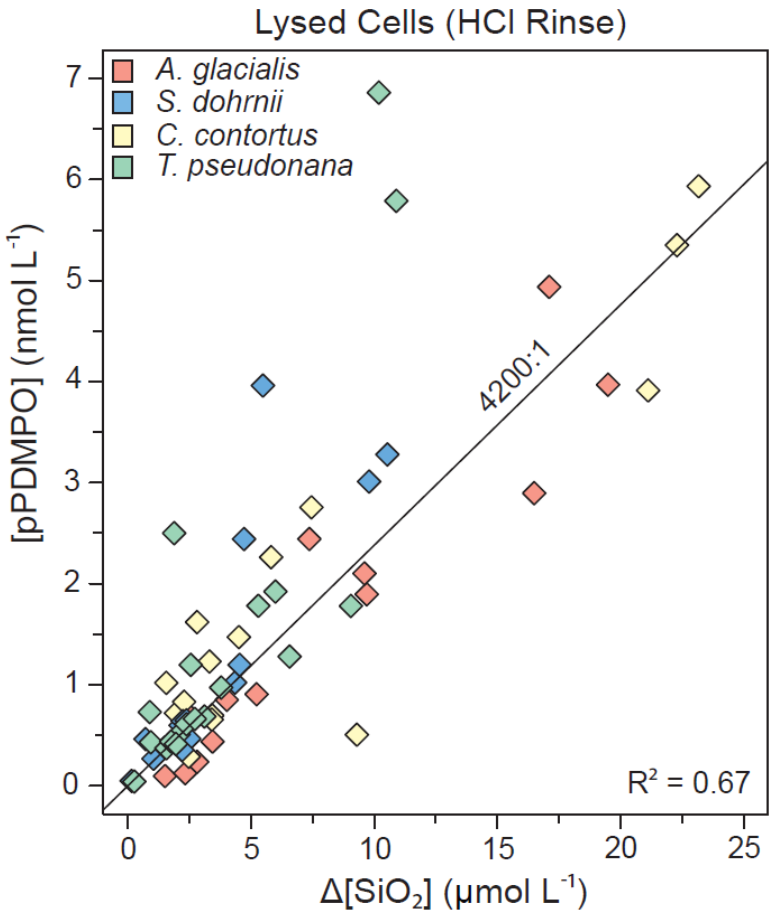

Figure 2.6: The concentration of pPDMPO vs. $\Delta[SiO_2]$. When incubations were terminated, cells on the filter lysed rinsing cells with 10% HCl. Colours indicate the different species tested. For each species the consecutive data points correspond to different incubation times (12, 18, 24, 36 and 48 h), with the lowest and highest concentrations of pPDMPO and $\Delta[SiO_2]$ corresponding to 12 and 48 hours respectively. The line of best fit for all four species pooled together is indicated.

2.3.2. Quantification of PDMPO Fluorescence by Microscopy

2.3.2.a Effect of Microscope Objective

When *C. wailesii* and *Pseudo-nitzschia* sp. fluorescence was quantified by microscopy, the fluorescence of both species measured with the 40x objective was higher than that measured with the 10x objective (Figure 2.7). The differences in absolute value of fluorescence measurements between configurations (i.e. 2P, 10x and 40x) are due to arbitrary differences in scaling, and do not impact comparisons between species. For 2P-normalized 10x and 40x fluorescence data, variability was greater for *Pseudo-nitzschia* sp. than for *C. wailesii*. This is likely due to the low absolute fluorescence of *Pseudo-nitzschia* spp. relative to *Coscinodiscus* spp., necessitating shorter than optimal exposure times for *Pseudo-nitzschia* spp. cells and consequently an increase in the noise associated with *Pseudo-nitzschia* spp. measurements. High fluorescence *Pseudo-nitzschia* sp. outliers were included, but their removal had little effect on the comparison between species. As measurements of *Pseudo-nitzschia* sp. had higher variance than those of *C. wailesii*, a Wilcoxon rank sum test was used to determine if the species differed significantly. When 10x/2P measurements were compared, the species were not significantly different ($p = 0.4$); however, fluorescence of *C. wailesii* was significantly higher than *Pseudo-nitzschia* sp. for 40x/2P measurements ($p < 0.001$).

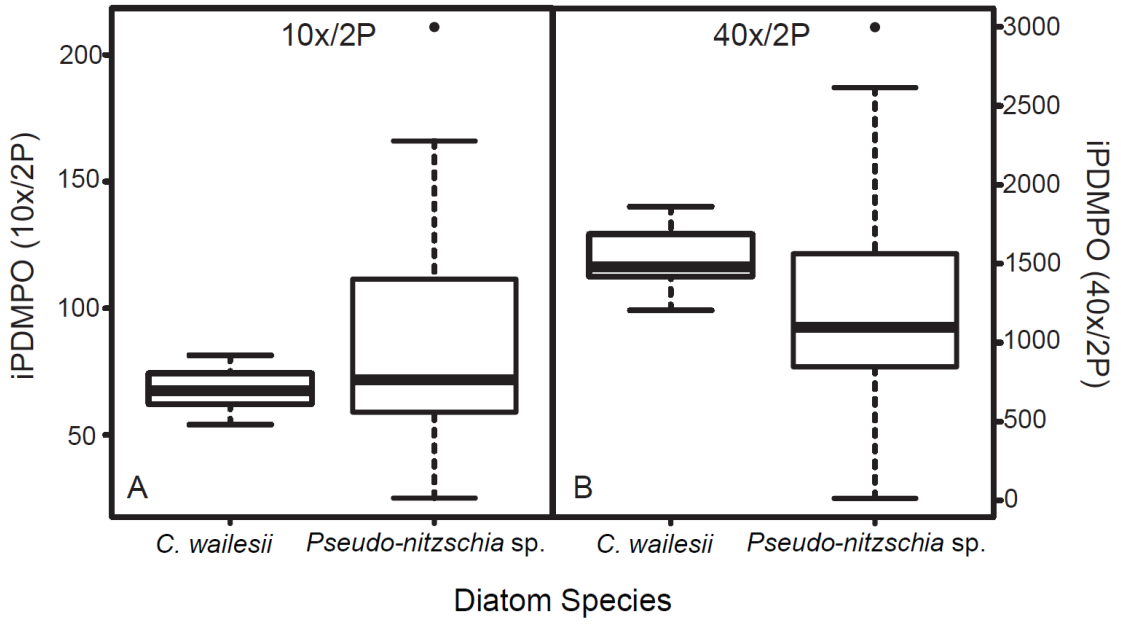

Figure 2.7: Boxplots of iPDMPO fluorescence per cell for *C. wailesii* (n = 23 cells) and *Pseudo-nitzschia* sp. (n = 54 cells) measured by fluorescence microscopy using either an A) 10x (0.25NA), or B) 40x (0.6NA) microscope objective then normalized to fluorescence of the same cell measured by 2P. The median of each box is indicated by the thick black line and the top and bottom of each box represents the first and third quartile respectively. Whiskers extend to 1.5x the range between the first and third quartile.

2.3.2.b Testing Relative PDMPO Quantification

PDMPO fluorescence was higher in *Pseudo-nitzschia* sp. than *C. wailesii* at the conclusion of the incubations, and accounted for 82 ± 4 % of the total PDMPO incorporation by both species when measured by fluorometry and 78 ± 12 when measured by microscopy (Figure 2.8). The relative proportion of PDMPO incorporated by each species measured by quantitative microscopy agreed well with results from fluorometry, suggesting that PDMPO fluorescence can be quantified reliably for different species within a mixed assemblage within the same slide.

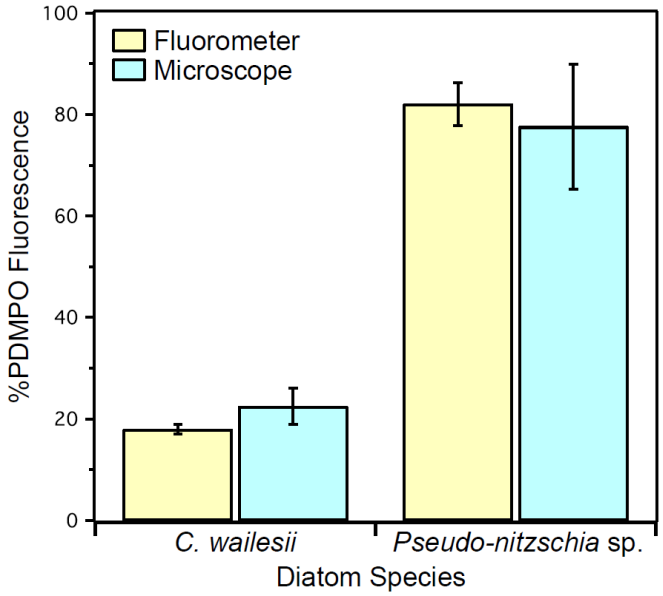

Figure 2.8: Percentage contribution of *C. wailesii* and *Pseudo-nitzschia* sp. to total PDMPO fluorescence of both diatom species, when measured on a fluorometer (yellow bars, rinsed with HCl) and with a microscope (blue bars). Error bars represent ± 1SE.

2.3.2.c Testing Absolute PDMPO Quantification

Similarly to when PDMPO was quantified by fluorometry (section 2.3.1b, Figure 2.5, 2.6), iPDMPO increased with $\Delta[SiO_2]$ in the four species tested (Figure 2.9). PDMPO fluorescence measured by microscopy was strongly correlated with $\Delta[SiO_2]$ ($R^2 = 0.78$), suggesting that quantifying PDMPO fluorescence by microscopy is a reliable method for measuring the concentration of PDMPO in diatom frustules. Both the slope and intercept of the relationship between PDMPO and $\Delta[SiO_2]$ were significant ($p < 0.05$), and the relationship was best described by

$$iPDMPO = 125{,}000 * \Delta[SiO2] - 212{,}000 \qquad \textbf{Equation 3}$$

where iPDMPO is the fluorescence measured by microscopy (arbitrary units), and $\Delta[SiO_2]$ is the concentration of SiO_2 less the concentration of SiO_2 when PDMPO was added (µmol L^{-1}). This relationship is dependent on several conditions: the concentration

of PDMPO applied (125 nmol L^{-1}), the mountant used to prepare slides (Shandon Immu-mount, pH 8.0), and the calibration slide used (Chroma yellow slide).

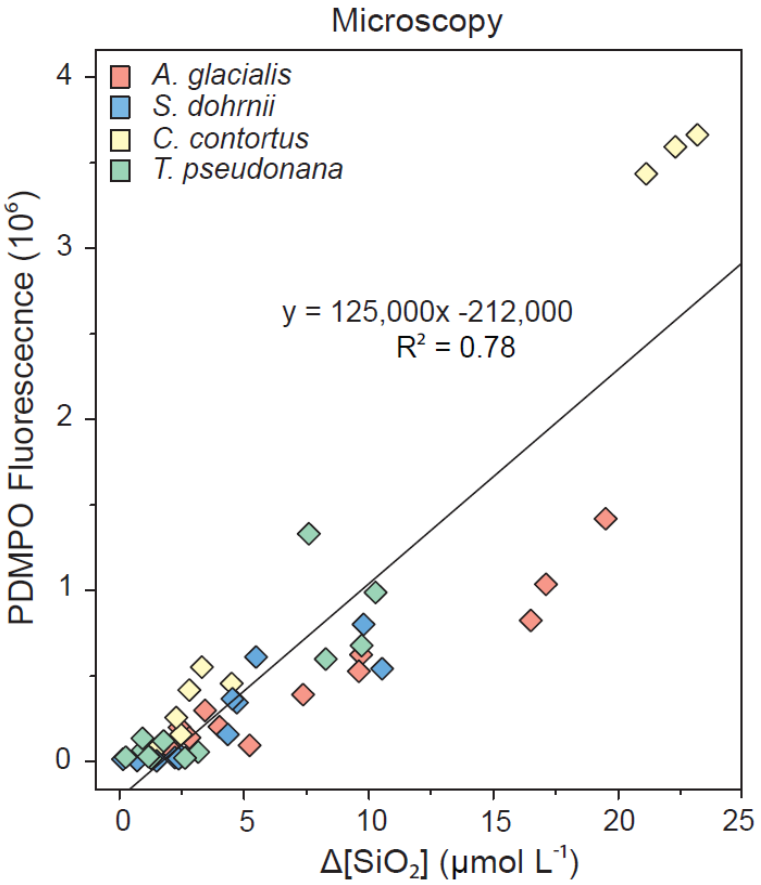

Figure 2.9: The fluorescence of PDMPO determined by microscopy vs. $\Delta[SiO_2]$ from experiments with *A. glacialis* (red), *S. dohrnii* (blue), *C. contortus* (yellow) and *T. pseudonana* (green) when fluorescence was quantified by microscopy from each triplicate culture and 12, 24, and 48 hour time points. The line of best fit when all species were pooled together is indicated.

2.3.3. Assessing the Performance of the PDMPO Technique in the Field

In all Saanich Inlet experiments, PDMPO incubations were conducted for 24 hours; therefore, when pPDMPO measurements are converted to $\Delta[SiO_2]$ this represents a daily rate of SiO_2 production (ρ_{PDMPO}). Generally, ρ_{PDMPO} and ρ_{GROSS} (determined using ^{32}Si) agreed well in Saanich Inlet (Figure 2.10). However, in August diatom cell counts were

low (320,000 cells L^{-1}), and ρ_{PDMPO} was 78 times higher than ρ_{GROSS} (data not shown). Although no reason for this large discrepancy is apparent, this measurement is likely erroneous and has been excluded from subsequent analyses.

The pPDMPO concentration was strongly correlated with ρ_{GROSS} in the Saanich Inlet samples (Figure 2.10A, $R^2 = 0.78$). When pPDMPO concentrations measured from lysed cells were converted to $\Delta[SiO_2]$ using a Si:PDMPO ratio of 4200 ± 380:1 (this chapter, section 2.3.1c) the slope of the fit of ρ_{PDMPO} vs. ρ_{GROSS} was 0.77 (Figure 2.10B). When the Leblanc and Hutchins (2005) ratio of 3230 ± 660:1 was used to convert measurements of PDMPO to $\Delta[SiO_2]$, the slope of the line of best fit was 18% lower than when a ratio of 4200 ± 380:1 was used (Figure 2.10C). For both Si:PDMPO conversion ratios, the slope of the line of best fit between ρ_{PDMPO} and ρ_{GROSS} was less than 1, suggesting that in both cases PDMPO under-estimated SiO_2 incorporation relative to ^{32}Si. However, when the lines of fit was forced through the origin the slopes increased for both Si:PDMPO ratios, to 1.10 for a ratio of 4200 ± 380:1, and to 0.85 for a ratio of 3230 ± 660:1. This suggests that ρ_{PDMPO} agreed better with ρ_{GROSS} at high ρ_{PDMPO}. Therefore, disagreements between ρ_{PDMPO} and ρ_{GROSS} were mostly due to over-estimation of SiO_2 incorporation rates by PDMPO when rates were low.

Three of the Saanich Inlet pPDMPO measurements appeared to be inflated relative to ρ_{GROSS} (coloured points, Figure 2.10). In two instances (June and September), these samples were collected when diatoms were very low in abundance (<5% of phytoplankton >5 µm), while dinoflagellates dominated (indicated in blue Figure 2.10). In the third case, diatoms dominated the phytoplankton, but $Si(OH)_4$ concentrations were the lowest measured during the study period (9.4 µmol L^{-1}, yellow point, May).

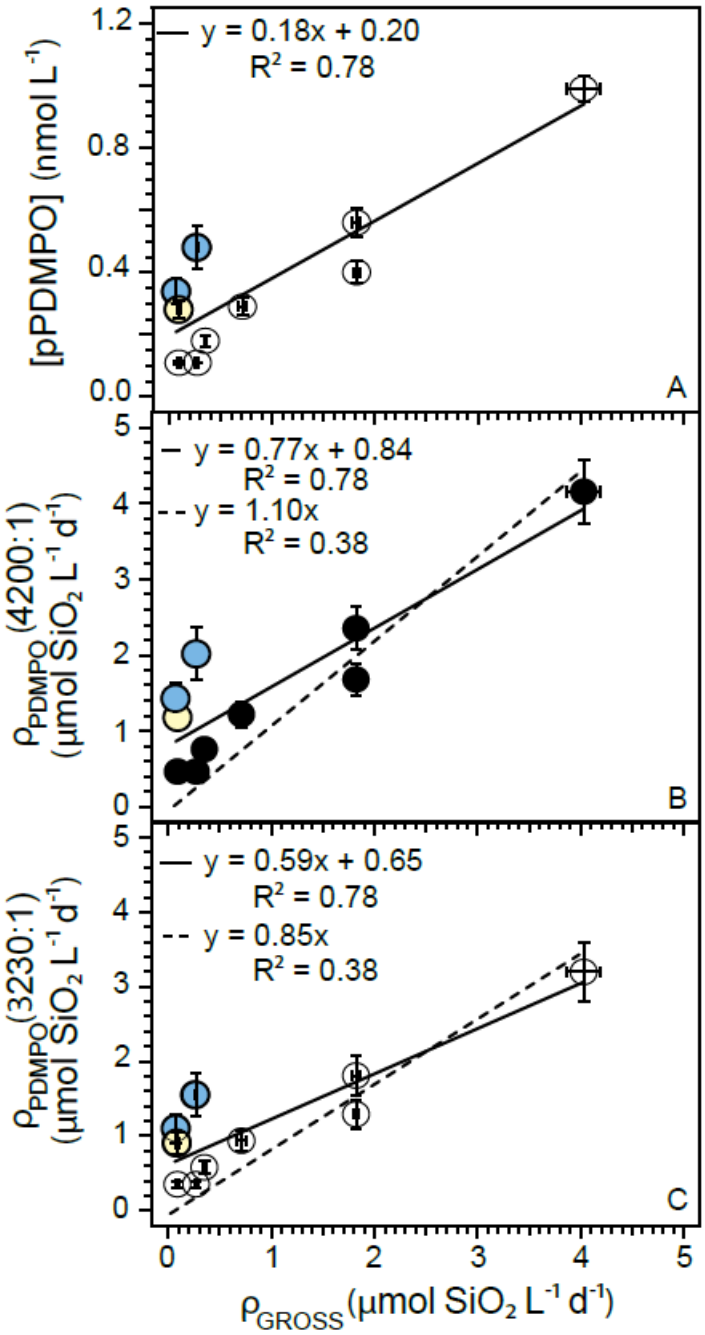

Figure 2.10: A) pPDMPO concentration vs. ρ_{GROSS}, B) ρ_{PDMPO} calculated using a Si:PDMPO ratio of 4200:1 (this chapter, section 2.3.1c) vs. ρ_{GROSS} and C) ρ_{PDMPO} calculated using a ratio of 3230:1 Si:PDMPO (Leblanc and Hutchins 2005) vs. ρ_{GROSS} from monthly sampling in Saanich Inlet from February to December 2013, (August 2013 excluded, see text). Solid lines indicate the line of best fit, while dashed lines show the fit when forced through the origin. Data points represent the mean of triplicate measurements and error bars ± 1 SE. Data points indicated in blue are for months when diatoms were low in abundance and dinoflagellates dominated the phytoplankton assemblage, while the data point indicated in yellow indicates the sample collected with the lowest $Si(OH)_4$ concentration (May 2013, 9.4 µmol L^{-1}).

During the March 2013 spring bloom, three diatom taxa made up the majority of diatom cell numbers (Figure 2.11). *Chaetoceros* spp. was the most abundant genus numerically, and represented 57% of diatom cells present. *Thalassiosira* spp. was the next most abundant genus and accounted for 33% of diatom cells. However, the contributions of these diatom genera to total diatom cell numbers were very different from the contributions of these genera to iPDMPO. *Chaetoceros* spp. accounted for only 2 ± 1 % of community iPDMPO, indicating that its contribution to community SiO_2 incorporation was minimal. *Thalassiosira* spp. was responsible for the majority of PDMPO fluorescence (96 ± 2 %), which corresponded to a ρ_{PDMPO} 3.6 ± 0.3 μmol L^{-1} d^{-1} from this genus alone. During this month samples the chlorophyll *a* maximum occurred at a depth corresponding to 48% of surface irradiance, suggesting that incubation light intensity (screened to 50%) would have matched ambient conditions (Table 4.1).

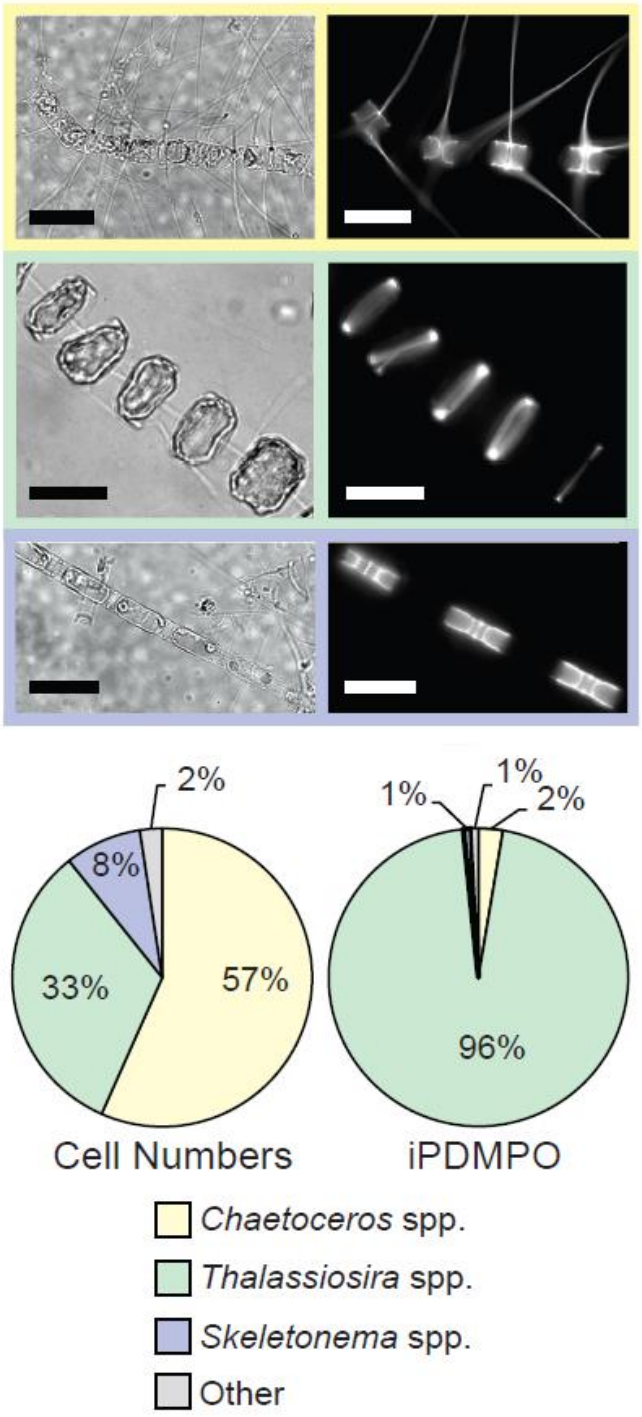

Figure 2.11: Panels showing images of abundant diatom genera in Saanich Inlet captured using brightfield (left column) and PDMPO fluorescence microscopy (right column). The percent contribution of these diatom genera to total diatom cell numbers (left pie chart) and total PDMPO fluorescence (iPDMPO, right pie chart) in Saanich Inlet during March 2013 are shown below the images. Colours of each genus match between pie charts and microscope image frames. All scale bars represent 25 µm.

2.4. Discussion

Throughout these experiments, PDMPO was useful as a tracer of SiO_2 incorporation of marine diatoms. Particulate PDMPO concentration was strongly correlated with the amount of new SiO_2 produced in laboratory cultures, and with SiO_2 incorporation determined using ^{32}Si in natural marine diatom assemblages. In addition, PDMPO could be reliably quantified using widefield fluorescence microscopy. As a result, total diatom community and taxa specific rates of SiO_2 incorporation can be determined using the PDMPO tracer.

2.4.1. PDMPO as a Tracer of SiO_2 Incorporation in Marine Diatoms

The incorporation of PDMPO was strongly related to the incorporation of SiO_2 in both laboratory cultures and natural marine diatom assemblages. However, PDMPO may be toxic to diatoms at high concentrations. The reduction of diatom growth rates in *T. pseudonana* at concentrations of $\geq$500 nmol L^{-1} (Figure 2.4A) observed in this study was an unexpected result, as the manufacturer of PDMPO recommends using 1000 nmol L^{-1} (Life Technologies Corporation 2013) for this type of experiment. In fact, this concentration has been used previously in several studies (Shimizu et al. 2001; Hazelaar et al. 2005; Heredia et al. 2008; Vartanian et al. 2009). In the present study, a reduction in growth rate was evident after 24 hours, in contrast to the results of Leblanc and Hutchins (2005) that showed reduced growth at 500 and 1000 nmol L^{-1} only after 96 hours of incubation. It is possible that some of this discrepancy may be due to differences in susceptibility between diatom species, as Leblanc and Hutchins (2005) assessed toxicity in a mixed natural assemblage, not in *T. pseudonana*. It is also possible that the decrease in growth rate was easier to detect with the higher precision cell count method used in this study (automated particle counting, average precision 3%) than by Leblanc and Hutchins (2005, microscope counts). My results support the recommendation of Leblanc and Hutchins (2005) that a PDMPO concentration of 125 nmol L^{-1} should be used and that concentrations greater than 500 nmol L^{-1} should be avoided to prevent toxic effects on diatoms.

The incorporation of PDMPO was strongly correlated with SiO_2 incorporation in experimental cultures. However, this relationship did not have a fixed Si:PDMPO stoichiometry. Rather, the Si:PDMPO of incorporation likely reflects the concentrations of $Si(OH)_4$ and PDMPO that reach the SDV. This has been suggested previously by Durkin et al. (2013), and they found that different ambient $Si(OH)_4$ concentrations affected the relationship between PDMPO fluorescence and SiO_2 incorporation. Here, the same effect was observed but when PDMPO concentrations were varied. As PDMPO concentrations in the culture medium of *T. pseudonana* increased, the Si:PDMPO of incorporation decreased (Figure 2.4D), in agreement with previous findings for the same diatom using a similar fluorescent dye (HCK- 123, Hervé et al. 2012). Although the mechanism of PDMPO's incorporation into the SiO_2 frustule is unknown, this result is consistent with what is known about the incorporation of PDMPO by diatom cells. PDMPO diffuses rapidly across the cell membrane and into the SDV (Shimizu et al. 2001; Life Technologies Corporation 2013), and as a result the accumulation of PDMPO within the SDV depends on its concentration gradient. In contrast, the incorporation of SiO_2 did not exhibit a trend with PDMPO concentration (Figure 2.4B), and as a result, Si:PDMPO will vary depending on the extracellular PDMPO concentration. This suggests that any factors that differentially affect PDMPO or $Si(OH)_4$ uptake into the cell may change the ratio of Si:PDMPO incorporated into the frustule, and could confound the quantification of SiO_2 incorporation based on PDMPO measurements.

The diatom taxa present is one factor that differentially affects $Si(OH)_4$ and PDMPO uptake into diatom cells, and consequently may affect the Si:PDMPO ratio of incorporation. Different diatom taxa vary in their ability to take up $Si(OH)_4$; the half saturation constant for $Si(OH)_4$ (K_{Si}) uptake varies by two orders of magnitude (Sarthou et al. 2005), and maximum $Si(OH)_4$ uptake rates vary by as much as five orders of magnitude between diatom species (Martin-Jézéquel et al. 2000). These differences between species would affect the rate of $Si(OH)_4$ uptake into the cell, and the amount present within the SDV. Therefore, the incorporation of SiO_2 in the frustule would be expected to occur differently for individual diatom species. In contrast, PDMPO uptake would be unaffected by taxonomic differences in $Si(OH)_4$ uptake, and consequently the

Si:PDMPO ratio would vary between taxa. Indeed, diatom species was a significant predictor of the relationship between $\Delta[SiO_2]$ and pPDMPO in diatom frustules, whether or not cells were lysed to get rid of intracellular PDMPO (Figure 2.5, 2.6). However, the species effect was small relative to the effect of $\Delta[SiO_2]$, and explained only 20% and 8% of the variability in the Si:PDMPO relationship when cells were intact (FSW rinse) or lysed (HCl rinse), respectively. When cells were lysed, *T. pseudonana* had a significantly lower ratio of Si:PDMPO than *C. contortus* and *A. glacialis*, but this largely due to two high pPDMPO measurements from *T. pseudonana*. When these measurements were excluded, the Si:PDMPO ratio was no longer significantly different between the species. Therefore, it is possible that different diatom species have different Si:PDMPO ratios when cells are lysed, but it is difficult to say for certain due to the variability between replicates for this species. Even when the effect of species was ignored, and species was not included as a predictor variable, the amount of pPDMPO was strongly predicted by the amount of SiO_2 produced whether or not cells were lysed ($R^2 > 0.65$). This suggests that PDMPO remains a useful tracer of SiO_2 incorporation even when the taxonomic composition of the diatom assemblage is unknown.

Interestingly, much of the difference between the diatom species tested when cells were unlysed was due to *A. glacialis*. For this species, the ratio of Si:PDMPO incorporated into the cell did not differ when cells were intact or lysed, suggesting that *A. glacialis* stores little or no PDMPO intracellularly. This is in contrast to the other species tested, in which pPDMPO concentrations decreased when cells were lysed. The disparity between *A. glacialis* and the other species tested may reflect a phylogenetic difference, as *A. glacialis* is an araphid pennate, while the other species are within the polar centric clade (Theriot 2010). Perhaps these clades differ in some physiological respect, such as the size or pH of the storage vacuole or SDV, which causes less accumulation of PDMPO within *A. glacialis* cells. Leblanc and Hutchins (2005) also found differences in intracellular PDMPO storage between the species that they tested, and suggested that this was due to greater PDMPO storage within larger cells. However, the proportion of PDMPO lost during cell lysis was not correlated with intracellular volume in the species tested in the present study.

When pPDMPO concentration was modelled as a function of $\Delta[SiO_2]$, R^2 values were similar between cells that were kept intact and cells that were lysed ($R^2 = 0.70$, and 0.67 respectively) when diatom species was not included as a predictor variable in the model. However, when species was included as a predictor variable, R^2 values were much higher for cells that remained intact ($R^2 = 0.90$ for intact cells, 0.75 for lysed cells). This suggests that species has a much larger effect on pPDMPO measurements when cells are intact (20% vs. 8%), but additionally implies that rinsing samples with HCl increases variability. When cells were not lysed, only 10% of the variability in pPDMPO measurements was not explained by species or $\Delta[SiO_2]$, while when cells were lysed 25% of the variability was unexplained. It is possible that not all of the PDMPO present in diatom cells is removed during the HCl lysis protocol, and that inconsistencies in the amount removed are responsible for this increased variability. Despite this, HCl rinsing reduced the effect of diatom species on the relationship between $\Delta[SiO_2]$ and PDMPO incorporation. Therefore, I agree with the recommendation of Leblanc and Hutchins (2005) that cells by lysed during filtration when determining $\Delta[SiO_2]$ from pPDMPO measurements.

From culture experiments in which diatoms were grown with 125 nmol L^{-1} PDMPO, $\Delta[SiO_2]$ was best predicted for all species from pPDMPO measurements using a Si:PDMPO ratio of 4200 ± 380:1. This Si:PDMPO ratio is 30% higher than the ratio reported by Leblanc and Hutchins (2005). Although there is considerable scatter in measurements of pPDMPO from lysed cells (Figure 2.6), the notable outliers are above the line of best fit and their exclusion increases the ratio further. It is possible that the discrepancy between the Si:PDMPO ratios reflects a methodological difference. Leblanc and Hutchins (2005) digested their samples with NaOH, while HF was used for digestion for Si:PDMPO ratio experiments in the present study. Digestion with NaOH may degrade PDMPO; however, this would decrease the ratio of Leblanc and Hutchins (2005) further, and could not explain the observed differences. Diatom taxa are also unlikely to explain the difference in ratios, as species from the two genera tested by Leblanc and Hutchins (2005) were also tested in this study. It is possible that more efficient cell lysis

could have increased the Si:PDMPO in my experiments relative to Leblanc and Hutchins (2005); however, the same protocol was used. Differences in the conditions of culture experiments could also have played a role in the difference in ratios. If $Si(OH)_4$ concentrations were limiting during the experiments described in Leblanc and Hutchins (2005), SiO_2 incorporation could have been reduced relative to PDMPO incorporation, resulting in a lower Si:PDMPO ratio. During my experiments, $Si(OH)_4$ concentrations were always >80 μmol L^{-1}, much higher than would be expected to cause uptake limitation (Sarthou et al. 2005). Additionally, cultures were in the exponential phase of growth for the duration of my experiments, while Leblanc and Hutchins (2005) do not specify growth of diatom cultures during their experiments.

Although PDMPO concentration and diatom species may affect the relationship between SiO_2 and PDMPO incorporation, the good agreement (R^2 >0.65) between pPDMPO concentration and $\Delta[SiO_2]$ in culture experiments suggest that the effect of these variables can be minimized. By controlling the concentration of extracellular PDMPO added and lysing diatom cells, PDMPO can be used as a tracer of SiO_2 production despite potential decoupling of its incorporation from SiO_2 into diatom frustules.

2.4.2. Assessing Performance of PDMPO for Determining Total Diatom Community SiO_2 Incorporation in Natural Assemblages

In laboratory diatom cultures, incorporation of PDMPO into the frustule was strongly correlated with $\Delta[SiO_2]$. This was also true for samples collected from Saanich Inlet; PDMPO incorporated into lysed cells was strongly correlated with ρ_{GROSS} measured using ^{32}Si (R^2 = 0.78, Figure 2.10A).

At high rates of ρ_{GROSS} (>1 μmol L^{-1} d^{-1}), ρ_{PDMPO} calculated using a Si:PDMPO ratio of 4200 ± 380:1 agreed with ρ_{GROSS}, while the Leblanc and Hutchins (2005) ratio predicted less ρ_{PDMPO}. However, ρ_{PDMPO} was over-estimated when calculated using either ratio when ρ_{GROSS} was low. In two months when ρ_{PDMPO} was substantially higher than ρ_{GROSS},

dinoflagellates dominated the large phytoplankton (>5 µm), and diatoms accounted for less than 5% of large phytoplankton cell numbers (Figure 2.10, blue points). Previous work has found that dinoflagellates may bind PDMPO extracellularly and add to the PDMPO signal (Alvarado 2012). Because of this, Alvarado (2012) recommends rinsing samples for the determination of ρ_{PDMPO} with antibiotics. However, Alvarado (2012) did not test the HCl rinse protocol used for Saanich Inlet samples. Consequently it is unknown how rinsing dinoflagellate bound PDMPO with HCl affects the pPDMPO concentration measured. In cases when dinoflagellates dominate the phytoplankton community (>95% of >5 µm cells present), diatom productivity is unlikely to account for a large share of phytoplankton productivity overall. Therefore rates of SiO_2 incorporation are unlikely to be informative about phytoplankton dynamics in these cases. However, it is important to assess the abundance of diatoms and dinoflagellates when PDMPO measurements are conducted, to ensure that dinoflagellates do not represent a source of error in measurements of ρ_{PDMPO}.

Even when samples from these two dinoflagellate-dominated months were excluded, ρ_{PDMPO} was 13.1x higher than ρ_{GROSS} in May 2013 (Figure 2.11, yellow). Diatoms were the dominant group of phytoplankton at this time, and dinoflagellate binding of PDMPO cannot explain the overestimation of ρ_{PDMPO}. May had the lowest $Si(OH)_4$ concentration (9.4 µmol L^{-1}) during Saanich 2013 sampling, which might explain the mismatch between rates of SiO_2 production determined using PDMPO and ^{32}Si as tracers. If $Si(OH)_4$ concentrations were low enough to limit uptake, the rate of Si accumulation within the SDV and the frustule could have been reduced relative to the rate of PDMPO accumulation. This would alter the Si:PDMPO ratio of incorporation relative to culture experiments, during which $Si(OH)_4$ concentrations were always >80 µmol L^{-1} and would not be limiting. However, the highest K_{Si} previously reported for any of the genera that are present in Saanich Inlet is 4.7 ± 0.5 µmol L^{-1} (Sarthou et al. 2005) suggesting that concentrations of $Si(OH)_4$ of 9.4 µmol L^{-1} should close to saturating for $Si(OH)_4$ transporters. As a result, it is surprising that $Si(OH)_4$ uptake when ambient concentrations are 9.4 µmol L^{-1} would be reduced enough to explain the 13.1x reduction in Si:PDMPO. Previous work by Durkin et al. (2013) found decoupling between SiO_2

incorporation and measured PDMPO fluorescence when cultures were grown with 20 μmol L^{-1} and 80 μmol L^{-1} $Si(OH)_4$. At these concentrations of $Si(OH)_4$, uptake by transporters would be expected to be maximal. However, not all $Si(OH)_4$ uptake occurs via transporters; above 30 μmol L^{-1} uptake is dominated by passive diffusion (Thamatrakoln and Hildebrand, 2008), and $Si(OH)_4$ uptake may continue to increase beyond this concentration. Therefore, it is possible that $Si(OH)_4$ concentration may affect the amount of SiO_2 incorporated and the Si:PDMPO ratio at concentrations above 10 μmol L^{-1} when transporter mediated uptake would be saturated. It is difficult to determine if ρ_{PDMPO} calculated for the remainder of the Saanich Inlet samples was affected by $Si(OH)_4$ concentrations (average 30 μmol L^{-1}) that were much lower than during culture experiments. The remaining Saanich Inlet samples collected had $Si(OH)_4$ concentrations >20 μmol L^{-1}, and inflation of pPDMPO measurements is not apparent. To ensure that PDMPO remains a robust tracer of SiO_2 incorporation regardless of ambient $Si(OH)_4$ concentration, further experimentation is needed. It is possible that the effect of $Si(OH)_4$ uptake limitation on the Si:PDMPO ratio could be modeled (Chapter 3, Appendix H), and corrected for in future studies.

When the samples from the dinoflagellate dominated and low $Si(OH)_4$ (<10 μmol L^{-1}) months are excluded, agreement between ρ_{PDMPO} and ρ_{GROSS} improves (R^2 = 0.93, both ratios). When the ratio of 4200 ± 380:1 was used to convert pPDMPO to ρ_{PDMPO} the slope of the line of best was 0.93, while a ratio of 3230 ± 660:1 yielded a slope of 0.72. This indicates that a ratio of 4200 ± 380:1 yields better agreement between ρ_{PDMPO} and ρ_{GROSS} than that of 3230 ± 660:1, which underestimated the amount of SiO_2 incorporation by 28%.

At present, ρ_{PDMPO} may be inaccurate when diatoms are very rare and dinoflagellates dominate the phytoplankton >5 μm (>95% of cells), and also when $Si(OH)_4$ concentrations are less than 10 μmol L^{-1}. Further improvements to the use of PDMPO as a tracer of SiO_2 incorporation should be investigated: in particular rinses to remove PDMPO bound to dinoflagellates, and experiments to determine whether correcting ρ_{PDMPO} for limitation of $Si(OH)_4$ uptake are warranted. Excluding cases when diatoms

are very rare and when $Si(OH)_4$ uptake is limited, PDMPO is a robust tracer of SiO_2 production natural diatom assemblages.

2.4.3. Quantification of PDMPO by Microscopy

A significant advantage of using PDMPO as a tracer of SiO_2 incorporation is that PDMPO fluorescence can be imaged for individual diatom cells by fluorescence microscopy. This allows SiO_2 production by different diatom taxa within the same mixed assemblage to be quantified separately. This goes beyond cell numbers, the conventional indicator of community composition, by detecting which cells are actively producing SiO_2, and indicating the amount produced.

Quantification of PDMPO by widefield fluorescence microscopy agreed with measurements of SiO_2 incorporation, for the protocols used in this study. The procedure used for quantifying PDMPO fluorescence differs from that used in previous studies. First, excitation light must be calibrated. Illumination from excitation light sources is variable with time, and a reduction in excitation light intensity will cause a corresponding reduction in fluorescence emitted. It is important to control for this variability, as has been done in several previous studies (Znachor and Nedoma 2008; Iluz et al. 2009; Znachor et al. 2011, 2013), but not all (Durkin et al. 2012). Although the correction used in previous studies accounts for differences in excitation light intensity with time, it does not account for differences in light intensity spatially across the field of view. Even when microscopes are properly aligned, illumination will be uneven across a FOV (Wolf et al. 2007). Therefore, it is necessary to perform a flat-field correction, and normalize the fluorescence intensity of pixels within a sample image by the intensity of pixels at the same location within the FOV of a reference image.

In addition to a different method for calibrating measured fluorescence intensities from previous studies, different microscope configurations were tested. Microscope objective lenses have different depths of field, indicated by the NA, and a lower NA objective will have a larger depth of focus (Figure 2.1). As diatom SiO_2 structures vary widely in

thickness, it is important that microscope objectives are chosen for PDMPO imaging that capture fluorescence throughout the depth of the cell. Otherwise, measurements of thick diatom species may be under-estimated, a concern that previous studies have raised (Durkin et al. 2012; Hervé et al. 2012). Optical sectioning methods (such as 2P) may overcome the limitation of a fixed depth of focus, because the depth of focus can be increased to capture the entirety of a cell. However, image capture is more time consuming using optical sectioning compared to widefield fluorescence, and widefield microscopes are more widely available.

When measurements of two differently sized diatom species were imaged using high and low NA objectives, measurements using the high NA objective differed between the two species relative to PDMPO fluorescence determined by optical sectioning (Figure 2.7B). In contrast to expectations, PDMPO fluorescence from the larger cells was not reduced with the higher NA and shorter depth of focus objective, but rather fluorescence was over-estimated. It is possible that out of focus fluorescence was captured, and that fluorescence closer to the detector was captured more effectively despite being above the plane of focus. Focus for images was adjusted manually, so that both *C. wailesii* and *Pseudo-nitzschia* spp. cells appeared to be in focus. Therefore, the plane of focus for most images would likely be within ~10 µm of the slide surface, as this is where flat *Pseudo-nitzschia* spp. cells would be in focus. However, thicker *C. wailesii* cells would protrude from the slide surface, closer to the detector. Perhaps this out of focus fluorescence was somehow over-estimated due to its close proximity to the objective lens. Regardless of the mechanism, the difference in 2P normalized fluorescence between the species of different size demonstrate that high NA microscope objectives should not be used to quantify PDMPO fluorescence between different diatom taxa. In contrast, measurements of the two species agreed with optical sectioning measurements when the low NA was used (Figure 2.7A). This suggests PDMPO fluorescence in diatom cells quantified using widefield fluorescence microscopy reasonably approximates the optical sectioning method provided that a low NA objective is used. The implications of this finding for the results of previous studies is unclear, as to my knowledge, not a single study quantifying PDMPO fluorescence microscopy specifies the NA of the microscope

objective used. Objectives of 20x (Znachor et al. 2008, 2013; Znachor and Nedoma 2008) and 40x (Durkin et al. 2012) magnification have been used previously, with others not specifying their magnification (Iluz et al. 2009; Quéguiner et al. 2011). As microscope objectives may confound measurements of PDMPO between species, it is critical that objectives with low NA are used to quantify PDMPO, and that microscope configurations are described in sufficient detail.

When variability in illumination intensity was controlled and a low NA objective was used, measurements of iPDMPO agreed with pPDMPO fluorescence measured by fluorometry and with measurements of $\Delta[SiO_2]$ (Figures 2.8, 2.9). Relative iPDMPO measurements (within the same slide) were not significantly different from fluorometric measurements, suggesting that comparisons of fluorescence determined for different cells within the same microscope slide reflect the amount of PDMPO incorporated (Figure 2.8). In samples from separate culture experiments, absolute PDMPO fluorescence (fluorescence determined as a concentration, compared between slides) quantified by microscopy was strongly correlated with $\Delta[SiO_2]$ concentration ($R^2 = 0.78$, Figure 2.9). The correlation between $\Delta[SiO_2]$ and PDMPO measured by microscopy was stronger than when PDMPO was measured by fluorometry ($R^2 = 0.70$ for intact cells, 0.67 for lysed cells). Although this may suggest that PDMPO can be reliably quantified between different microscope slides, I emphasize that the results presented here are for controlled laboratory experiments. It is likely that comparisons between different slides prepared from natural assemblages would be less reliable due to additional sources of variability inherent in field work. For slides prepared from natural assemblages on the west coast of Vancouver Island (Chapter 3 of this thesis), microscopic measurements of PDMPO did not indicate SiO_2 incorporation as reliably as SiO_2 incorporation determined from pPDMPO concentrations or ^{32}Si incorporation. Therefore, measurements of PDMPO fluorescence by microscopy should not be used alone to determine absolute rates of SiO_2 incorporation, but rather in combination with another method that determines bulk community SiO_2 incorporation rates.

Using relative measurements of PDMPO obtained with microscopy it was possible to determine the contributions of different diatom taxa to SiO_2 production during the 2013 spring bloom (Figure 2.11). In this case, the genus that was dominant numerically did not dominate the SiO_2 incorporation of the entire diatom assemblage. This is in agreement with the few previous comparisons of PDMPO fluorescence and cell numbers for different diatom taxa within natural assemblages (Quéguiner et al. 2011; Durkin et al. 2012), but due to the low number of samples (4, including this chapter) it is unclear how often this may be the case. An alternative explanation for the discrepancy between the contribution of taxa to cell numbers and iPDMPO is that PDMPO incubation experiments did not adequately simulate *in situ* conditions, and enhanced the growth of *Thalassiosira* spp. relative to *Chaetoceros* spp. While it is difficult to simulate *in situ* conditions, incubation experiments were conducted outdoors in natural light, bottles were shaded to the same irradiance as the depth of collection, and the temperature of the incubation tank was matched to *in situ* temperatures. Therefore, the observed discrepancy between cell numbers and iPDMPO likely reflects a real difference in the composition of the diatom community present and the diatom community actively silicifying. If taxa specific SiO_2 incorporation consistently differs from cell numbers, the use of PDMPO as a tracer may considerably alter interpretation of diatom community composition.

2.5. Recommendations and Implications of this work

Overall, PDMPO was a useful tracer of SiO_2 incorporation in marine diatoms. The incorporation of PDMPO into diatom frustules was strongly correlated with the incorporation of SiO_2 in laboratory cultures and natural assemblages of diatoms. However, the relationship between SiO_2 and PDMPO incorporation did not have a fixed stoichiometry and changed with extracellular PDMPO concentration. In addition, concentrations of PDMPO $\geq$500 nmol L^{-1} may reduce diatom growth. Therefore, I recommend that PDMPO be added to a final concentration of 125 nmol L^{-1} for use as a tracer of SiO_2 incorporation in marine diatoms. When this concentration is used, the amount of SiO_2 produced since the time of PDMPO addition can be calculated from the

pPDMPO concentration measured in cells lysed with HCl (frustule only pPDMPO) using the Si:PDMPO ratio of 4200 ± 380:1.

This ratio consistently predicted more ρ_{PDMPO} than the Leblanc and Hutchins (2005) ratio, and better agreed with ρ_{GROSS} measured in Saanich Inlet. Measurements of pPDMPO were strongly correlated with ρ_{GROSS} in a marine location when ρ_{GROSS} was high (>1 µmol L^{-1} d^{-1}) but ρ_{PDMPO} sometimes over-estimated SiO_2 incorporation relative to ρ_{GROSS} when rates were low. In some cases, this was due to high dinoflagellate abundance relative to diatoms (dinoflagellates >95%). In these cases, PDMPO should not be used as a tracer of SiO_2 incorporation. In addition, PDMPO appeared to over-estimate SiO_2 production when $Si(OH)_4$ concentrations were below 10 µmol L^{-1}. The extent of this effect is difficult to determine, and can only be assessed with further experimentation. However, the strong correlation between ρ_{GROSS} and ρ_{PDMPO} in marine samples suggests that PDMPO remains a good tracer of SiO_2 incorporation when concentrations of $Si(OH)_4$ are above this 10 µmol L^{-1} threshold.

As a useful tracer of SiO_2 incorporation, PDMPO presents advantages over other methods used to determine total diatom SiO_2 incorporation. PDMPO is more affordable and less controlled by regulation than ^{32}Si, and is more sensitive for detecting increases in SiO_2 than measurements of unlabelled diatom frustules. As a result, PDMPO should allow more measurements of SiO_2 incorporation in the marine environment. This will enable better understanding of the processes that drive diatom productivity and the links between Si and carbon cycling in the ocean.

Not only can PDMPO be used to measure total diatom community SiO_2 production, but it can also be used to determine cell specific SiO_2 incorporation. This is because PDMPO can be reliably quantified by widefield fluorescence microscopy. In order to quantify PDMPO by microscopy, I emphasize that calibration is necessary to account for differences in excitation light intensity and also unevenness of illumination across the FOV. In addition, low NA microscope objectives should be used to maximize the depth

of focus captured, and avoid biased measurements between different species that may be introduced by high NA objectives. When these recommendations are followed, PDMPO fluorescence can quantified on a per cell basis by widefield microscopy.

By measuring PDMPO fluorescence per cell, the contribution of diatom taxa to community SiO_2 incorporation can be determined, which may frequently differ from the contribution of taxa to cell numbers. Cell numbers are most commonly used to assess the contribution of diatom species to the community, and if the importance of taxa to cell numbers consistently differs from the importance of taxa to PDMPO measurements, this could considerably change understanding of diatom community dynamics. The PDMPO tracer allows actively productive cells to be distinguished from inactive, and the most significant taxa to diatom SiO_2 incorporation to be determined. This is important, because diatom taxa vary in their ability to take up nutrients, the grazing pressure they experience, and the efficiency at which they are exported to depth. Therefore the taxonomic composition of the assemblage contributing to productivity has consequences for its fate. By determining the contribution of different taxa to community production rates, PDMPO has the potential to illuminate the relationship between cellular activity and community scale productivity. This will enable better understanding of the role of diatom community composition in elemental cycling within the ocean.

Chapter 3: Illuminating Diatom Community Dynamics on the West Coast of Vancouver Island

3.1. Introduction

The west coast of Vancouver Island has the highest annual average phytoplankton biomass of the entire west coast of North America (Ware and Thomson 2005). Large nutrient inputs to the continental shelf support the high phytoplankton biomass observed in this region, which in turn supports highly productive fisheries. Typically, these nutrients would be supplied from deeper waters being upwelled onto the shelf, a wind-driven process that occurs along much of the west coast of North America in summer (Hickey and Banas 2008). While this process does supply nutrients to the west coast of Vancouver Island, upwelling in this region is weaker compared to areas further south (Thomson 1981), and consequently plays less of a role in supporting the high phytoplankton biomass observed. Rather the high nutrient concentrations result from a large nutrient supply originating at the south of Vancouver Island due to strong tidal mixing within the Strait of Juan de Fuca. The nutrients supplied by the Strait of Juan de Fuca are roughly equivalent to the supply from upwelling across the whole of the Vancouver Island and Washington continental shelves (Hickey and Banas 2008, Whitney et al., 2005). This nutrient rich Strait of Juan de Fuca water is less saline than oceanic waters, and flows out the strait at the surface of the ocean onto the shelf. Combined with the wide continental shelf at the south of the island (Hickey and Banas 2008) these large nutrient inputs contribute to the high phytoplankton biomass of this region.

Nelson et al. (1995) observed that diatoms often dominate phytoplankton communities at times and locations of high productivity, and this is true off the coast of Vancouver Island (Harris et al. 2009). However, diatoms are not well studied in this region. As diatoms require silicic acid ($Si(OH)_4$, Del Amo and Brzezinski, 1999) in order to produce their silica (SiO_2) frustules, measuring biogenic SiO_2 concentrations ($bSiO_2$) and production rates are a useful for examining the diatom component of the phytoplankton communities in natural waters. Though previous work has determined diatom cell

numbers (Harris et al. 2009) and the $bSiO_2$ content of sediment traps (Pena et al. 1999), no studies have reported $bSiO_2$ concentrations or production in surface waters of this region.

In order to better understand diatom community dynamics, the fluorescent dye PDMPO (Lysosensor DND-160, Life Technologies) can be used to label newly produced $bSiO_2$ (Shimizu et al. 2001). The incorporation of PDMPO into diatom cells is proportional to SiO_2 incorporation (Leblanc and Hutchins 2005, Chapter 2 of this thesis), which allows PDMPO to be used as a quantitative tracer of $bSiO_2$ production. Although the use of PDMPO to quantitatively label newly synthesized $bSiO_2$ in diatom cells has been known for a decade (Leblanc and Hutchins 2005), few studies have used this method. This is likely due to uncertainty regarding the technique, as only one study (Leblanc and Hutchins 2005) has compared $bSiO_2$ production determined by PDMPO with established methods (using the tracer ^{32}Si) for measuring of $bSiO_2$ production in the field. To increase confidence in the PDMPO method, more comparisons are needed with established techniques for determining $bSiO_2$ production.

One advantage of the PDMPO technique over other methods is that PDMPO can be quantified per cell by fluorescence microscopy (Znachor and Nedoma 2008; Durkin et al. 2012, Chapter 2) allowing the determination of $bSiO_2$ production per species in a mixed diatom assemblage. In controlled laboratory experiments, measurements of PDMPO fluorescence by microscopy were as reliable a tracer of SiO_2 incorporation in diatoms as PDMPO measured by fluorometry (Chapter 2). However, it is currently unknown whether this agreement between methods will hold for field samples, as additional variability between samples (e.g. sample storage length, minor differences in sample preparation) could affect microscopic measurements of PDMPO.

Prior to the development of the PDMPO method, cell numbers were conventionally used as an indicator of the importance of different diatom species to the phytoplankton community. However, diatom species vary by several orders of magnitude in size (Sarthou et al. 2005), and $bSiO_2$ per cell is correlated with diatom surface area

(Brzezinski 1985; Marchetti and Harrison 2007). As a result, two diatom cells could contribute equally to cell numbers, but contain very different amounts of $bSiO_2$ if they differed in size. Additionally, cell numbers are a measure of concentration, while in many cases it would be useful to relate community composition to production rates. Neither cell numbers nor $bSiO_2$ concentrations are rate measurements, whereas PDMPO can indicate $bSiO_2$ production rates for different taxa within a mixed community. For the few comparisons between cell numbers and PDMPO incorporation that exist, diatom community composition determined by cell numbers was not the same as determined by PDMPO (Quéguiner et al. 2011; Durkin et al. 2012, Chapter 2). However, together these studies represent only four samples, so it is yet unknown whether cell numbers and PDMPO fluorescence often yield different information about diatom community dynamics.

The objectives of the present study are to:

1. Investigate the diatom community on the west coast of Vancouver Island by:
    a. Determining the spatial distribution of diatoms and $bSiO_2$ production during spring and late summer
    b. Examining diatom community composition using cell numbers and PDMPO microscopy
2. Assess the performance of the PDMPO method by:
    a. Comparing $bSiO_2$ production rates determined using PDMPO with other established methods
    b. Determining the agreement between measurements of PDMPO fluorescence by fluorometry and microscopy in natural assemblages

3.2. Methods

3.2.1. Study Area and Sampling

Sampling was conducted during two cruises aboard the CCGS John P. Tully in May and September 2012 (Fisheries and Oceans Canada (DFO) cruises 2012-25 and 2012-59 respectively). Eight stations were sampled per cruise, generally with an on shelf and off

shelf station paired perpendicular to the coast (Figure 3.1). Stations were considered to be on shelf or off shelf if the bottom depth was less or more than 200 m, respectively. All seawater samples were collected from the depth of the chlorophyll *a* (chl *a*) maximum as determined from *in situ* fluorescence profiles determined with a Seabird SBE911 conductivity, temperature and depth (CTD) profiler equipped with sensors for chl *a* fluorescence and photosynthetically active radiation (PAR). Water samples were collected in 10 L Niskin bottles as part of a rosette sampling system combined with the CTD profiler. For the measurements of dissolved nutrient, chl *a* and $bSiO_2$ concentrations, and for phytoplankton identification and counts, seawater was collected into acid washed carboys and kept cool and in the dark until subsampling. For determination of $bSiO_2$ production rates, acid cleaned polycarbonate incubation bottles were filled with seawater directly from the Niskin bottles. Additional details of sample collection can be found in Table 3.1.

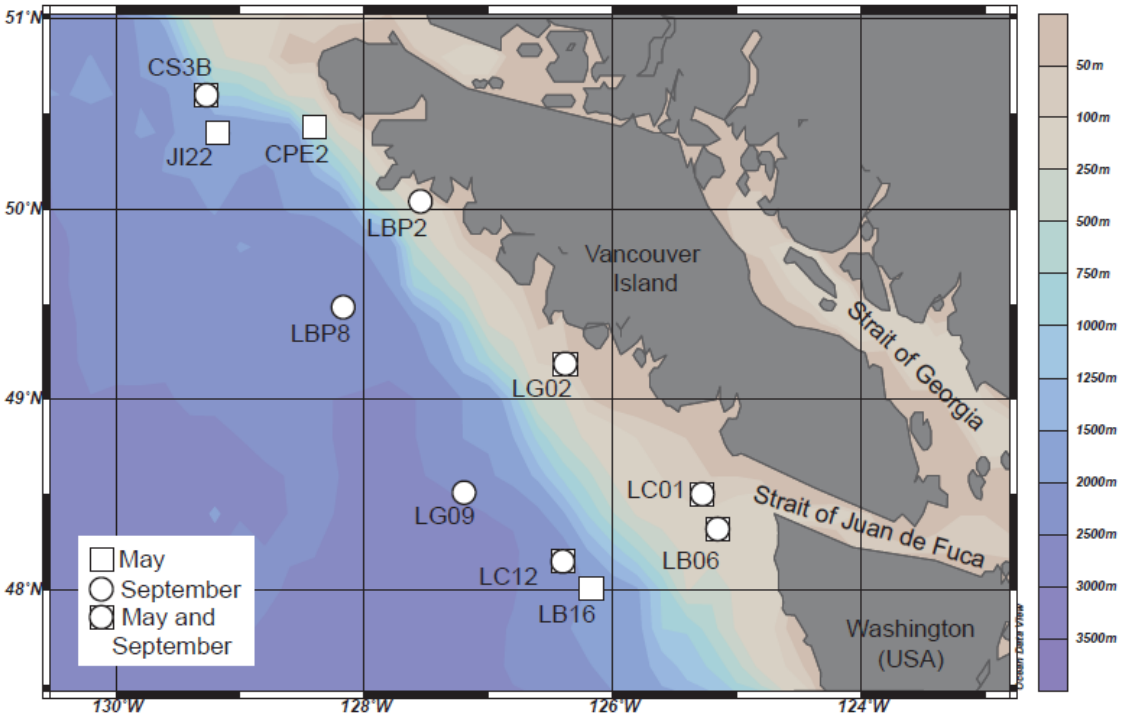

Figure 3.1: Map showing the locations of stations sampled in May and September of 2012 off the west coast of Vancouver Island. Squares indicate that stations were sampled in May, circles indicate September stations, while both shapes indicate stations that were sampled during both cruises.

Table 3.1: General sampling information and dissolved nutrient concentrations for stations sampled during May and September of 2012 (DFO cruise numbers 2012-25 and 2012-59 respectively). All samples were collected from the depth of the chlorophyll maximum. The percentage surface PAR at the depth of sampling is indicated when available. Stations are ordered from shallowest to deepest within each month.

Date	Station	Longitude ^{0}W	Latitude ^{0}N	Time	Sample Depth (m)	Bottom Depth (m)	PAR (%)	$[NO_3^-]$ (µmol L^{-1})	$[PO_4^{-3}]$ (µmol L^{-1})	$[Si(OH)_4]$ (µmol L^{-1})
May 15	LC01	125.27.73	48.40.44	9:22	5	95	49	9.33	1.03	16.85
May 15	LG02	127.19.64	48.51.14	16:30	7.5	97	29	7.87	0.86	11.66
May 13	LB06	125.15.80	48.32.12	11:26	20	115	3	1.34	0.41	2.51
May 17	CPE2	128.39.78	50.42.98	10:11	15	127	10	10.01	1.08	15.70
May 18	CS3B	129.26.99	50.59.97	15:48	11.5	218	-	4.51	0.63	10.04
May 17	JI22	129.17.33	50.39.73	15:08	8	1339	30	4.54	0.63	8.88
May 14	LB16	126.16.98	48.00.59	10:13	40	1778	2	4.77	0.70	8.59
May 14	LC12	126.39.93	48.14.99	16:34	42	2517	26	2.88	0.56	5.51
Sept 03	LC01	125.27.73	48.40.44	1:59	8	97	17	9.13	0.93	10.76
Sept 05	LBP2	127.54.36	50.04.11	4:10	13	97	-	6.95	1.04	8.08
Sept 04	LG02	127.19.64	48.51.14	8:30	8	99	21	5.55	0.86	9.36
Sept 01	LB06	125.15.80	48.32.12	9:30	10	115	28	2.00	0.38	4.06
Sept 06	CS3B	129.26.99	50.59.97	15:01	13	220	13	7.35	0.78	8.77
Sept 03	LG09	126.38.29	49.18.68	17:10	7	2060	-	1.17	0.25	2.22
Sept 04	LBP8	128.16.79	49.48.61	16:11	5	2074	62	0.24	0.24	2.10
Sept 02	LC12	126.39.93	48.14.99	8:00	27	2522	10	3.94	0.68	3.09

3.2.2. Nutrient Concentrations and Phytoplankton Biomass

Samples for measurement of dissolved nutrient concentrations (30 mL) were filtered through combusted 0.7 µm glass fiber (GF) filters and then were frozen until analysis. Samples were analyzed after return to shore on an Astoria Autoanalyzer equipped with nitrate and nitrite (hereafter referred to as NO_3^-), orthophosphate (PO_4^{-3}), and silicic acid ($Si(OH)_4$) channels according to the methods described in Barwell-Clarke and Whitney (1996). Filtration of nutrient samples with GF filters did not cause an increase in measured in $Si(OH)_4$ concentrations; however, frozen storage of these samples may cause a reduction in $Si(OH)_4$ concentrations by 15% (Chapter 4, section 4.2.2).

Samples for phytoplankton identification and enumeration (250 mL) were preserved using acidic Lugol's solution and stored in amber glass bottles. Samples were gently mixed and then 50 mL subsamples were settled for 24 hours. Settled cells were counted on an IX-70 Olympus inverted microscope using a 40x objective (Utermöhl 1958). As the focus of this study is diatom distribution and community composition, non-diatom plankton cells were grouped into two size categories: cells smaller than 5 µm, which were small coccoid or flagellate cells, and cells larger than 5 µm, which were dinoflagellate, and flagellate cells. Diatom cells were identified to genus. For simplicity, *Rhizosolenia* spp. and *Proboscia* spp. were counted together as were *Neodenticula* spp. and *Fragilariopsis* spp. due to their similar morphologies.

Samples were also collected to determine chl *a* concentrations as an indicator of phytoplankton biomass. For size fractionated chl *a* concentrations during the May cruise, triplicate samples (500 mL) were filtered through 5 µm polycarbonate (PC) filters, and the filtrate through a 0.7 µm GF filter to give two size fractions: >5 µm and 0.7-5 µm. In September, samples (500 mL) were first filtered through a 20 µm PC filter by gravity, and then through stacked 5 µm and 2 µm filters by low vacuum pressure, giving three size fractions: >20 µm, 5-20 µm and 2-5 µm. Additionally, total chl *a* concentrations were determined by filtering directly through a 0.7 µm GF filter. For consistency, results for September will be described for size fractions as in May (i.e. >5 µm and 0.7-5 µm),

with the >5 µm size fraction representing the sum of the September 20 µm and 5 µm size fractions and <5 µm size fraction calculated as the total >0.7 µm concentration less the >5 µm size fraction. Filters were placed in glass scintillation vials and frozen at -80°C until return to shore. Pigments were extracted at -20°C using 90% acetone and chl *a* concentrations determined using a calibrated Turner Designs 10-AU fluorometer using the acidification method of Parsons et al. (1984).

Seawater samples for $bSiO_2$ concentration measurement (1- 2.2L) were collected in triplicate, except at LC01 and CPE2 in May when only duplicate samples were obtained. Samples were filtered through 0.6 µm PC filters which were folded in quarters, placed in polypropylene (PP) centrifuge tubes, and frozen at -80°C until return to shore. At the laboratory, filters were dried for one week at 56°C, and then stored in a dessicator until measurement. To solubilize $bSiO_2$, samples were digested with hot NaOH for 30 minutes following the methods of Paasche (1973a) as modified by Brzezinski and Nelson (1989). Then concentrations were measured using the silicomolybdic acid assay with a modified reagent blank (Brzezinski and Nelson 1986, 1989) by determining absorbance at 810 nm on a Beckman DU UV/Vis spectrophotometer.

3.2.3. Biogenic Silica Production Rates

Biogenic silica production rates (ρ in units of µmol SiO_2 L^{-1} d^{-1}) were determined using independent incubations for three different measurements: PDMPO (ρ_{PDMPO}), change in $bSiO_2$ concentration (ρ_{NET}), and ^{32}Si (ρ_{GROSS}, September only). All incubations were conducted in an acrylic incubation tank supplied with flowing surface seawater and shaded with mesh screening to 50% of surface irradiance. However, for the majority of samples, irradiance at the depth of sampling was below 50%, and ranged from 2- 62% (Table 1). Consequently, rates of $bSiO_2$ production are likely over-estimates of the *in situ* rate at many stations, and represent potential $bSiO_2$ production. However, this should not affect comparisons between the three different methods used to determine $bSiO_2$ production rates.

PDMPO-based $bSiO_2$ production rates (ρ_{PDMPO}) were determined by spiking triplicate samples (400 mL) with PDMPO (Lysosensor DND-160, Life Technologies) as described in Leblanc and Hutchins (2005) and with modifications from Chapter 2. Samples were incubated for 24 hours with 125 nmol L^{-1} PDMPO, filtered onto 0.6 µm PC filters, and lysed with HCl at the conclusion of filtration (Leblanc and Hutchins 2005, Chapter 2). Samples were then frozen at -80°C in PP centrifuge tubes until return to shore where they were dried at 56°C for one week then stored dry. Although freezing PDMPO samples at -20°C may reduce PDMPO fluorescence, freezing samples at -80°C and then drying samples does not significantly affect PDMPO fluorescence (Appendix B). The first replicate of all May samples were analyzed after hot NaOH digestion; however, subsequent work has found that this may reduce PDMPO fluorescence (Appendix C). Other replicates were digested with 0.5 M HF for 48 hours, and digestions were stopped by adding saturated boric acid (Appendix D). Though May replicate 1 PDMPO concentrations may have been reduced, any reduction was small relative to the inherent variability between replicates. No significant differences were detected between replicate 1 and replicates 2 and 3; therefore, all replicates were included in the calculation of the average ρ_{PDMPO} for each station. PDMPO fluorescence was measured on a Trilogy fluorometer (350/80 nm excitation 410 – 600 nm emission, crude oil module). The PDMPO concentration was determined by comparing fluorescence of samples to a calibration curve of PDMPO standards prepared in the appropriate matrix (NaOH-HCl for May replicate 1, HF and boric acid for all others). Standards were prepared with a range of 0 – 100 nmol L^{-1}, and curves had low noise ($R^2 \geq 0.995$). The PDMPO fluorescence measured from these samples represents PDMPO incorporated into particles >0.6 µm, and is thus denoted pPDMPO, to distinguish from PDMPO measurements by microscopy. Measurements of pPDMPO were then converted to the amount of SiO_2 produced during the 24 hour incubation using the ratio 4200 ± 380:1 (Chapter 2), to yield a daily rate of $bSiO_2$ production based on PDMPO (ρ_{PDMPO}).

The difference in $bSiO_2$ concentrations before and after incubation was also measured from samples (2.2 L) incubated separately, to yield a net $bSiO_2$ production rate (ρ_{NET}). Unlabelled water samples were incubated for 48 hours and $bSiO_2$ concentrations were

determined at the start and end of incubation as described above. The initial concentration was subtracted from the final concentration divided by the incubation time (in days) to get a daily rate. In September, replicates from stations LC01, LB06 and LC12 were lost. Consequently, data from September LC01 is from a single bottle, September LB06 and LC12 from duplicates, while all others results presented are from triplicate incubations.

Gross silica production rates (ρ_{GROSS}) were measured by incubation of samples (300 mL) spiked with high specific activity $^{32}Si(OH)_4$ (Brzezinski and Phillips 1997; Krause et al. 2011a). Incubation bottles were spiked to a final activity of 22.2kBq (0.01 µCi) with ^{32}Si and incubated for 24 hours. Following incubation, samples were filtered onto 0.6 µm PC filters and rinsed with 0.6 µm-filtered seawater to remove excess tracer not incorporated into particles. Filters were dried at room temperature on nylon discs and, once dry, covered with Mylar film. Upon reaching secular equilibrium (~120 days), ^{32}Si activity of the samples was measured using gas-flow proportional counting (Krause et al., 2011) using a low-level beta multicounter system (Risø GM-25-5A, DTU Nutech). Gross $bSiO_2$ production rates were calculated as in Brzezinski and Phillips (1997). Unfortunately due to permitting restrictions on DFO ships these measurements were not conducted in May therefore only data from September are presented.

3.2.4. Genus Specific $bSiO_2$ Production

PDMPO fluorescence per cell was determined by microscopy as described in Chapter 2. To distinguish PDMPO quantified in particles by fluorometry from PDMPO quantified by microscopy, microscopic measurements of PDMPO fluorescence are denoted iPDMPO.

Aliquots from PDMPO incubations were used to make microscope slides by filtering samples then freeze transferring cells (Chapter 2). Diatom cell densities were assessed to determine the optimal volume for filtration, and then a subsample from the PDMPO

incubation was filtered onto a 0.6 µm PC filter. This filter was placed on a 15 µL droplet of deionized water on a microscope slide so that cells were within the droplet. Then the reverse of the slide was frozen, the filter removed and the slide was allowed to dry. Then slides were coverslipped using Pro-Long Gold mountant and stored frozen until analysis (Leblanc and Hutchins 2005). Cells were imaged using an Olympus IX-71 inverted epifluorescence microscope using a 10x (0.25 NA) objective, DAPI excitation filter (377/50nm), custom emission filter (500/140nm), and X-cite 120 PC (EXFO) light source. Incident light was calibrated at the start of each imaging session using a yellow fluorescent slide (Chroma Technology Corp, 1.5mm thick, Chapter 2). Thirty to 50 images of each slide were captured using both brightfield and PDMPO fluorescence configurations with a 12-bit QImaging camera controlled by a computer with µManager and ImageJ software (Edelstein et al. 2010; Rasband 2012). Three slides were analyzed from each station, one from each replicate incubation bottle.

Images for iPDMPO quantification were randomly selected from the images captured. Prior to quantification, the fluorescence intensity of each pixel within the sample image was normalized to the intensity of the calibration image, and then the background intensity was subtracted (Chapter 2). The fluorescence of each particle (detectable with the PDMPO fluorescence configuration, diatom cells and others) was then determined using ImageJ's particle analysis function (Chapter 2). These fluorescence values were normalized by exposure time to correct for differences between images (Znachor and Nedoma 2008).

Particles were identified using PDMPO fluorescence and brightfield images, and were categorized as Si containing (diatoms and silicoflagellate cells) or non Si (all other particles). The fluorescence of particles per mL was calculated using Equation 2 from Chapter 2, and this was determined for Si containing particles as well for all particles (non Si + Si containing). Measurements of fluorescence per mL for Si containing cells were converted to a concentration of SiO_2 produced since the addition of PDMPO using

the relationship determined from culture experiments (Chapter 2, section 2.3.2c, Equation 3):

$$\Delta[SiO_2] = \frac{iPDMPO + 212{,}000}{125{,}000}$$

where $\Delta[SiO_2]$ is the amount of SiO_2 produced since the time of PDMPO addition and iPDMPO is the fluorescence of PDMPO measured by microscopy (per mL). As all experiments were conducted for 24 hours, the $\Delta[SiO_2]$ determined yields a daily rate of $bSiO_2$ production.

The number of FOVs analyzed varied depending on the sample. Additional FOVs were analyzed until the iPDMPO of the dominant diatom genera (>15 % of total diatom iPDMPO, present in all three replicate slides) was adequately quantified. A genus was considered adequately quantified when the standard deviation between replicate slides was less than 15%. Fluorescence per genus was summed within each slide in order to determine the percentage contribution of each genus to total iPDMPO.

Surface area (SA) was also determined for 8 key genera (Table 3.2). Cell dimensions were measured from brightfield images of slides analyzed, and then SA was calculated for different genera using the formulas of Sun and Liu (2003).

3.3. Results

3.3.1. Spatial and Seasonal Distribution of Nutrients, Phytoplankton, and $bSiO_2$ Production

In general, phytoplankton cell numbers, chl *a* concentrations, and $bSiO_2$ concentrations were higher in May than in September, and higher at on shelf than off shelf stations (Figure 3.2). Similar seasonal or on/off shelf patterns were not observed for nutrient concentrations (Table 3.1). Non-diatom cells <5 µm were present in high numbers at most times and places (Figure 3.2A, B), while non-diatom cells >5 µm were found in

higher numbers during September and at some off shelf stations in May. Diatoms were most abundant in May and more abundant at on shelf than off shelf stations at this time. However, there were some exceptions; during May off shelf station JI22 had high diatom cell numbers, as did on shelf station LC01 during September. Concentrations of >5 µm chl *a* and $bSiO_2$ showed similar spatial and seasonal patterns to diatom cell numbers (Figure 3.2C, D, E, F). In contrast, <5 µm chl *a* concentrations were did not show a clear on/off shelf trend during May (Figure 3.2C), but dominated (>50%) the chl *a* present in September at all stations except LC01 and LB06 (Figure 3.2D). Overall, May off shelf and September stations had a greater proportion of non-diatom cells, while May on shelf stations had the highest diatom cell numbers, >5 µm chl *a* and $bSiO_2$ concentrations.

Silica production rates showed similar spatial and seasonal patterns to diatom cell numbers, >5 µm chl *a* and $bSiO_2$ concentrations: high in May at on shelf stations and JI22, low in September at all stations except LC01 (Figure 3.3). Patterns in ρ were similar regardless of the measurement method used, though in some cases ρ_{NET} rates were lower than ρ_{GROSS} or ρ_{PDMPO}. Times and locations of high ρ coincided with high diatom cell numbers and biomass ($bSiO_2$ concentrations).

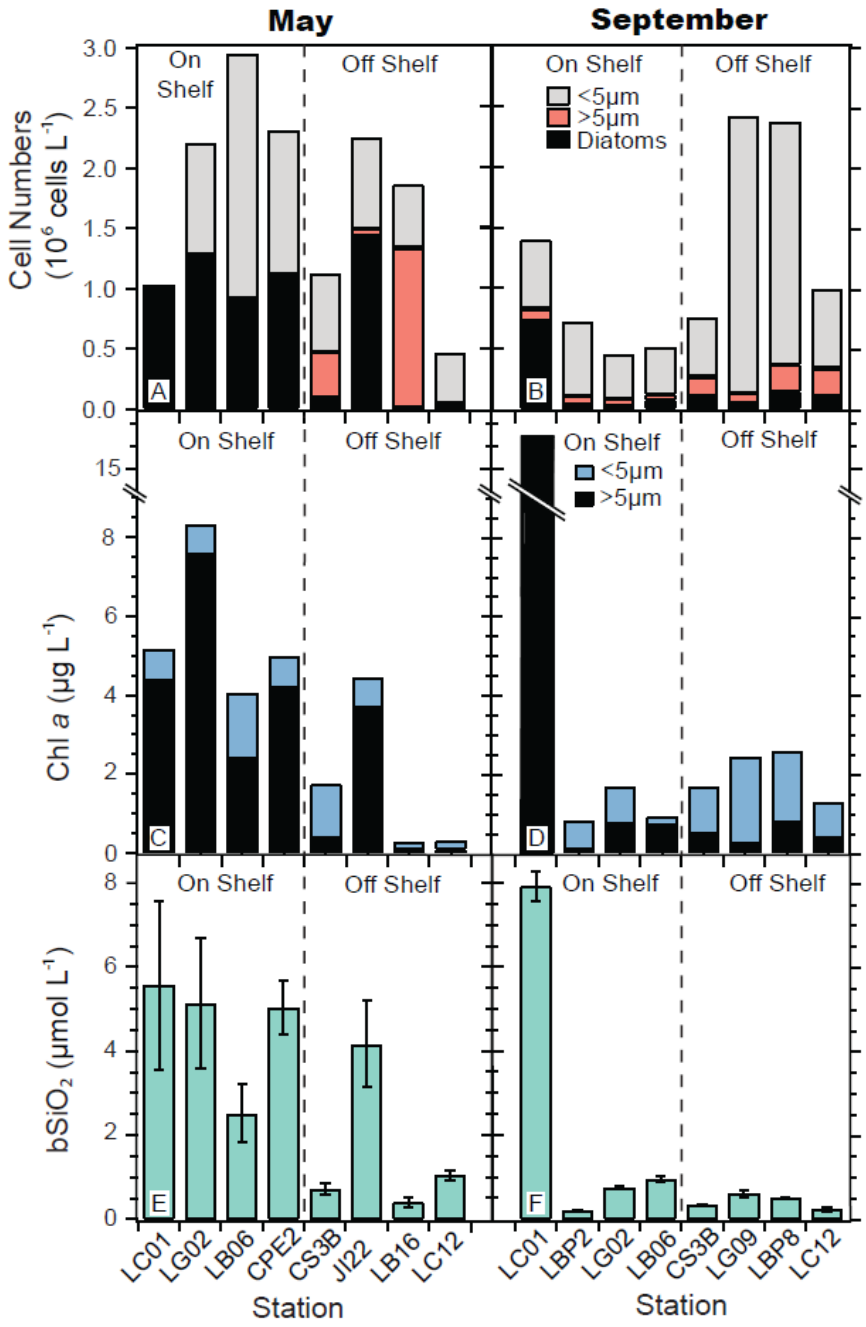

Figure 3.2: Phytoplankton cell numbers (A, B), chl *a* concentration (C, D), and $bSiO_2$ concentration (E, F) at stations sampled in May (A, C, E) and September (B, D, F). A, B) Cells were grouped into three classes: non-diatom cells <5 µm, non-diatom cells >5 µm, and diatom cells. C, D) Two size fractions of chl *a* were determined, smaller and larger than 5 µm. Stations were considered "On Shelf" if bottom depth was shallower than 200 m, or "Off Shelf" if bottom depth was >200 m. The bars for chl *a* and $bSiO_2$ concentrations represent the mean of triplicate samples (except for $bSiO_2$ in LC01 and CPE2 during May when n=2), with $bSiO_2$ error bars representing one standard deviation around the mean.

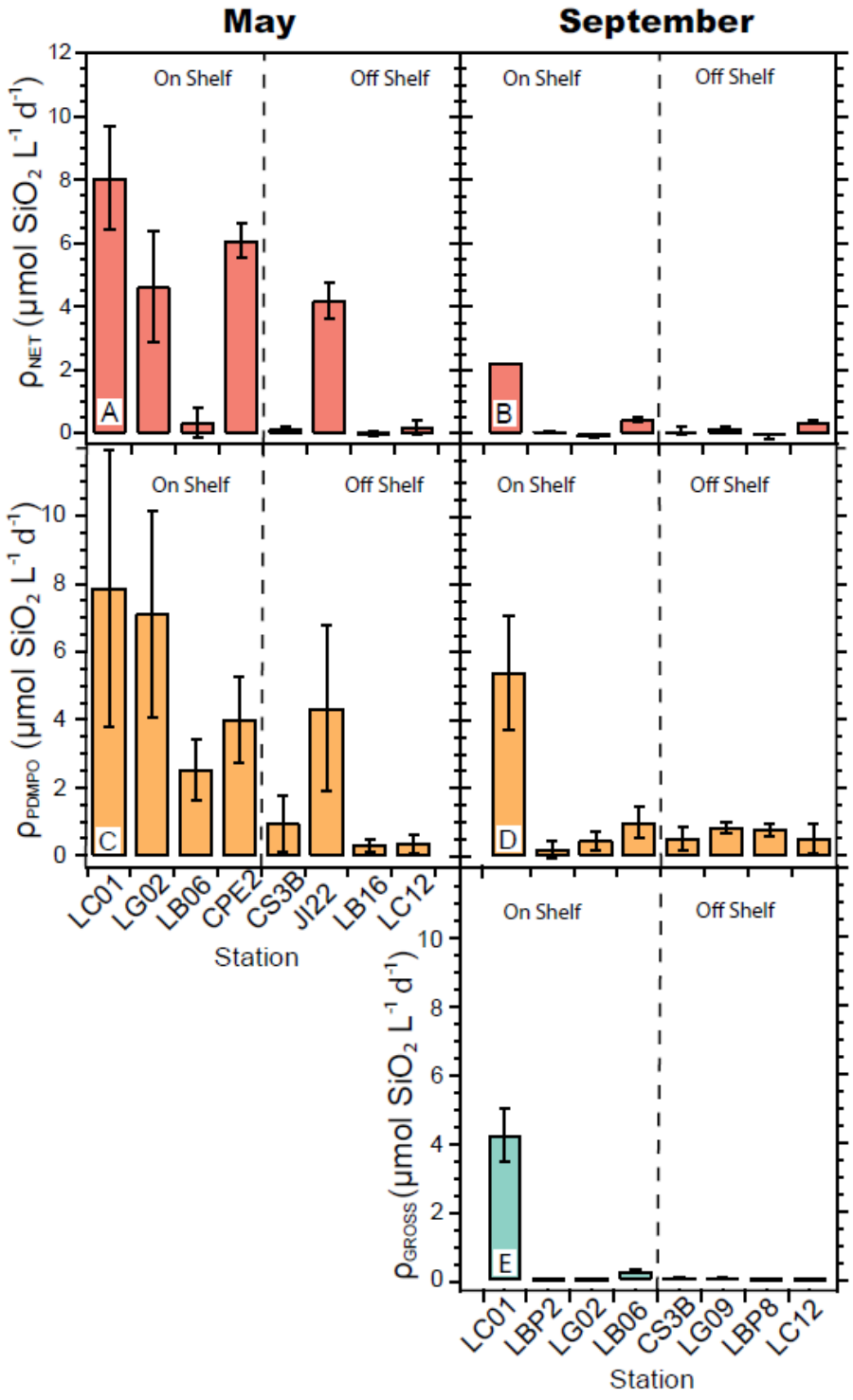

Figure 3.3: Silica production rates (ρ) determined using three different methods: net (A, B), PDMPO (converted to SiO_2 using a Si:PDMPO ratio of 4200:1) (C, D) and gross (^{32}Si) (E) for May (A, C) and September (B, D, E). For net measurements in September n = 1 for LC01, and n = 2 for LB16 and LC12, all others n = 3. For PDMPO samples, n = 4 for May LB06, LC01 and JI22; n = 2 for September LBP8 and n = 3 for all others. For ^{32}Si n = 3 for all. Error bars represent one standard deviation.

3.3.2.Diatom Community Composition on the West Coast of Vancouver Island

Eight groups of diatoms were responsible for the majority of iPDMPO measured during the sampling period (Figure 3.4, Table 3.2). Different diatom genera dominated iPDMPO at different stations with high ρ (>1 μmol SiO_2 L^{-1} d^{-1}, Figure 3.5A, C, thick pie outline). During May, iPDMPO at stations with high ρ were dominated by *Chaetoceros* spp. in the south, and *Skeletonema* spp. in the north (Figure 3.5A). During September, high $bSiO_2$ production rates occurred only at LC01, and iPDMPO at this station was dominated by *Thalassiosira* spp. At stations with low ρ (Figure 3.5A, C, thin pie outlines) *Chaetoceros* spp. and *Thalassiosira* spp. were also important to iPDMPO, with *Thalassionema* spp. and *Neodenticula* spp. contributing in addition. The contribution of different species to iPDMPO was not consistent between high or low $bSiO_2$ production stations; therefore, no assemblage type was indicative of high or low production.

Table 3.2: Cell sizes of common genera sampled. Cell dimensions were measured and surface area and volume calculated using the geometric shapes described in Sun et al. (2003).

Genus	Surface Area (μm^2)	Volume (μm^3)
Chaetoceros spp.	690	1,200
Skeletonema spp.	644	1,300
Thalassiosira spp.	2,200	7,100
Pseudo-nitzschia spp.	840	2,100
Thalassionema spp.	1,700	1,700
Rhizosolenia spp.	15,000	100,000
Fragilariopsis spp.	160	150
Coscinodiscus spp.	38,000	520,000

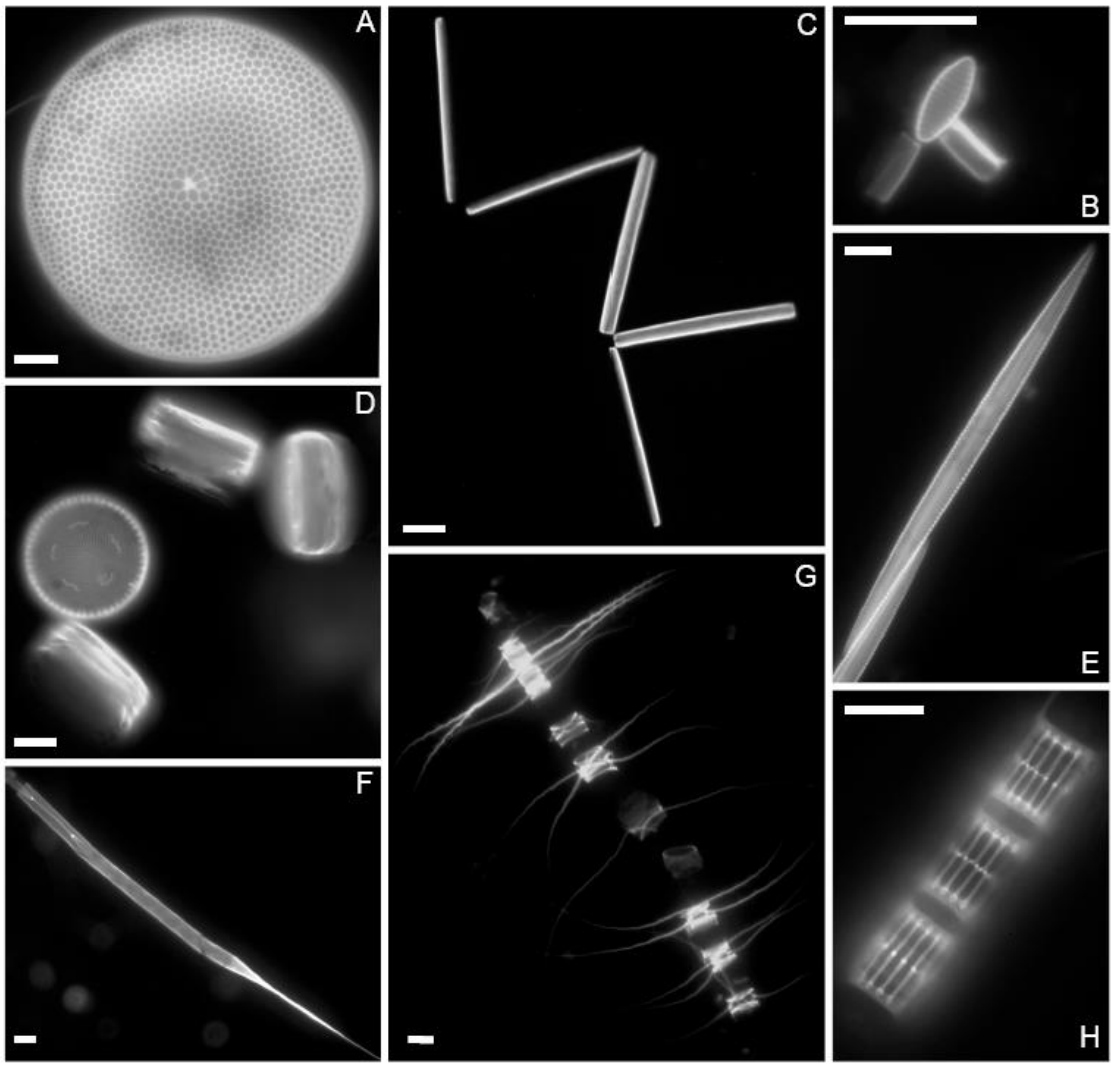

Figure 3.4: PDMPO fluorescence images of main diatom genera observed during this study: A) *Coscinodiscus* sp., B) *Fragilariopsis* sp., C) *Thalassionema* sp., D) *Thalassiosira* sp., E) *Pseudo-nitzschia* sp., F) *Rhizosolenia* sp., G) *Chaetoceros* sp., and H) *Skeletonema* sp. Scale bars represent 10 µm in all panels. Images of PDMPO labelled $bSiO_2$ were captured by fluorescence microscopy with the same microscope configuration for image analysis (see text), although higher magnification objective lenses were used (40x (0.6 NA) for B, D, F, G, or 100x (1.35 NA) for A, C, E, H).

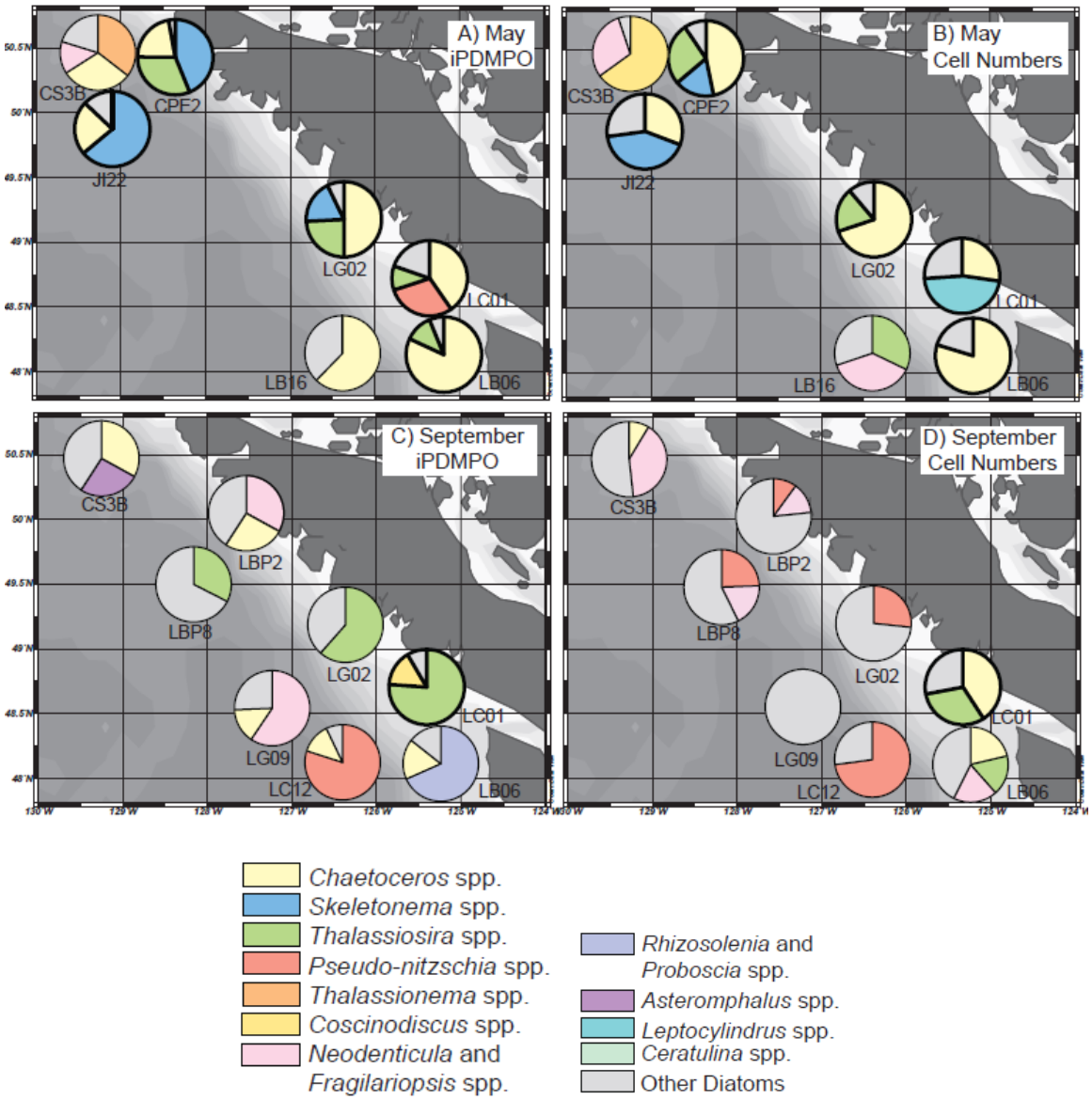

Figure 3.5: Relative contribution of diatom genera to total iPDMPO (A, C) and cell numbers (B, D) during May (A, B) and September (C, D). Pie charts are located at the approximate latitude and longitude of each station (see Figure 3.1 for exact locations). PDMPO labelled microscope slides from LC12 in May were lost, so results from this station are not presented. Colours indicate diatom genera. For simplicity, only a few genera (4 or less) are shown in each pie chart, and represent the most important to PDMPO fluorescence or cell numbers. "Other Diatoms" includes less important genera that were <10% of the total. In some cases, "Other Diatoms" represents a suite of many different genera with low contribution to the total (e.g. September LG02 cell numbers, 10 genera with <10 %). Low $bSiO_2$ production stations (less than 1 µmol SiO_2 L^{-1} d^{-1}) are indicated by thin pie outlines, while stations with higher $bSiO_2$ production are indicated with thicker outlines.

The composition of the diatom community from inferred cell numbers differed from the contribution of genera to iPDMPO (Figure 3.5B, D). In some cases, genera had high cell numbers, but contributed little to iPDMPO (e.g. *Leptocylindrus* spp. at LC01 in May, 47% of diatom cells, 0% of iPDMPO). In other cases, genera that were major contributors to iPDMPO had low cell numbers (e.g. *Rhizosolenia* spp. at LB06 during September, 68% of iPDMPO and 9% of cell numbers). Overall, the contribution of a given genus to cell numbers had little relationship to its contribution to iPDMPO (Figure 3.6).

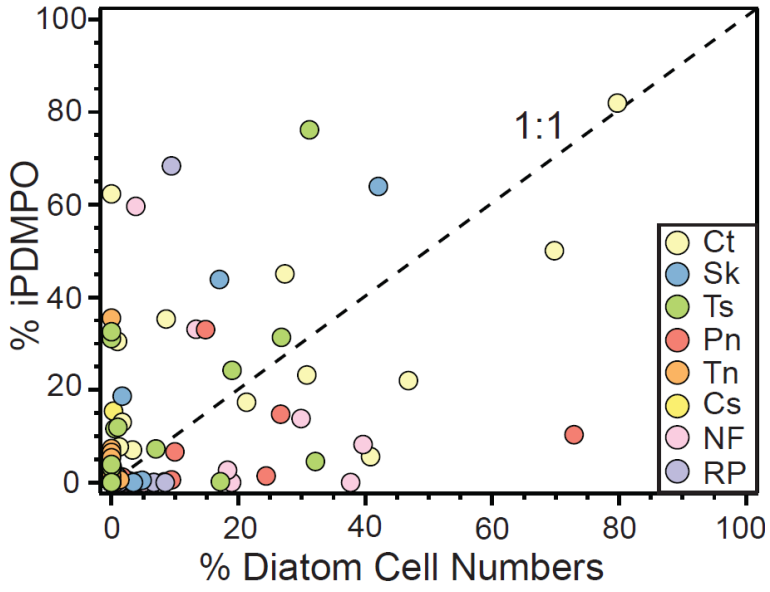

Figure 3.6: Relationship between the percentage contribution of diatom genera to PDMPO fluorescence and to cell numbers. The dashed line indicates a 1:1 relationship and colours indicate the different genera (Ct = *Chaetoceros* spp., Sk = *Skeletonema* spp., Ts = *Thalassiosira* spp., Pn = *Pseudo-nitzschia* spp., Tn = *Thalassionema* spp., Cs = *Coscinodiscus* spp., NF = *Neodenticula* spp. and *Fragilariopsis* spp., and RP = *Rhizosolenia* spp. and *Proboscia* spp.).

3.3.3. Assessing PDMPO as a Tracer of $bSiO_2$ Production

Spatial and seasonal patterns of ρ_{PDMPO} were similar to ρ_{NET} and ρ_{GROSS} (Figure 3.3). Measurements of ρ_{PDMPO} were correlated with ρ_{NET}, but with large uncertainties (Figure 3.7A). In all but one case (May CPE2), ρ_{PDMPO} incorporation was equal to or greater than ρ_{NET}. During September, ρ was only greater than 1 $\mu mol\ L^{-1}\ d^{-1}$ at one station, LC01

(Figure 3.7B, LC01 in red). Unfortunately, this limits the comparison between ρ_{PDMPO} and ρ_{GROSS} measurements. At LC01, ρ_{PDMPO} and ρ_{GROSS} were similar, and both were higher than ρ_{NET}. Consequently, when all September data was pooled, ρ_{PDMPO} and ρ_{GROSS} agreed well ($y = 1.16x + 0.41$, $R^2 = 0.99$, Figure 3.7B). However, when LC01 was excluded, ρ_{PDMPO} was 2x higher than ρ_{GROSS} on average (Figure 3.7C). Overall, ρ_{PDMPO} was generally higher than ρ_{NET} and higher than ρ_{GROSS} when rates were low (<1 µmol L^{-1} d^{-1}), but agreed with ρ_{GROSS} when ρ was higher.

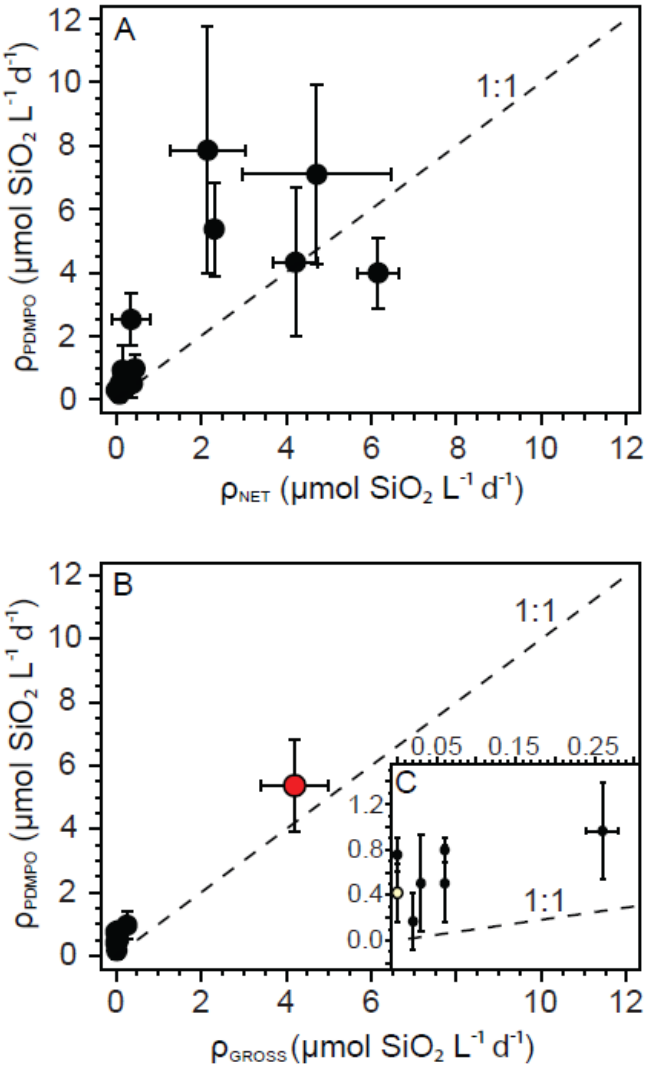

Figure 3.7: A comparison of $bSiO_2$ production rates determined using PDMPO (ρ_{PDMPO}**)** with A) net $bSiO_2$ production rates (ρ_{NET}) and B, C) gross $bSiO_2$ production rates (ρ_{GROSS}). Inlay (C) excludes LC01 (red) shown in B. Station LG02 in September is indicated in yellow in (C), and all error bars represent one standard deviation. Dashed lines indicate a 1:1 relationship.

In many cases ρ_{PDMPO} rates were higher than ρ_{GROSS} and ρ_{NET}. In order to determine whether this could be due to PDMPO labelling of non-Si containing particles, the contribution of these particles to iPDMPO was assessed. During analysis of microscope images, dinoflagellates and other non-Si particles were detected with the PDMPO fluorescence configuration (Appendix I). When the contribution of all detected particles (those with and without Si) to iPDMPO was compared with iPDMPO from only Si containing particles (diatoms and in rare occasions, silicoflagellates), the measurements were strongly correlated ($R^2 = 0.99$, Figure 3.8A). The slope of the line of best fit was 1.03, suggesting that including non-Si particles in iPDMPO measurements increased fluorescence by only 3% overall. However, at one station (LG02 in September, indicated in yellow Figure 3.8A) the majority of iPDMPO was from non-Si particles (99 ± 83 %), albeit with high variability between replicates. As the contribution of non-Si particles to iPDMPO was low at most stations, non-Si particles are unlikely to cause systemic inflation of pPDMPO measurements.

Next, the agreement between $bSiO_2$ production rates determined using pPDMPO and absolute iPDMPO measurements was assessed. Measurements of $bSiO_2$ production by the two methods were correlated ($R^2 = 0.55$). When both measurements were converted to ρ using the relationships determined from culture experiments in Chapter 2, iPDMPO determined rates generally agreed with pPDMPO rates, though with large uncertainties (Figure 3.8B).

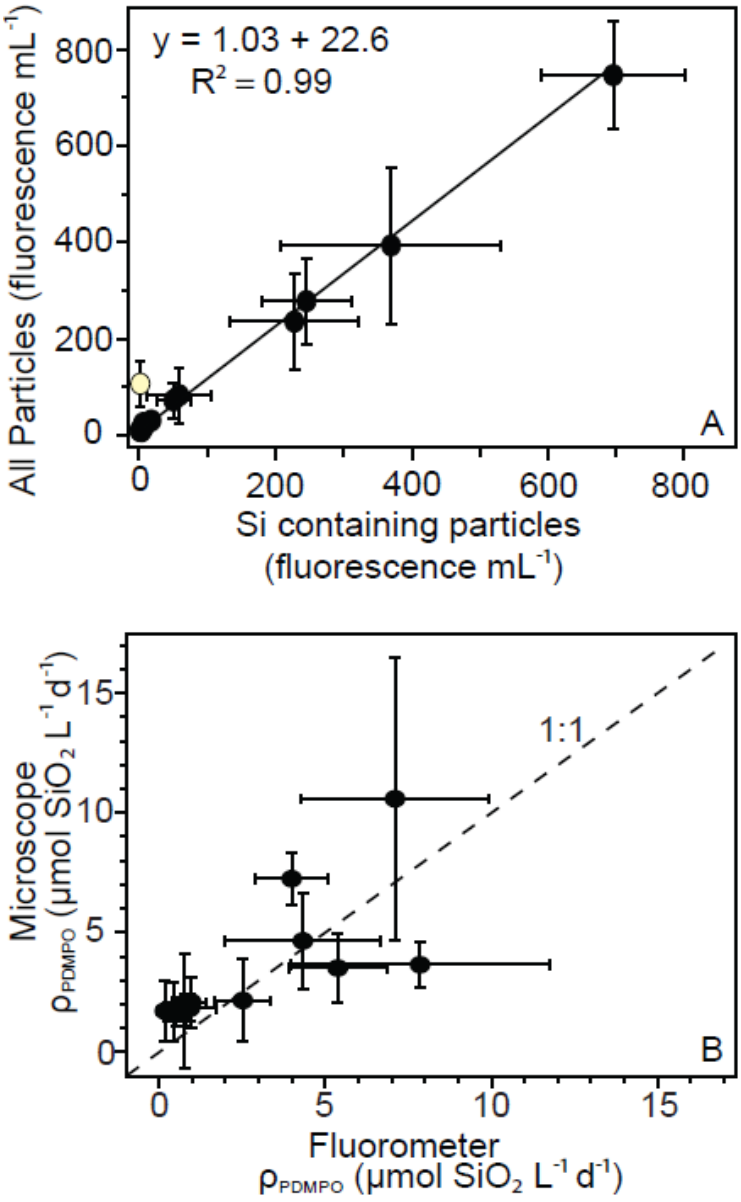

Figure 3.8: A) iPDMPO for all particles vs. iPDMPO of diatom and silicoflagellate particles (Si containing only) with Station LG02 shown in yellow. The solid line indicates the line of best fit. B) ρ_{PDMPO} determined from measurements of PDMPO by microscopy vs. fluorometry using relationships for conversion of PDMPO from Chapter 2. In panel B, microscopy values are shown only for Si containing particles, with the dashed line representing a 1:1 relationship. Microscope measurements from LG02 in May were not included, for all other stations n = 3 and error bars represent 1 standard deviation.

3.4. Discussion

3.4.1. Spatial and Seasonal Distribution of Nutrients, Phytoplankton, and $bSiO_2$ Production

Average phytoplankton biomass off the west coast of Vancouver Island is the highest of the west coast of North America (Ware and Thomson 2005). Previously, diatoms have been observed to dominate high biomass and productivity patches in this area (Denman et al. 1981; Harris et al. 2009). This is consistent with results presented here; at stations with high phytoplankton biomass (as indicated by chl *a*), diatom cell numbers and $bSiO_2$ concentrations were also high (Figure 3.2). At these stations the majority of chl *a* was from cells > 5 µm in size, and microscopic observations indicated that these large cells were almost exclusively diatoms when chl *a* concentrations were high. Overall, 76% of chl *a* was >5 µm, and therefore the majority of phytoplankton biomass sampled during this study was diatoms.

Diatom biomass and production differed between the two cruises. During spring, diatom biomass and production were higher than in the late summer (Figures 3.2, 3.3). This is typical for temperate regions, where a spring phytoplankton bloom occurs when light availability is high enough for net phytoplankton population growth (Lalli and Parsons 1997). Satellite data shows that the highest spring 2012 chl *a* concentrations in this region occurred from May 8th – May 15th, so sampling likely captured the peak of the spring bloom (Costa et al. 2013). Following the spring bloom, phytoplankton biomass is typically limited by nutrient availability, as nutrients are consumed during the bloom and not replenished until fall or winter (Lalli and Parsons 1997) except by wind mixing events. However, this is not the case for the west coast of Vancouver Island, as coastal upwelling and the Strait of Juan de Fuca supply nutrients throughout the summer (Hickey and Banas 2008; Crawford and Peña 2013). During 2012, the upwelling season did not end until October (Dewey et al. 2013), suggesting that upwelling likely supplied additional nutrients during September, though nutrient concentrations were patchy at this time (Table 3.1). Previous studies disagree regarding the seasonality of phytoplankton biomass in this region. Harris (2009) found that phytoplankton biomass was highest

during summer, and did not differ between April and October. However, samples from Harris et al. (2009) were collected during a large Pacific decadal oscillation, and may not reflect typical conditions. A peak in diatom biomass during spring is suggested by sediment trap data (Pena et al. 1996, 1999), which show high $bSiO_2$ flux out of the euphotic zone at the end of May, suggesting that diatom biomass in the surface waters may have been high earlier in spring, similar to results presented here.

Although diatom biomass and productivity was lower at most stations in September than in May, there was one major exception. Station LC01 in September had the highest chl *a* and $bSiO_2$ concentrations measured of any station during the study period, suggesting a diatom bloom (Figure 3.2). The elevated diatom biomass at this station could be due to the influence of the Juan de Fuca Eddy, an upwelling eddy that is centered over Tully Canyon (MacFadyen et al. 2008; Crawford and Peña 2013). However, station LB06 is closer to Tully Canyon, but did not have elevated chl *a* and $bSiO_2$ concentrations at this time. Previous work suggests that phytoplankton biomass may be elevated at the Juan de Fuca eddy margin, but remain low at the center (MacFadyen et al. 2008). It is possible that LC01 was at the eddy edge, leading to elevated diatom biomass, while LB06 was too close to the eddy center for this to occur. Nutrient concentrations at LC01 were the highest of September stations (Table 3.1), but concentrations at several stations remained above expected thresholds for uptake limitation (Sarthou et al. 2005). Thus nutrient concentrations alone are unlikely to explain the large biomass differences between September stations. Of all stations sampled during September, 91% of the $bSiO_2$ production occurred at LC01 (Figure 3.3E). Consequently, diatom blooms with small spatial scales may play a large role in overall production.

In addition to a seasonal pattern, diatom biomass and production also exhibited a spatial pattern. During May, most on shelf stations had higher diatom biomass and production than off shelf (Figure 3.2, 3.3). This was not observed in September, as diatom biomass and production were low at all stations except LC01. Previous studies

have found elevated chl *a* on the shelf (Mackas et al. 1980; Mackas and Yelland 1999; Harris et al. 2009), as well as higher $bSiO_2$ sinking fluxes (Pena et al. 1999). No on/off shelf pattern in nutrient concentration was observed in contrast to Mackas et al. (1980) but in agreement with Harris et al. (2009) and Peña et al. (1999). This suggests that nutrient availability is not the driver of on/off shelf patterns in diatom biomass, and that physical factors may play a more important role. Along the shelf, the buoyant Vancouver Island Coastal Current flows northwards during summer (Crawford and Peña 2013), which may increase stratification on the shelf and increase light availability to phytoplankton. This is supported by the results of Harris et al. (2009) which indicate that mixed layers off the shelf were twice as deep as on the shelf, but was not clearly evident from CTD data during 2012 sampling.

One factor that could play a role in explaining the observed differences in diatom productivity is dissolved iron (Fe) concentrations. Availability of Fe is known to limit phytoplankton productivity further offshore in the northeast subarctic Pacific (Martin and Fitzwater 1998; Boyd et al., 2004). Previous work has also found that Fe availability may limit phytoplankton productivity in the coastal upwelling region off the coast of California (Hutchins and Bruland 1998); however, Fe was sufficient for phytoplankton growth where the continental shelf is wide (Bruland et al., 2001). Off the coast of Vancouver Island, Cullen et al. (2009) found that surface water Fe concentrations decreased from a station at the shelf break to a station off the shelf. Yet even at the off shelf station, Cullen et al. (2009) observed that macronutrients were depleted, suggesting that Fe concentrations were not limiting to the phytoplankton present. Therefore, due to the wide continental shelf and previous measurements of Fe concentration, it seems unlikely that Fe limitation can explain the low phytoplankton biomass and moderate macronutrient concentrations on the continental shelf during September. Limitation by Fe could have had a role in the differences in diatom productivity between on and off shelf stations, but this is impossible to determine without measurements of Fe concentration or Fe stress within the phytoplankton present. Although no one mechanism clearly explains the spatial pattern, diatom biomass and productivity is enhanced on the continental shelf relative to off shelf regions.

Overall, diatoms dominated phytoplankton biomass during this study. As sampling was conducted only in spring and late summer, the contribution of diatoms to phytoplankton biomass may differ somewhat for an entire annual cycle. However, sampling captured the spring bloom, which is usually the time of highest phytoplankton biomass in temperate regions. Therefore, diatoms are clearly an important component of the phytoplankton in this region. On the west coast of North America, phytoplankton biomass is a strong predictor of the biomass of higher trophic levels, such as fish yield (Ware and Thomson 2005). Because much of the unusually high phytoplankton biomass on the west coast Vancouver Island is due to diatoms, this group is also an important contributor to the high fish yields in this area (Ware and Thomson 2005).

3.4.2. Diatom Community Composition

The composition of the diatom community is an important determinant of the function of an assemblage. Assemblage characteristics such as susceptibility to nutrient limitation, growth rates, and sinking rates vary based on the species present (Sarthou et al. 2005; Waite et al. 2011). Yet the composition of diatom communities has not been well studied on the west coast of Vancouver Island. During this study, *Chaetoceros* spp., *Skeletonema* spp., and *Leptocylindrus* spp. had the highest cell concentrations during spring (Figure 3.5B), as observed previously by Harris et al. (2009). When cell numbers from all stations were pooled, *Chaetoceros* spp. had the highest cell numbers (45%) overall.

Previous studies in this region have noted which species are most important to cell numbers (Mackas et al. 1980; Denman et al. 1981; Harris et al. 2009), but these may not be the most important to productivity. For the few comparisons between cell counts and PDMPO that exist (Quéguiner et al. 2011, Durkin et al. 2012, Chapter 2) cell numbers did not indicate which species were most important to PDMPO fluorescence. In this study, a consistent mismatch between the contribution of genera to cell numbers and iPDMPO was observed (Figure 3.6). Several reasons could exist for this discrepancy. It

is unlikely that the addition of PDMPO itself could have differentially affected diatom growth rate; previous work suggests that the concentration used in this study (125 nmol L^{-1}) does not decrease growth rate in laboratory cultures and field assemblages (Chapter 2, Figure 2.4, Leblanc and Hutchins 2005). Additionally, the most common genera present during sampling (*Thalassiosira* spp., *Chaetoceros* spp., and *Skeletonema* spp.) were used previously in culture experiments to determine the relationship between SiO_2 and PDMPO incorporation (Chapter 2) and grew exponentially throughout these experiments in the presence of 125 nmol L^{-1} PDMPO.

Results from Chapter 2 suggest that diatom species is a significant determinant of the relationship between SiO_2 and PDMPO incorporation. These experiments suggested that *Thalassiosira pseudonana* and *Skeletonema dohrnii* may have lower Si:PDMPO ratios than *Chaetoceros contortus*, though there was much variability in the data (Chapter 2, Figure 2.6). If *Chaetoceros* spp. did have a lower Si:PDMPO ratio than the other diatom taxa present, this might explain some of the discrepancy between cell numbers and iPDMPO observed. However, the contribution of *Chaetoceros* spp. to iPDMPO was less than its contribution to cell numbers in only 3 of 15 cases. This suggests that systemic underestimation of *Chaetoceros* spp. $bSiO_2$ production by iPDMPO relative to other taxa cannot explain the discrepancy between iPDMPO and cell numbers for this genus. Even when *Chaetoceros* spp. contributed substantially less to iPDMPO than cell numbers at station LC01 in September, this could not be entirely explained by differences between taxa in Si:PDMPO incorporation ratios. If the incorporation of Si:PDMPO is truly 2x lower in *Chaetoceros* spp. than *Thalassiosira* spp., as may be suggested by results from Chapter 2, this cannot account for the 7x less iPDMPO than cell numbers for *Chaetoceros* spp. at LC01 in September. While it is possible that species specific differences in the relationship between SiO_2 and PDMPO incorporation may contribute to some of the discrepancy between cell numbers and iPDMPO, this effect cannot entirely explain the observed results.

The contribution of diatom taxa to iPDMPO may have differed from their contribution to cell numbers because of mismatch between incubation and *in situ* conditions. For the

majority of stations, shading incubation bottles to 50% of surface irradiance would have resulted in greater light intensity than phytoplankton would have experienced *in situ* (Table 3.1). This is somewhat complicated by mixing within the water column; in some cases the chl *a* maximum was within the mixed layer and phytoplankton at this depth would have experienced a different light intensity than if they had been stationary at the depth of collection. As diatom cells likely experienced higher light intensities while incubated with PDMPO than *in situ*, it is possible that some of the observed differences between cell numbers and iPDMPO reflect a shift within incubation bottles towards species that are favoured by increased irradiance. If this were the case, a shift towards the same high light adapted taxon might be expected to occur between different stations, but this was not observed. Though some taxa were generally over-represented in iPDMPO measurements relative to cell numbers (e.g. *Skeletonema* spp.), no genus consistently dominated iPDMPO. While it is probable that increased light played a role in the discrepancy between iPDMPO and cell numbers, it is unlikely to explain the diversity of genera that contributed more to iPDMPO than to cell numbers.

Diatom species vary by several orders of magnitude in size (Sarthou et al. 2005), and among the 8 genera important for $bSiO_2$ production during this study the largest genus (*Coscinodiscus* spp.) had a SA 240 times that of the smallest genus (*Fragilariopsis* spp., Table 3.2). Consequently, if a cell of each genus were to divide once, a *Coscinodiscus* spp. cell would be expected to produce 240 times more $bSiO_2$ than a cell of *Thalassionema* spp. because $bSiO_2$ quotas per cell are correlated with cell SA (Brzezinski 1985; Marchetti and Harrison 2007). Therefore, larger cells could be expected to contribute more to $bSiO_2$ production than to cell numbers. This is apparent at station LC01 in September, where *Coscinodiscus* spp. was 15% of $bSiO_2$ production but only 0.3% of diatom cells (Figure 3.5C, D). This proportion of $bSiO_2$ production translates into 0.86 μmol L^{-1} d^{-1} from *Coscinodiscus* spp. alone, greater than the total community production from any other September station. This agrees with results from Durkin et al. (2012) which found that large rare diatom cells were important for $bSiO_2$ production at Ocean Station Papa. Therefore, large diatom species may play a significant role in community $bSiO_2$ production despite low cell numbers.

In addition to cell size, cell division rate is also an important determinant of $bSiO_2$ production, as frustule production is closely linked to the cell cycle (Martin-Jézéquel et al. 2000). When a diatom divides it produces a new frustule, with half becoming part of each new daughter cell. Consequently, the majority of $bSiO_2$ production occurs during cell division, and a genus that is not dividing will contribute little to $bSiO_2$ production. This is evident at station LC01 during May where *Leptocylindrus* spp. was 47% of diatom cells but 0% $bSiO_2$ production (Figure 3.5A, B). This is surprising, as buoyancy maintenance in diatoms requires energy (Waite et al. 2011), and cells without energy to divide would likely also lack the energy to resist sinking.

In other cases, genera that were rare numerically were important contributors to $bSiO_2$ production despite small cell sizes. At CPE2 in May, *Chaetoceros* spp. dominated cell numbers, while *Skeletonema* spp. dominated $bSiO_2$ production (Figure 3.5A, B). This discrepancy was not explained by differences in size, as the two genera had similar SAs (Table 3.2). Therefore, *Skeletonema* spp. likely had a higher cell division rate leading to higher $bSiO_2$ production by this genus.

Interestingly, $bSiO_2$ production of high productivity assemblages (> 1 μmol Si L^{-1} d^{-1}) was dominated by different genera at different stations (Figure 3.5). *Chaetoceros* spp. dominated $bSiO_2$ production at southern stations on the shelf in May, and was responsible for 34% of $bSiO_2$ production overall. Northern stations in May were dominated by *Skeletonema* spp. (17% of $bSiO_2$ production overall), while *Thalassiosira* spp. dominated $bSiO_2$ production at LC01 during September and was responsible for 25% overall. In contrast, *Chaetoceros* spp. was much more dominant numerically (45% of total diatom cells), while *Skeletonema* spp. and *Thalassiosira* spp. were rarer (12 and 13% of total diatom cells respectively). Differences in species composition during May at high productivity stations did not seem to be driven by differences in nutrient concentration, which did not have an obvious spatial trend. However, at the southernmost *Chaetoceros* spp. dominated stations (LB06 and LC01) surface seawater was 1.7 °C warmer and 1.6

psu fresher than stations where *Skeletonema* spp. dominated (CPE2 and JI22). During May, $Si(OH)_4$ concentrations were 1.8 ± 0.2x higher than nitrate concentrations, while at LC01 in September $Si(OH)_4$ and nitrate concentrations were similar. Perhaps the lower availability of $Si(OH)_4$ relative to nitrate at this station contributed to dominance of *Thalassiosira* spp. with respect to $bSiO_2$ production. As different genera dominated $bSiO_2$ production at different high productivity stations, no genus indicated high $bSiO_2$ production rates.

Both cell numbers and genus specific $bSiO_2$ production rates are useful to describe the diatom community. Cell numbers represent the concentration of cells present, whereas $bSiO_2$ production represents a rate. Both concentration and rate measurements are important for understanding the role of the diatom community in the ecosystem. In order to link community composition to inventory measurements (e.g. POC, chl *a*, and $bSiO_2$ concentrations; particulate ratios) cell counts are not as useful as biomass measurements, because of large variability between diatom species in cell size. But many measurements of the diatom community are rates, for example uptake, productivity and export rates. In these cases cell numbers are not useful, and species specific productivity rates are more informative. It is possible to infer species specific $bSiO_2$ production rates using PDMPO, which should insight into the relationship between community composition and community wide fluxes.

3.4.3. PDMPO as a Tracer of $bSiO_2$ Production

PDMPO was a useful tracer of $bSiO_2$ production in this study. Spatial and seasonal patterns of $bSiO_2$ production determined from PDMPO largely matched those determined using net and gross methods. Silica production rates determined with PDMPO were generally higher than net $bSiO_2$ production (Figure 3.7A). The net $bSiO_2$ method production measures the difference in unlabelled $bSiO_2$ concentrations between two time points. As both production and dissolution affect the amount of unlabelled $bSiO_2$ measured after incubation, this yields a net rate. However, dissolution is unlikely to affect tracer based measurements of $bSiO_2$ production (e.g. PDMPO, ^{32}Si) during

incubations conducted for only 24 hours. This is because dissolution rates in healthy diatoms are low (Bidle and Azam 1999), and for a tracer to become incorporated into the frustule a diatom must be producing $bSiO_2$. While dissolution may be occurring, the small amount of $bSiO_2$ that dissolves during the incubation will likely not be labelled. The probability is low that a tracer could become incorporated into the frustule, and then this labelled SiO_2 could subsequently dissolve during a 24 hour incubation. As a result, tracer methods yield closer to a gross rate of $bSiO_2$ production. Therefore, PDMPO likely represents a gross measurement of $bSiO_2$ production, and ρ_{PDMPO} is expected to be greater than ρ_{NET}.

When compared to ρ_{GROSS}, ρ_{PDMPO} agreed at LC01 where $bSiO_2$ production rates determined by all methods was high (Figure 3.7B). However, at other stations in September, $bSiO_2$ production rates were low (Figure 3.3D, E) and pPDMPO over-estimated $bSiO_2$ production relative to ^{32}Si by 37% on average, with much variability between stations (Figure 3.4C). Overestimation of $bSiO_2$ production measured by pPDMPO at rates below 1 $\mu mol\ L^{-1}\ d^{-1}$ has been observed previously in Saanich Inlet (Chapter 2) and in some cases this occurred when dinoflagellates dominated the phytoplankton. During this study, dinoflagellates were observed with the PDMPO fluorescence microscope configuration (Appendix I), suggesting that dinoflagellates may incorporate PDMPO in some way, or alternatively have endogenous fluorescence in the same spectrum. Previous work has suggested that dinoflagellate cells may bind PDMPO extracellularly and contribute to measurements of pPDMPO (Alvarado 2012). However, fluorescence of dinoflagellates observed appeared to be within the cell in the present study (Appendix I). Overall, dinoflagellates contributed little to measurements of iPDMPO (Figure 3.8A). At station LG02 in September, the contribution of non-diatoms to fluorescence was higher, though it is unclear why this might be. Regardless, the high iPDMPO measured at LG02 during September did not correlate with inflated ρ_{PDMPO} relative to ρ_{GROSS} (Figure 3.7B). Perhaps fluorescence associated with dinoflagellates and non-diatom cells was removed similarly to intracellular diatom fluorescence by rinsing with HCl during pPDMPO sample filtration. Therefore, dinoflagellates are

unlikely to be the cause of over-estimation of $bSiO_2$ production rates by PDMPO during September experiments.

Another factor that may increase PDMPO incorporation relative to $bSiO_2$ production is decoupling between PDMPO and SiO_2 incorporation into the frustule. As the relationship between PDMPO and SiO_2 incorporation into the frustule reflects their respective concentrations within the silicon deposition vesicle (SDV, Durkin et al. 2013, Chapter 2) factors that differentially affect PDMPO or SiO_2 accumulation within the SDV will decouple their incorporation into the frustule. Low $Si(OH)_4$ concentrations may limit uptake of $Si(OH)_4$ by diatom cells, reducing SiO_2 accumulation within the SDV without a corresponding effect on PDMPO accumulation. It is likely that this caused an overestimation of PDMPO incorporated into $bSiO_2$ during this study relative to culture experiments (in which $Si(OH)_4$ was always present at high concentrations, >80 µmol L^{-1}), and could explain the greater $bSiO_2$ production measured by PDMPO compared to that measured by ^{32}Si. There is some evidence for this in Saanich Inlet, where ρ_{PDMPO} was over-estimated relative to ρ_{GROSS} in the only sample where $Si(OH)_4$ concentrations were less than 10 µmol L^{-1}. Silicic acid concentrations ranged from 2.10–10.76 µmol L^{-1} during the September cruise, and these concentrations are low enough to reduce $Si(OH)_4$ uptake in some species (Sarthou et al. 2005). However, it may be possible to correct for the effect of reduction in $Si(OH)_4$ uptake assuming Michelis-Menten kinetics of $Si(OH)_4$ uptake. Such a correction could have the form:

$$\rho\text{PDMPOc} = \text{pPDMPO} \times 4200 \times \frac{[Si(OH_4)]}{([Si(OH_4)] + 4)} \qquad \textbf{Equation 4}$$

where ρ_{PDMPOc} is the rate of $bSiO_2$ production based on pPDMPO after correction, pPDMPO is the concentration of PDMPO measured from HCl lysed samples, 4200 is the ratio of Si:PDMPO from Chapter 2, $[Si(OH)_4]$ is the silicic acid concentration, and 4 was chosen as an approximate K_{Si} value as it is the average for diatoms (Sarthou et al. 2005). When such a correction was applied to pPDMPO measurements from September samples with $Si(OH)_4$ concentrations below 10 µmol L^{-1}, the agreement between ρ_{PDMPOc} with

ρ_{GROSS} was improved (R^2 = 0.67, y = 1.03x + 0.222). Therefore, it is probable that low $Si(OH)_4$ causes reduced accumulation of SiO_2 relative to PDMPO within the frustule, and this effect needs to be considered when utilizing the PDMPO method to estimate $bSiO_2$ production. However, this does not appear to affect $bSiO_2$ production rates >1 μmol L^{-1} d^{-1}, and further experimentation is needed to determine how to best account for the effect $Si(OH)_4$ concentration when calculating ρ_{PDMPO}.

Previous work has suggested that iPDMPO measurements may be as reliable for quantifying $bSiO_2$ production as pPDMPO (Chapter 2, Figure 2.9). This suggests that measurements of community scale $bSiO_2$ production (net, gross and pPDMPO based) could be replaced by iPDMPO measurements. During this study, iPDMPO measurements agreed with pPDMPO measurements for determining $bSiO_2$ production (Figure 3.8B). Accurate quantification of several of the dominant genera in this region (*Chaetoceros* spp., *Skeletonema* spp., *Thalassiosira* spp., *Pseudo-nitzschia* spp. and *Coscinodiscus* spp.) have been confirmed previously with the microscope configuration used here (Chapter 2), which improves confidence in these measurements. This is despite differences in the preparation of the microscope slides between studies- slides from Chapter 2 were prepared using Immu-mount mountant whereas in this study they were prepared with ProLong Gold. However, the relationship used to convert iPDMPO to ρ_{PDMPO} is specific to the microscope configuration, and intercalibration would be necessary before this relationship could be more widely applied. Although microscopy and fluorometry measurements of PDMPO generally agreed, this was with high variability in measurements. This suggests absolute PDMPO fluorescence determined from microscopy cannot be reliably converted to absolute $bSiO_2$ production rates, and therefore this method should not be relied on as a substitute for pPDMPO measurements or other measurements of $bSiO_2$ production rates. Therefore, relative contributions of different diatom taxa to community $bSiO_2$ production can be determined by microscopy and should be combined with community scale measurements of $bSiO_2$ production in order to determine both the contribution of different genera and absolute rates.

3.5. Conclusions

During this study, the majority of phytoplankton biomass was composed of diatoms. Diatom biomass and productivity were generally higher during spring than late summer, and higher on than off the continental shelf. Consequently, diatoms are key contributors to the high phytoplankton biomass and may be responsible for the high fisheries yields in this area.

The composition of the diatom community is an important determinant of the role of the community within the ecosystem. Different diatom genera dominated $bSiO_2$ production at different locations, and the importance of a genus to $bSiO_2$ production was not correlated with its contribution to cell numbers. In order to link community scale fluxes to assemblage composition, the composition of the productive assemblage must be determined. This differs from the composition of the assemblage present, and can be determined using PDMPO.

PDMPO was a useful tracer of $bSiO_2$ production and more closely approximates a gross rather than net rate of production. The tracer was reliable when $bSiO_2$ production rates were high (> 1 μmol L^{-1} d^{-1}), but over-estimated production when rates were low. This was not due to PDMPO staining of dinoflagellates, and was likely due to variability in $Si(OH)_4$ concentrations, though more work is needed to assess this effect. In this study, measurements of PDMPO fluorescence by microscopy agreed with measurements by fluorometry, but with large associated uncertainty. Therefore, measurements of PDMPO by microscopy should be used in combination with other methods to determine the productivity of different groups within the diatom community.

Chapter 4: Highlighting Taxa Specific Production of Diatoms in Saanich Inlet

4.1. Introduction

Diatoms are microscopic phytoplankton estimated to account for 32- 40% of marine primary production (Nelson et al. 1995; Uitz et al. 2010). This large role in global primary productivity makes them a key component of the global carbon cycle as well as the foundation of many productive food webs. Because diatoms require $Si(OH)_4$ to build their hydrated biogenic silica ($bSiO_2$) frustules (Del Amo and Brzezinski 1999; Kröger and Poulsen 2008), diatoms link the biogeochemical cycles of carbon and silicon in the ocean.

Although diatoms share many traits and belong to the same taxonomic group, the Stramenopiles, large differences can be found among species. Physiologically, diatoms species can differ in their ability to take up nutrients. For example the half saturation constant for $Si(OH)_4$ (K_{Si}), a key determinant of $Si(OH)_4$ uptake and limitation, varies by over 2 orders of magnitude between species (Sarthou et al. 2005) and therefore it is possible for different diatom species to be differentially limited within the same community (Poulton et al. 2007). Such differences in nutrient physiology within members of the diatom community affect the nutrient uptake kinetics of the community as a whole (Blain et al. 1997; Mosseri et al. 2008). Community composition also affects the export of carbon from the system, as species experience differences in grazing pressure (Frost 1972; Sunda and Hardison 2010), as well as differ in the efficiency with which they are exported from the euphotic zone to depth (Waite and Nodder 2001; Annett et al. 2009; Smetacek et al. 2012). Thus, diatom community composition affects the fluxes to the rest of the marine ecosystem.

In the past 15 years a new method has been developed for investigating diatom community composition using the fluorescent dye 2-(4-pyridyl)-5-((4-(2-

dimethylaminoethylaminocarbamoyl)methoxy)-phenyl)oxazole (PDMPO). This dye labels newly produced $bSiO_2$ (Shimizu et al. 2001), and the incorporation of PDMPO is strongly correlated with $bSiO_2$ production (Leblanc and Hutchins 2005, Chapter 2). Since relative amounts of PDMPO can be accurately quantified by fluorescence microscopy (Chapter 2), this tracer allows $bSiO_2$ production for different diatom species to be determined in a mixed assemblage. This determines a production rate, unlike the most common assessment of diatom community composition, diatom cell numbers, which yields a concentration. Previous work with PDMPO suggests that the composition of the diatom community responsible for $bSiO_2$ production differs from the composition determined from cell numbers (Quéguiner et al. 2011; Durkin et al. 2012, Chapter 2, Chapter 3).

This difference between $bSiO_2$ production and cell numbers could be due to differences between diatom taxa in the amount of $bSiO_2$ per cell, or differences in the rate of $bSiO_2$ production per amount of $bSiO_2$ (specific $bSiO_2$ production rate). The amount of $bSiO_2$ per cell is related to a cell's size, and because $bSiO_2$ is found at the periphery of a cell it is dependent on a cell's surface area (Brzezinski 1985; Marchetti and Harrison 2007). The results of Quéguiner et al. (2011) and Durkin et al. (2012) are consistent with differences in $bSiO_2$ production between diatom taxa due to differences in cell size. However, differences between taxa could also reflect differences in specific $bSiO_2$ production rate. If specific $bSiO_2$ production rates did not vary between taxa, the cumulative surface area of a taxon would likely explain most of the variability between taxa in $bSiO_2$ production rate, making PDMPO measurements unnecessary. No previous studies have used PDMPO to calculate specific $bSiO_2$ production rates for different diatom taxa within a mixed assemblage. Therefore, further work is needed to determine the roles that $bSiO_2$ cell quota and specific $bSiO_2$ production rate play in explaining taxa specific $bSiO_2$ production.

Specific $bSiO_2$ production rates may also be useful as an indicator of growth rate. Only $bSiO_2$ produced when PDMPO is present is fluorescently labelled by the tracer (Shimizu

et al. 2001). This makes it possible to distinguish diatom cells actively depositing $bSiO_2$ from those that are inactive, and PDMPO has been used for this purpose in previous studies (Leblanc and Hutchins 2005; Ichinomiya et al. 2010). Znachor et al. (2013) expand on this premise by suggesting that PDMPO fluorescence could be used as a proxy for diatom growth rate when comparing PDMPO measured for cells of the same diatom species. Technically, PDMPO measures a $bSiO_2$ production rate and when normalized to some measure of $bSiO_2$ this yields a specific $bSiO_2$ production rate, which is not strictly the same as growth rate (cell division rate). Specific $bSiO_2$ production rates are equivalent to growth rate when conditions are constant (MacIntyre and Cullen 2005), but constant environmental conditions are not possible in natural environments due to daily cycles in light intensity. Additionally, the amount of SiO_2 per diatom cell is relatively flexible, and generally diatom cells that grow slower deposit more SiO_2 before dividing (Martin-Jézéquel et al. 2000). An increase in SiO_2 per cell has been demonstrated when reductions in growth rate occur due to decreased temperature (Durbin 1977, Claquin et al. 2002), nitrogen limitation (Harrison et al. 1977, Claquin et al. 2002), phosphorous limitation (Claquin et al, 2002), and iron limitation (Marchetti and Harrison 2007). Concentrations of $Si(OH)_4$ also affect the amount of SiO_2 per cell, with $Si(OH)_4$ limitation resulting in a reduction in SiO_2 per cell (Harrison et al. 1977, Brzezinski et al. 1990) while excess $Si(OH)_4$ may cause increased SiO_2 per cell in some cases (Durkin et al. 2013). As a result, the many factors that affect the amount of SiO_2 per cell could confound the relationship between $bSiO_2$ production (indicated by PDMPO incorporation) and growth rate.

If PDMPO could indicate diatom growth rate for different taxa, it could be useful for predicting shifts in diatom community composition, before a corresponding increase in biomass. This would allow the precise timing of growth initiation to be determined, which would enable changes in diatom community composition to be better linked to their casual factors. However, Znachor et al. (2013) did not use PDMPO as an indicator of growth rate between different diatom taxa, so it is not yet known whether PDMPO would be useful for this application.

In the present study, PDMPO was used to investigate diatom community composition in Saanich Inlet. This inlet is a highly productive fjord (Takahashi et al. 1977; Timothy and Soon 2001; Grundle et al. 2009), and is one of the best-studied basins in the global ocean (Tunnicliffe et al. 2005). Diatoms are the dominant group of phytoplankton within the inlet (Parsons et al. 1983; Grundle et al. 2009), and the community composition and seasonal succession have been previously characterized using cell counts from surface water samples (Takahashi et al. 1977; Hobson 1981, 1983; Parsons et al. 1983; Sancetta and Calvert 1988; Grundle et al. 2009), sediment traps (Sancetta and Calvert 1988) and a 91 year sediment core record (McQuoid and Hobson 1997).

The aim of this study is to expand upon existing understanding of diatom community dynamics within Saanich Inlet using the PDMPO method by determining (1) if the contribution of different diatom genera to $bSiO_2$ production (based on PDMPO) can be predicted by cell count or biomass data, (2) which genera are most important to $bSiO_2$ production within the inlet, and (3) whether PDMPO can indicate shifts in diatom assemblage composition.

4.2. Methods

4.2.1. Sample Collection

Samples were collected from UBC station (48.35500 N, 123.30300 W) in Saanich Inlet from March 2012 to December 2013 aboard the RV Strickland. Samples were collected monthly for most of this time period, except during fall and winter 2012/2013 (August 2012 to February 2013) when samples were collected every two months. A Seabird 911 conductivity temperature depth profiler (CTD) equipped with chlorophyll *a* (chl *a*) fluorescence and photosynthetically active radiation (PAR) sensors was used to determine the depth of the chl *a* maximum. Samples were collected from the depth of the chl *a* maximum which varied between 2- 20 m depth, and averaged 6.5 m during the study period. Seawater was collected in 12 L Go-Flo bottles which were drained through tubing into an acid washed carboy. This carboy was kept cool and in the dark until return

to shore. Samples for all measurements described below were subsampled from this carboy, which was continually mixed to homogenize its contents. The dates and depths of sample collection are presented in Table 4.1.

4.2.2. Nutrient Concentrations

Macronutrient concentrations were determined by filtering seawater samples through pre-combusted 0.7 µm glass fiber filters (GF) using acid cleaned syringes and swinnex holders. The filtrate (30 mL) was collected in acid cleaned polypropylene bottles which were frozen at -20°C until analysis. Concentrations of nitrate and nitrite ($NO_3^- + NO_2^-$), phosphate (PO_4^{-3}), and silicic acid ($Si(OH)_4$) were determined using an Astoria 2 Nutrient Autoanalyzer, according to the methods described in Barwell-Clarke and Whitney (1996). During 2013, separate samples were collected for determination of $Si(OH)_4$ concentration. Unlike samples for other nutrients, these were pre-filtered using 0.6 µm polycarbonate (PC) filters to avoid potential leaching of Si from GF filters. Additionally, these samples were stored at 4°C until analysis, as freezing samples with high concentrations of $Si(OH)_4$ may cause polymerization (Barwell-Clarke and Whitney 1996). These separate $Si(OH)_4$ samples had 15.0 ± 4.3 % (mean ± SE, n = 10) higher $Si(OH)_4$ concentrations than those that were collected for analysis of other nutrients. This suggests that leaching of Si from GF filters did not cause inflation of $Si(OH)_4$ measurements; however, $Si(OH)_4$ concentrations presented here may underestimate actual concentrations. This may have been due to loss of $Si(OH)_4$ due to polymerization of $Si(OH)_4$ when samples were frozen or thawed.

Table 4.1: Dates and depths of sample collection, with corresponding temperature (T), salinity (S) and nutrient nitrate (NO_3^-), orthophosphate (PO_4^{-3}) and silicic acid ($Si(OH)_4$)) concentrations. The depths noted below corresponds to the depth of the chl *a* maximum from which all samples were collected. Photosynthetically active radiation (PAR) is also indicated for the depth of sampling as a percentage of the surface irradiance.

Year	Month	Day	Depth (m)	T (^{0}C)	S (psu)	PAR (%)	$[NO_3^- + NO_2^-]$ (µmol L^{-1})	$[PO_4^{-3}]$ (µmol L^{-1})	$[Si(OH)_4]$ (µmol L^{-1})
2012	March	14	5	7.2	29.4	75	25.8	2.1	21.8
2012	April	11	8	8.1	29.3	26	13.4	1.2	9.5
2012	May	9	15	8.2	29.4	9	12.4	1.3	12.9
2012	June	14	5	11.2	29.0	31	2.1	0.45	13.9
2012	July	11	7	12.6	28.1	40	0.15	0.25	9.9
2012	August	1	8	13.1	27.8	92	5.3	0.89	14.3
2012	October	10	7	12.3	28.9	38	0.42	0.59	11.6
2012	December	12	2	7.9	25.3	65	17.4	1.5	29.3
2013	February	13	5	8.4	29.5	70	23.1	2.3	31.2
2013	March	13	3	7.8	29.4	48	16.1	1.5	28.1
2013	April	17	8	8.5	29.3	4	19.5	-	33.3
2013	May	8	20	9.4	29.2	2	8.7	-	9.4
2013	June	13	7	12.0	28.0	100	2.2	-	12.5
2013	July	10	5	15.5	25.3	50	6.0	-	33.0
2013	August	1	4	16.8	28.0	35	0.44	-	19.4
2013	September	11	3.5	16.0	28.9	97	6.8	-	33.8
2013	October	9	3.5	11.8	28.5	80	13.3	-	23.2
2013	November	13	3	-	-	-	13.9	-	26.2
2013	December	9	5	8.8	28.5	34	20.6	-	35.0

4.2.3. Phytoplankton and Diatom Biomass

Triplicate samples were collected for determination of phytoplankton biomass, measured as chl *a*. Chlorophyll *a* concentrations were determined for the total phytoplankton assemblage by filtering seawater (300- 500 mL) through 0.7 µm GF filters. Chlorophyll *a* concentrations were also determined for different size fractions, and filtration procedures differed between 2012 and 2013. During both years, seawater (300 – 500 mL) was first filtered through a 20 µm PC filter by gravity. In 2012 this was followed by low vacuum pressure (<5 psi) filtration through stacked 5 µm and 2 µm PC filters. In 2013, the 20 µm filtrate was filtered through 5 µm PC filters, and then 0.7 µm GF filters. For simplicity, size fractions are described as >5 µm (20 µm + 5 µm chl *a*, both years) and <5 µm (>0.7 µm less the >5 µm fraction in 2012, or 5 µm >chl *a* >0.7 µm in 2013). In April and May 2013 no GF samples were collected for chl *a* analysis, so the <5 µm size fraction in these months represents phytoplankton biomass between 5 µm and 2 µm in size. This may under-estimate phytoplankton biomass overall, as very small cells between 2 µm and 0.7 µm would not have been collected. However, microscope cell counts indicate that during both these months diatoms dominated cell numbers (>75%), implying that the contribution of small phytoplankton cells (<2 µm) to phytoplankton biomass would have been minimal. Filters were stored in glass scintillation vials, and frozen at -20°C until analysis. Pigments were extracted at -20°C for 24 hours in 90% acetone, and then chl *a* concentrations were determined on a calibrated Turner 10-AU fluorometer. Concentrations were corrected for phaeopigment interference by acidification as described in Parsons et al. (1984).

Biogenic silica concentrations were also determined by filtering triplicate seawater samples (1 L) through 0.6 µm PC filters. Filters were folded, placed in polypropylene centrifuge tubes, and dried at 56°C for several days. Samples were stored dry until analysis. Then samples were digested to convert $bSiO_2$ to $Si(OH)_4$ for spectrophotometric analysis. Samples were digested for 30 minutes using the NaOH digestion procedure of Paasche (1973a) as modified by Brzezinski and Nelson (1989). Then concentrations of $Si(OH)_4$ were measured using the silicomolybdic acid assay with

a modified reagent blank (Brzezinski and Nelson 1986, 1989) at 810 nm using a Beckman DU UV/Vis spectrophotometer.

4.2.4. Production Rates

Production rates of $bSiO_2$ (ρ, units of μmol SiO_2 L^{-1} d^{-1}) and organic carbon (primary production) were determined from incubation experiments. All incubations were conducted in an acrylic tank outdoors exposed to ambient light conditions. The tank was supplied with flowing seawater that matched the temperature of the sampling depth. Samples were incubated in acid cleaned polycarbonate bottles. These bottles were incubated in tubes shaded with blue photographic film (Lee Filters 202 Half C. T. Blue) to simulate ~50% of ambient irradiance.

Primary production rates were determined by spiking seawater samples (1.2 L) with approximately 10% (203 μmol L^{-1} $NaH^{13}CO_3$) of ambient DIC levels. These samples were incubated for 4 hours, except in November and December 2013. For these 2 months, 24 hour incubations were conducted because incubations began late in the day when light levels were low. Four hour incubation lengths were preferred, to minimize the possibility of tracer depletion during experiments. Primary productivity rates measured over 4 hours are expected to yield closer to a gross rate of primary production, while 24 hour incubation rates would tend towards a net measurement. Consequently, ^{13}C labelled organic carbon may have been respired during 24 hour incubations during November and December 2013, which could have reduced the primary productivity rate during these months relative to the others sampled. Samples were filtered onto pre-combusted 0.7 μm GF filters and kept in the dark during filtration. Then filters were folded in half, placed in polystyrene petri dishes, dried at 56°C for 5 days, and stored in a dessicator until measurement of the isotopic composition and total carbon content at the UC Davis Stable Isotope Facility using an elemental analyzer interfaced with an isotope ratio mass spectrometer (EA-IRMS). Hourly primary production rates were calculated as described in Hama et al. (1983). Hourly rates were converted to daily primary production rates by multiplying by the fraction of daily insolation during the incubation time (Grundle et al.

2009, Harris et al. 2009). Daily insolation profiles were retrieved from the School-Based Weather Station Network University of Victoria Science Building insolation sensor (data available at victoriaweather.ca). Dissolved inorganic carbon (DIC) concentrations used in the calculation of primary productivity rates were estimated from measurements of CTD temperature and salinity based on the relationship between density and DIC determined for Saanich Inlet by Grundle (2007).

Biogenic silica production rates were determined using two methods. Beginning in May 2012, $bSiO_2$ production was measured using PDMPO (ρ_{PDMPO}) as described in Chapter 2. Triplicate samples (400 mL) were incubated with 125 nmol L^{-1} PDMPO (Lysosensor DND-160, Life Technologies) for 24 hours. Then samples were filtered onto 0.6 µm PC filters. Once all seawater had passed through the filters, they were coated with 10% HCl for 2 minutes to lyse cells (Leblanc and Hutchins 2005, Chapter 2), and then rinsed thoroughly with deionized water. Filters were placed in polypropylene centrifuge tubes, dried at 56°C for several days (Chapter 2, Appendix B) and stored dry until analysis. Then the concentration of PDMPO incorporated into particles on the filter (pPDMPO) was determined. First, samples were digested to solubilize pPDMPO in order to measure it fluorometrically. Some replicates from May 2012 to August 2012 were digested using hot NaOH, as for $bSiO_2$. However, subsequent work (Appendix C) has found that this may degrade PDMPO fluorescence, so HF (Appendix D) was used to digest the remaining samples. For months where replicates were digested using both methods, replicates were not significantly different, and therefore all replicates have been included in the calculation of the average. Although digestion with NaOH likely caused a reduction in pPDMPO measured during these cases, the variability between replicates was high enough to mask any decrease. For HF digestions, HF (0.2 mL) was added to the filter, allowed to digest for 48 hours, and then 4.8 mL of saturated boric acid was added to bind remaining fluorine ions (Chapter 2). Then the dissolved PDMPO concentrations were determined using a Turner Trilogy fluorometer (350/80 nm excitation 410 – 600 nm emission, crude oil module). Dissolved PDMPO concentrations were determined by comparing fluorescence measured from samples with the fluorescence of PDMPO standards prepared in the appropriate matrix (NaOH-HCl for

samples digested with NaOH, and HF-boric acid for samples digested with HF). Standard curves were prepared for the PDMPO concentration range of 0 – 200 nmol L^{-1} ($R^2 \geq 0.994$). The incorporation of PDMPO during incubations was converted to SiO_2 using a ratio of 4200 ± 380:1 (Chapter 2). As all experiments were conducted for 24 hours, the amount of SiO_2 calculated is equivalent to ρ_{PDMPO} (units of units of µmol SiO_2 L^{-1} d^{-1}).

Gross $bSiO_2$ production rates (ρ_{GROSS}) were also determined during 2013 using ^{32}Si. Seawater (300 mL) was spiked with high specific activity $^{32}Si(OH)_4$ (Los Alamos National Laboratory) to a final activity of 22.2 kBq (0.01 µCi). After 24 hours of incubation, samples were filtered onto 0.6 µm PC filters which were rinsed with filtered sea water to remove unbound ^{32}Si. Filters were then placed on nylon discs and dried at room temperature. Once dry, filters were covered with Mylar film and stored dry until secular equilibrium was reached (~120 days). Activity of ^{32}Si was determined by gas-flow proportional counting according to Krause et al. (2011a) using a low-level beta multicounter system (Risø GM-25-5A, DTU Nutech). Gross $bSiO_2$ production rates were then calculated as described in Brzezinski and Phillips (1997).

4.2.5. Community Composition

Diatom cells were identified using both brightfield and PDMPO fluorescence microscopy. For phytoplankton cell counts, seawater (125 mL) was stored in amber glass bottles and preserved using acidic Lugol's solution. Bottles were gently mixed to homogenize the contents and then a subsample (50 mL) was settled for 24 hours. Then cells were counted on an IX-70 Olympus inverted microscope using a 40x objective (Utermöhl 1958). As the focus of this study is diatoms, non-diatom cells were not identified in detail and were grouped according to size. Non-diatom cells smaller than 5 µm in length were small coccoid and flagellate cells, while larger non diatom cells were mostly dinoflagellates but also included some larger flagellate or coccoid cells. Diatom cells were identified to genus.

The contribution of different diatom genera to $bSiO_2$ production was determined by measuring PDMPO fluorescence per cell by microscopy. To distinguish from measurements of PDMPO by fluorometry, measurements of PDMPO by microscopy have been denoted iPDMPO. Aliquots from triplicate PDMPO incubations were used to prepare microscope slides as described in Chapter 2. First, the cell density of unlabelled water was assessed by microscopy, and the optimal aliquot volume chosen. Next aliquots were filtered onto 0.6 µm PC filters, and filters were placed onto a microscope slide with a 15 µL droplet of deionized water such that the cells on the surface of the filter were within the droplet of water. Then the reverse of the microscope slide was frozen using canned freeze spray, the filter peeled off, and the slide allowed to dry. Once slides had dried, a drop of mountant (Pro-Long Gold for 2012 samples, Immu-mount for 2013 samples) and coverslip were placed on each slide. Slides were stored frozen. Unfortunately, Immu-mount mountant is water based, so frozen slides developed ice crystals, and an additional heating step was required to clear the mountant prior to imaging.

Fluorescence of PDMPO stained diatom cells was imaged and quantified as described in Chapter 2. An Olympus IX-71 inverted microscope with DAPI excitation filter (377/50 nm), custom emission filter (500/140 nm), and X-cite 120 PC (EXFO) light source was used to image PDMPO fluorescence. Images for PDMPO analysis were captured using a 10x (0.25 NA) objective, while images showing the morphology of the dominant diatom genera were captured using higher magnification objective lenses (40x (0.6 NA) or 100x (1.35 NA)). Images of brightfield and PDMPO fluorescence were captured using a 12-bit Retiga QImaging camera coupled with a computer running µManager for ImageJ software (Edelstein et al. 2010; Rasband 2012). Prior to imaging diatom cells, 10 FOVs of a calibration slide (Chroma Technologies yellow autofluorescent slide, 1.5mm thick) were imaged (Chapter 2). Then 30-50 FOVs of sample slides were imaged using both brightfield and PDMPO fluorescence illumination. Focus for images were adjusted manually, and exposure times adjusted to be as long as possible without saturating pixels (Chapter 2).

Then images were analyzed. For each sample, FOVs were randomly selected from the images captured for analysis. First, the fluorescence intensity of each pixel in the original image was divided by the intensity of the pixel from the calibration image at the same location within the FOV. Then background was measured and subtracted (Chapter 2). Background measurements were low (160) relative to the range of the camera (0 – 4096). Then automated particle analysis was conducted as described in Chapter 2. If cells of different diatom genera overlapped, either the cells were excluded or the overlapping pixels were manually excluded. Fluorescence intensity per cell was normalized by exposure time to account for differences between images (Znachor and Nedoma 2008). Cells were identified to genus using both brightfield and PDMPO fluorescence images. For each sample, additional FOVs were analyzed until iPDMPO was adequately quantified. Sample fluorescence was considered adequately quantified when the coefficient of variation (standard deviation divided by the average) was <15% for diatom genera that contributed >10% to iPDMPO. Then the iPDMPO measurements of all diatom cells within a genus were summed up within a sample and the percentage contribution of each genus to the total was determined. Measurements presented here represent the average of triplicate sample slides. For slides prepared with Immu-mount, an additional heating step was required to clear ice crystals from the mountant. Heating has been found to degrade PDMPO fluorescence when PDMPO is not bound within $bSiO_2$ (Appendix C), and it is possible that heating these slides may have reduced PDMPO fluorescence within diatom cells. However, all results presented are from relative measurements of different diatom genera within the same slide, and comparisons between months are combined with ρ_{PDMPO} to account for differences between months (see below). Even if this heating step caused a decrease in iPDMPO overall, this effect would not be expected to differentially affect diatom genera and the results presented here.

Surface area (SA) was also determined for the six most important diatom genera. Cell dimensions were measured from brightfield images of diatom cells from slides prepared above. The SA per cell for each genus was calculated using the geometric formulas of

Sun and Liu (2003). The total SA for each genus was calculated as the SA per cell multiplied by the cell concentration.

Specific $bSiO_2$ production rates (V_{PDMPO}) were also estimated for each genus based on iPDMPO. This was calculated by normalizing the percentage contribution of a genus to iPDMPO by its contribution to total diatom SA. Because $bSiO_2$ per cell is correlated with SA per cell (Brzezinski 1985), normalizing $bSiO_2$ production per genus (iPDMPO, Chapter 2) to total diatom SA for a given genus approximates a specific $bSiO_2$ production rate. For genera that were very rare (< 3% of cells counted), cell numbers could not be reliably quantified. Consequently iPDMPO normalized to the SA of genera with low cell numbers were often extremely high, and likely inaccurate. Therefore, V_{PDMPO} calculated for very rare genera (<3% of cells counted) have been excluded.

In order to examine seasonality, samples were grouped together into three seasons: spring (February to May), summer (June to August), and fall/winter (October to January). For each month, the fraction of iPDMPO from different taxa was multiplied by the total community $bSiO_2$ production rate (ρ_{PDMPO}) for that month to determine the $bSiO_2$ production rate for each taxon within each month. The monthly contributions of a genus to $bSiO_2$ production were summed for each season, and then divided by the total for all of the months within the season to yield the proportion of $bSiO_2$ production measured attributable to each genus.

4.3. Results

4.3.1. Biomass and Production in Saanich Inlet

The two years sampled differed in their seasonal patterns. During April and May 2012 a large spring bloom was detected (Figure 4.1) with high chl *a* and $bSiO_2$ concentrations. Primary productivity rates were the highest measured during April 2012, though May 2012 rates were only moderate. Phytoplankton biomass was much lower in spring (February – May) 2013 than 2012; and total spring chl *a* concentrations in 2012 were 6.3 ± 0.3 times higher than in 2013. The highest phytoplankton biomass during 2013

occurred during fall/winter in November. Smaller peaks in phytoplankton biomass occurred during summer of both years, and were associated with high primary production and ρ_{PDMPO} during July 2012. Thus, peaks in phytoplankton biomass and production occurred during all seasons. For August 2013 the calculation of ρ_{PDMPO} produced an improbably high value (~100x ρ_{GROSS}). Since diatom cell numbers and $bSiO_2$ concentrations were low at that time, and few diatoms were observed labelled by PDMPO via microscopy, then this measurement is likely erroneous and has been excluded from the dataset.

Despite the strong differences between years, spring (February - May) had the highest phytoplankton (chl *a* average of 11.6 ± 1.3 µg L^{-1}) and diatom biomass ($bSiO_2$, average of 9.6 ± 1.4 µmol L^{-1}) overall. Spring also accounted for the majority of primary production (average 24 ±1.7 µmol C L^{-1}). Fall/winter (October-January) had the next highest phytoplankton biomass (chl *a* 6.5 ± 0.33 µg L^{-1}), while summer (June-September) had the second highest primary production (11.0 ± 0.4 µmol C L^{-1}).

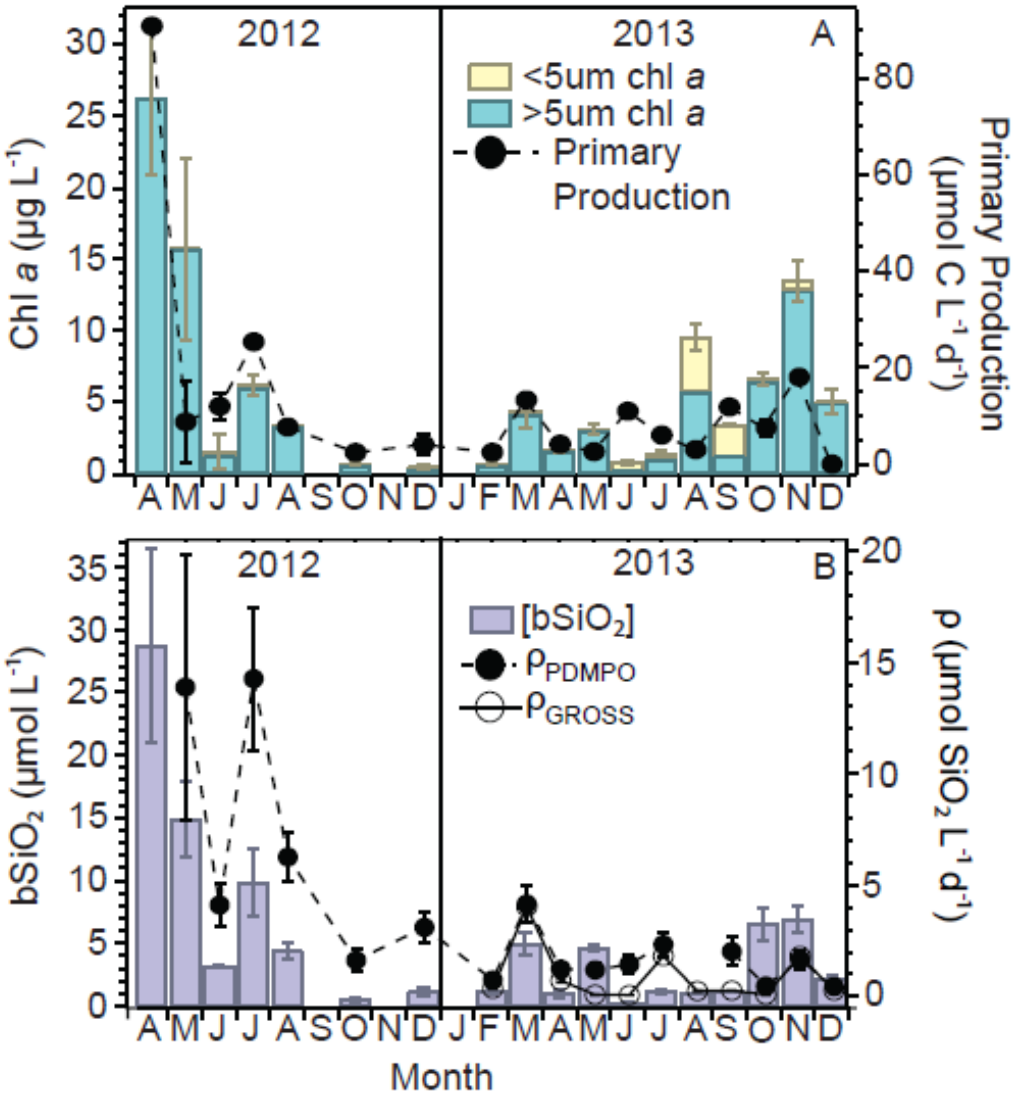

Figure 4.1: A) Chlorophyll *a* concentrations (bars) for the >5µm (green) and <5µm (yellow) size fractions and primary production rates (circles and dashed lines) for all samples. B) Biogenic silica concentrations (purple bars) and ρ (circles and lines) determined using either pPDMPO (filled circles) or ^{32}Si (open circles) as a tracer. All measurements represent the average of triplicate samples, with error bars representing ± 1 standard deviation.

At all times the >5 µm size fraction dominated chl *a* concentrations (Figure 4.1A). Dinoflagellates contributed little to cell numbers during the study period (data not shown), so the larger size fraction chl *a* generally represents diatom biomass. Only during December 2012, June 2013, August 2013, and September 2013 did the <5 µm size fraction account for more than 40% of total chl *a*. As diatoms generally dominated biomass and production during sampling, excluding non-diatom phytoplankton by using

Si based methods to investigate biomass and production should still be informative about the majority of phytoplankton biomass and productivity at this location.

On average, *Thalassiosira* spp. dominated $bSiO_2$ production (determined from the combination of iPDMPO and pPDMPO measurements) over the entire study period (Figure 4.2A), and was responsible for 32% of total $bSiO_2$ production. This differed from cell numbers, in which *Chaetoceros* spp. accounted for 51% of the total number of diatom cells and *Thalassiosira* spp. was only 16% (Figure 4.2B). However, the contribution of different genera to cell numbers and $bSiO_2$ production differed depending on the season. In spring, *Thalassiosira* spp. dominated $bSiO_2$ production (79%, Figure 4.2C), while accounting for only 38% of diatom cells (Figure 4.2D). *Chaetoceros* spp., *Skeletonema* spp., and *Pseudo-nitzschia* spp. were all abundant during spring (20, 23 and 15% of cells respectively), but were less important to $bSiO_2$ production (11%, 2% and 6% respectively). During summer, *Chaetoceros* spp. and *Skeletonema* spp. were both important to $bSiO_2$ production (39% and 32% respectively, Figure 4.2E), though *Chaetoceros* spp. was far more abundant than *Skeletonema* spp. during this time (73% and 23% of cells respectively, Figure 4.2F). Fall/winter $bSiO_2$ production was dominated by *Ditylum* spp. (29%, Figure 4.2G), although this genus accounted for only 6% of diatom cells (Figure 4.2H). *Thalassiosira* spp. and *Thalassionema* spp. were rare at this time (2% and 3% of cells respectively), but contributed relatively more to $bSiO_2$ production (11% and 13% respectively). *Chaetoceros* spp. dominated cell numbers during fall/winter (46%) but contributed less to $bSiO_2$ production (15%).

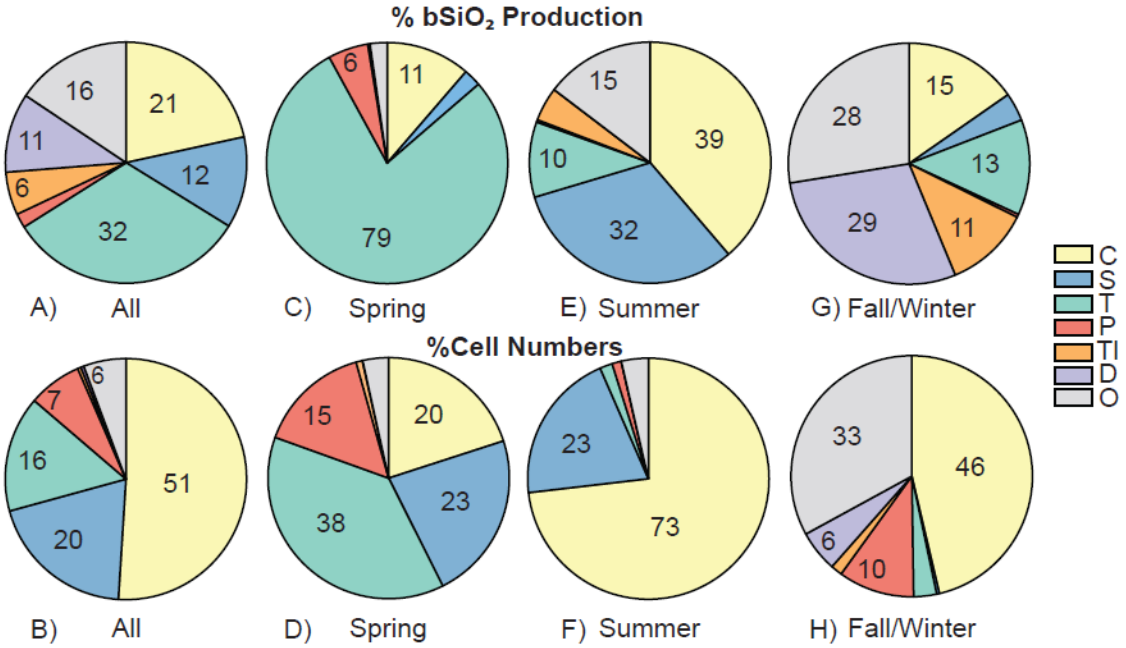

Figure 4.2: The contribution of diatom genera to $bSiO_2$ production determined from combined fluormetry and microscopy measurements of PDMPO (A, C, G, E) and cell numbers (B, D, H, F) for the entire sampling period (A, B), during spring (C, D), summer (E, F), and fall/winter (G, H). Colours indicate the six dominant diatom genera during the study period: *Chaetoceros* spp. (C), *Skeletonema* spp. (S), *Thalassiosira* spp. (T), *Pseudo-nitzschia* spp. (P), *Thalassionema* spp. (Tl), and *Ditylum* spp. (D), while grey indicates other diatom species.

During the study period, six diatom genera (*Chaetoceros* spp., *Skeletonema* spp., *Thalassiosira* spp., *Pseudo-nitzschia* spp., *Thalassionema* spp., and *Ditylum* spp., Figure 4.3) dominated diatom cell numbers (94%), and iPDMPO (84%). To simplify presentation of the results, diatoms other than the 6 dominant genera are categorized as "other diatoms". Other diatom species contributed more than 5% to the community total $bSiO_2$ production in summer and fall/winter, and cell numbers in fall/winter (Figure 4.2). For summer $bSiO_2$ production, other diatoms present were *Asterionellopsis* spp., *Asteromphalus* spp., *Actinoptychus* spp. and small centric genera. In the fall/winter other diatom genera that contributed to $bSiO_2$ production included *Asterionellopsis* spp. and *Coscinodiscus* spp., while cell numbers also included *Rhizosolenia* spp., *Melosira* spp., *Bacillaria* spp., *Navicula* spp., *Eucampia* spp., *Cylindrotheca* spp., and *Thalassionema* spp. During each season, a different genus was the dominant contributor to $bSiO_2$

production, in contrast to cell numbers which were dominated by *Chaetoceros* spp. cells except in spring.

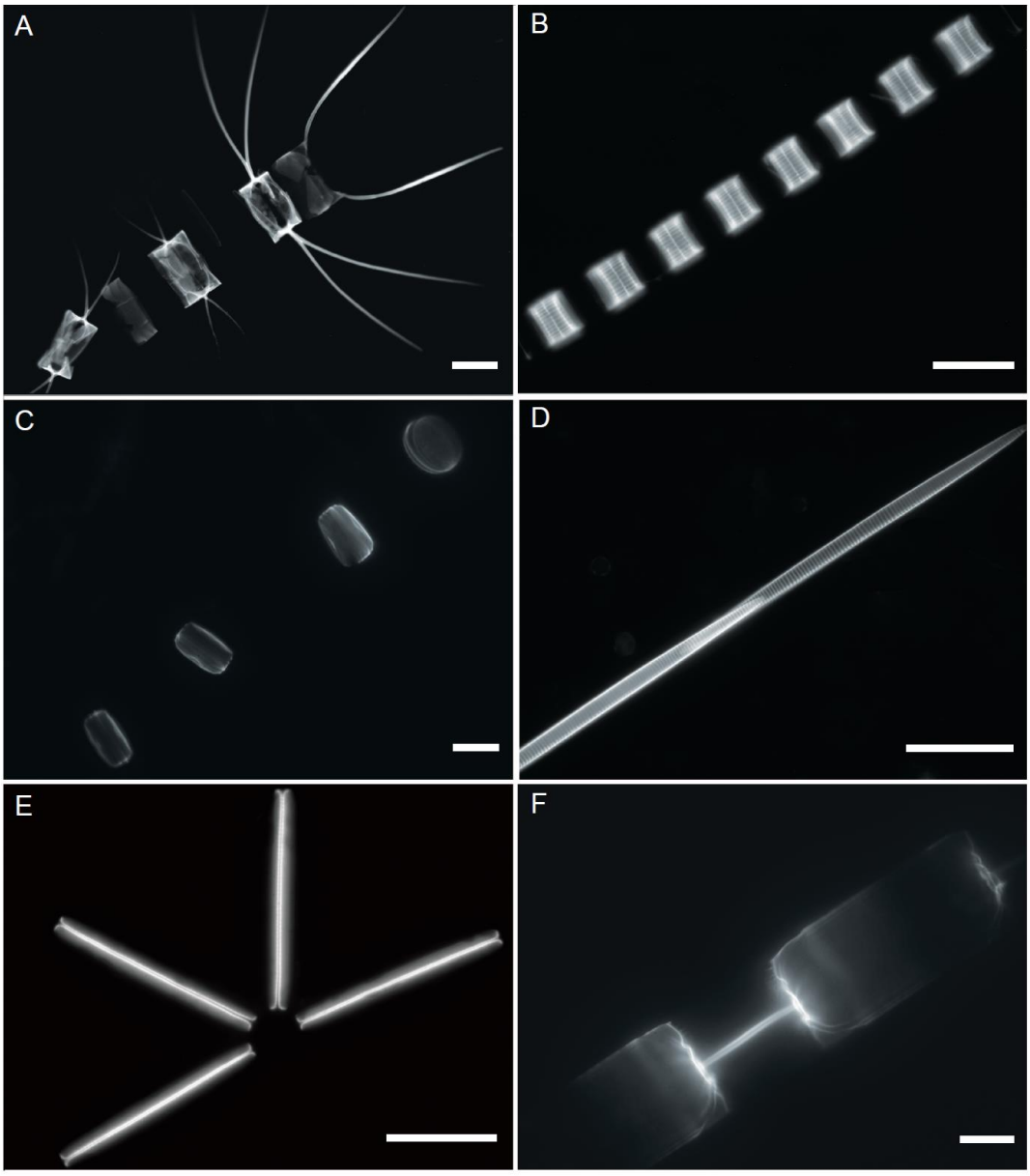

Figure 4.3: Dominant diatom genera in Saanich Inlet labeled with PDMPO: A) *Chaetoceros* spp., B) *Skeletonema* spp., C) *Thalassiosira* spp. D) *Pseudo-nitzschia* spp., E) *Thalassionema* spp., and F) *Ditylum* spp. All scale bars represent 25µm. Images of PDMPO labelled $bSiO_2$ were captured by fluorescence microscopy with the same microscope configuration for image analysis (see text), although higher magnification objective lenses were used (40x (0.6 NA) for A, B, C, F; or 100x (1.35 NA) for D, E).

4.3.2.Measurements of Diatom Community Composition

Contributions of the six dominant diatom genera to iPDMPO were compared with their contributions to cell numbers and total diatom SA. The %iPDMPO fluorescence of a genus was not correlated with its percentage contribution to diatom cell numbers (Figure 4.4A). The %iPDMPO fluorescence better matched %SA (Figure 4.4B), but only in some cases. At certain times, one genus dominated the diatom assemblage, and contributed similarly to iPDMPO, cell numbers and SA. For example, during May 2013 *Pseudo-nitzschia* spp. accounted for 98% of iPDMPO, 97% of diatom cells and 99% of diatom SA (Figure 4.5). More frequently, the opposite was also true, meaning that when a genus was unimportant to iPDMPO, it was also rare and contributed little to total diatom SA (e.g. *Pseudo-nitzschia* spp. in July 2012 contributed 0.1% of iPDMPO, 0.5% of cells and 0.5% of diatom SA, Figure 4.6). Intermediate cases were less common, and occurred when a genus was neither rare nor dominant, but its contribution to iPDMPO and SA agreed (e.g. *Ditylum* spp. November 2013 was 71% of iPDMPO, 8% of diatom cells and 75% of diatom SA, Figure 4.7).

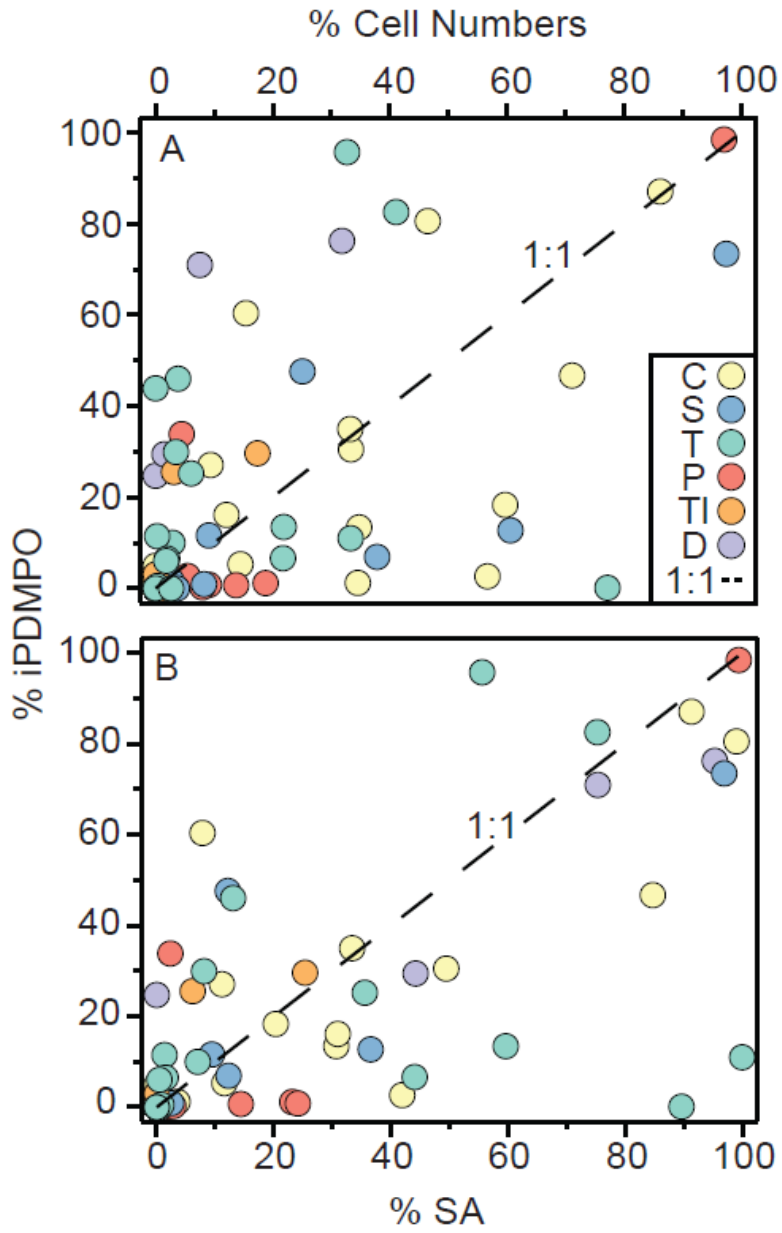

Figure 4.4: The percentage contribution of dominant diatom genera in Saanich inlet to iPDMPO vs. A) cell numbers and B) total diatom surface area (SA). Dashed lines indicate 1:1 relationship, and different genera are indicated by colour. The genera included are *Chaetoceros* spp. (C), *Skeletonema* spp. (S), *Thalassiosira* spp. (T), *Pseudo-nitzschia* spp. (P), *Thalassionema* spp. (Tl) and *Ditylum* spp. (D).

However, in many cases the contribution of a genus to iPDMPO did not match its contribution to SA, suggesting that specific $bSiO_2$ production rates differed between genera. This was clear for *Thalassiosira* spp. during spring 2013 (Figure 4.5). During March 2013, *Thalassiosira* spp. contributed more to iPDMPO than to abundance or SA

(96%, 33% and 56% respectively). However, in the following month, April 2013, *Thalassiosira* spp. cells were the most abundant (77%) and the largest contributor to SA (90%), but accounted for only 0.1% of iPDMPO. Therefore, neither cell numbers nor surface area consistently predicted the importance of a genus to iPDMPO fluorescence and, by extension, $bSiO_2$ production.

Parameters of diatom community composition are presented for only select months in Figure 4.5, 4.6, and 4.7, to showcase diatom blooms during each of the three seasons (March 2013 in spring, July 2012 in summer and November 2013 in fall/winter). Complete results are presented in Appendix J.

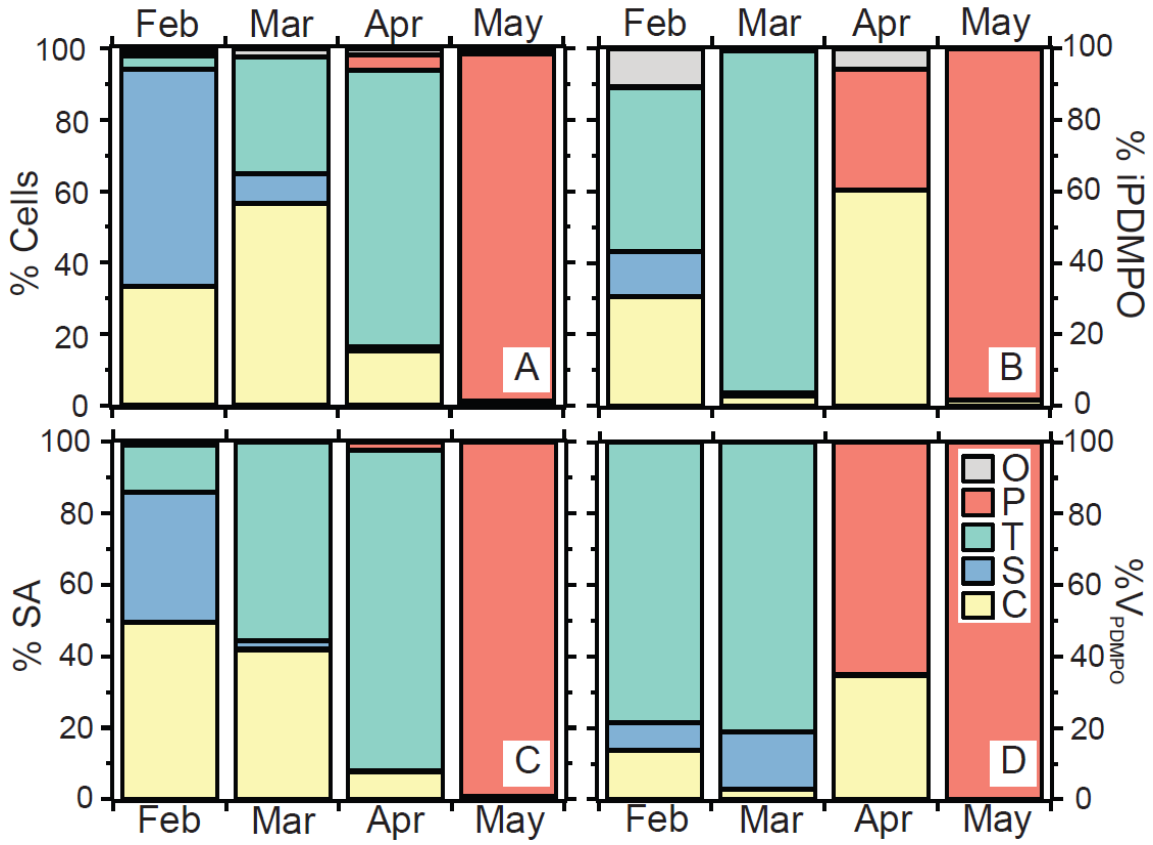

Figure 4.5: The percentage contribution of diatom genera to A) cell numbers, B) iPDMPO, C) total diatom surface area (SA), and D) V_{PDMPO} (PDMPO normalized to SA) during spring 2013 Diatoms included are *Chaetoceros* spp. (C), *Skeletonema* spp. (S), *Thalassiosira* spp. (T), *Pseudo-nitzschia* spp. (P), and other diatom species (O).

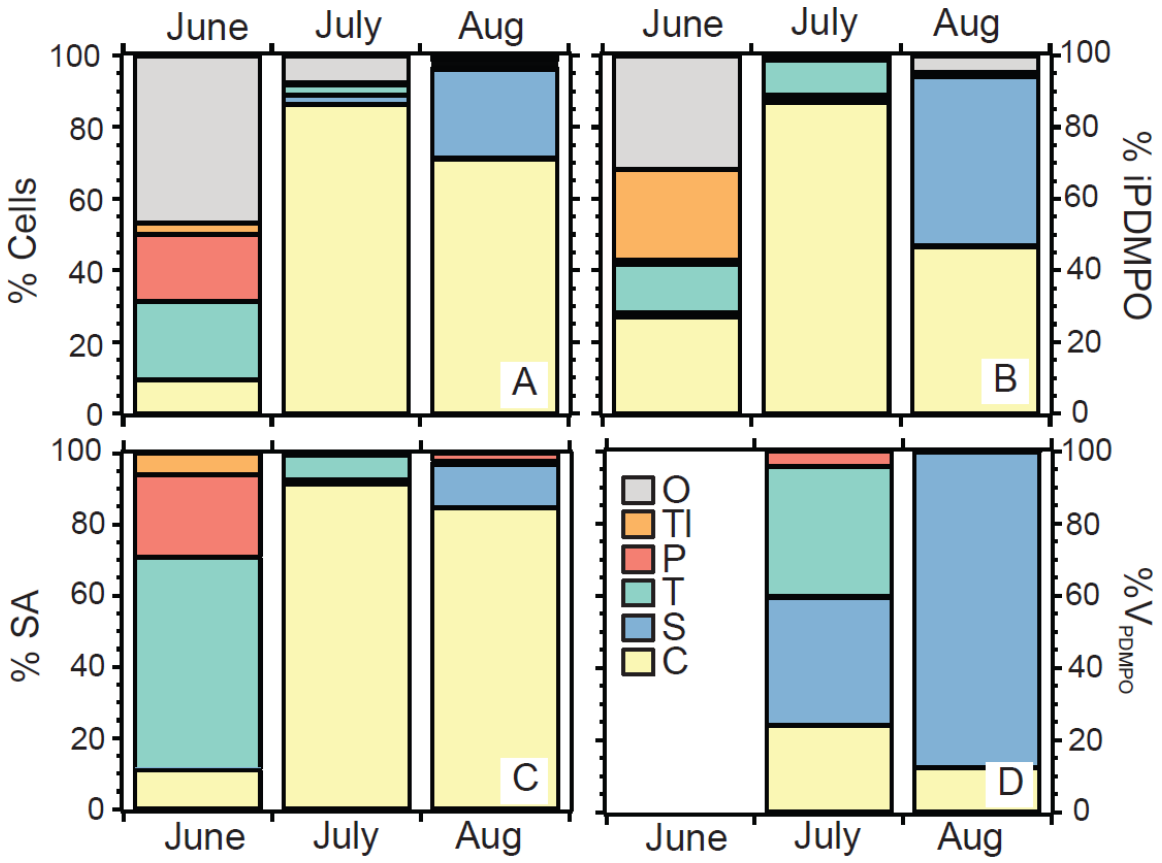

Figure 4.6: The percentage contribution of diatom genera to A) cell numbers, B) iPDMPO, C) diatom surface area (SA) and D) V_{PDMPO} (PDMPO normalized to SA) during summer 2012 in Saanich Inlet. June V_{PDMPO} values are not reported as cell numbers of all diatom genera was too low for V_{PDMPO} to be accurately determined. Diatoms included are *Chaetoceros* spp. (C), *Skeletonema* spp. (S), *Thalassiosira* spp. (T), *Pseudo-nitzschia* spp. (P), *Thalassionema* spp. (Tl) and other diatom species (O).

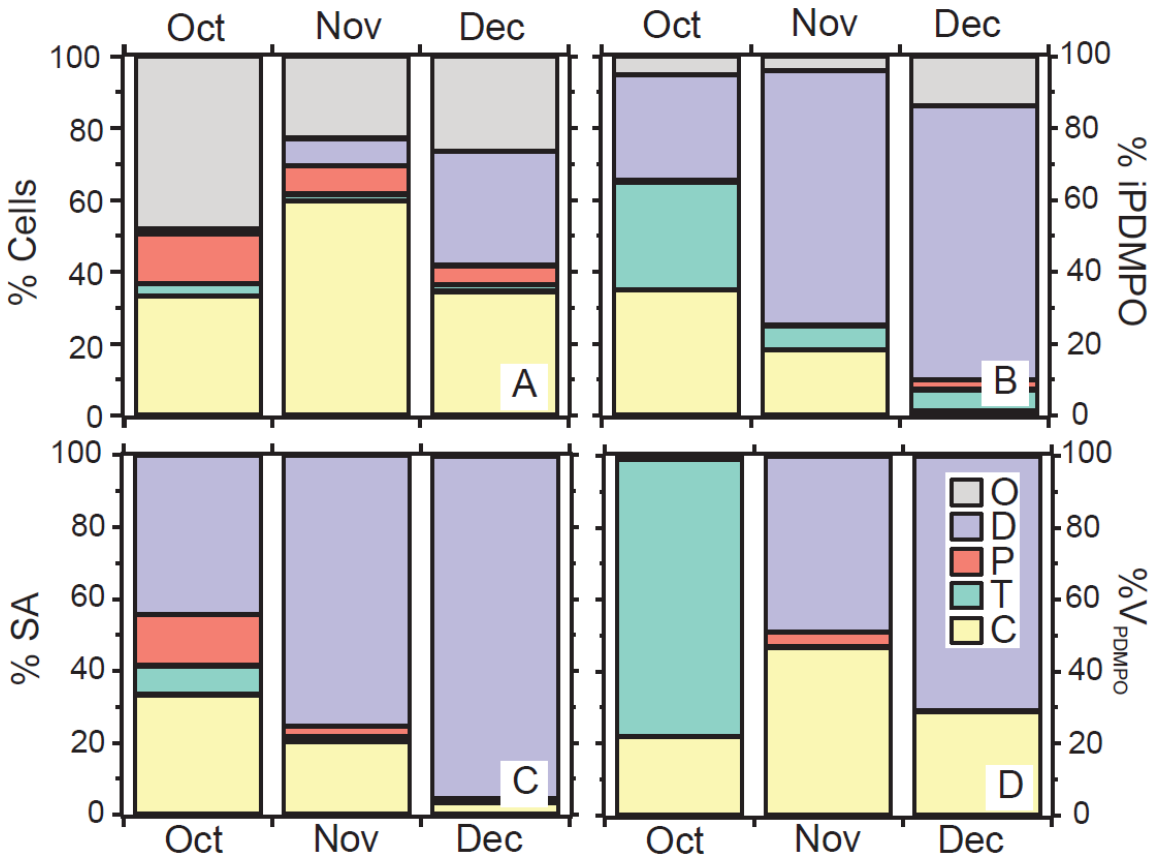

Figure 4.7: The percentage contribution of diatom genera to A) cell numbers, B) iPDMPO, C) diatom surface area (SA) and D) V_{PDMPO} (PDMPO normalized to SA) during fall/winter 2013 in Saanich Inlet. Diatoms included are *Chaetoceros* spp. (C), *Thalassiosira* spp. (T), *Pseudo-nitzschia* spp. (P), *Ditylum* spp. (D) and other diatom species (O).

4.3.3. Using PDMPO to Pinpoint Assemblage Transitions

As a proxy for specific $bSiO_2$ production rate, a genus' contribution to iPDMPO was normalized by its contribution to total diatom SA (V_{PDMPO}). In some cases, a genus that dominated V_{PDMPO} in one month dominated cell numbers the following month. This was most evident during spring 2013 (Figure 4.5). Cell numbers indicated that the community was initially dominated by *Skeletonema* spp. in February, it shifted to a *Thalassiosira* spp. and *Chaetoceros* spp. mixed community in March, to *Thalassiosira* spp. in April, and a *Pseudo-nitzschia* spp. dominated community in May (Figure 4.5A). However, community $bSiO_2$ production was already dominated by *Thalassiosira* spp. in February (Figure 4.5B). This was followed by *Chaetoceros* spp. and *Pseudo-nitzschia* spp. dominated $bSiO_2$ production in April and then *Pseudo-nitzschia* spp. exclusively in

May. High *Thalassiosira* spp. V_{PDMPO} during February and March preceded the high *Thalassiosira* spp. cell numbers and SA observed during April. Likewise, *Pseudo-nitzschia* spp. had the highest V_{PDMPO} during April, which was followed by the almost exclusively *Pseudo-nitzschia* spp. assemblage sampled during May. In these cases, V_{PDMPO} indicated high specific $bSiO_2$ production rate of the genera that dominated the community the subsequent month.

Although V_{PDMPO} indicated the transitions between the dominant diatom species present during spring 2013, it was not a consistent predictor during other times of the year. For example, *Skeletonema* spp. and *Thalassiosira* spp. had higher V_{PDMPO} than *Chaetoceros* spp. in July 2012, but *Chaetoceros* spp. continued to dominate diatom cell numbers and SA in August 2012 (Figure 4.6). Of the 10 months when V_{PDMPO} was measured in a month prior to measurements of cell numbers, the genus with the greatest V_{PDMPO} dominated cell numbers the following month in only 3 instances. Also, from a total of 30 measurements, the percentage contribution of a genus to V_{PDMPO} was within 20% of its contribution to cell numbers the following month in 16 cases. Although V_{PDMPO} predicted changes in cell numbers during spring 2013, it was not a consistent indicator throughout the study period.

4.4. Discussion

4.4.1. Measurements of Diatom Community Composition

Previous work that investigated diatom community composition in Saanich Inlet has used cell numbers as a metric for the contribution of different species to the phytoplankton community (Hobson 1981, 1983; Parsons et al. 1983; Sancetta and Calvert 1988; McQuoid and Hobson 1997; Grundle et al. 2009). However, my results suggest that numerically dominant diatom genera are not necessarily the most important in terms of diatom production (Figure 4.4). Prior to the development of PDMPO as a tracer of $bSiO_2$ production in diatoms (Shimizu et al. 2001; Leblanc and Hutchins 2005; Chapter 2), no convenient method existed to determine the contribution of individual diatom

species to total diatom production. Because PDMPO incorporation is closely related to SiO_2 incorporation in diatom frustules (Leblanc and Hutchins 2005, Chapter 2), the contribution of a particular taxa to iPDMPO indicates its contribution to community $bSiO_2$ production.

When the relative contribution of diatom genera to cell numbers was compared with their contribution to iPDMPO, little relationship was evident (Figure 4.4A). This is in agreement with findings from the few previous studies. Quéguenir et al. (2011) found that *Rhizosolenia* spp. dominated iPDMPO while contributing far less to cell numbers (18%). At Ocean Station Papa, Durkin et al. (2012) observed that *Fragilariopsis* spp. <5 μm had high cell numbers, but contributed little to iPDMPO. Similarly, cell numbers were poorly correlated with iPDMPO for several samples from the west coast of Vancouver Island (Chapter 3).

The methodology used to quantify iPDMPO in previous studies differed from that used in this study and in Chapter 3. Quéguenir et al. (2011) do not describe their methods, so it is not possible to determine how differences in methodology may affect comparison with my results. Durkin et al. (2012) quantified iPDMPO using a 40x objective with unspecified numerical aperture (NA), and did not calibrate excitation light intensity. Numerical aperture and differences in excitation light intensity between images or across the FOV may confound measurements of PDMPO (Chapter 2 and Appendix G), so it is possible that the measurements of Durkin et al. (2012) may be confounded by these effects. Therefore, the differences between cell numbers and iPDMPO measured in these previous studies could reflect inaccurate measurements of iPDMPO between diatom species, and not a true discrepancy between iPDMPO and cell numbers. In contrast, reliable quantification of PDMPO fluorescence by microscopy has been confirmed with the microscope configuration used in the present study, and was tested with several of the diatom genera within Saanich Inlet (Chapter 2).

Previous studies also differ in how the relative contribution of different species to iPDMPO was calculated. Durkin et al. (2012) and Znachor et al. (2013) quantified the average PDMPO fluorescence per cell, and then multiplied this value by the cell numbers of the species or genus to get a relative contribution of the particular taxa to total PDMPO fluorescence. If unlabelled cells were not included in the calculation of average PDMPO per cell, this could result in over-estimation of PDMPO fluorescence per species. During 24 hour incubations, many cells will not deposit $bSiO_2$. This fraction of inactive cells may be ≥70% (Leblanc and Hutchins 2005, Figure 4.5 in this study for *Thalassiosira* spp. in April). As Durkin et al. (2012) and Znachor et al. (2013) prepared microscope slides by directly mounting black polycarbonate filters, it would not have been possible to determine the fraction of unlabelled cells by brightfield illumination. This could result in over-estimates of the average fluorescence for cells from a particular genus, and cause over-estimation of the genus' contribution to $bSiO_2$ production. In the present study, PDMPO fluorescence per genus was quantified within a FOV. Thus differences in cell numbers and fluorescence intensity between species were not determined separately, but both contribute to the total measured. As this method does not rely on determining a per cell average fluorescence, there is no possibility of over-estimation of fluorescence due to inactive diatom cells being erroneously excluded from an average measurement. As a result, the discrepancy between cell numbers, SA, and iPDMPO observed here reflects a real difference between the contributions of genera to each of these measurements.

Although Quéguenir et al. (2011) and Durkin et al. (2012) used different methods to quantify iPDMPO, the discrepancy between cell numbers and iPDMPO that they observed could be explained by differences in size between diatom species. Diatom cell size can range by several orders of magnitude (Sarthou et al. 2005), and larger diatoms with larger frustules result in more $bSiO_2$ per cell. Thus large cells would be expected to contribute more to iPDMPO than small cells. In the Quéguenir et al. (2011) study, large *Rhizosolenia* sp. cells were more important for $bSiO_2$ production than the other smaller genera present. Likewise, Durkin et al. (2012) observed small cells of *Fragilariopsis* sp. were very abundant, but accounted for little iPDMPO. Durkin et al. (2012) also observed that large diatom cells low in abundance were important for $bSiO_2$ production, which was

also evident at some sampling locations described in Chapter 3 of this thesis. To account for differences between diatom cells measured in $bSiO_2$ quota, the contribution of genera to iPDMPO was compared to their contribution to SA (Figure 4.4B). Since $bSiO_2$ is found at the cell periphery, SA is correlated with $bSiO_2$ per cell (Brzezinski 1985; Marchetti and Harrison 2007). Therefore the contribution of a genus to SA approximates its share of community $bSiO_2$. Although SA was correlated better with iPDMPO than cell numbers, this correlation was not strong. Therefore the relationship between iPDMPO and SA (indicated by iPDMPO:SA, V_{PDMPO}) frequently differed between diatom genera sampled, and confounded the relationship between iPDMPO and SA.

It is possible that the discrepancy between iPDMPO and SA observed is due to factors affecting iPDMPO measurements, and does not reflect a true difference between $bSiO_2$ production and SA. It is unlikely that the addition of PDMPO itself could be such a factor, as PDMPO was added to a final concentration of 125 nmol L^{-1}, and PDMPO toxicity has not been observed to occur at concentrations below 500 nmol L^{-1} (Chapter 2, Leblanc and Hutchins 2005).

Light intensity during incubations with PDMPO (50% surface irradiance) often did not match *in situ* conditions which varied between 2 and 100% of surface irradiance (Table 4.1). It is possible that this mismatch could explain some of the discrepancy between iPDMPO, cell number and total diatom SA measurements, and this effect likely varies between samples. During spring 2013 iPDMPO, cell numbers and SA strongly disagreed in March and April (Figure 2.5). During March, *Thalassiosira* spp. dominated iPDMPO (95%) but accounted for only 33% of cell numbers. As the *in situ* irradiance at the depth of sample collection was 48%, differences in irradiance cannot explain the discrepancy observed in this case. In the following month (April 2013), *Thalassiosira* spp. accounted for 77% of cells, but virtually no iPDMPO. This could have been due to increased growth of other genera due to enhanced light during incubation (50%) relative to *in situ* (4%). Yet the genus with the highest V_{PDMPO} at this time (*Pseudo-nitzschia* spp.) dominated cell numbers following month, suggesting a real difference in growth rates between genera *in situ*. While it is likely that differences in light intensity between

incubations and *in situ* conditions played a role in the discrepancies observed between iPDMPO, cell numbers and SA, this effect is not sufficient to explain all of the disagreement between these measurements.

Previous work suggests that diatom species may be a significant predictor of the relationship between SiO_2 and PDMPO incorporation (Chapter 2). If this is the case, iPDMPO measurements could be confounded by taxonomic differences. When cells were kept intact, no significant differences in ratio were observed between *Chaetoceros* spp., *Thalassiosira* spp., and *Skeletonema* spp. (Chapter 2, Table 2.2). However, it is unlikely that cells remain intact during preparation of microscope slides as cells are immersed in de-ionized water and then dried. When cells were lysed, *Thalassiosira pseudonana* had a significantly lower Si:PDMPO ratio than *Chaetoceros contortus*, while *Skeletonema dohrnii* was intermediate between them. If these ratios are more representative of PDMPO incorporation as measured by iPDMPO, this taxonomic difference could affect results as presented here. However, when genus specific ratios were applied to iPDMPO measurements, correlations of iPDMPO with cell numbers and SA did not change ($R^2 = 0.32$ for cell numbers, $R^2 = 0.49$ for SA). While taxonomic differences in the ratio of Si:PDMPO incorporation would affect the contributions of taxa to total assemblage $bSiO_2$ production, they do not change the discrepancy between iPDMPO, cell numbers and SA measurements presented here.

The discrepancy between the contribution of a species to iPDMPO and cell numbers or SA likely reflects fundamental differences in these measurements. Cell numbers and total diatom SA (or other indicators of biomass) indicate concentrations, while iPDMPO indicates a rate. When relating assemblage composition to the characteristics of the assemblage overall, it is important that these measurements are matched appropriately. For example, measurements of particulate concentrations (e.g. chl *a*, $bSiO_2$) should be related to measurements of biomass (e.g. volume for chl *a*, SA for $bSiO_2$). In contrast, rate measurements (e.g. primary production, ρ) are more related to the composition of the productive assemblage, which can be determined using PDMPO. Therefore, PDMPO

measurements should provide insight into the relationship between diatom assemblage composition and community wide fluxes.

4.4.2. Dynamics of Diatom Biomass and Production

Six diatom genera dominated diatom cell numbers and $bSiO_2$ production in Saanich Inlet (Figure 4.3). The seasonal succession in cell numbers observed for these genera (Figure 4.2) agreed with descriptions from previous studies that determined cell numbers from seawater samples (Takahashi et al. 1977; Hobson 1981, 1983; Parsons et al. 1983; Sancetta and Calvert 1988; Grundle et al. 2009), sediment traps (Sancetta and Calvert 1988), and a 91 year sediment core record (McQuoid and Hobson 1997). Numerically, *Chaetoceros* spp. dominated overall within the Inlet, and in summer and fall/winter (Figure 4.2B, F, H; Hobson 1981; Sancetta and Calvert 1988; McQuoid and Hobson 1997; Grundle et al. 2009). Only in spring did other genera dominate cell numbers, primarily *Thalassiosira* spp. and *Skeletonema* spp. (Figure 4.2D, Hobson 1981, 1983; Sancetta and Calvert 1988; McQuoid and Hobson 1997). However, the community composition determined from cell numbers did not correspond to the composition of the $bSiO_2$ producing community as inferred from iPDMPO (Figure 4.2). Although cell numbers suggest a diatom community dominated by *Chaetoceros* spp.; *Thalassiosira* spp., *Skeletonema* spp., and *Ditylum* spp. were each responsible for a similar or greater share of $bSiO_2$ production during every season.

It is possible that taxonomic differences in the relationship between SiO_2 and PDMPO incorporation could affect these results. As discussed above in section 4.4.2., different diatom genera may have different ratios of Si:PDMPO incorporation (Chapter 2). Were genus specific ratios of Si:PDMPO adopted for *Thalassiosira* spp., *Skeletonema* spp., and *Chaetoceros* spp. (Chapter 2, Table 2.2) assuming that cells on microscope slides are lysed, the balance of $bSiO_2$ production throughout an annual cycle shifts somewhat between taxa. Adopting genera specific Si:PDMPO ratios decreases the proportion of $bSiO_2$ production from *Thalassiosira* spp. in spring, but this genus still dominates (64%). The share of $bSiO_2$ production from *Chaetoceros* spp. in spring increases to 21%. In

summer, the share of $bSiO_2$ production due to *Chaetoceros* spp. increases to 49%, while *Skeletonema* spp. decreases to 24% when genus specific Si:PDMPO ratios are applied. During fall, adopting genus specific Si:PDMPO ratios causes little difference (6% or less) in the contributions of different taxa. If genus specific ratios from Chapter 2 are applied, *Chaetoceros* spp. dominates $bSiO_2$ production (29%) while the proportion from *Thalassiosira* spp. decreases to 20% over an annual cycle within Saanich Inlet. Consequently, the role of *Thalassiosira* spp. in annual $bSiO_2$ production could be over-estimated in results presented in Figure 4.2 if the ratio determined for this genus with high uncertainty in Chapter 2 is accurate. However, this genus would still dominate $bSiO_2$ production during the spring bloom.

In order to determine the controls on diatom production throughout an annual cycle, it is useful to combine cell count and iPDMPO measurements. Although cell numbers indicated that *Skeletonema* spp. dominated cell numbers in early spring, iPDMPO measurements suggest that this genus contributed little to $bSiO_2$ production at this time (Figure 4.5). Therefore, *Skeletonema* spp. growth must have occurred even earlier in the season (prior to February in 2013) in order to explain the cell numbers observed. Late winter/early spring blooms of *Skeletonema* spp. have been observed in the nearby Strait of Georgia (Hobson and McQuoid 1997), suggesting that this species is present early in the annual succession, likely because it is a superior competitor when irradiance is low.

During February 2013, March 2013, and May 2012, *Thalassiosira* spp. dominated community $bSiO_2$ production, inferred from iPDMPO. This agrees with the observations of others (Hobson 1981, 1983; Sancetta and Calvert 1988; McQuoid and Hobson 1997) which suggest that *Thalassiosira* spp. is a major component of the spring bloom, presumably due to its high growth rate relative to other genera when nutrient concentrations are high and light is sufficient. In both years, this was followed by low diatom abundance and biomass during June. During July and August, *Chaetoceros* spp. and *Skeletonema* spp. were the major contributors to cell numbers and $bSiO_2$ production, as has been observed previously (Hobson, 1983; Sancetta and Calvert, 1988). When summer nitrate concentrations were moderate (NO_3^- ~5 µmol L^{-1}, August 2012 and July

2013) *Skeletonema* spp. tended to be more important to cell numbers and $bSiO_2$ production, while *Chaetoceros* spp. dominated when nitrate levels were lower (NO_3^- <0.5 µmol L^{-1}, July 2012, August 2013).

During fall and winter, *Chaetoceros* spp., *Thalassionema* spp., and *Thalassiosira* spp. were present and contributed to $bSiO_2$ production. However, the largest contributor to $bSiO_2$ production during fall was *Ditylum* spp. (Figure 2.4), which dominated $bSiO_2$ production and diatom biomass in November 2013 (Figure 2.7). This is in agreement with previous studies that have observed *Ditylum* spp. in the fall (Takahashi 1977, McQuoid and Hobson 1997). As only one *Ditylum* spp. bloom was observed during the present study it is not possible to determine how widespread blooms of this genus are. In contrast to previous studies, no summer *Ditylum* spp. blooms were observed (Sancetta and Calvert 1988, McQuoid and Hobson 1997). Although *Rhizosolenia* spp. was present during fall 2013 as has been observed in previous work (Sancetta and Calvert 1988, McQuoid and Hobson 1997) this genus never contributed significantly to $bSiO_2$ production determined from PDMPO.

In this study, the composition of the productive assemblage was determined for $bSiO_2$ production rates because this is possible using the PDMPO tracer. However, when linking the diatom community to food webs or global biogeochemical cycles, carbon (C) is usually the currency of choice, instead of Si. The contribution of a genus to primary production may not be the same as its contribution to $bSiO_2$ production. While $bSiO_2$ is at cell periphery and related to cell SA, C is found throughout the cell and more closely related to cell volume (V, Brzezinski 1985; Marchetti and Harrison 2007). Therefore, a large species (e.g. *Ditylum* spp.) with a low SA:V would be expected to have a lower cellular Si:C, and contribute less to $bSiO_2$ production than primary production. The contribution of a genus to $bSiO_2$ production could also differ from its contribution to primary production if the incorporation of Si and C into the cell were decoupled. Cellular $bSiO_2$ content may vary relative to C, and cellular Si:C may be affected by growth rate and macronutrient availability (Martin-Jézéquel et al. 2000; Claquin et al. 2002; Brzezinski et al. 2005; Marchetti and Harrison 2007; Durkin et al. 2013). But when

nutrients are plentiful and growth rates are high, such decoupling is less likely. Nutrient concentrations were low (NO_3^- + NO_2^- <5 µmol L^{-1}, Table 4.1) in only four months sampled, mostly during summer. Consequently, the contribution of summer genera to $bSiO_2$ production may not match primary production if species within the community were differentially NO_3^- limited (Claquin et al. 2002). However, during most months sampled during this study nutrient concentrations were high (NO_3^- + NO_2^- > 5 µmol L^{-1}, Table 4.1), and these high nutrient months accounted for most of the primary production measured during this study (77 ± 5 %). Therefore, Si and C decoupling is less likely for most of the production measured in this study, and the contributions of different species to $bSiO_2$ production may generally reflect their contribution to primary production.

Measured primary production differed substantially between the two years (Figure 4.1). However, much of this is likely due to the timing of sample collection rather than a real difference between years. The majority of the difference observed between 2012 and 2013 was due to spring primary production, and satellite data suggests that this may be due to mismatch between the timing of sample collection and the spring bloom. In the nearby Strait of Georgia, satellite data suggests that chl *a* concentrations were highest during April 2012 at the time of sample collection, while the highest chl *a* in 2013 occurred between March and April sampling (Costa et al. 2013; Allen et al. 2014). Remote sensing data also suggests that the Strait of Georgia bloom in 2013 was two weeks shorter (Costa et al. 2013; Gower 2014), so it is likely that there was also some real difference in phytoplankton biomass between the years. Despite the lower than expected phytoplankton biomass and primary production measured during spring 2013, spring still accounted for more than half of the primary production measured over the entire study period (53 ± 4%). *Thalassiosira* spp. accounted for the majority of spring $bSiO_2$ production (79%), and if the contribution of this genus to the primary production of the whole assemblage matched its contribution to $bSiO_2$ production, *Thalassiosira* spp. alone would account for 42% of primary production within Saanich Inlet.

The seasonality of primary production measured in this study may not reflect a typical cycle for this location; other studies have found that primary production rates are high in summer, and may be more important than spring production to the annual total (Timothy and Soon 2001; Grundle et al. 2009; Suchy 2014). Tidally driven inputs replenish nutrients during summer, leading to higher phytoplankton biomass at this time than is typical for many temperate marine locations (Takahashi et al. 1977; Gargett et al. 2003). As these tidally driven nutrient inputs occur every two weeks, monthly sampling is inadequate to resolve these events and any subsequent phytoplankton response. During the present study, measurements during summer months were likely influenced by the different tidal regimes that occurred during sampling. In July 2012, the highest summer productivity rate was observed (Figure 4.1), likely because a spring tide had occurred one week before (Fisheries and Oceans Canada, data available at http://tides.gc.ca/eng/data). This likely caused resupply of nutrients which were subsequently consumed by phytoplankton by the time of sample collection (Table 4.1) and contributed to the high diatom biomass and productivity observed during this month. In contrast, August 2012 and July 2013 were sampled during spring tide, which could explain the higher nutrient concentrations measured at this time. However, diatoms likely would not have had enough time to respond to the increase in nutrients, which could explain why diatom biomass was lower during these months than during July 2012. August 2013 sampling took place 9 days after the spring tide, and nutrient concentrations at this time were depleted. Although chl *a* concentrations were moderate at this time, productivity rates were low, perhaps a result of nutrient exhaustion.

In a previous study, Timothy and Soon (2001) observed different seasonality in primary production than in the present study. They found that primary production in summer was higher than in spring and accounted for 60% of the annual total at the mouth of the inlet and 40% at the head. Although they too sampled monthly, if this seasonality is more representative of an average cycle in Saanich Inlet than observed in my study, the role of *Thalassiosira* spp. in annual primary production would be less than estimated above. If the contribution of different diatom taxa to primary production was the same as their contribution to $bSiO_2$ production, and if summer accounted for 60% of primary

production (Timothy and Soon, 2001), *Thalassiosira* spp. would still dominate annual primary production (25%) but *Chaetoceros* spp. and *Skeletonema* spp. would contribute only slightly less (23% and 19% respectively).

The composition of the community responsible for primary production has consequences for its fate. Diatom species differ in their sinking rates, larger species sink faster (Waite et al. 2011), and a higher proportion may sink to depth than smaller species (Annett et al. 2009). In Saanich Inlet, the *Thalassiosira* spp. present in spring is larger on average than the *Chaetoceros* spp. or *Skeletonema* spp. (2.3 and 5.7 times greater SA, respectively). Additionally, zooplankton grazing affects these taxa differently. Sancetta (1989) observed that fragmentation of diatom valves in Saanich Inlet sediments was greater for late spring and summer *Chaetoceros* spp. and *Skeletonema* spp. than the *Thalassiosira* spp. that occurred early in the spring. If more intact cells of *Thalassiosira* spp. are exported to depth, less of the associated organic carbon may be respired before reaching the sediments. Consequently, the 25 – 42% of primary production produced by *Thalassiosira* spp. may be exported to depth more effectively than that from *Chaetoceros* spp. and *Skeletonema* spp., and contribute more to carbon burial in the sediments. Fjords such as Saanich Inlet are important to the global carbon cycle; they represent only 0.1% of ocean surface area but account for 11% of marine carbon burial on the planet (Keil 2015). Therefore, seasonally occurring *Thalassiosira* spp. blooms may play a significant role in global carbon cycling.

4.4.3. Using PDMPO to Indicate Diatom Assemblage Transitions

One of the most striking patterns in phytoplankton ecology is the rapid seasonal accumulation of phytoplankton biomass during spring in temperate regions, which is usually dominated by diatoms (Uitz et al. 2010). Sverdrup's (1953) classic theory posits that this occurs due to the alleviation of light limitation, allowing phytoplankton to rapidly consume the nutrients that have accumulated over winter. Blooms are normally detected by high concentrations of diatom biomass, but the initiation of growth that could have caused the bloom would have occurred prior to this.

By estimating V_{PDMPO} it is possible to detect an increase in diatom cellular activity before a resulting increase in cell numbers. This does not strictly indicate growth rate; V_{PDMPO} is an estimate of specific $bSiO_2$ production rate which can be equivalent to growth rate when growth is balanced, and the proportions of cellular constituents (e.g. C, Si) are constant (MacIntyre and Cullen 2005). Balanced growth occurs when phytoplankton are grown under constant conditions, which is not possible in the natural environment because of daily variability in light. In the case of V_{PDMPO} measurements, changes in $bSiO_2$ per cell would confound their relationship with growth rate, as in these cases the accumulation of $bSiO_2$ per genus would not reflect the rate of cell division. How often this may be the case is unknown. However, Znachor et al. (2013) found a strong correlation between PDMPO fluorescence per cell and growth rate in three diatom species from a eutrophic reservoir. This suggests that PDMPO may be a useful proxy for diatom growth rate even if environmental conditions are not constant.

Znachor et al. (2013) also found that the relationship between PDMPO fluorescence and growth rate (determined from cell numbers) differed between the species tested, and reflected differences in cell size. Here, V_{PDMPO} was calculated as a proxy for growth rate. The calculation of V_{PDMPO} differs from the calculation of Znachor et al. (2013) in that iPDMPO for a genus was normalized to its SA, while Znachor et al. (2013) determined fluorescence per cell by normalizing PDMPO to diatom cells that had chl *a* fluorescence. Surface area may over-estimate the amount of living diatom biomass, as cells counted may no longer be alive. This would result in under-estimation of the growth rate of living diatom cells. In contrast, detecting only those cells with chl *a* should exclude non-living cells, though it may be hard to identify diatom cells based on chl *a* fluorescence alone as only the chloroplasts would be visible. This could cause living diatom cells not labelled with PDMPO to be missed from measurements of the average PDMPO per cell for a given genus, and growth rates over-estimated. An additional advantage of normalizing PDMPO fluorescence by SA is that differences between genera in $bSiO_2$ quota due to differences in size are accounted for, allowing comparisons between them.

This does not account for differences in $bSiO_2$ thickness, which may vary. In laboratory experiments, Durkin et al. (2013) found that differences in $Si(OH)_4$ concentration caused a 2.5 fold change in $bSiO_2$ per cell. However, differences in SA between genera are often much larger than this. For the key diatom species within Saanich Inlet, the largest genus (*Ditylum* spp.) had a SA 72 times greater than the smallest diatom (*Skeletonema* spp.). Thus, differences between genera in SA are likely to account for much of the variability in $bSiO_2$ quota. Therefore, normalizing total iPDMPO to the total SA for different diatom taxa should be a reasonable proxy for specific $bSiO_2$ production rates, which may be useful as an indicator of growth rate under certain conditions.

During spring 2013, increases in V_{PDMPO} preceded a genus' dominance of diatom cell numbers (Figure 4.5). A close relationship between V_{PDMPO} and cell numbers the following month was not observed for other times of the year (Figure 4.6, 4.7). This may be due to more transient changes in environmental conditions, for example tidally driven nutrient inputs during summer (Gargett et al. 2003). Samples were collected only every month, and would not capture increases in V_{PDMPO} and cell numbers on time scales shorter than this. As changes in V_{PDMPO} occur on time scales of hours to days, monthly sampling has inadequate temporal resolution to capture these processes. In addition, loss processes are unlikely to be constant throughout an annual cycle. Zooplankton biomass and grazing in Saanich Inlet are higher during summer than in spring (Suchy 2014, Sancetta 1989), and consequently summer phytoplankton blooms may experience more grazing pressure than spring blooms. Accumulation of cell numbers reflects net population growth; therefore, an increase in intrinsic phytoplankton growth rate may not result in accumulation if mortality exceeds growth. The lack of relationship between V_{PDMPO} and cell numbers except in spring 2013 does not necessarily mean that V_{PDMPO} was a poor indicator of growth rate, but rather that an increase in growth rate alone was not sufficient to generate an increase in cell numbers that was detectable the following month.

During spring 2013, V_{PDMPO} was a useful indicator of diatom assemblage transitions. *Thalassiosira* spp. dominated $bSiO_2$ production for the spring season overall, and had the highest cell numbers and SA during April (Figure 4.5). However, V_{PDMPO} suggests that *Thalassiosira* spp. had the highest specific $bSiO_2$ production rate earlier in the season, in February and March. If the growth of *Thalassiosira* spp. increased due to increased light availability in spring, the threshold of irradiance required for an increase in *Thalassiosira* spp. differs when its dominance of cell numbers or V_{PDMPO} are considered. In the week prior to sampling in April, average insolation was 3.5 times higher than in February (School Based Weather Station Network), suggesting that light required for *Thalassiosira* spp. growth may be substantially less than previously thought. In this case, PDMPO was useful to pinpoint the timing of *Thalassiosira* spp. growth initiation, which was prior to the biomass accumulation observed.

PDMPO was useful as a tracer to indicate diatom $bSiO_2$ production rates, which could not be predicted from cell numbers or biomass. As a proxy for specific $bSiO_2$ production rate, V_{PDMPO} should allow better understanding of the controls on diatom productivity. For example, determining when the initiation of diatom growth leading to the spring bloom occurs will allow more accurate determination of the factors (e.g. light intensity) that caused it. This should be useful for model parameterization, which make predictions about the spring bloom based on light intensity (e.g. Collins et al. 2009). Additionally, $bSiO_2$ production rates derived using PDMPO as a proxy should be useful for distinguishing the processes that lead to biomass accumulation. Both phytoplankton intrinsic growth rates and mortality rates determine whether phytoplankton population numbers and biomass increase. The relative importance of these processes to the development of the spring bloom may not be as simple as described by Sverdrup (1953), and is currently debated (Behrenfeld 2010; Fischer et al. 2014). As a sensitive method for indicating diatom growth rate, PDMPO has the potential to illuminate the processes that control diatom productivity in the global ocean.

4.5. Conclusions

The PDMPO tracer shed new light on diatom community dynamics within Saanich Inlet. The composition of the assemblage contributing to $bSiO_2$ production was determined using PDMPO fluorescence microscopy, and could not be inferred from the composition of cell numbers or biomass. By combining microscopic and fluorometric measurements of PDMPO, it was possible to translate the proportion of $bSiO_2$ production by a given genus to its absolute $bSiO_2$ production for the study period overall. In addition, PDMPO was useful as an indicator of taxon specific $bSiO_2$ production rates, and detected transitions in assemblage composition prior to their observation from cell numbers during a spring bloom. This suggests that PDMPO has the potential to substantially enhance investigation of the interplay between diatom community composition, growth rates, and productivity. Consequently, the critical role that diatoms fill in marine food webs and elemental cycling can be better understood.

Chapter 5: General Conclusions

5.1. Summary of Major Findings

This thesis presents several optimizations for the use of PDMPO as a tracer of $bSiO_2$ production in marine diatoms. Additionally, results of field work in two marine locations using PDMPO to investigate diatom community dynamics are described.

5.1.1. Basis of PDMPO as a Tracer of $bSiO_2$ Production

The incorporation of PDMPO into diatom frustules did not have a fixed stoichiometric relationship with SiO_2. The Si:PDMPO relationship of incorporation was altered by PDMPO concentration, suggesting that factors that differentially affected transport of $Si(OH)_4$ or PDMPO to the SDV determine the ratio of incorporation. The Si:PDMPO incorporation relationship was significantly affected by diatom species, though this effect was smaller when cells were lysed.

From laboratory cultures, a ratio of 4200 ± 380:1 best fit pPDMPO concentrations as a function of SiO_2 concentrations produced since the addition of PDMPO, when cells were lysed during filtration and cells were grown in the presence of 125 nmol L^{-1} PDMPO. This relationship predicts 30% more SiO_2 incorporation from a given amount of PDMPO incorporation than previous work (Leblanc and Hutchins 2005) and performed better in a field comparison between $bSiO_2$ production determined by PDMPO and by ^{32}Si. However, PDMPO over-estimated rates of $bSiO_2$ production when $bSiO_2$ production rates were low (<1 µmol L^{-1} d^{-1}). In a few cases, this may have been related to dinoflagellate abundance as reported in previous work (Alvarado 2012), but more often appeared due to differences in ambient $Si(OH)_4$ concentration. Therefore, further optimizations of the technique are necessary to ensure that PDMPO remains a robust tracer of $bSiO_2$ production when diatoms dominate the phytoplankton assemblage and when $Si(OH)_4$ concentrations are below 10 µmol L^{-1}.

5.1.2. Quantification of PDMPO by Microscopy

Laboratory tests confirmed that quantification of PDMPO by microscopy agreed with measurements of PDMPO by fluorometry, suggesting that both methods are useful for determining $bSiO_2$ production in diatoms. However, microscope measurements of thick diatom species were over-estimated for different sizes of diatoms when objective lenses with high numerical apertures were used. When a low numerical aperture objective was used to quantify PDMPO, these measurements agreed with fluorometric measurements. This was true for both relative measurements of PDMPO fluorescence from different species within the same slide, and for absolute measurements of PDMPO incorporated per mL of diatom laboratory culture. Although microscope and fluorometric measurements generally agreed between field samples, variability in microscope measurements of PDMPO was large, suggesting that microscope measurements of PDMPO should not be used to replace total diatom community measurements of $bSiO_2$ production. Instead, microscope measurements of PDMPO fluorescence should be used in combination with total community measurements of $bSiO_2$ production to determine absolute $bSiO_2$ production rates for different taxa within mixed assemblages.

5.1.3. Using PDMPO to Investigate Diatom Community Dynamics in Marine Environments

When the PDMPO method was employed in marine locations, it provided novel information about diatom community dynamics. The contribution of different genera to PDMPO florescence was not correlated with their contribution to cell numbers. In some cases, a genus' surface area was better correlated with PDMPO fluorescence, but this was not consistent. As a result, the genera that were most dominant numerically were often not the most important for $bSiO_2$ production. This reflects the differences between these parameters, as cell numbers and surface area are concentrations whereas PDMPO indicates a production rate. The PDMPO tracer was also useful for distinguishing actively growing diatom cells from inactive cells. When normalized to a genus' surface area, PDMPO fluorescence was useful as a proxy for specific $bSiO_2$ production rate. In

some cases this predicted shifts in composition within the diatom community, and better indicated when assemblage transitions occurred.

5.2. Improving Measurements of $bSiO_2$ Production Based on PDMPO

5.2.1. The Effect of $Si(OH)_4$ on the Si:PDMPO Ratio of Incorporation

One of the major questions raised by this work is how extracellular $Si(OH)_4$ concentrations affect the Si:PDMPO ratio of incorporation. In the laboratory, Si:PDMPO was strongly dependent on extracellular PDMPO concentration, so it seems likely that converse would also be true and that $Si(OH)_4$ concentration would affect incorporation. Previous work with laboratory cultures by Durkin et al. (2013) suggests that this may be the case, and that increases in $bSiO_2$ per cell associated with high $Si(OH)_4$ concentrations (20 and 80 μmol L^{-1}) affect the Si:PDMPO ratio of incorporation.

In marine field tests ρ_{PDMPO} was sometimes higher than ρ_{GROSS} when ρ_{GROSS} was less than 1 μmol L^{-1} d^{-1}. In many of these cases, $Si(OH)_4$ concentrations were low enough that they may have limited uptake by transporters. But in a few cases, $Si(OH)_4$ concentrations were high enough to saturate transporters, but below the threshold expected for a switch to uptake dominated by diffusion. It is possible that both transporter limitation and uptake mode may reduce $Si(OH)_4$ uptake into the cell, and consequently incorporation rate of SiO_2 into the frustule. As $Si(OH)_4$ concentration is unlikely to affect PDMPO incorporation rates, reduced uptake of $Si(OH)_4$ would cause an enrichment of PDMPO in the frustule, leading to the over-estimation of ρ_{PDMPO} relative to ρ_{GROSS}.

In order to assess the effect of $Si(OH)_4$ on PDMPO's performance as a tracer of $bSiO_2$ production it is necessary to conduct further experiments with laboratory cultures. Concentrations of $Si(OH)_4$ in the range of 0-10 μmol L^{-1} should be prioritized, as this is when uptake limitation of $Si(OH)_4$ would occur. In addition, concentrations above and below the 30 μmol L^{-1} switch between uptake modes (Thamatrakoln and Hildebrand

2008) should be tested to assess if uptake mode has an effect. If $Si(OH)_4$ affects the Si:PDMPO relationship of incorporation it may be possible to include it as a parameter in the relationship describing Si:PDMPO incorporation. Preliminary attempts to account for differences in $Si(OH)_4$ concentration yielded better agreement between ρ_{PDMPO} relative to ρ_{GROSS} (Appendix H) suggesting that PDMPO will remain useful as a tracer in low $Si(OH)_4$ conditions. However, more experimentation is necessary before applying a correction for $Si(OH)_4$ concentration to PDMPO measurements is warranted.

5.2.2. Optimizing Microscope Configurations for PDMPO Quantification

Diatom cells vary widely in size in morphology, which make it difficult to reliably quantify PDMPO fluorescence from the variety of diatom cells present in a natural mixed assemblage. Measurements of thicker species were over-estimated when a high numerical aperture objective was used to quantify PDMPO fluorescence by widefield microscopy. Optical sectioning imaging ensures that fluorescence from the entire depth of a cell is captured, but is far more time consuming than widefield fluorescence imaging. To compromise between time and measurement quality, a low numerical aperture objective and widefield fluorescence microscope were used to quantify PDMPO in this thesis. However, low numerical apertures objectives are inefficient at light collection because they capture fewer angles of light.

It is possible that a superior microscope configuration could be designed to meet the unusual challenges of quantifying PDMPO within diatom cells. It may be possible to minimize the trade-off between a long depth of focus (longer with low numerical aperture objectives) and light capture (more light captured with high numerical apertures) by using a collimated excitation light source. If excitation light reached the sample in a collimated beam, rays of light within the beam would be parallel to one another, and not focused. Consequently, this excitation would theoretically have an infinite depth of focus, and the entire depth of the cell could be illuminated.

Most widefield fluorescence microscopes are configured for epifluroescence: the excitation and emission light pass through the same objective. This reduces the excitation light that returns to the objective, as the majority of excitation light will pass through the sample to the side opposite the objective lens. This is less important with PDMPO than with other fluorophores, as it has a relatively large Stoke's shift: the excitation and emission wavelengths are dissimilar. Thus, it may be possible to screen out excitation light from the fluorescence emitted from PDMPO even if a transmission fluorescence microscope configuration was used. Were this possible, the excitation and emission light would not pass through the same objective, instead excitation light would pass through the sample to the detector. This could allow a collimated light source to be used for excitation, while using a microscope objective to focus fluorescence emitted. This configuration would have a limited depth of focus for the detection of fluorescence, defined by the numerical aperture of the objective used to capture emitted fluorescence. But unlike epifluorescence microscopes, excitation of fluorescence would not have a limited depth of focus, and as a result measurements of PDMPO fluorescence using a transmission configuration could be less affected by mismatch between depth of focus and diatom cell size. This would improve quantification of PDMPO fluorescence in diatoms by reducing effect of depth of focus on PDMPO measurements by microscopy.

5.3. Application of PDMPO to Investigate Diatom Ecology

5.3.1. Inactive Diatoms in the Water Column

A consistent finding of this thesis is that rarely does the contribution of a diatom genus to cell numbers indicate its contribution to $bSiO_2$ production. Even when surface area per genus, a proxy for $bSiO_2$, was compared with $bSiO_2$ production the contribution of a genus was rarely similar to both. These discrepancies indicate that relative production rates are poorly correlated with biomass within a community, and reflect differences in specific production rates between genera. In some cases, the genus that dominated $bSiO_2$ accounted for almost none of the $bSiO_2$ produced. This suggests that at some times the majority of $bSiO_2$ present is in cells that are not producing $bSiO_2$.

It is possible that diatoms not labelled by PDMPO were living, but did not produce $bSiO_2$ during the incubation. Production of $bSiO_2$ is closely linked to the cell cycle; new $bSiO_2$ is produced when a cell divides. If a genus divided only once every several days, many of the cells would not be labelled with PDMPO during a 24 hour incubation, and appear inactive despite producing organic matter. Alternatively, cells not labelled with PDMPO may no longer be living. As $bSiO_2$ dissolution is generally slower than organic matter respiration, empty frustules may be present after cells have died. However, these empty frustules would be expected to sink rapidly, as $bSiO_2$ is dense and buoyancy maintenance requires energy in diatoms (Waite et al. 2011). In spite of this, high concentrations of inactive $bSiO_2$ have been previously documented in the water column. For example, Brzezinski et al. (2008) estimate that greater than 65% of $bSiO_2$ present during sampling in the Equatorial Pacific may have been detrital. This is in agreement with results from this thesis, as in several cases, one genus accounted for a large share of $bSiO_2$ (90%), but was less than 1% of $bSiO_2$ production at the depth of the chlorophyll maximum. Therefore the rapid sinking rate of non-living diatoms and high concentrations of detrital $bSiO_2$ in the water column present an apparent contradiction.

PDMPO may be able to shed light on this contradiction, as it labels newly produced $bSiO_2$. By conducting time series incubations with mixed natural assemblages, it would be possible to assess the proportion of diatom cells that divided over different time periods. This would allow slow growing and non-living diatoms to be distinguished. If non-living diatom frustules remained in the surface water for longer than previously expected (e.g. several days), this could allow time for dissolution of $bSiO_2$ and an additional $Si(OH)_4$ source to diatom cells.

In addition, determining the proportion of labelled cells could improve estimates of maximum specific $bSiO_2$ production rates. Specific $bSiO_2$ production rates are calculated by normalizing the $bSiO_2$ production determined for a community to the concentration of $bSiO_2$ present. However, cells that do not deposit any $bSiO_2$ would contribute to $bSiO_2$ measured and reduce the specific $bSiO_2$ production rate. Using PDMPO, it would be

possible to determine the proportion of inactive cells, and exclude these from measurements of specific $bSiO_2$ production rate. This would yield a rate for the active diatom community, and be more representative of processes occurring in living diatoms on a cellular scale.

5.3.2. Dynamics of Diatom Bloom Initiation

Determining the causes of accumulations of biomass and phytoplankton production is one of the central goals of biological oceanography. Yet even the cause of the spring bloom in the North Atlantic, one of the largest scale patterns in oceanography, is currently debated (Fischer et al. 2014). In 1953, Sverdrup postulated the Critical Depth Hypothesis which predicts that the spring bloom in the North Atlantic occurs annually due to the shoaling of the mixed layer. Once the mixed layer is shallower than a threshold light intensity required for phytoplankton growth (the critical depth) phytoplankton biomass begins to accumulate and the bloom occurs. This suggests that the bloom occurs due to an increase in phytoplankton growth rate, and is not dependant on mortality rates.

In the 60 years since Sverdrup's theory, other hypotheses have arisen to explain the sudden occurrence of spring blooms (see Fischer et al. 2014 for a review). In contrast to Sverdrup (1953) theory, Behrenfeld (2010) suggests that the spring bloom is not the result of an increase in phytoplankton growth rate, but rather a decrease in mortality rate. Behrenfeld (2010) makes the argument that the timing of biomass accumulation is not the same as the timing of initiation of diatom growth. This is evident in results from Saanich Inlet presented in this thesis, which found an increase in specific $bSiO_2$ production rates determined using PDMPO prior to accumulation of $bSiO_2$ for the genera present during the spring.

PDMPO allows $bSiO_2$ production rates to be quantified for individual diatom cells by fluorescence microscopy. This yields a cellular production rate, independent of cell numbers. Therefore, an increase in PDMPO fluorescence per cell during spring when the

mixed layer shoals prior to the spring bloom would indicate an increase in diatom cellular activity, and support Sverdrup's (1953) theory regarding bloom formation. In contrast, if the theory of Behrenfeld (2010) was correct, an increase in PDMPO incorporation per cell would not precede the spring bloom. If a decrease in grazing rates caused the spring diatom bloom, this would not affect the amount of PDMPO fluorescence per cell, simply the number of cells present. Therefore PDMPO could be useful for distinguishing the processes that lead to spring blooms in the North Atlantic, and the marine environment overall.

Bibliography

Adjou, M., P. Tréguer, C. Dumousseaud, R. Corvaisier, M. A. Brzezinski, and D. M. Nelson. 2011. Particulate silica and Si recycling in the surface waters of the Eastern Equatorial Pacific. Deep Sea Res. Part II Top. Stud. Oceanogr. **58**: 449–461.

Albright, L. J., C. Z. Yang, and S. Johnson. 1993. Sub-lethal concentrations of the harmful diatoms, *Chaetoceros concavicornis* and *C. convolutus*, increase mortality rates of penned Pacific salmon. Aquaculture **117**: 215–225.

Alldredge, A. L., and C. G. Gotschalk. 1989. Direct observations of the mass flocculation of diatom blooms: characteristics, settling velocities and formation of diatom aggregates. Deep Sea Res. **36**: 159–171.

Allen, J. T., L. Brown, R. Sanders, C. M. Moore, A. Mustard, S. Fielding, M. Lucas, M. Rixen, G. Savidge, S. Henson, and D. Mayor. 2005. Diatom carbon export enhanced by silicate upwelling in the northeast Atlantic. Nature **437**: 728–32.

Allen, S. E., D. J. Latornell, B. Moore-Maley, and D. Ianson. 2014. Spring Phytoplankton Bloom in the Strait of Georgia, p. 97–106. *In* R.I. Perry [ed.], State of the physical, biological and selected fishery resources of Pacific Canadian marine ecosystems in 2013. Can. Tech. Rep. Fish. Aquat. Sci. 3102.

Alvarado, N. D. 2012. A Modified Protocol for Monitoring Silicic Acid Uptake in Natural Phytoplankton Assemblages. University of California, Santa Cruz.

Del Amo, Y., and M. A. Brzezinski. 1999. The chemical form of dissolved Si taken up by marine diatoms. J. Phycol. 1162–1170.

Annenkov, V. V., E. N. Danilovtseva, S. N. Zelinskiy, T. N. Basharina, T. A. Safonova, E. S. Korneva, Y. V. Likhoshway, and M. A. Grachev. 2010. Novel fluorescent dyes based on oligopropylamines for the in vivo staining of eukaryotic unicellular algae. Anal. Biochem. **407**: 44–51.

Annett, A. L., D. S. Carson, X. Crosta, A. Clarke, and R. S. Ganeshram. 2009. Seasonal progression of diatom assemblages in surface waters of Ryder Bay, Antarctica. Polar Biol. **33**: 13–29.

Armbrust, E. V. 2009. The life of diatoms in the world's oceans. Nature **459**: 185–92.

Azam, F., B. B. Hemmingsen, and B. E. Volcani. 1974. Role of silicon in diatom metabolism. V. Silicic acid transport and metabolism in the heterotrophic diatom *Nitzschia alba*. Arch. Microbiol. **97**: 103–114.

De Baar, H. J. W., P. W. Boyd, K. H. Coale, M. R. Landry, A. Tsuda, P. Assmy, D. C. E. Bakker, Y. Bozec, R. T. Barber, M. A. Brzezinski, K. O. Buesseler, M. Boyé, P. L. Croot, F. Gervais, M. Y. Gorbunov, P. J. Harrison, W. T. Hiscock, P. Laan, C. Lancelot, C. S. Law, M. Levasseur, A. Marchetti, F. J. Millero, J. Nishioka, Y. Nojiri, T. van Oijen, U. Riebesell,

M. A. Rijkenberg, H. Saito, S. Takeda, K. R. Timmermans, M. J. W. Veldhuis, A. M. Waite, and C.-S. Wong. 2005. Synthesis of iron fertilization experiments: From the Iron Age in the Age of Enlightenment. J. Geophys. Res. **110**: 1–24.

Barwell-Clarke, J., and F. A. Whitney. 1996. Institute of Ocean Sciences nutrient methods and analysis, Fisheries and Oceans Canada.

Behrenfeld, M. J. 2010. Abandoning Sverdrup's Critical Depth Hypothesis on phytoplankton blooms. Ecology **91**: 977–89.

Benitez-Nelson, C. R., R. R. Bidigare, T. D. Dickey, M. R. Landry, C. L. Leonard, S. L. Brown, F. Nencioli, Y. M. Rii, K. Maiti, J. W. Becker, T. S. Bibby, W. Black, W.-J. Cai, C. A. Carlson, F. Chen, V. S. Kuwahara, C. Mahaffey, P. M. McAndrew, P. D. Quay, M. S. Rappé, K. E. Selph, M. P. Simmons, and E. J. Yang. 2007. Mesoscale eddies drive increased silica export in the subtropical Pacific Ocean. Science **316**: 1017–21.

Berges, J. A., D. J. Franklin, and P. J. Harrison. 2001. Evolution of an Artificial Seawater Medium: Improvements in Enriched Seawater, Artificial Water Over the Last Two Decades. J. Phycol. **37**: 1138–1145.

Bessey, C. E. 1900. The Modern Conception of the Structure and Classification of Diatoms, with a Revision of the Tribes and Rearrangement of the North American Genera. Trans. Am. Microsc. Soc. **21**: 61–86.

Bidle, K. D., and F. Azam. 1999. Accelerated dissolution of diatom silica by marine bacterial assemblages. Nature **397**: 508–512.

Blain, S., A. Leynaert, and P. Tréguer. 1997. Biomass , growth rates and limitation of Equatorial Pacific diatoms. Deep Sea Res. I **44**: 1255–1275.

Blain, S., B. Quéguiner, L. Armand, S. Belviso, B. Bombled, L. Bopp, A. Bowie, C. Brunet, C. Brussaard, F. Carlotti, U. Christaki, A. Corbière, I. Durand, F. Ebersbach, J.-L. Fuda, N. Garcia, L. Gerringa, B. Griffiths, C. Guigue, C. Guillerm, S. Jacquet, C. Jeandel, P. Laan, D. Lefèvre, C. Lo Monaco, A. Malits, J. Mosseri, I. Obernosterer, Y.-H. Park, M. Picheral, P. Pondaven, T. Remenyi, V. Sandroni, G. Sarthou, N. Savoye, L. Scouarnec, M. Souhaut, D. Thuiller, K. Timmermans, T. Trull, J. Uitz, P. van Beek, M. Veldhuis, D. Vincent, E. Viollier, L. Vong, and T. Wagener. 2007. Effect of natural iron fertilization on carbon sequestration in the Southern Ocean. Nature **446**: 1070–4.

Bowler, C., A. E. Allen, J. H. Badger, J. Grimwood, K. Jabbari, A. Kuo, U. Maheswari, C. Martens, F. Maumus, R. P. Otillar, E. Rayko, A. Salamov, K. Vandepoele, B. Beszteri, A. Gruber, M. Heijde, M. Katinka, T. Mock, K. Valentin, F. Verret, J. a Berges, C. Brownlee, J.-P. Cadoret, A. Chiovitti, C. J. Choi, S. Coesel, A. De Martino, J. C. Detter, C. Durkin, A. Falciatore, J. Fournet, M. Haruta, M. J. J. Huysman, B. D. Jenkins, K. Jiroutova, R. E. Jorgensen, Y. Joubert, A. Kaplan, N. Kröger, P. G. Kroth, J. La Roche, E. Lindquist, M. Lommer, V. Martin-Jézéquel, P. J. Lopez, S. Lucas, M. Mangogna, K. McGinnis, L. K. Medlin, A. Montsant, M.-P. Oudot-Le Secq, C. Napoli, M. Obornik, M. S. Parker, J.-L. Petit, B. M. Porcel, N. Poulsen, M. Robison, L. Rychlewski, T. a Rynearson, J. Schmutz, H. Shapiro, M. Siaut, M. Stanley, M. R. Sussman, A. R. Taylor, A. Vardi, P. von Dassow, W. Vyverman, A. Willis, L. S. Wyrwicz, D. S. Rokhsar, J. Weissenbach, E. V. Armbrust, B. R.

Green, Y. Van de Peer, and I. V Grigoriev. 2008. The *Phaeodactylum* genome reveals the evolutionary history of diatom genomes. Nature **456**: 239–44.

Boyd, P. W., C. S. Law, C. S. Wong, Y. Nojiri, A. Tsuda, M. Levasseur, S. Takeda, R. Rivkin, P. J. Harrison, R. Strzepek, J. Gower, M. McKay, E. Abraham, M. Arychuk, J. Barwell-Clarke, W. Crawford, D. Crawford, M. Hale, K. Harada, K. Johnson, H. Kiyosawa, I. Kudo, A. Marchetti, W. Miller, J. Needoba, J. Nishioka, H. Ogawa, J. Page, M. Robert, H. Saito, A. Sastri, N. Sherry, T. Soutar, N. Sutherland, Y. Taira, F. Whitney, S.-K. E. Wong, and T. Yoshimura. 2004. The decline and fate of an iron-induced subarctic phytoplankton bloom. Nature **428**: 549–53.

Bradbury, S., and G. L. Turner, eds. 1967. Historical Aspects of Microscopy, Royal Microscopical Society.

Bruland, K. W., E. L. Rue, and G. J. Smith. 2001. Iron and macronutrients in California coastal upwelling regimes: Implications for diatom blooms. Limnol. Oceanogr. **46**: 1661–1674.

Brzezinski, M. A. 1985. The Si:C:N ratio of marine diatoms: interspecific variability and the effect of some environmental variables. J. Phycol. 347–357.

Brzezinski, M. A. 2008. Mining the diatom genome for the mechanism of biosilicification. Proc. Natl. Acad. Sci. U. S. A. **105**: 1391–1392.

Brzezinski, M. A., and D. J. Conley. 1994. Silicon deposition during the cell cycle of *Thalassiosira weissflogii* (Bacillariophyceae) determined using dual rhodamine 123 and propidium iodide staining. J. Phycol. **30**: 45–55.

Brzezinski, M. A., J. L. Jones, and M. S. Demarest. 2005. Control of silica production by iron and silicic acid during the Southern Ocean Iron Experiment (SOFeX). Limnol. Oceanogr. **50**: 810–824.

Brzezinski, M. A., and D. M. Nelson. 1986. A solvent extraction method for the colorimetric determination of nanomolar concentrations of silicic acid in seawater. Mar. Chem. **19**: 139–151.

Brzezinski, M. A., and D. M. Nelson. 1989. Seasonal changes in the silicon cycle within a Gulf Stream warm-core ring. Deep Sea Res. Part A. Oceanogr. Res. Pap. **36**: 1009–1030.

Brzezinski, M. A., R. J. Olson, and S. W. Chisholm. 1999. Silicon availability and cell-cycle progression in marine diatoms. Mar. Ecol. Prog. Ser. **67**: 83–96.

Brzezinski, M. A., and D. R. Phillips. 1997. Evaluation of ^{32}Si as a tracer for measuring silica production rates in marine waters. Limnol. Oceanogr. **42**: 856–865.

Brzezinski, M., T. Villareal, and F. Lipschultz. 1998. Silica production and the contribution of diatoms to new and primary production in the central North Pacific. Mar. Ecol. Prog. Ser. **167**: 89–104.

C, M. 1703. Two Letters from a Gentleman in the Country, relating to Mr. Leuwenhoeck's Letter in Transaction, No. 283. Philos. Trans. **23**: 1494 – 1501.

Chassot, E., S. Bonhommeau, N. K. Dulvy, F. Mélin, R. Watson, D. Gascuel, and O. Le Pape. 2010. Global marine primary production constrains fisheries catches. Ecol. Lett. **13**: 495–505.

Claquin, P., V. Martin-Jézéquel, J. C. Kromkamp, M. J. W. Veldhuis, and G. W. Kraay. 2002. Uncoupling of silicon compared with carbon and nitrogen metabolisms and the role of the cell cycle in continuous cultures of *Thalassiosira pseudonana* (Bacillariophyceae) under light, nitrogen and phosphorus control. J. Phycol. **38**: 922–930.

Collins, K. A., S. E. Allen, and R. Pawlowicz. 2009. The role of wind in determining the timing of the spring bloom in the Strait of Georgia. Can. J. Fish. Aquat. Sci. **66**: 1597–1616.

Costa, M., T. Carswell, E. Young, R. Sweeting, J. Gower, R. Pawlowicz, and G. Borstad. 2013. Spatial-temporal phytoplankton bloom metrics in the Strait of Georgia derived from MODIS imagery: 2012 and previous years, p. 117–120. *In* R.I. Perry [ed.], State of physical, biological, and selected fishery resources of Pacific Canadian marine ecosystems in 2012. DFO Can. Sci. Advis. Sec. Res. Doc. 2013/032.

Cox, J. D. 1885. Some Diatom Hoops: The Question of Thier Mode of Growth (*Aulacodiscus kittoni*). Proc. Am. Soc. Microsc. **7**: 33–37.

Crawford, W. R., and M. A. Peña. 2013. Declining Oxygen on the British Columbia Continental Shelf. Atmosphere-Ocean **51**: 37–41.

Cullen, J. T., M. Chong, and D. Ianson. 2009. British Columbian continental shelf as a source of dissolved iron to the subarctic northeast Pacific Ocean. Global Biogeochem. Cycles **23**: GB4012.

Demarest, M. S., M. A. Brzezinski, D. M. Nelson, J. W. Krause, J. L. Jones, and C. P. Beucher. 2011. Net biogenic silica production and nitrate regeneration determine the strength of the silica pump in the Eastern Equatorial Pacific. Deep Sea Res. Part II Top. Stud. Oceanogr. **58**: 462–476.

Denman, K. L., D. L. Mackas, H. J. Freeland, M. J. Austin, and S. H. Hill. 1981. Persistent upwelling and mesoscale zones of high productivity off the west coast of Vancouver Island, Canada, p. 514–521. *In* F.A. Richards [ed.], Coastal Upwelling. American Geophysical Union.

Desclés, J., M. Vartanian, A. El Harrak, M. Quinet, N. Bremond, G. Sapriel, J. Bibette, and P. J. Lopez. 2008. New tools for labeling silica in living diatoms. New Phytol. **177**: 822–9.

Dewey, R., S. Mihaly, and M. Jefferies. 2013. Water properties from Ocean Networks Canada: VENUS and NEPTUNE, p. 48–51. *In* J.R. Irvine and W.R. Crawford [eds.], State of physical, biological, and selected fishery resources of Pacific Canadian marine ecosystems in 2012. DFO Can. Sci. Advis. Sec. Res. Doc. 2013/032.

Donkin, A. S. 1858. On the marine Diatomaceae of Northumberland, with a description of eighteen new species. Trans. Microsc. Soc. London **2**: 12–34.

Dugdale, R. C., and F. P. Wilkerson. 1998. Silicate regulation of new production in the equatorial Pacific upwelling. Nature **391**: 270–273.

Dugdale, R., F. Chai, R. Feely, C. Measures, A. Parker, and F. Wilkerson. 2011. The regulation of equatorial Pacific new production and pCO_2 by silicate-limited diatoms. Deep Sea Res. Part II Top. Stud. Oceanogr. **58**: 477–492.

Durbin, E. G. 1977. Studies on the autoecology of the marine diatom. J. Phycol. **13**: 150–155.

Durkee, R. P. H. 1884. The Structure of the Diatom Valve. Proc. Am. Soc. Microsc. **6**: 105–109.

Durkin, C. A., S. J. Bender, K. Yu Karen Chan, K. Gaessner, D. Grünbaum, and E. Virginia Armbrust. 2013. Silicic acid supplied to coastal diatom communities influences cellular silicification and the potential export of carbon. Limnol. Oceanogr. **58**: 1707–1726.

Durkin, C. A., A. Marchetti, S. J. Bender, T. Truong, R. Morales, T. Mock, and E. Virginia Armbrust. 2012. Frustule-related gene transcription and the influence of diatom community composition on silica precipitation in an iron-limited environment. Limnol. Oceanogr. **57**: 1619–1633.

Durkin, C. A., T. Mock, and E. V. Armbrust. 2009. Chitin in diatoms and its association with the cell wall. Eukaryot. Cell **8**: 1038–50.

Edelstein, A., N. Amodaj, K. Hoover, R. Vale, and N. Stuurman. 2010. Computer Control of Microscopes Using μManager. Curr. Protoc. Mol. Biol. , doi:10.1002/0471142727.mb1420s92

Emerson, S. R., and J. I. Hedges. 2008. Chemical oceanography and the marine carbon cycle, Cambridge University Press.

Field, C. B., M. J. Behrenfeld, J. T. Randerson, and P. G. Falkowski. 1998. Primary Production of the Biosphere: Integrating Terrestrial and Oceanic Components. Science (80-.). **281**: 237–240.

Fischer, A. D., E. A. Moberg, H. Alexander, E. F. Brownlee, K. R. Hunter-Cevera, K. J. Pitz, S. Z. Rosengard, and H. M. Sosik. 2014. Sixty Years of Sverdrup. Oceanography , doi:http://dx.doi.org/10.5670/oceanog.2014.26

Fripiat, F., K. Leblanc, M. Elskens, A. Cavagna, L. Armand, L. André, F. Dehairs, and D. Cardinal. 2011. Efficient silicon recycling in summer in both the Polar Frontal and Subantarctic Zones of the Southern Ocean. Mar. Ecol. Prog. Ser. **435**: 47–61.

Frost, B. W. 1972. Effects of size and concentration of food particles on the feeding behavior of the marine planktonic copepod *Calanus pacificus*. Limnol. Oceanogr. **17**.

Gargett, A. E., D. Stucchi, and F. Whitney. 2003. Physical processes associated with high primary production in Saanich Inlet, British Columbia. Estuar. Coast. Shelf Sci. **56**: 1141–1156.

Geider, R. J., T. Platt, and J. A. Raven. 1986. Size dependence of growth and photosynthesis in diatoms: a synthesis. Mar. Ecol. Ser. **30**: 93–104.

Gower, J. 2014. Strait of Georgia Spring Bloom Timing 2013, p. 101– 106. *In* R.I. Perry [ed.], State of the physical, biological and selected fishery resources of Pacific Canadian marine ecosystems in 2013. Can. Tech. Rep. Fish. Aquat. Sci. 3102.

Gröger, C., M. Sumper, and E. Brunner. 2008. Silicon uptake and metabolism of the marine diatom Thalassiosira pseudonana: Solid-state ^{29}Si NMR and fluorescence microscopic studies. J. Struct. Biol. **161**: 55–63.

Grundle, D. S. 2007. Temporal and Spatial Variations in Primary Productivity, Phytoplankton Assemblages and Dissolved Nutrient Concentrations in Saanich Inlet, a British Columbia Fjord. University of Victoria.

Grundle, D. S., D. A. Timothy, and D. E. Varela. 2009. Variations of phytoplankton productivity and biomass over an annual cycle in Saanich Inlet, a British Columbia fjord. Cont. Shelf Res. **29**: 2257–2269.

Harris, S. L., D. E. Varela, F. W. Whitney, and P. J. Harrison. 2009. Nutrient and phytoplankton dynamics off the west coast of Vancouver Island during the 1997/98 ENSO event. Deep Sea Res. Part II Top. Stud. Oceanogr. **56**: 2487–2502.

Harrison, P. J., H. L. Conway, R. W. Holmes, and C. O. Davis. 1977. Marine diatoms grown in chemostats under silicate or ammonium limitation. III. Cellular chemical composition and morphology of *Chaetoceros debilis*, *Skeletonema costatum*, and *Thalassiosira gravida*. Mar. Biol. **43**: 19–31.

Hazelaar, S., H. J. Van Der Strate, W. W. C. Gieskes, and E. G. Vrieling. 2005. Monitoring Rapid Valve Formation in the Pennate Diatom *Navicula salinarum* (Bacillariophyceae). J. Phycol. **41**: 354–358.

Hendry, K. R., and M. A. Brzezinski. 2014. Using silicon isotopes to understand the role of the Southern Ocean in modern and ancient biogeochemistry and climate. Quat. Sci. Rev. **89**: 13–26.

Heredia, A., H. J. van der Strate, I. Delgadillo, V. A. Basiuk, and E. G. Vrieling. 2008. Analysis of organo-silica interactions during valve formation in synchronously growing cells of the diatom *Navicula pelliculosa*. Chembiochem **9**: 573–84.

Hervé, V., J. Derr, S. Douady, M. Quinet, L. Moisan, and P. J. Lopez. 2012. Multiparametric Analyses Reveal the pH-Dependence of Silicon Biomineralization in Diatoms. PLoS One **7**, doi:10.1371/journal.pone.0046722

Hewes, C. D., and O. Holm-Hansen. 1983. A method for recovering nanoplankton from filters for identification with the microscope : The filter-transfer-freeze (FTF) technique. Limnol. Oceanogr.

Hickey, B., and N. Banas. 2008. Why is the Northern End of the California Current System So Productive? Oceanography **21**: 90–107.

Hildebrand, M., L. G. Frigeri, and A. K. Davis. 2007. Synchronized Growth of *Thalassiosira pseudonana* (Bacillariophyceae) Provides Novel Insights Into Cell-Wall Synthesis Processes in Relation To the Cell Cycle 1. J. Phycol. **43**: 730–740.

Hobson, L. A. 1981. Seasonal variations in maximum photosynthetic rates of phytoplankton in Saanich Inlet, Vancouver Island, British Columbia. J. Exp. Mar. Bio. Ecol. **52**: 1–13.

Hobson, L. A. 1983. Phytoplankton crops, bacterial metabolism and oxygen in saanich inlet, a fjord in Vancouver Island, British Columbia. Sediment. Geol. **36**: 117–130.

Hobson, L. A., and M. R. McQuoid. 1997. Temporal variations among planktonic diatom assemblages in a turbulent environment of the southern Strait of Georgia, British Columbia. Mar. Ecol. Prog. Ser. **150**: 263–274.

Hogg, J. 1869. The Microscope: It's History, Construction and Application, G. Routledge & Sons.

Honjo, S., S. J. Manganini, R. a. Krishfield, and R. Francois. 2008. Particulate organic carbon fluxes to the ocean interior and factors controlling the biological pump: A synthesis of global sediment trap programs since 1983. Prog. Oceanogr. **76**: 217–285.

Hutchins, D. A., and K. W. Bruland. 1998. Iron-limited diatom growth and Si:N uptake ratios in a coastal upwelling regime. Nature **393**: 65–68.

Ichinomiya, M., Y. Gomi, M. Nakamachi, T. Ota, and T. Kobari. 2010. Temporal patterns in silica deposition among siliceous plankton during the spring bloom in the Oyashio region. Deep Sea Res. Part II Top. Stud. Oceanogr. **57**: 1665–1670.

Iluz, D., G. Dishon, E. Capuzzo, E. Meeder, R. Astoreca, V. Montecino, P. Znachor, D. Ediger, and J. Marra. 2009. Short-term variability in primary productivity during a wind-driven diatom bloom in the Gulf of Eilat (Aqaba). Aquat. Microb. Ecol. **56**: 205–215.

Ingalls, A. E., K. Whitehead, and M. C. Bridoux. 2010. Tinted windows: The presence of the UV absorbing compounds called mycosporine-like amino acids embedded in the frustules of marine diatoms. Geochim. Cosmochim. Acta **74**: 104–115.

Johnston, C. 1872. The Preparation of Diatomaceae. Lens; A Q. J. Microsc. Allied Nat. Sci.

Kain, C. H. 1891. Recent Contributions to the Literature of the Diatomaceae. Bull. Torrey Bot. Club 11–13.

Kaluzhnaya, O. V, and Y. V Likhoshway. 2007. Valve morphogenesis in an araphid diatom *Synedra acus* subsp. *radians*.

Keil, R. 2015. Carbon cycle: Hoard of fjord carbon. Nat. Geosci. 1–2.

Kemp, A. E. S., R. B. Pearce, I. Grigorov, J. Rance, C. B. Lange, P. Quilty, and I. Salter. 2006. Production of giant marine diatoms and their export at oceanic frontal zones: Implications for Si and C flux from stratified oceans. Global Biogeochem. Cycles **20**: GB4S04.

Kemp, A., J. Pike, R. Pearce, and C. Lange. 2000. The "Fall dump" — a new perspective on the role of a "shade flora" in the annual cycle of diatom production and export flux. Deep Sea Res. Part II Top. Stud. Oceanogr. **47**: 2129–2154.

Krause, J. W., M. A. Brzezinski, R. Goericke, M. R. Landry, M. D. Ohman, M. R. Stukel, and A. G. Taylor. 2015. Variability in diatom contributions to biomass, organic matter production and export across a frontal gradient in the California Current Ecosystem. J. Geophys. Res. Ocean. **120**: 1–16.

Krause, J. W., M. A. Brzezinski, and J. L. Jones. 2011a. Application of low-level beta counting of 32Si for the measurement of silica production rates in aquatic environments. Mar. Chem. **127**: 40–47.

Krause, J. W., D. M. Nelson, and M. a. Brzezinski. 2011b. Biogenic silica production and the diatom contribution to primary production and nitrate uptake in the eastern equatorial Pacific Ocean. Deep Sea Res. Part II Top. Stud. Oceanogr. **58**: 434–448.

Krause, J. W., D. M. Nelson, and M. W. Lomas. 2009. Biogeochemical responses to late-winter storms in the Sargasso Sea, II: Increased rates of biogenic silica production and export. Deep Sea Res. Part I Oceanogr. Res. Pap. **56**: 861–874.

Krause, J. W., D. M. Nelson, and M. W. Lomas. 2010. Production, dissolution, accumulation, and potential export of biogenic silica in a Sargasso Sea mode-water eddy. Limnol. Oceanogr. **55**: 569–579.

Kröger, N. 2007. Prescribing diatom morphology: toward genetic engineering of biological nanomaterials. Curr. Opin. Chem. Biol. **11**: 662–9.

Kröger, N., and N. Poulsen. 2008. Diatoms-from cell wall biogenesis to nanotechnology. Annu. Rev. Genet. **42**: 83–107.

Kucki, M., and T. Fuhrmann-Lieker. 2012. Staining diatoms with rhodamine dyes: control of emission colour in photonic biocomposites. J. R. Soc. Interface **9**: 727–33.

Kusurkar, T. S., I. Tandon, N. K. Sethy, K. Bhargava, S. Sarkar, S. K. Singh, and M. Das. 2013. Fluorescent silk cocoon creating fluorescent diatom using a "Water glass-fluorophore ferry". Sci. Rep. **3**: 3290.

Lalli, C. M., and T. R. Parsons. 1997. Biological Oceanography: An Introduction, 2nd ed. Butterworth-Heinemann.

Laruelle, G. G., P. Regnier, O. Ragueneau, M. Kempa, B. Moriceau, S. Ni Longphuirt, A. Leynaert, G. Thouzeau, and L. Chauvaud. 2009. Benthic–pelagic coupling and the seasonal silica cycle in the Bay of Brest (France): new insights from a coupled physical–biological model. Mar. Ecol. Prog. Ser. **385**: 15–32.

Leblanc, K., and D. A. Hutchins. 2005. New applications of a biogenic silica deposition fluorophore in the study of oceanic diatoms. Limnol. Oceanogr. Methods 462–476.

Leng, X., Y. Feng, X. Li, and J. Sun. 2015. *Skeletonema* cf . *costatum* biogenic silica production rate determinated by PDMPO method. Adv. Environ. Sci. Energy Plan. 255–260.

Li, C. W., M. Chu, and M. Lee. 1989. Characterizing the silica deposition vesicle of diatoms. Protoplasma **151**: 158–163.

Life Technologies Corporation. 2013. LysoTracker ® and LysoSensor ^{TM} Probes. 1–6.

MacFadyen, A., B. M. Hickey, and W. P. Cochlan. 2008. Influences of the Juan de Fuca Eddy on circulation, nutrients, and phytoplankton production in the northern California Current System. J. Geophys. Res. **113**: C08008.

MacIntyre, H. L., and J. J. Cullen. 2005. Using cultures to investigate the physiological ecology of microalgae, p. 287– 326. *In* R.A. Andersen [ed.], Algal Culturing Techniques. Elsevier Academic Press.

Mackas, D. L., G. C. Louttit, and M. J. Austin. 1980. Spatial Distribution of Zooplankton and Phytoplankton in British Columbian Coastal Waters. Can. J. Fish. Aquat. Sci. **37**: 1476–1487.

Mackas, D. L., and D. R. Yelland. 1999. Horizontal flux of nutrients and plankton across and along the British Columbia continental margin. Deep Sea Res. II **46**: 2941–2967.

Marchetti, A., and P. J. Harrison. 2007. Coupled changes in the cell morphology and elemental (C, N, and Si) composition of the pennate diatom *Pseudo-nitzschia* due to iron deficiency. Limnol. Oceanogr. **52**: 2270–2284.

Marchetti, A., D. E. Varela, V. P. Lance, Z. Johnson, M. Palmucci, M. Giordano, and E. V. Armbrust. 2010. Iron and silicic acid effects on phytoplankton productivity, diversity, and chemical composition in the central equatorial Pacific Ocean. Limnol. Oceanogr. **55**: 11–29.

Martin, J. H. 1990. Glacial-Interglacial CO_2 Change: The Iron Hypothesis. Paleoceanography **5**: 1–13.

Martin, J. H., and S. E. Fitzwater. 1988. Iron deficiency limits phytoplankton growth in the north-east Pacific subarctic. Nature **336**: 403–405.

Martin-Jézéquel, V., M. Hilderand, and M. A. Brzezinski. 2000. Silicon Metabolism in Diatoms: Implications for Growth. J. Phycol. **840**: 821–840.

McQuoid, M. R., and L. A. Hobson. 1997. A 91-year record of seasonal and interannual variability of diatoms from laminated sediments in Saanich Inlet, British Columbia. J. Plankton Res. **19**: 173–194.

Mock, T., M. P. Samanta, V. Iverson, C. Berthiaume, M. Robison, K. Holtermann, C. Durkin, S. S. Bondurant, K. Richmond, M. Rodesch, T. Kallas, E. L. Huttlin, F. Cerrina, M. R. Sussman, and E. V. Armbrust. 2008. Whole-genome expression profiling of the marine diatom *Thalassiosira pseudonana* identifies genes involved in silicon bioprocesses. Proc. Natl. Acad. Sci. U. S. A. **105**: 1579–84.

Model, M. a, and J. K. Burkhardt. 2001. A standard for calibration and shading correction of a fluorescence microscope. Cytometry **44**: 309–16.

Mosseri, J., B. Quéguiner, L. Armand, and V. Cornetbarthaux. 2008. Impact of iron on silicon utilization by diatoms in the Southern Ocean: A case study of Si/N cycle decoupling in a naturally iron-enriched area. Deep Sea Res. Part II Top. Stud. Oceanogr. **55**: 801–819.

Nelson, D. M., and J. J. Goering. 1977. A stable isotope tracer method to measure silicic acid uptake by marine phytoplankton. Anal. Biochem. **78**: 139–147.

Nelson, D. M., P. Treguer, and M. A. Brzezinski. 1995. Production and dissolution of biogenic silica in the ocean: Revised global estimates, comparison with regional data and relationship to biogenic sedimentation. Global Biogeochem. Cycles **9**: 359–372.

Nikon Instruments Inc. 2013. 1st Place, 2013 Photomicrography Competition.

Nomura, M., T. Nakayama, and K. Ishida. 2014. Detailed process of shell construction in the photosynthetic testate amoeba *Paulinella chromatophora* (euglyphid, Rhizaria). J. Eukaryot. Microbiol. **61**: 317–21.

Ogane, K., A. Tuji, N. Suzuki, T. Kurihara, and A. Matsuoka. 2009. First application of PDMPO to examine silicification in polycystine Radiolaria. Plankt. Benthos Res. **4**: 89–94.

Paasche, E. 1973a. Silicon and the Ecology of Marine Plankton Diatoms . II . Silicate-Uptake Kinetics in Five Diatom Species. Mar. Biol. **19**: 262–269.

Paasche, E. 1973b. Silicon and the ecology of marine plankton diatoms. I. *Thalassiosira pseudonana* (*Cyclotella nana*) grown in a chemostat with silicate as limiting nutrient. Mar. Biol. **19**: 117–126.

Palmer, T. C., and F. J. Keeley. 1900. The Structure of the Diatom Girdle. Proc. Acad. Nat. Sci. Philadelphia **52**: 465–479.

Parsons, T. R., Y. Maita, and C. M. Lalli. 1984. A manual of biological and chemical methods for seawater analysis, Pergamon Press, Oxford.

Parsons, T. R., R. I. Perry, E. D. Nutbrown, W. Hsieh, and C. M. Lalli. 1983. Frontal Zone Analysis at the Mouth of Saanich Inlet, British Columbia, Canada. Mar. Biol. **73**: 1–5.

Passow, U., A. Engel, and H. Ploug. 2003. The role of aggregation for the dissolution of diatom frustules. FEMS Microbiol. Ecol. **46**: 247–55.

Peña, M. A., K. L. Denman, J. R. Forbes, S. E. Calvert, and R. E. Thomson. 1996. Sinking particle fluxes from the euphotic zone over the continental slope of an eastern boundary current region. J. Mar. Res. **54**: 1097–1122.

Peña, M., K. Denman, S. S. E. Calvert, R. E. Thompson, and J. R. Forbes. 1999. The seasonal cycle in sinking particle Fluxes off Vancouver Island, British Columbia. Deep Sea Res. II **46**: 2969–2992.

Pondaven, P., M. Gallinari, S. Chollet, E. Bucciarelli, G. Sarthou, S. Schultes, and F. Jean. 2007. Grazing-induced changes in cell wall silicification in a marine diatom. Protist **158**: 21–8.

Poulton, A. J., C. Mark Moore, S. Seeyave, M. I. Lucas, S. Fielding, and P. Ward. 2007. Phytoplankton community composition around the Crozet Plateau, with emphasis on diatoms and *Phaeocystis*. Deep Sea Res. Part II Top. Stud. Oceanogr. **54**: 2085–2105.

Quéguiner, B., K. Leblanc, V. Cornet-barthaux, L. Armand, F. Fripiat, and D. Cardinal. 2011. Using a new fluorescent probe of silicification to measure species-specific activities of diatoms under varying environmental conditions H.-J. Ceccaldi, I. Dekeyser, M. Girault, and G. Stora [eds.]. Glob. Chang. Mankind-Marine Environ. Interact. , doi:10.1007/978-90-481-8630-3

Le Quéré, C., R. Moriarty, R. M. Andrew, G. P. Peters, P. Ciais, P. Friedlingstein, and S. D. Jones. 2015. Global carbon budget 2014. Earth Syst. Sci. Data **7**: 47–85.

R Core Team. 2013. R: A language and environment for statistical computing.

R Studio. 2012. R Studio: Integrated development environment for R.

Rasband, W. S. 2012. ImageJ.

Raven, J. A., and A. M. Waite. 2004. The evolution of silicification in diatoms: inescapable sinking and sinking as escape? New Phytol. **162**: 45–61.

Renzi, M., L. Roselli, A. Giovani, S. E. Focardi, and A. Basset. 2014. Early warning tools for ecotoxicity assessment based on *Phaeodactylum tricornutum*. Ecotoxicology **23**: 1055–72.

Richthammer, P., M. Börmel, E. Brunner, and K.-H. van Pée. 2011. Biomineralization in diatoms: the role of silacidins. Chembiochem **12**: 1362–6.

Riebesell, U., K. G. Schulz, R. G. J. Bellerby, M. Botros, P. Fritsche, M. Meyerhöfer, C. Neill, G. Nondal, A. Oschlies, J. Wohlers, and E. Zöllner. 2007. Enhanced biological carbon consumption in a high CO_2 ocean. Nature **450**: 545–8.

Round, F. E., R. M. Crawford, and D. G. Mann. 1990. The Diatoms, Cambridge University Press.

Sabine, C. L., R. A. Feely, N. Gruber, R. M. Key, J. L. Bullister, R. Wanninkhof, C. S. Wong, D. W. R. Wallace, B. Tilbrook, F. J. Millero, T. Peng, A. Kozyr, T. Ono, and A. F. Rios. 2004. The Oceanic Sink for Anthropogenic CO_2. Science (80-.). **305**: 367–371.

Sancetta, C. 1989. Processes controlling the accumulation of diatoms in sediments: a model derived from British Columbian fjords. Paleoceanography **4**: 235–251.

Sancetta, C., and S. E. Calvert. 1988. The annual cycle of sedimentation in Saanich Inlet , British Columbia: implications for the interpretation of diatom fossil assemblages. Deep Sea Res. **35**: 71–90.

Sarmiento, J. L., and N. Gruber. 2006. Ocean Biogeochemical Dynamics,.

Sarthou, G., K. R. Timmermans, S. Blain, and P. Tréguer. 2005. Growth physiology and fate of diatoms in the ocean: a review. J. Sea Res. **53**: 25–42.

Saxton, M. A., N. A. D'souza, R. A. Bourbonniere, R. M. L. McKay, and S. W. Wilhelm. 2012b. Seasonal Si:C ratios in Lake Erie diatoms — Evidence of an active winter diatom community. J. Great Lakes Res. **38**: 206–211.

Schickore, J. 2003. Cheese mites and other delicacies: The introduction of test objects into microscopy. Endeavour **27**: 134–138.

Scholin, C. A., F. Gulland, G. J. Doucette, S. Benson, M. Busman, F. P. Chavez, J. Cordaro, R. DeLong, A. De Vogelaere, J. Harvey, M. Haulena, K. Lefebvre, T. Lipscomb, S. Loscutoff, L. J. Lowenstine, R. Marin, P. E. Miller, W. A. McLellan, P. D. Moeller, C. L. Powell, T. Rowles, P. Silvagni, M. Silver, T. Spraker, V. Trainer, and F. M. Van Dolah. 2000. Mortality of sea lions along the central California coast linked to a toxic diatom bloom. Nature **403**: 80–4.

Schröder, H.-C., S. Perovic-Ottstadt, M. Rothenberger, M. Wiens, H. Schwertner, R. Batel, M. Korzhev, I. M. Muller, and W. E. G. Muller. 2004. Silica transport in the demosponge *Suberites domuncula*: fluorescence emission analysis using the PDMPO probe. **673**: 665–673.

Shimizu, K., Y. Del Amo, M. A. Brzezinski, G. D. Stucky, and D. E. Morse. 2001. A novel Fluorescent silica tracer for biological silicification studies. Chem. Biol. **8**: 1051–1060.

Shipe, R. F., and M. A. Brzezinski. 1999. A study of Si deposition synchrony in *Rhizosolenia* (Bacillariophyceae) mats using a novel ^{32}Si Autoradiographic method. J. Phycol. **1004**: 995–1004.

Smetacek, V., C. Klaas, V. H. Strass, P. Assmy, M. Montresor, B. Cisewski, N. Savoye, A. Webb, F. d'Ovidio, J. M. Arrieta, U. Bathmann, R. Bellerby, G. M. Berg, P. Croot, S. Gonzalez, J. Henjes, G. J. Herndl, L. J. Hoffmann, H. Leach, M. Losch, M. M. Mills, C. Neill, I. Peeken, R. Röttgers, O. Sachs, E. Sauter, M. M. Schmidt, J. Schwarz, A. Terbrüggen, and D. Wolf-Gladrow. 2012. Deep carbon export from a Southern Ocean iron-fertilized diatom bloom. Nature **487**: 313–9.

Spitta, E. J. 1920. Microscopy: The construction, theory and use of the microscope,.

De Stefano, L., I. Rea, I. Rendina, M. De Stefano, and L. Moretti. 2007. Lensless light focusing with the centric marine diatom Coscinodiscus walesii. Opt. Express **15**: 18082–18088.

Suchy, K. D. 2014. The response of crustacean zooplankton production to variations in food quantity, quality, and primary production in coastal marine ecosystems. University of Victoria.

Sun, J., and D. Liu. 2003. Geometric models for calculating cell biovolume and surface area for phytoplankton. J. Plankton Res. **25**: 1331–1346.

Sunda, W. G., and D. R. Hardison. 2010. Evolutionary tradeoffs among nutrient acquisition, cell size, and grazing defense in marine phytoplankton promote ecosystem stability. Mar. Ecol. Prog. Ser. **401**: 63–76.

Sunda, W., K. Shertzer, and D. Hardison. 2009. Ammonium uptake and growth models in marine diatoms: Monod and Droop revisited. Mar. Ecol. Prog. Ser. **386**: 29–41.

Sverdrup, H. U. 1953. On conditions for the vernal blooming of phytoplankton. J. du Cons.

Takahashi, M., D. L. Seibert, and W. H. Thomas. 1977. Occasional blooms of phytoplankton during summer in Saanich Inlet, B.C., Canada. Deep Sea Res. **24**: 775–780.

Tesson, B., C. Gaillard, and V. Martin-Jézéquel. 2009. Insights into the polymorphism of the diatom *Phaeodactylum tricornutum* Bohlin. Bot. Mar. **52**: 104–116.

Tesson, B., and M. Hildebrand. 2010a. Dynamics of silica cell wall morphogenesis in the diatom *Cyclotella cryptica* : Substructure formation and the role of microfilaments. J. Struct. Biol. **169**: 62–74.

Tesson, B., and M. Hildebrand. 2010b. Extensive and intimate association of the cytoskeleton with forming silica in diatoms: control over patterning on the meso- and micro-scale. PLoS One **5**: e14300.

Tesson, B., and M. Hildebrand. 2013. Characterization and localization of insoluble organic matrices associated with diatom cell walls: insight into their roles during cell wall formation. PLoS One **8**: e61675.

Thamatrakoln, K., and M. Hildebrand. 2008. Silicon uptake in diatoms revisited: a model for saturable and nonsaturable uptake kinetics and the role of silicon transporters. Plant Physiol. **146**: 1397–407.

Theriot, E. C. 2010. A preliminary multigene phylogeny of the diatoms (Bacillariophyta): challenges for future research. Plant Ecol. Evol. **143**: 278–296.

Thomson, R. E. 1981. Oceanography of the British Columbia Coast, Department of Fisheries and Oceans.

Timothy, D. A., and M. Y. S. Soon. 2001. Primary production and deep-water oxygen content of two British Columbian fjords. Mar. Chem. **73**: 37–51.

Tréguer, P. 2002. Silica and the cycle of carbon in the ocean. Comptes rendus l'Académie des Sci. **334**: 3–11.

Tréguer, P. J., and C. L. De La Rocha. 2012. The World Ocean Silica Cycle. Ann. Rev. Mar. Sci. 1–25.

Tunnicliffe, V., R. Dewey, and D. Smith. 2005. Research Plans for a Mid-depth Cabled Seafloor Observatory in Western Canada. Oceanography **16**: 53–59.

Twining, B. S., S. D. Nodder, A. L. King, D. A. Hutchins, G. R. Lecleir, J. M. Debruyn, E. W. Maas, S. Vogt, S. W. Wilhelm, and P. W. Boyd. 2014. Differential remineralization of major and trace elements in sinking diatoms. **59**: 689–704.

Uitz, J., H. Claustre, B. Gentili, and D. Stramski. 2010. Phytoplankton class-specific primary production in the world's oceans: Seasonal and interannual variability from satellite observations. Global Biogeochem. Cycles **24**: 1–19.

Utermöhl, H. 1958. Zur Vervollkommnung der quantitativen Phytoplankton-Methodik. Int. Vereinigung für Theor. und Angew. Limnol. Kom. für Limnol. Methoden **9**: 1–39.

Vartanian, M., J. Desclés, M. Quinet, S. Douady, and P. J. Lopez. 2009. Plasticity and robustness of pattern formation in the model diatom *Phaeodactylum tricornutum*. New Phytol. **182**: 429–42.

Vrieling, E. G., W. W. C. Gieskes, T. P. M. Beelen, and N. G. Hustedt. 1999. Silicon deposition in diatoms: control by the pH inside the silicon deposition vesicle. J. Phycol. **35**: 548–559.

Waite, A. M., and S. D. Nodder. 2001. The effect of in situ iron addition on the sinking rates and export flux of Southern Ocean diatoms. Deep Sea Res. II **5**: 2635–2654.

Waite, A. M., P. A. Thompson, and P. J. Harrison. 2011. Does energy control the sinking rates of marine diatoms? **37**: 468–477.

Walker-Arnott, G. A. 1860. On *Cyclotella*. Q. J. Microsc. Sci. **1**: 244–248.

Wang, W., T. Gutu, D. K. Gale, J. Jiao, G. L. Rorrer, and C. Chang. 2009. Self-Assembly of Nanostructured Diatom Microshells into Patterned Arrays Assisted by Polyelectrolyte Multilayer Deposition and Inkjet Printing. 4178–4179.

Ware, D. M., and R. E. Thomson. 2005. Bottom-up ecosystem trophic dynamics determine fish production in the Northeast Pacific. Science (80-.). **308**: 1280–4.

Weaver, A., and E. Weibe. 2014. School-Based Weather Station Network.

Whitney, F. A., W. R. Crawford, and P. J. Harrison. 2005. Physical processes that enhance nutrient transport and primary productivity in the coastal and open ocean of the subarctic NE Pacific. Deep Sea Res. II **52**: 681–706.

Wolf, D. E., C. Samarasekera, and J. R. Swedlow. 2007. Quantitative analysis of digital microscope images. Methods Cell Biol. **81**: 365–96.

Znachor, P., and J. Nedoma. 2008. Application of the PDMPO Technique in Studying Silica Deposition in Natural Populations of *Fragilaria crotonensis* (Bacillariophyceae) At Different Depths in a Eutrophic Reservoir. J. Phycol. **44**: 518–525.

Znachor, P., and J. Nedoma. 2009. Importance of dissolved organic carbon for phytoplankton nutrition in a eutrophic reservoir. J. Plankton Res. **32**: 367–376.

Znachor, P., J. Nedoma, and P. Rychtecký. 2011. Kinetics of glucose stimulatory effect on silica deposition and growth of natural populations of *Fragilaria crotonensis*. Phycol. Res. **59**: 123–128.

Znachor, P., V. Visocká, J. Nedoma, and P. Rychtecký. 2013. Spatial heterogeneity of diatom silicification and growth in a eutrophic reservoir. Freshw. Biol. **58**: 1889–1902.

Znachor, P., E. Zapomělová, K. Řeháková, J. Nedoma, and K. Šimek. 2008. The effect of extreme rainfall on summer succession and vertical distribution of phytoplankton in a lacustrine part of a eutrophic reservoir. Aquat. Sci. **70**: 77–86.

Appendix A: Growth vs. Irradiance Curves

A.1. Introduction

Light intensity is an important determinant of phytoplankton growth rates. To ensure that cultures are growing optimally during experiments, the light intensity at which a diatom strain grows at the greatest rate must be determined. The objective of this work was to determine the irradiance at which growth rate is highest for the diatom species used in experiments.

A.2. Methods

Diatom cultures were obtained from the National Center for Marine Algae and Microbiota. Cultures were grown in enriched seawater, artificial water (ESAW) media (Berges et al. 2001) at 18°C with continuous light. For each species, triplicate cultures were grown at 10, 30, 50, 100, 150, 200, 250 and 300 µmol photons m^{-2} s^{-1} and in vivo chlorophyll *a* fluorescence monitored to indicate biomass. Cultures were maintained semi-continuously in exponential growth. After ten generations of acclimation, growth rates were determined as the change in the natural logarithm of in vivo chlorophyll *a* fluorescence over time over the exponential phase of growth. Growth rate was determined for each replicate for three successive transfers, and then averaged within a replicate and between replicates to yield the average growth rate for the given light intensity.

A.3. Results

Chaetoceros contortus, *Coscinodiscus wailesii*, and *Skeletonema dohrnii* had the fastest growth rates when cultured at 100 µmol photon m^{-2} s^{-1}, while *Asterionellopsis glacialis* grew faster at 150 µmol photon m^{-2} s^{-1} (Figure A.1, Table A.1).

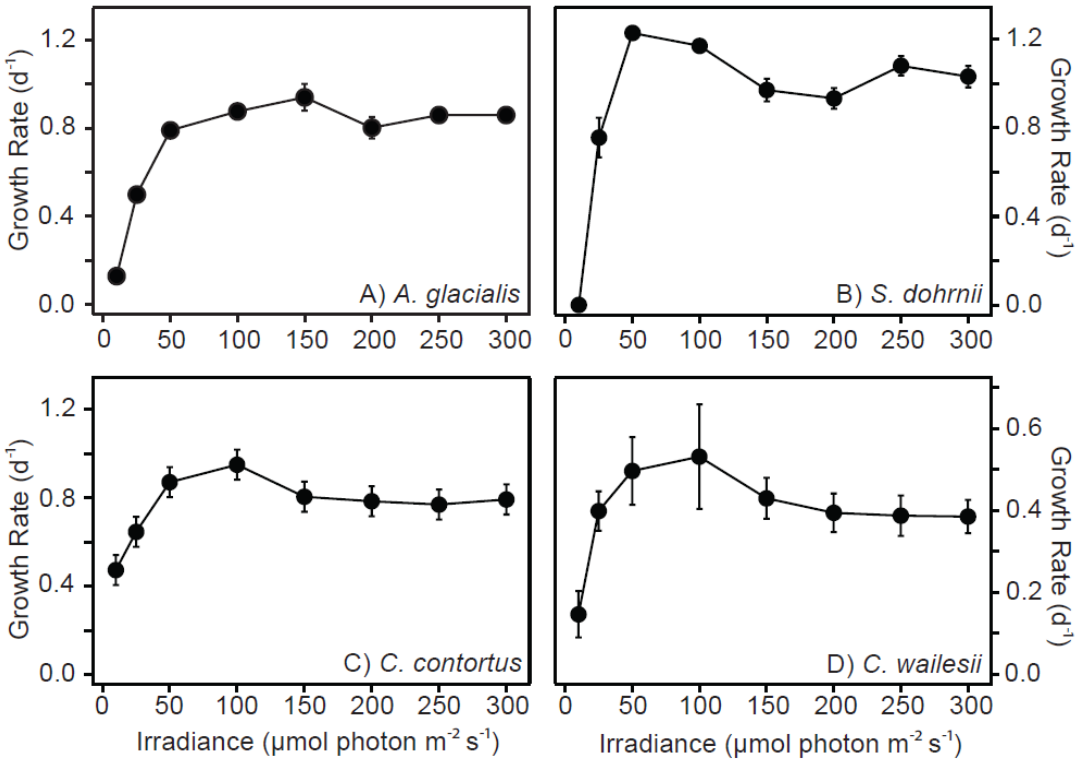

Figure A.1: Growth vs. irradiance curves for A) *A. glacialis*, B) *S. dohrnii*, C) *C. contortus*, and D) *C. wailesii*. All data points represent the mean of triplicate cultures, and error bars indicate one standard deviation.

Table A.1: Characteristics of diatom cultures used for experiments.

Species	Strain # (CCMP)	Optimal Irradiance (µmol photon m^{-2} s^{-1})	Maximum Growth Rate (day^{-1})		
			Mean	StDev	n
Asterionellopsis glacialis	139	150	0.94	0.06	3
Skeletonema dohrnii	785	100	1.24	0.10	3
Chaetoceros contortus	1578	100	0.95	0.03	3
Coscinodiscus wailesii	2513	100	0.53	0.13	3
*Thalassiosira pseudonana**	1014	200	1.93	0.04	3

* *T. pseudonana* growth vs. irradiance measurements were conducted by Marcos Lagunas

A.4. Conclusion

Experimental cultures should be grown at 100 µmol photon m^{-2} s^{-1} irradiance for *S. dohrnii*, *C. contortus*, and *C. wailesii*, while light intensities of 150 µmol photon m^{-2} s^{-1} and 200 µmol photon m^{-2} s^{-1} are preferable for *A. glacialis* and *T. pseudonana* respectively.

Appendix B: Storage of pPDMPO Samples

B.1. Introduction

It is not always possible to analyze field samples immediately, and it in many cases is preferable to analyze samples at a convenient time after collection. However, samples must be stored in such a way that the storage does not affect the signal to be measured. Slides prepared for iPDMPO measurements may be stored frozen at -20°C without a reduction in fluorescence (Leblanc and Hutchins 2005), and $bSiO_2$ samples are usually stored dry prior to measurement (Brzezinski and Nelson 1989). Additionally samples on the CCGS John P. Tully were stored by freezing at -80°C, and then dried upon return to shore. It is not known how these different storage methods would affect pPDMPO samples. The objectives of these experiments are to compare PDMPO fluorescence determined from fresh pPDMPO filters with samples that have been stored: 1) dry, or frozen at -20°C and 2) stored frozen at -80°C and then dried.

B.2. Methods

T. pseudonana was incubated with 125 nmol L^{-1} PDMPO for 24 hours. Then equal volumes of culture were filtered onto nine 0.6 µm PC filters. Three filters were digested immediately using hot NaOH digestion and pPDMPO was determined using a Turner TD-700 fluorometer as described in Chapter 2. The remaining six filters were split into two treatments: three filters were frozen at -20°C and three were dried at 56°C for 5 days and then stored dry. After one month of storage, the frozen and dried filters were digested as for the samples that were not stored.

In a second test, samples were stored similarly to field samples collected from the west coast of Vancouver Island. *T. pseudonana* was incubated with PDMPO as above, and then split into six equal volumes and filtered. Three filters were digested immediately (as above) and three were frozen at -80°C for one week, then dried at 56°C for five days and

stored dry. After one month, the three stored filters were digested and pPDMPO determined as above.

B.3. Results

Freezing samples at -20°C significantly reduced pPDMPO concentrations measured by 40 ± 3 % relative to freshly analyzed samples (Table B.1). Drying samples did not significantly reduce pPDMPO measured.

Table B.1: pPDMPO concentrations determined from samples digested immediately (Fresh), samples stored frozen at -20°C for one month (Frozen), and samples that were stored dry for one month (Dried).

Treatment	pPDMPO (nmol L^{-1})			p value*
	Mean	SE	n	
Fresh	20	0.7	3	
Frozen (-20°C)	12	0.3	3	0.00016
Dried	23	0.5	3	0.013

*when compared to the 'fresh' treatment.

Freezing samples at -80°C and then drying samples did not significantly alter pPDMPO measurements relative to fresh samples (Table B.2).

Table B.2: pPDMPO concentrations determined from samples digested and analyzed immediately (Fresh) and samples frozen at -80°C for one week then dried and stored dry for one month (Stored).

Sample	pPDMPO (nmol L^{-1})		
	Mean	SE	n
Fresh	1.8	0.2	3
Frozen (-80°C) and Dried	1.9	0.3	3

B.4. Conclusions

Drying pPDMPO samples preserves PDMPO fluorescence while freezing at -20°C may degrade PDMPO fluorescence. Storing pPDMPO samples by freezing at -80°C and then drying does not affect PDMPO fluorescence.

Appendix C: Degradation of PDMPO During NaOH Digestion

C.1. Introduction

When Leblanc and Hutchins (2005) compared $bSiO_2$ digestion protocols for analysis of pPDMPO samples, they found that NaOH digestion recovered less PDMPO than when digesting filters with HF, but this difference was not significant. However, in an experiment (Chapter 2, sections 2.2.1 and 2.3.1) where NaOH digestion was used for pPDMPO sample analysis, not all PDMPO added was recovered (Figure C1).

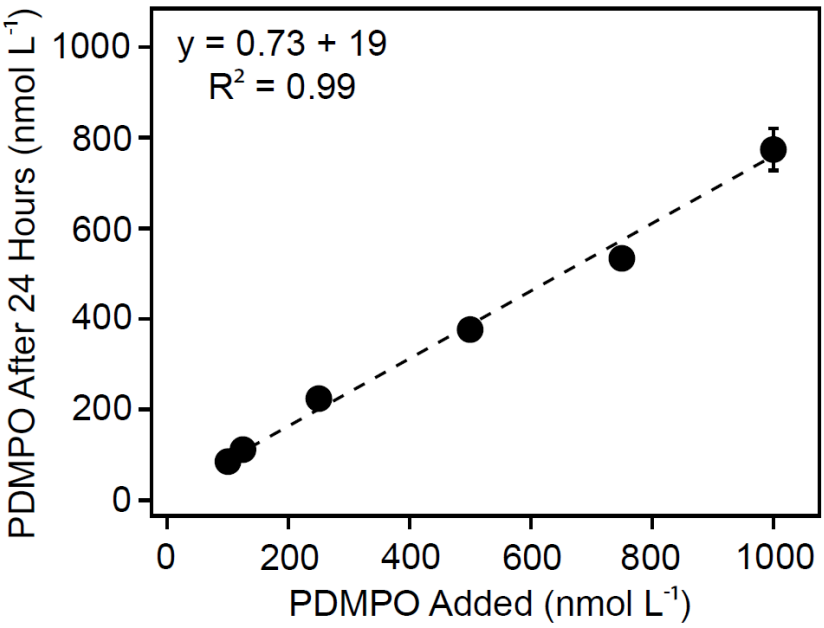

Figure C.1: PDMPO after 24 hours of incubation (dPDMPO + pPDMPO) vs. the concentration of PDMPO added at the start of incubation. All data points represent the mean of triplicate samples with error bars represent one standard deviation.

Instead, the total PDMPO measured after 24 hours (dissolved + particulate) was 27% less on average (indicated by slope of Figure C.1) than the amount of PDMPO added. It is possible that heating of samples during NaOH digestion may be detrimental to PDMPO fluorophores, and that degradation of PDMPO due to heating was responsible for this

PDMPO loss. The objective of this work was to determine the effect of heat during the NaOH digestion protocol on PDMPO fluorescence.

C.2. Methods

Fifteen 50 nmol L^{-1} PDMPO solutions were prepared in 0.2 mol L^{-1} NaOH. Ten of these solutions were heated to 95°C in a water bath, as per the $bSiO_2$ digestion protocol of Paasche (1973) as modified by Brzezinski and Nelson (1985). The remaining five solutions were kept at room temperature in the dark. After 1 hour, 1 mL of 1 mol L^{-1} HCl was added to each sample. Then PDMPO concentration was measured on a Turner TD-700 fluorometer as described in Chapter 2, section 2.2.1a.

C.3. Results

Heating pPDMPO samples to 95°C caused a decrease in PDMPO fluorescence of 23 ± 3% relative to unheated samples.

Table C.1: Fluorescence of 50 nmol L^{-1} PDMPO exposed to heat (95°C) or kept at room temperature (No Heat).

Treatment	PDMPO Fluorescence			
	Mean	**SE**	**n**	**p value**
95^0C	157	7	10	0.00006
No Heat	205	8	5	

C.4. Conclusion

Heating pPDMPO samples may degrade PDMPO and reduce fluorescence measured. Alternate digestion procedures would be preferable.

Appendix D: Solubilizing Frustule Bound PDMPO Using HF

D.1. Introduction

The NaOH digestion protocol caused degradation of PDMPO fluorescence, due heat (Appendix C). Biogenic silica may also be digested using HF, and this procedure does not require heat. The objective of this test is to compare NaOH and HF digestion protocols for the determination of pPDMPO concentration.

D.2. Methods

A dense culture of *Asterionellopsis glacialis* was cultured with 125 nmol L^{-1} PDMPO for 24 hours. Then samples of 15 mL, 30 mL and 45 mL were filtered onto 0.6 µm filters and rinsed with 10% HCl at the end of filtration (Chapter 2, section 2.2.1a). Six replicates were filtered for each volume, 3 of which were digested with the NaOH digestion method (Chapter 2, section 2.2.1a). The remaining 3 replicates were digested by adding 0.2 mL of 0.5 mol L^{-1} HF to each filter, and allowed to digest for 48 hours. Then 4.8 mL saturated boric acid was added to bind the remaining fluorine ions. PDMPO concentrations were determined for each sample using the Turner Trilogy fluorometer (Chapter 2, section 2.2.1b).

D.3. Results

The HF digestion procedure resulted in more PDMPO measured (Figure D.1). However, this difference was only significant when 45 mL of culture were filtered ($p < 0.02$), presumably because the PDMPO signal was lower when less volume was filtered, and degradation not as sensitively detected.

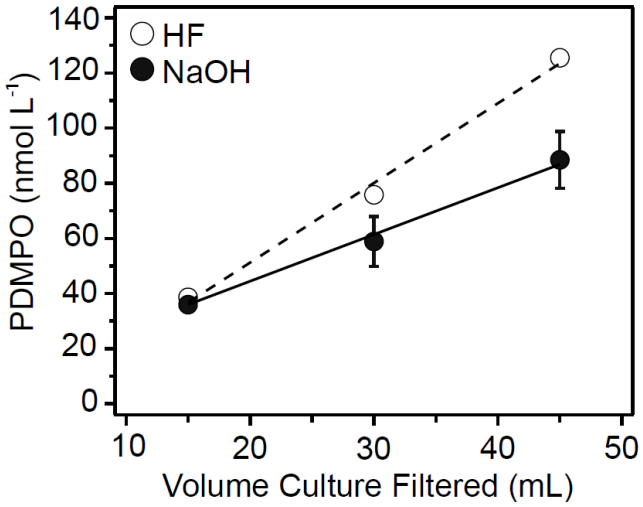

Figure D.1: The PDMPO concentration measured vs. the volume filtered for pPDMPO samples digested with either HF (open circles, dashed line) or NaOH (closed circles, solid line). All data points represent the average of triplicate samples, and error bars represent one standard error.

When data for different volumes filtered was pooled for each treatment, the NaOH treatment resulted in 28 ± 3 % less pPDMPO measured ($p < 0.005$, Table D.1).

Table D.1: pPDMPO concentrations (PDMPO incorporated per volume of culture) measured for samples digested with either HF or NaOH.

Digestion	**pPDMPO (nmol L^{-1})**		
	Mean	**SE**	**n**
HF	13.2	0.3	9
NaOH	9.5	0.6	9

D.4. Conclusion

The HF procedure was superior to NaOH for analysis of pPDMPO samples.

Appendix E: Modelling PDMPO Incorporation

E.1. Introduction

The effect of diatom species on the relationship between PDMPO and SiO_2 incorporation was investigated in order to determine if PDMPO would be useful as a tracer for diatom assemblages with variable taxonomic composition. Additionally, the relationship between PDMPO and SiO_2 incorporation was determined so that measurements of pPDMPO could be converted to an amount of SiO_2 produced during incubation with the tracer.

E.2. Methods

Experimental cultures and sample analysis are described in Chapter 2 (section 2.2.1b). All modelling was conducted in R with R Studio (R Studio 2012; R Core Team 2013). Measurements of $\Delta[SiO_2]$ and pPDMPO incorporated are repeat measurements from the same triplicate incubation bottles. Duplicate pPDMPO samples were collected at each time point, one in which cells were kept intact by rinsing cells with filtered seawater (FSW) and another in which cells were lysed by rinsing with 10% HCl. These two datasets have been analyzed separately.

E.3. Results

To start, the relationship between pPDMPO and $\Delta[SiO_2]$ was modelled in the most complex scenario. Initially, mixed effects models were used, which account for the effect of repeat measurements from the same incubation bottles through time. However, mixed effects models were not significantly different from simpler linear models, so linear models were preferred. In the most complex case, pPDMPO was modelled as a function of $\Delta[SiO_2]$, with each of the four diatom species best fit with its own slope and intercept (Figures E.1and E.2). This was compared to a simpler model, in which each all species had the same slope but different intercepts, but the fit of the simpler model was significantly worse. For both FSW and HCl rinsed pPDMPO samples, species was a

significant predictor variable in the model, and the slope of the pPDMPO vs. $\Delta[SiO_2]$ best fit line differed significantly between the species. In all cases, the intercepts fit were not significant; therefore, relationships between pPDMPO and $\Delta[SiO_2]$ are presented as Si:PDMPO ratios calculated from the slopes of best fit lines.

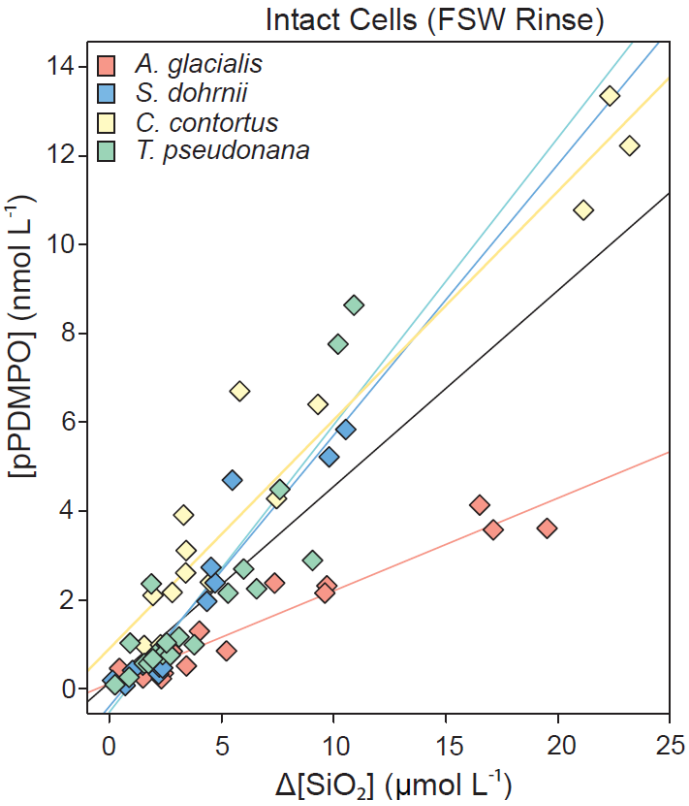

Figure E.1: The concentration of pPDMPO from intact diatom cells vs. $\Delta[SiO_2]$ from culture experiments described in section 2.3.1.b. The fit of individual species fit by the model are indicated, as is the fit when species is not included as a predictor variable (black). When species was included in the model as a predictor variable (coloured lines of best fit) the R^2 was 0.90. When species was not included as a predictor variable in the model (black line) the R^2 was 0.70.

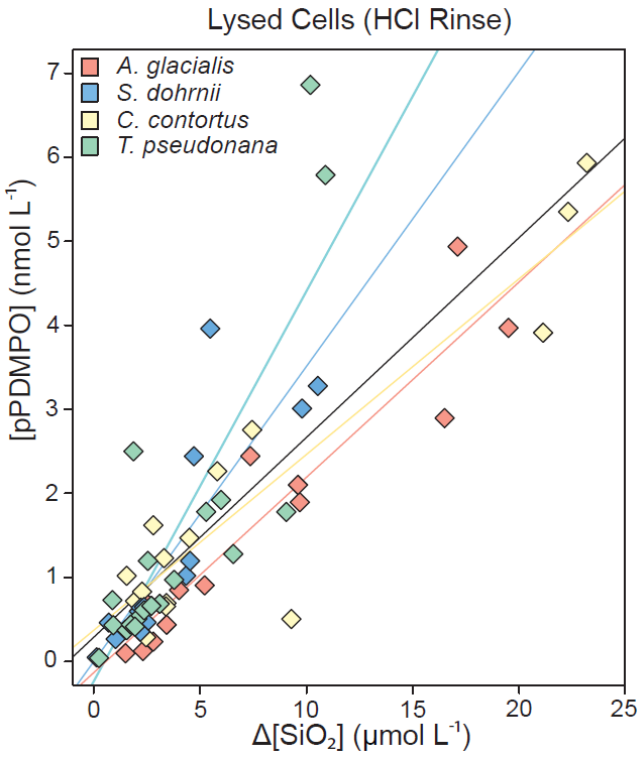

Figure E.2: The concentration of pPDMPO from lysed diatom cells vs. $\Delta[SiO_2]$ from culture experiments described in section 2.3.1.b. The fit of individual species fit by the model are indicated, as is the fit when species is not included as a predictor variable (black). When species was included in the model as a predictor variable (coloured lines of best fit) the R^2 was 0.75. When species was not included as a predictor variable in the model (black line) the R^2 was 0.67.

In results from lysed cells, *Thalassiosira pseudonana* had a significantly higher Si:PDMPO ratio than *Asterionellopsis glacialis* and *Chaetoceros contortus*. However, this appeared to be due to two data points with high pPDMPO concentrations (Figure E.3, red circles). These two data points were from t = 48, while the other two replicates from this time for this species were in line with the majority of points from the other species. If pPDMPO measured in these samples was erroneously over-estimated (perhaps due to incomplete cell lysis), the slope of the best fit for *T. pseudonana* decreased, and no longer differed significantly from the other species present.

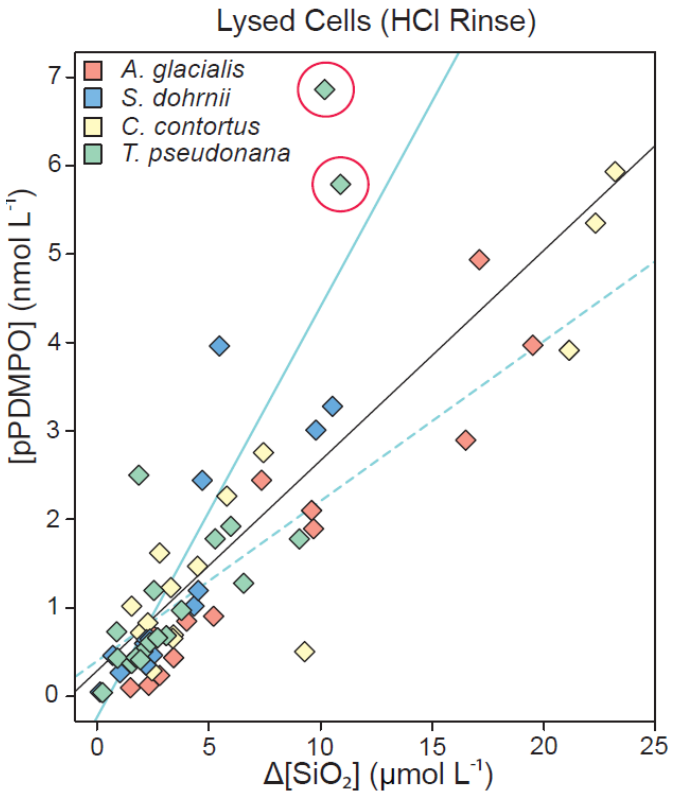

Figure E.3: The concentration of pPDMPO from lysed diatom cells vs. $\Delta[SiO_2]$ from culture experiments described in section 2.3.1.b. Data is the same as shown as Figure E.2, but with different fits indicated. Red circles indicate two *T. pseudonana* outliers, solid green fit is with outliers included while dashed green line shows the fit with outliers excluded. As in Figure E.2, the black line indicates the fit when species are not included as a model predictor.

Although species was a significant predictor in both models, pPDMPO concentration was also modeled as a function of $\Delta[SiO_2]$ without including species a predictor. When species was not included as a predictor variable, model R^2 values decreased for both intact and lysed cells (0.70 and 0.67 respectively).

When checking model fits using residual plots (Figure E.4), it is clear that there is not equal variance across the range of pPDMPO concentrations. At higher concentrations of pPDMPO and $\Delta[SiO_2]$ there was more variability between replicate measurements. This was the case whether or not cells were lysed, and regardless of whether species was included as a predictor variable. It would be possible to use a natural logarithm (Ln) transformation on both pPDMPO and $\Delta[SiO_2]$ measurements so that the model assumptions of equal variance were met. However, a Ln transformation would reduce

the effect of higher pPDMPO and $\Delta[SiO_2]$ data points on the model, and increase the effect of lower data points. As pPDMPO and $\Delta[SiO_2]$ measurements at the high range have a clearer signal of incorporation, these measurements are the most important for the calculation of the relationship between pPDMPO and $\Delta[SiO_2]$. Consequently, a Ln transformation was not used.

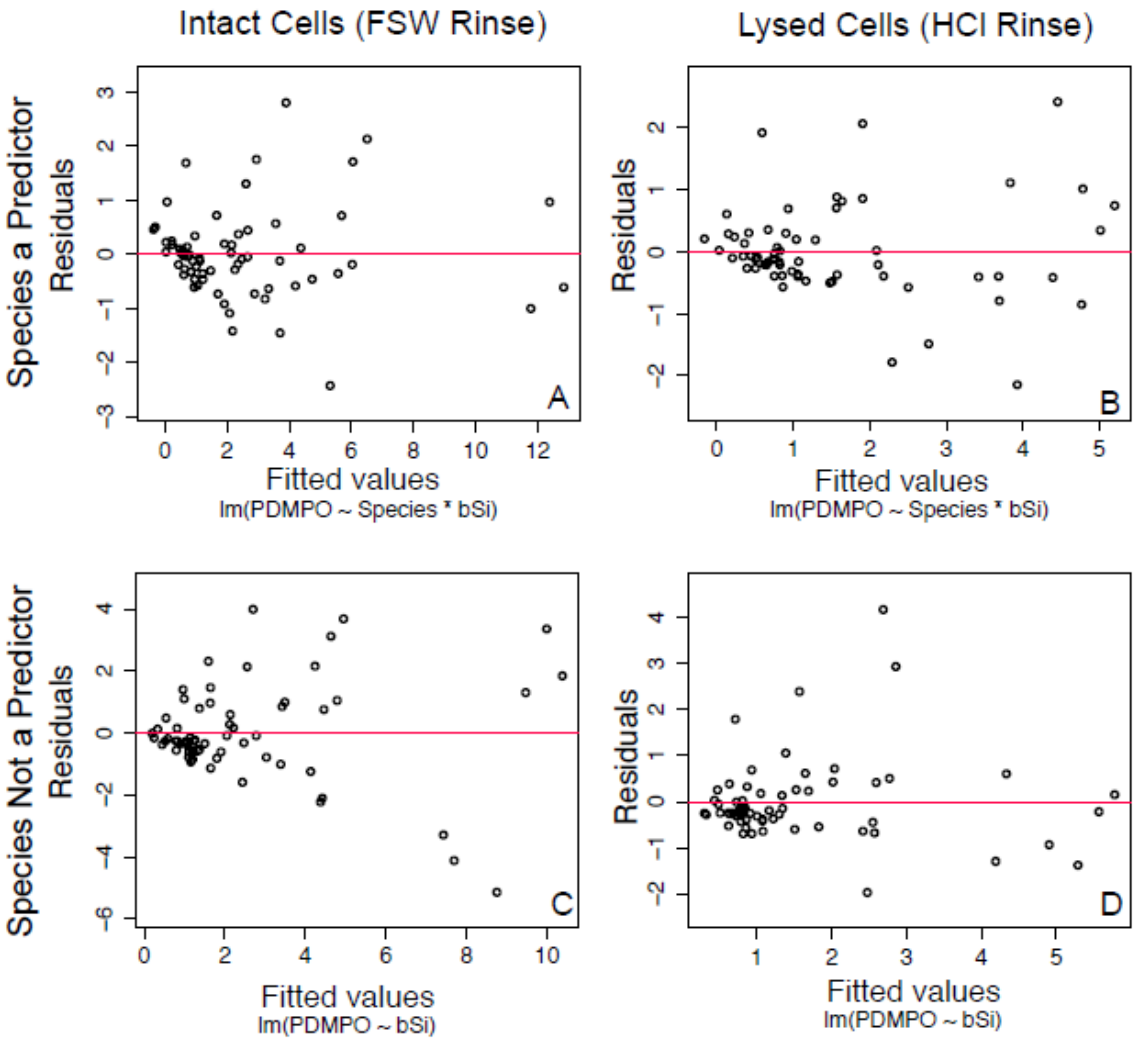

Figure E.4: Plots of model residuals vs. fitted values for models with species included (A, B) or not included (C, D) as a predictor variable for intact cells (A, C) and lysed cells (B, D). Fitted values are the y value predicted by the model, while residuals are the difference between the fitted values and the y values predicted from the model. Red lines indicate a residual of 0, i.e. agreement between predicted and actual values.

E.4.Conclusions

The relationship between PDMPO and SiO_2 incorporation was best fit when diatom species were each fit with separate slopes and intercepts, regardless of whether or not cells were lysed. However, species did not have a significant effect on the relationship between PDMPO and SiO_2 incorporation for lysed cells when two high pPDMPO data points from *T. pseudonana* were excluded. Although model residuals were not equal across the range of pPDMPO values modelled, data was not transformed, in order to better reflect the underlying biological processes.

Appendix F: Cell Density of Slides Prepared by Freeze Transfer

F.1. Introduction

Previous work has prepared slides for PDMPO microscopy by filtering cells onto black polycarbonate filters, then mounting the entire filter on a slide (Leblanc and Hutchins 2005, Znachor and Nedoma 2008). However, black filters obscure transmitted light; consequently, cells on slides prepared using this method cannot be observed using light microscopy (brightfield illumination). Another method for preparing slides of diatom cells is freeze transfer. Preparation of slides by freeze transfer was originally described by Hewes and Holm-Hansen (1983), and has been subsequently modified by Shipe and Brzezinski (1999) and Franck and Brzezinski (pers. comm.). Slides prepared by freeze transfer can be readily observed using brightfield illumination. This would be valuable for PDMPO microscopy with field assemblages, as observation by brightfield microscopy would aid species identification. However, if cells of different species were not transferred equally, this procedure could bias relative measurements of PDMPO fluorescence. In order to determine if slides prepared by freeze transfer are suitable for PDMPO microscopy, it is necessary to assess whether cells are transferred effectively. The objective of this experiment was to compare cell densities determined from slides prepared by freeze transfer, with densities determined from non-transfer methods.

F.2. Methods

Three diatom species were chosen that differed in size: the large diatom *C. wailesii* (cell length 100 µm), the smaller *A. glacialis* (cell length 25 µm), and the intermediately sized *Odontella* sp. (cell length 65 µm). Each species was grown with 125 nmol L^{-1} PDMPO and triplicate slides were prepared by freeze transfer as described in section 2.2.2a. For *Odontella* sp. and *A. glacialis*, slides were prepared by filtering the same volume of culture onto black polycarbonate filters. These filters were placed on top of a drop of immersion oil on a slide as described in Leblanc and Hutchins (2005). PDMPO fluorescence per slide was then quantified for slides prepared by freeze transfer and black filters as described in Chapter 2, section 2.2.2a. Cell densities of *C. wailesii* were too low to reliably quantify PDMPO fluorescence per slide. Instead, the cell density of slides prepared by freeze transfer was determined by counting cells using brightfield

illumination. This was compared to cell densities determined counts using a Sedgewick Rafter counting chamber.

F.3. Results

The freeze transfer had no significant effect on the PDMPO fluorescence measured (*Odontella* sp. and *A. glacialis*) or cell densities measured (*C. wailesii*) for any of the species tested (Table F.1, Figure F.1).

Table F.1: Cell densities (*C. wailesii*) and PDMPO fluorescence (*A. glacialis* and *Odontella* sp.) determined for slides prepared by freeze transfer and by no transfer methods.

Species	Cell Length (µm)	Freeze Transfer		No Transfer	
		Mean	SE	Mean	SE
*Coscinodiscus wailessii**	100	432	50	402	20
Odontella sp. [0]	65	2.14	0.50	2.08	0.29
Asterionellopsis glacialis [0]	25	9.1	3.1	7.9	0.7

*Values indicate cells L^{-1} for freeze transfer and Sedgewick Rafter counts (No Transfer)

[0] Values indicate PDMPO fluorescence per mL for slides prepared by freeze transfer and by mounting black polycarbonate filters (No Transfer)

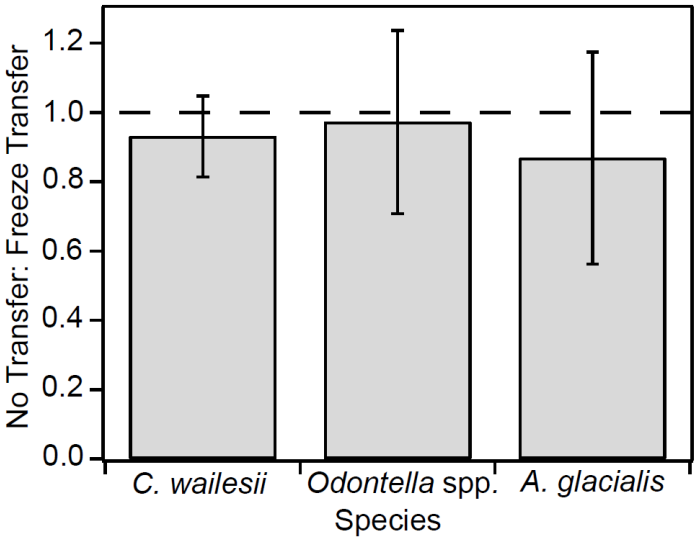

Figure F.1: The ratio of no transfer to freeze transferred cell densities (*C. wailesii*) or PDMPO fluorescence (*Odontella* sp. and *A. glacialis*) for the different species. The dashed line indicates 1, and no difference between the two protocols. All bars represent the mean of triplicate measurements, with error bars indicating one standard error.

F.4. Conclusion

Diatom cell densities on microscope slides prepared by freeze transfer did not differ significantly from slides prepared by non-transfer methods. Therefore, measurements of PDMPO fluorescence from microscope slides prepared by freeze transfer should not be biased between different taxa due to poor transfer of cells.

Appendix G: Comparing Calibrants for Fluorescence Microscopy

G.1. Introduction

Fluorescence measured by microscopy is dependent on the intensity of excitation light reaching the sample. However, illumination intensity may vary with time as excitation source bulbs gradually become fainter. Illumination intensity also varies across a field of view. To reliably measure fluorescence, this variability in excitation light intensity must be accounted for. Previous studies have used fluorescein solutions to calibrate excitation light intensity (Model and Burkhardt 2001; Znachor and Nedoma 2008). Yet solid autofluorescent slides are available, and would be a convenient alternative to preparing new slides of solution each imaging session. However, solid standards have thicker planes of fluorescence, and may perform differently than fluorescein solutions for calibration. The objective of this test is to compare fluorescein solution with a yellow fluorescent slide for flat-field correction.

G.2.Methods

A fluorescein solution was prepared by dissolving 0.28g Na-fluorescein in 100 mL 0.1 mol L^{-1} $NaHCO_3$. Previous studies have used higher concentrations of fluorescein (Model and Burkhardt 2001; Znachor and Nedoma 2008); however, it was not possible to prepare higher concentrations without many undissolved particles present. Therefore a lower concentration was used, but even at this concentration the fluorescein solution had much higher fluorescence intensity than PDMPO stained diatom cells. A fluorescein calibration slide was prepared by pipetting 10 µL of the fluorescein solution onto a coverslip, and placing another coverslip on top. A yellow fluorescent slide from Chroma Technology Corp was compared to the fluorescein solution. Both the yellow slide and fluorescein solution were imaged using the PDMPO microscope configuration (Chapter 2.2). Ten fields of view (FOVs) were imaged per slide at different locations, to minimize the effect of variability within a slide. These ten images were averaged together for each slide to generate the calibration image.

Next, plots of fluorescence intensity across the field of view were generated. The yellow slide had higher fluorescence than the fluorescein solution, so both calibration images were normalized to the highest measured fluorescence value then multiplied by 255 (the maximum intensity for 8 bit images). This normalized for overall differences in fluorescence intensity, to aid comparisons of relative intensity within a FOV.

Additionally, the slides were compared for their performance as calibrants for images of diatom cells. A PDMPO stained pennate diatom was imaged at left, center, and right positions within the FOV. The fluorescence of this cell was determined at each location using calibration images from each slide, as described in Chapter 2, section 2.2.2a.

G.3. Results

The profiles of fluorescence across the FOV were similar between yellow Chroma and fluorescein calibrants, but the yellow Chroma slide had higher intensity at the right edge (Figure G.1).

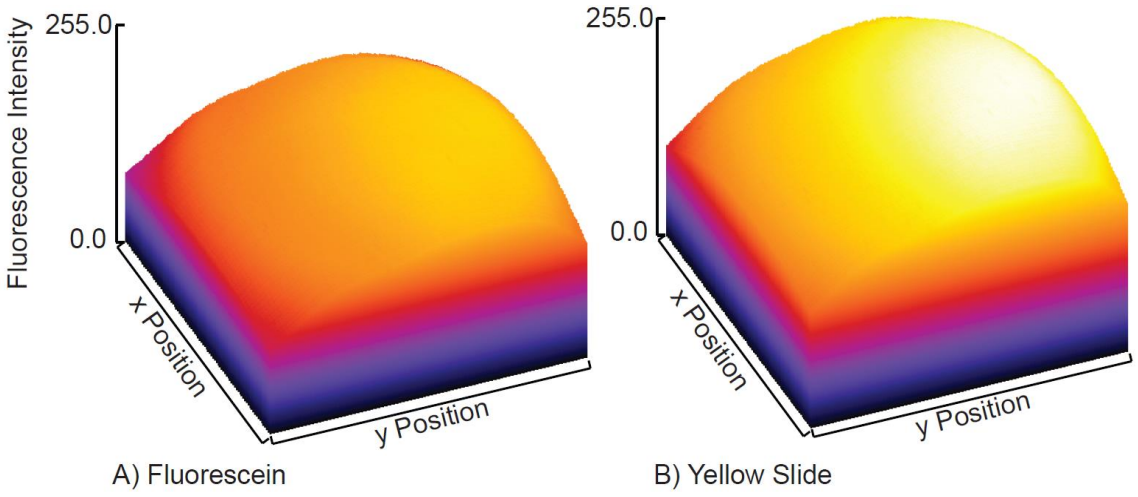

Figure G.1: The fluorescence intensity of calibration images of the fluorescein (A) and yellow slide (B). Intensities have been normalized to the maximum from each slide. Colours and height indicate the fluorescence intensity for each position within the FOV.

When the same PDMPO stained diatom cell was measured at different locations in the FOV, normalizing images by the yellow Chroma slide produced more consistent measurements of intensity than the fluorescein standard. The coefficient of variation was

less for measurements normalized by the yellow Chroma slide (12 %) than the fluorescein slide (21 %).

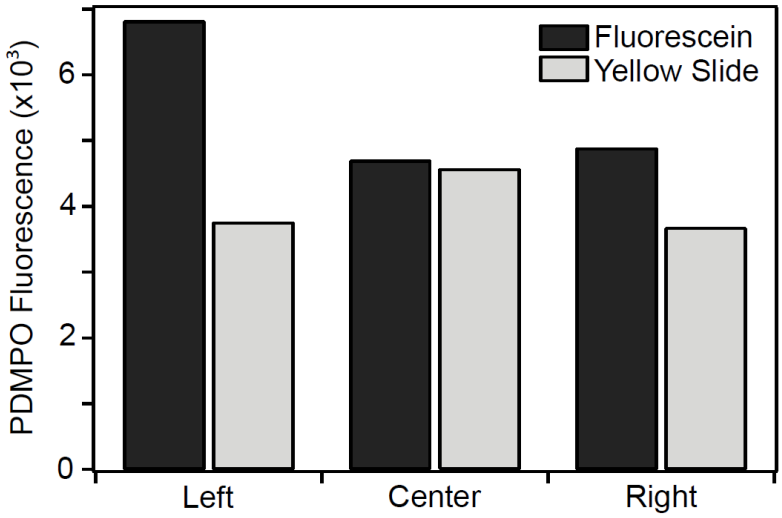

Figure G.2: PDMPO fluorescence measured for the same PDMPO stained pennate diatom cell at different positions within the FOV. Diatom fluorescence intensity was calibrated using either a fluorescein solution (black) or yellow slide (light grey).

G.4. Conclusions

The yellow Chroma and fluorescein calibrants had similar patterns of illumination intensity, but varied in magnitude across the field of view. Despite these differences, the yellow Chroma slide was superior for flat-field correction.

Appendix H: Effect of [$Si(OH)_4$] on Si:PDMPO Incorporation

H.1.Introduction

The incorporation of PDMPO into SiO_2 does not have a fixed stoichiometric relationship (Chapter 2). The ratio of Si:PDMPO incorporation likely reflects their ratio within the silicon deposition vesicle (SDV). Therefore, factors that differentially affect the transport of either PDMPO or Si to the SDV will likely affect the Si:PDMPO ratio of incorporation.

Silicic acid concentrations are expected to have no effect on PDMPO transport to the SDV, but may have a large effect on Si transport to the SDV. Low $Si(OH)_4$ concentrations may limit its uptake into the cell, and would result in reduced accumulation of Si within the SDV. This would cause a reduction in the Si:PDMPO ratio of incorporation. Consequently, SiO_2 incorporation calculated from PDMPO incorporation would be over-estimated under these conditions. The associated inflation of pPDMPO would be larger at low $Si(OH)_4$ concentrations as this would cause a greater reduction in SiO_2 incorporation and a larger discrepancy between SiO_2 and PDMPO incorporation. Paired measurements of ρ_{GROSS} and ρ_{PDMPO} from field sites indicate that ρ_{PDMPO} is higher than ρ_{GROSS} when rates are low (Chapter 2, 3). It is possible that the poor agreement between measurement methods in these cases could be due to low $Si(OH)_4$ concentrations. The objective of this section is to assess the effect of $Si(OH)_4$ concentration on $bSiO_2$ production rates measured by PDMPO.

H.2. Methods

Data presented here have been presented previously in Chapters 2 and 3. In addition, samples from April 2014 in Saanich Inlet are included. Instead of being collected from the depth of the chl *a* maximum, samples were collected from depths corresponding to 100%, 50%, 15% and 1% surface irradiance. Triplicate samples were collected on at the 100% depth, for the remainder only single samples were collected. Incubations with PDMPO and ^{32}Si and sample analysis were conducted as for Chapter 2, section 2.2.3.

In addition to comparing ρ_{PDMPO} with ρ_{GROSS}, PDMPO incorporation was also compared to ^{32}Si disintegrations per minute (DPM). Measurements of DPMs indicate the amount of ^{32}Si incorporated into $bSiO_2$, before correcting for the concentration of $Si(OH)_4$ (Brzezinski and Phillips 1997).

Two methods were used to calculate ρ_{PDMPO}: a ratio of 4200 ± 380:1 from Chapter 2 and Equation 4 presented in Chapter 3, section 3.4.3. Equation 3 attempts to account for the effect of $Si(OH)_4$ concentration on $Si(OH)_4$ uptake and the Si:PDMPO ratio of incorporation. This equation assumes SiO_2 incorporation depends on $Si(OH)_4$ with a half saturation constant of 4, the average for diatoms (Sarthou et al. 2005). Using this equation, PDMPO incorporation is reduced based on the expected reduction in $Si(OH)_4$ uptake. Equation 4 has been applied to samples with $Si(OH)_4$ concentrations below 10 μmol L^{-1}.

H.3. Results

The incorporation of pPDMPO was generally correlated with ^{32}Si DPMs except in two cases (Figure H.1A). In August 2013 and April 2014 at the 15% light depth (red circles), pPDMPO incorporation was much higher than expected from DPMs. These high pPDMPO concentrations are likely erroneous. When these samples were excluded, PDMPO incorporation was strongly correlated with DPMs ($R^2 = 0.92$).

When ^{32}Si DPMs were converted to ρ_{GROSS}, two samples with low ambient $Si(OH)_4$ concentrations were no longer in line with other samples (Figure H.1B, $Si(OH)_4 < 1$ μmol L^{-1} , purple circles). When a ratio of 4200 ± 380:1 was used to convert pPDMPO incorporation to ρ_{PDMPO} these samples remained out of alignment with others, and ρ_{PDMPO} calculated for these samples was 20-46x higher than ρ_{GROSS} (Figure H.1C, E). Samples indicated in green circles are samples when dinoflagellates were >95% of phytoplankton >5 μm which may also cause inflation of pPDMPO measurements as discussed in Chapter 2. When samples in red and green circles were excluded, the fit between ρ_{PDMPO} and ρ_{GROSS} was poor ($R^2 = 0.17$), but improved substantially when samples with $Si(OH)_4$ <1 μmol L^{-1} were excluded ($R^2 = 0.93$).

When pPDMPO was converted to ρ_{PDMPO} using Equation 4 for samples with $Si(OH)_4$ less than 10 µmol L^{-1}, the samples with $Si(OH)_4$ <1 µmol L^{-1} were much closer to the 1:1 line (Figure H.1D, F). When data points in red and green circles were excluded, ρ_{PDMPO} calculated using Equation 4 was strongly correlated with ρ_{GROSS} ($y = 1.04x + 0.3$, $R^2 = 0.95$, Figure H.1F).

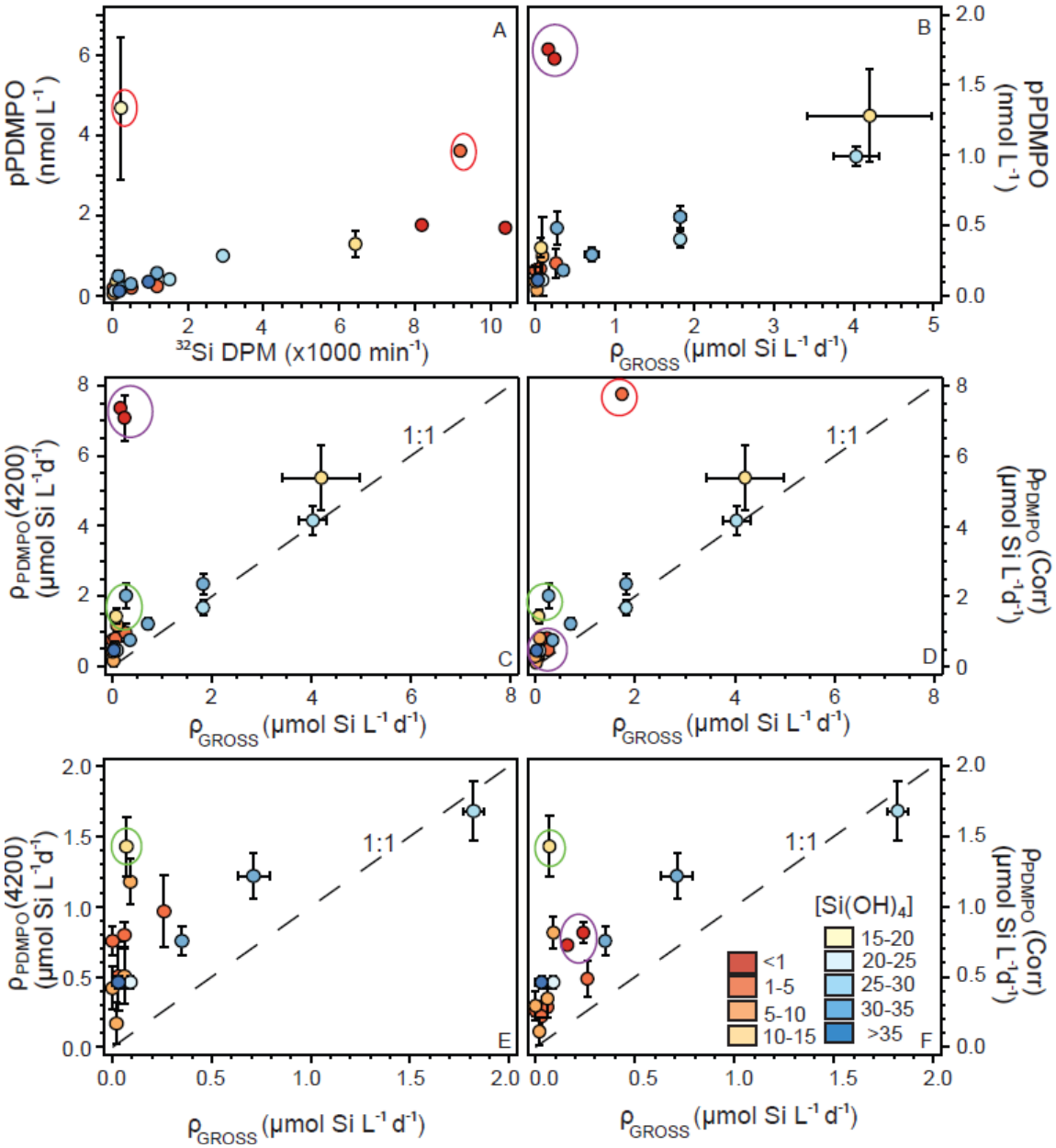

Figure H.1: All PDMPO and paired ^{32}Si measurements from natural field assemblages. PDMPO incorporation vs. ^{32}Si disintegrations per minute (DPM, A), pPDMPO concentration vs. ρ_{GROSS} (B), and ρ_{PDMPO} vs. ρ_{GROSS} for ρ_{PDMPO} calculated using a ratio of 4200 ± 380:1 from Chapter 2 (C, E), or using Equation 4 (D, F). Panels E and F present the same data as C and D, but with different axis scaling. August 2013 and April 2014 15% samples with inexplicably high pPDMPO concentration are indicated in red circles. Purple circles indicate April 100% and 15% samples when $Si(OH)_4$ concentrations were less than 1 μmol L^{-1}. Green circles indicate June and September 2013, when dinoflagellates made up >95% of the >5 μm phytoplankton cell numbers. Colours of data points indicate $Si(OH)_4$ concentration with blue the highest (> 35 μmol L^{-1}) and red the lowest (< 1 μmol L^{-1}). The dashed line indicates a 1:1 relationship. In all cases

except April 2014, 50%, 15% and 1% data points indicate the mean of triplicate samples with error bars indicating one standard deviation.

H.4. Conclusions

When $Si(OH)_4$ concentrations were below 1 µmol L^{-1}, ρ_{PDMPO} was higher (≥30x) than ρ_{GROSS}. It may be possible to correct for the effect of $Si(OH)_4$ on ρ_{PDMPO} by parameterizing ρ_{PDMPO} as a function of $Si(OH)_4$ concentration (e.g. Equation 4), but more work is needed to assess this affect before such a correction can be recommended.

Appendix I: PDMPO Fluorescence In Cells Without $bSiO_2$

I.1. Introduction

When microscope slides were analyzed for iPDMPO incorporation into diatoms, non-diatom cells were sometimes imaged by microscopy fluorescing in the same spectrum as PDMPO. Alvarado (2012) found that PDMPO may bind to the exterior of dinoflagellate cells, and contribute to pPDMPO measurements. It is unknown how these non-diatom sources of fluorescence may affect PDMPO measurements using the protocols in this thesis. The objective of this section is to investigate sources of fluorescence in the same spectrum as PDMPO from taxa not known to produce SiO_2.

I.2. Methods

Images presented here are from iPDMPO samples from the west coast of Vancouver Island, described in Chapter 2.

I.3. Results

In some cases, non-diatom cells were observed to fluoresce in the same spectrum as PDMPO (Figure I.1). Non-diatom sources of fluorescence may be due to PDMPO accumulation within cells, or due to another fluorophore (not PDMPO) that is found in these cells. In some cases, non-diatom fluorescence was as bright as diatom fluorescence (Figure I.1A, B, red circles), while in other cases non-diatom cells were not as bright as diatom fluorescence (yellow circles, green circles). In contrast to the results of Alvarado (2012), dinoflagellate fluorescence was located interior to the theca (Figure I.1C, D). Additionally, some non-diatom fluorescence was due to copepods, not dinoflagellates (Figure I.1E, F).

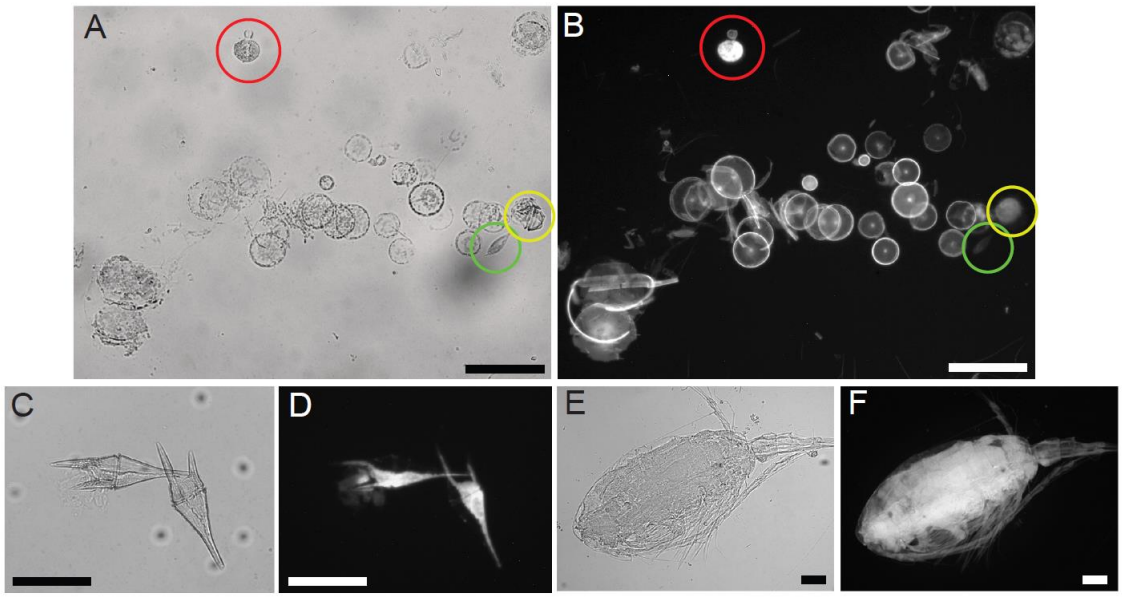

Figure I.1: Brightfield (A, C, E) and PDMPO fluorescence (B, D, F) images of cells from the west coast of Vancouver Island. A mixed assemblage of PDMPO stained diatoms and dinoflagellates from LC01 in September (A, B) with an unknown cell circled in red, and dinoflagellate cells indicated in yellow and green. *Ceratium* sp. (C, D) and a copepod (E, F) from station LG02 in September**.**

I.4. Conclusions

Certain non-diatom cells may exhibit fluorescence in the same spectrum as PDMPO. However, in this study, these cells generally contribute little to PDMPO fluorescence when measured by microscopy (3%, Chapter 3, Figure 3.8A), and seem to affect ρ_{PDMPO} only when diatoms are in very low abundance (<5% of cells >5 µm, Chapter 2 and Chapter 3).

Appendix J: Diatom Community Composition in Saanich Inlet

Figure J.1: The percentage contribution of the six most important diatom genera in Saanich Inlet to A) cell numbers, B) iPDMPO, C) total diatom SA, and D) V_{PDMPO}. Select results were presented in Chapter 4, in Figures 4.5, 4.6 and 4.7.